UNIVERSITAT DE BARCELONA

Characterization of Endothelial Cells dysfunction associated to Acute Myocardial Infarction: modulation of metabolic pathways as a new therapeutic approach

Erika Zodda

Doctoral Program in Biotechnology

Departament de Bioquímica i Biomedicina Molecular
Facultat de Farmàcia i Ciències de l'Alimentació

Characterization of Endothelial Cells dysfunction associated to Acute Myocardial Infarction: modulation of metabolic pathways as a new therapeutic approach

Doctoral Thesis submitted by Erika Zodda to obtain PhD degree from the Universitat de Barcelona and Universitá degli studi di Milano in the frame of dual degree agreement

Prof. Dr. Marta Cascante Serratosa
Co-Supervisor and Tutor

Prof. Dr. Marina Carini
Co-Supervisor

Dr. Timothy M. Thomson Okatsu
Co-Supervisor

Erika Zodda
Doctoral Student
2019

TABLE OF CONTENTS

Abbreviations and Acronyms

2DG 2-deoxy-D-glucose

ABRO1 Abraxas brother 1

ACE angiotensin converting enzyme

ACSS2 Acyl-CoA Synthetase Short chain 2

ADP/ATP adenosine diphosphate/ adenosine triphosphate

AIR Abraxas-interaction region

AK4 Adenylate kinase 4

AMI Acute Myocardial Infarction

AMPK AMP-activated protein kinase

ANT ADP/ATP translocase

AS Alternative Splicing

ASCT2 Alanine, Serine, Cysteine Transporter 2

ATCC American Type Culture Collection

ATF4 Activating Transcription Factor 4

ATM ataxia telangiectasia mutated

ATR ataxia telangiectasia and Rad3-related protein

bFGF basic Fibroblast growth factor

BARD1 BRCA1 Associated RING Domain 1

BLCA bladder carcinoma

BRCA1 BReast CAncer gene

BRCC36 BRCA1/BRCA2-containing complex subunit 36

BRISC BRCC36 isopeptidase complex

CABG coronary artery bypass grafting

CAMs Cell adhesion molecules

CCCP Carbonyl cyanide m-chlorophenyl hydrazone

CD44 Cluster of Differentiation 44

CHOL cholangiocarcinoma

COAD colon adenocarcinoma

CVD Cardiovascualr disease

DAPI 4',6-diamidino-2-phenylindole

DSBs Double Strand Breaks

DSK Desmoplakin

EC Endothelial cells

EDTA Ethylenediamine tetraacetic acid

EGF Epidermal growth factor

EMT Epithelial-to-Mesenchymal transition

ENAH enabled homolog gene

e-NOS Endothelial Nitric Oxide Synthase

EpCam epithelial cell adhesion

ESRP Epithelial Splicing Regulatory Protein

F-6-P Fructose-6-Phosphate

FACs fluorescence-activated cell sorter

$FADH_2$ Flavin adenine dinucleotide

FBS Fetal bovine serum

FGFR2 Fibroblast growth factor receptor

FNI Fibronectin

G6PDH *Glucose-6-phosphate dehydrogenase*

GAC Glutaminase C

GBM glioblastoma

GLDH Glutamate dehydrogenase

GLS Glutaminase

GSEA Gene Set Enrichment Analysis

GSH Glutathione

GTP Guanosine-5'-triphosphate

H3 histone3

HCAECs Human Coronary Artery Endothelial Cells

HCY homocysteine

HDL High density lipoprotein

HDR homology-dependent DNA repair

HERPUD homocysteine and ER stress-induced protein with an ubiquitin domain 1

HIF Hypoxia Inducible Factor

HK Hexokinase

HMG-CoA 3-hydroxy-3-methyl-glutaryl-coenzyme A reductas

HNSC head and neck squamous carcinoma

HR homologous recombination

hsCRP high-sensitivity C reactive protein

HTS high throughput sequencing

IFNAR1 IFN heterodimeric transmembrane receptor1

IMM Inner Mitochondrial membrane

KGA Kidney-type glutaminase

LC-MS Liquid Chromatography - Mass Spectrometry

LDL Low density lipoprotein

LIHC liver hepatocellular carcinoma

LUAD lung adenocarcinoma

LUSC lung squamous carcinoma

MCT1/MCT4 Monocarboxylate transporter 1/4

MET Mesenchymal to Epithelial transition

MI myocardial infarction

miRNAs microRNA

MPs microparticles

mTOR mammalian target of rapamycin

MTT 3-(4,5-Dimethylthiazol-2-yl)-2,5-diphenyltetrazolium bromide

NADH nicotinamide adenine dinucleotide

NHEJ Non-homologous end joining

NLRP3 NACHT, LRR and PYD domains-containing protein 3

NMR Nuclear magnetic resonance

NO Nitric OxidE

NOACs non-vitamin K antagonist oral anticoagulant

OXPHOS oxidative phosphorylation

PBS Phosphate-buffered saline

PC Prostate Cancer

PCCB Propionyl CoA carboxylase β

PCI percutaneous coronary intervention

PCYT1A Phosphate Cytidylyltransferase 1, Choline, Alpha

PDH Pyruvate Dehydrogenase

PECAM1 Platelet endothelial cell adhesion molecule

PFK1 Phosphofructokinase-1

PFKFB3 6-phosphofructo-2-kinase/fructose-2,6-biphosphatase 3

PFKFB4 6-phosphofructo-2-kinase/fructose-2,6-biphosphatase 4

PI propidium iodide

PPAR Peroxisome Proliferator-Activated Receptor

PPP pentose phosphate pathway

PRAD prostate adeno carcinoma

PSI percent spliced-in

PVDF Polyvinylidene fluoride or polyvinylidene difluoride

RAP80 Receptor Associated Protein 80

READ rectum adenocarcinoma

ROS Reactive Oxygen Species

RT Room temperature

SAH S-adenosylhomocysteine

SHMT2 Serine hydroxymethyltransferase 2

SKT25 serine/threonine kinase

snRNPs small nuclear ribonucleo proteins

SRC-3 steroid receptor coactivator-3

STEMI segment elevation myocardial infarction

SUMO Small Ubiquitin-like Modifier

TCA Tricarboxylic acid cycle

TCGA The Cancer Genome Atlas

TGF-β Transforming growth factor beta

TIGAR TP53-induced glycolysis and apoptosis regulator

TKT transketolase

TME tumor microenvironment

TOP3A DNA topoisomerase III α

TP53 Tumor Protein 53

UIMC-1 Ubiquitin Interaction Motif Containing 1

UPL Universal ProbeLibrary

UPR unfolded protein response

V-CAM1 Vascular cell adhesion protein 1

vWF von Willebrand factor

αKG αketoglutarate

γPPAR peroxisome proliferator-activating receptor γ

ABSTRACT

The endothelium plays a pivotal role in the development of cardiovascular disease (CVD), and emerging evidences indicate that the onset of the pathological blood vessels and endothelial dysfunctions are associated with metabolic alterations in endothelial cells (ECs).

This project aims at performing a complete characterization of the metabolic profiles of an endothelial pathological Acute Myocardial Infarction (AMI) cell model from 8 patients. The results discussed throughout this thesis are part of this attempt, and brought to the identification of the causes of the AMI pathology, as a consequence of the metabolic alterations related to the endothelium dysfunction.

Patients-derived cells displayed a low proliferation rate and unveiled a dependence on mitochondrial metabolism, which results in increased ROS-oxidative stress.

Patients-derived cells displayed slow growth, poor migration, and defective tubulogenesis, associated with less glucose consumption and higher lactate efflux in AMI patient-derived endothelial cells. Moreover, these cells showed also a glutamine-dependent metabolism to proliferate, and glutamine plays an important role as a precursor for the synthesis of glutathione to counter the high level of ROS detected in patients-derived cells. Additionally, the high content of glutaminase C (GAC) identified is fundamental to neutralize the acidic pH, which results from the lactate production.

The previous observations indicate a profound metabolic reprogramming in AMI patient-derived endothelial cells. This suggests the occurrence of a broad and complex dysfunction in these cells, that should be reflected in global processes. Systematic analysis by RNA-seq led us to discover that the adaptor protein RAP80, a critical actor in homology-directed repair (HDR), is regulated by ESRP1/2 and controls cell growth and response to genotoxic stress. RAP80 presents two isoforms, which express differentially in epithelial or in mesenchymal phenotypes.

Our analysis of the expression of these two isoforms in breast cancer demonstrates the clinical relevance of the alternative splicing event in the early prognosis of cancer disease. So we propose RAP80 as a possible target to reduce aggressive phenotypes in

breast and prostate cancers, and we hypothesize a possible direct implication of this gene in the DNA-damage associated to some endothelial dysfunction

1. INTRODUCTION

1 INTRODUCTION

1.1 Angiogenesis

The process of forming blood vessels from pre-existing ones is called angiogenesis. In the course of adulthood, endothelial cells remain inactive, except in situations such as wound healing, pregnancy, and in many pathological conditions when these cells are activated to form blood vessels (Nihed Draoui, De Zeeuw, and Carmeliet 2017a). A continuous supply of oxygen and nutrients is, in fact, essential for every cell, tissue, and organ of the body for its survival and development, in addition to eliminating waste products; therefore, a meticulously organized system of blood circulation guarantees these vital processes. Several pathologies have been identified associated with excessive blood vessel formation, such as cancer (Braunschweig et al. 2014; Cansby et al. 2018) (Hanahan and Weinberg 2011), arthritis (S.-J. Kim et al. 2013) and diabetes (Willard and Herman 2012). At the same time, pathological conditions associated with insufficient growth of blood vessels have also been identified, such as cardiac ischemia (Kalogeris et al. 2012) and stroke (S. J. Park et al. 2018). When a tissue has insufficient vessels to meet its blood and oxygen requirements, ischemia ensues (Kalogeris et al. 2012) which results in the degradation of its functions, whereas a blood vessel network in excess of tissue requirements may favor the growth of malignant cells in neoplasia or an inflammatory state (Kalogeris et al. 2012; Pahwa et al. 2019).

Angiogenesis is a biologically complex process in which the delicate balance of the factors responsible for its induction and regression need to be exquisitely orchestrated. The current understanding of fundamental mechanisms of angiogenesis has permitted to explain the defective development of blood vessels under pathological conditions, a knowledge crucial for the development of new therapeutic strategies targeting aberrant angiogenesis. Angiogenesis is considered one of the hallmarks of cardiovascular diseases and a key player in maintaining tumor tissues and preventing death and metastasis (Hanahan and Weinberg 2011). As such, factors responsible for the induction of angiogenesis have been described that favor the revascularization of ischemic tissues and cognate inhibitors were developed and proven to reduce vascular growth in diseases such as cancer (Goveia, Stapor, and Carmeliet 2014; Stapor et al. 2014). A

rational consideration in favor of anti-angiogenic strategies in the treatment for cancer is that, while tumor cells are genetically heterogeneous and unstable and eventually develop resistance to therapies directed at them, endothelial cells are normally stable and thus therapeutic targets to which resistance through genetic selection is unlikely to develop (Hida et al. 2018). In spite of the large body of knowledge that has been accrued on the molecular bases of angiogenesis, key aspects are yet to be determined in detail, notably the metabolic pathways underlying each step of physiological angiogenesis or the aberrant angiogenesis associated with human pathology. Emerging evidences indicate that metabolic plasticity exert both permissive and decisive roles in angiogenesis and, as such, a deeper understanding of the metabolism of endothelial cells should reveal new mechanisms of disease and new metabolic-targeted therapies that, either as single agents or in combination with conventional drugs, may improve anti-angiogenic therapeutic strategies in cardiovascular disease or cancer.

1.2 Cardiovascular diseases

Cardiovascular diseases (CVD) are the leading causes of death in the world. In 2015, The World Health Organization (WHO) estimated that 17.7 million people died from CVD, representing 31% of all global deaths(Townsend et al. 2015) Death from CVD is associated with increasing age, with 1.4 million deaths in individuals under 75 and 700,000 in individuals under 65 (Townsend et al. 2016) CVD encompass a range of diseases affecting the functions of the heart and blood vessels, driven by diverse underlying mechanisms. In this study, we will focus on acute myocardial infarction (AMI), a type of coronary artery disease characterized by an altered endothelium conducive to atherosclerosis, a consequent narrowing of arteries, compromised blood flow and reduced oxygen and nutrient supply to the vascular cells, eventually leading to cardiac hypertrophy and myocardial infarction.

1.3 Atherosclerosis

Atherosclerosis, or the formation of atherosclerotic plaques, underlies the majority of CVD (Townsend et al. 2015), with an estimated 16.7 million attributed deaths in 2015

(Hyder et al. 2007; Leopold and Loscalzo 2005). Atherosclerotic plaque formation and rupture is one of most common pathogenic mechanisms of coronary artery disease, stroke and peripheral artery disease (Grootaert et al. 2015). Atherogenesis is the result of complex sequences of events associated with processes such as endothelial dysfunction, neovascularization, vascular proliferation, apoptosis, matrix degradation, inflammation, oxidative stress and thrombosis (Hansson 2005). All these processes affect the inner lining of the artery. Eventually, arteries become thicker under an accumulation of calcium, fat deposits, and inflammatory cells, leading to the formation of the atherosclerotic plaque (N. R. Shah and Mahmoudi 2015). Although the pathophysiological mechanisms of atherosclerosis are yet to be fully unveiled, increasing evidences point to a critical role played by endothelial and metabolic dysregulation involving oxidative phosphorylation and fatty acid metabolism (**Figure 1.1**). A complete understanding of endothelial metabolic reprogramming underlying atherosclerosis requires further investigation and could open new avenues in the prevention and treatment of this disease (Moreno-Viedma et al. 2016).

Acute myocardial infarction (AMI) occurs as a result of insufficient myocardial perfusion leading to cell necrosis. This is most commonly due to the obstruction of the coronary artery by ruptured atherosclerotic plaques and thrombosis. Damaged ischemic and necrotic myocardial cells release pro-inflammatory substances in tissue and plasma, leading to a systemic inflammatory response. A profound systemic inflammatory response during ischemia/reperfusion injury disrupts the endothelial glycocalyx and detachment of endothelial cells that express von Willebrant factor (vWF). Circulating vWF+ can act as antigen-presenting cells that interact directly with T and NK cells and indirectly by cytokine and chemokine, promoting an inflammatory response (Rakic et al. 2018). The identification and analysis of pro-inflammatory factors produced in circulating vWF+ cells in patients with AMI could be crucial to determine, in the early period of AMI, the severity of the pro-inflammatory event according to the level of endothelial dysfunction detected (Rakic et al. 2018).

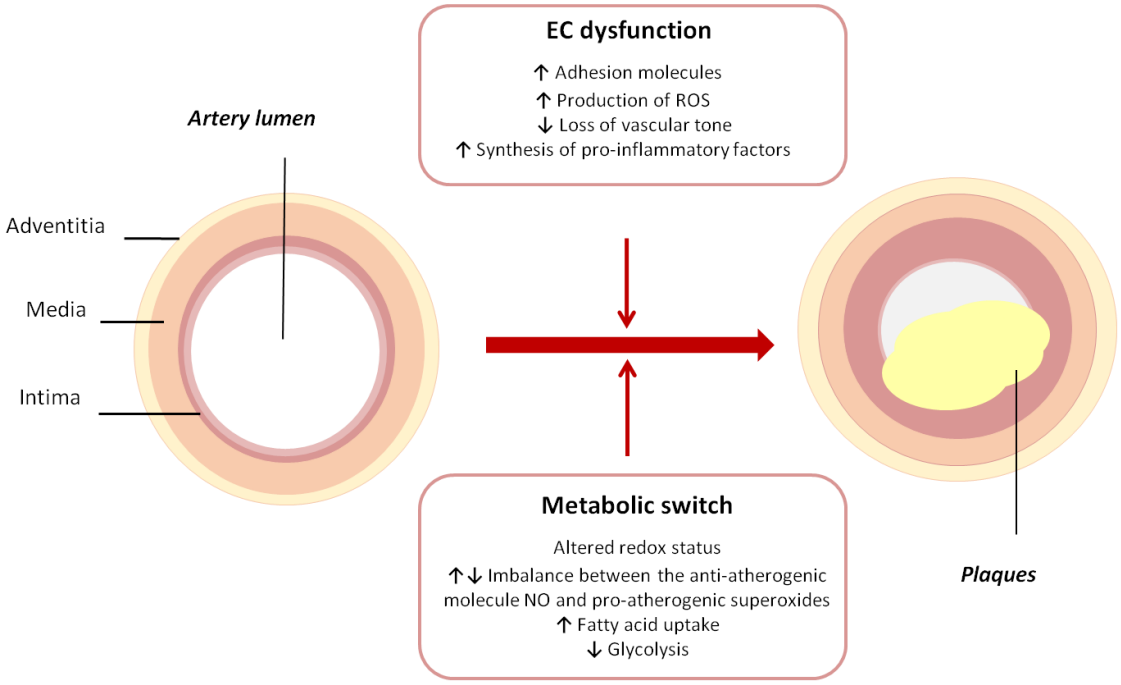

Figure1.1: Graphical representation of vascular changes occurring in atherosclerosis
Narrowing of the artery lumen is caused by intimal proliferation and by plaque formation and is a result of disease-specific EC dysfunction and cellular metabolic switches. EC, endothelial cell; NO, nitric oxide, ROS, reactive oxygen species. Figure adapted from Smolders VF., Zodda E. *et al*. Metabolic alterations in cardiopulmonary vascular dysfunction. Front. Mol. Biosci. 5, 120 (2019).

1.3.1 Current therapies in atherosclerosis and AMI

The four major risk factors for developing atherosclerosis are hypercholesterolemia, diabetes, hypertension, and cigarette smoking (Bergheanu, Bodde, and Jukema 2017) Recent studies have shown that adequate control of blood lipoprotein levels reduces the risk of atherosclerosis events. As such, a modification in the daily diet, an increase in physical activity, and cessation of smoking constitute the cornerstones of any intervention aimed at the prevention and/or treatment of atherosclerosis. While the role of the other parameters is still not clear, TG (triglycerides), LDL-C (low-density lipoprotein cholesterol), and HDL-C (high-density lipoprotein cholesterol) remain very strong predictors of premature atherosclerosis (Catapano et al. 2016). Hypercholesterolemia alters vascular permeability, allowing the leaking of LDL cholesterol and deposition on the arterial walls. There, LDL is subject to modifications that include oxidation, enzymatic processing, and aggregation, that render the lipoprotein particles proinflammatory and induce an immune response. As part of this

response, monocytes are recruited to the sub-endothelial space where they differentiate into macrophages. Macrophages may also derive from pluripotent cells associated with blood vessels. Regardless of their origin, macrophages in atherosclerotic lesions actively participate in lipoprotein ingestion and accumulation giving rise to foam cells filled with cholesterol-rich lipid droplets. These processes lead to vascular modifications visible as fatty streaks, intimal thickening, and ruptured plaques, causing acute coronary disease (Bergheanu, Bodde, and Jukema 2017). Vulnerable plaques contain monocytes, macrophages and T cells, which account for their instability.

The critical role played by LDL-C in atherosclerosis has prompted the development of rational strategies to counter the pathogenic effects of hypercholesterolemia. The use of statins (inhibitors of HMG-CoA reductase, the rate-controlling enzyme of the mevalonate and cholesterol synthesis pathways) as a pharmacological approach to lower cholesterol levels is one of the most widely used therapies in the treatment of atherosclerosis and acute coronary syndromes, as these drugs show consistent clinical event reductions with a very good safety profile (Adams, Sekhon, and Wright 2014). Other clinical studies reveal that the use of ezetimibe (an inhibitor of intestinal cholesterol absorption) considerably reduces LDL-C blood levels when combined with statins (Catapano et al. 2016). An alternative approach is the administration of fibrates, a particular class of agonists of the peroxisome proliferator-activated receptor α (PPAR-α) a regulator of lipoprotein metabolism, showing a good effect in lowering TG levels as mono-therapy, even though the results are not as promising as for the statins (Adams, Sekhon, and Wright 2014). When the combination of a healthier diet, lifestyle and pharmacological treatments fail to improve the pathological and clinical conditions in atherosclerotic patients with associated coronary disease, surgical intervention is considered the best option. Coronary artery thrombosis with complete occlusion typically leads to ST-segment elevation myocardial infarction (STEMI). Partial occlusion, or occlusion in the presence of collateral circulation, results in non-STEMI or unstable angina, an acute coronary syndrome without ST-segment elevation. Once a definitive or likely diagnosis of an acute coronary syndrome without ST-segment elevation has been made, the patient is triaged to either an invasive strategy or an ischemia-guided

strategy. An invasive strategy leads to improved outcomes and is favored for the majority of patients (Anderson and Morrow 2017).

In patients presenting with an unstable condition or with STEMI, urgent percutaneous coronary intervention (PCI) is performed. An ischemia-guided strategy is chosen for patients at low risk of recurrent ischemia, especially for women. Although PCI is currently the intervention of choice for most of these patients, individual coronary anatomy and clinical features may dictate the use of a different approach, such as coronary artery bypass grafting (CABG), a surgery that reinstates cardiac blood flow (Parsa et al. 2011a). In some cases, current guidelines also recommend antiplatelet therapy combined with non-vitamin K antagonist oral anticoagulant (NOACs) therapy (Husted et al. 2014).

Indeed, the rates of major complications of acute myocardial infarction have declined dramatically with early reperfusion (PCI) associated with antiplatelet therapy (French et al. 2010). Nevertheless, complications are still a leading cause of death and deserve careful consideration. Several new therapeutic approaches, such as reducing inflammation, mitigating reperfusion injury, or inducing myocardial regeneration, are under active investigation, although, except for angiotensin converting enzyme (ACE) inhibition, have so far not proved beneficial in the acute care setting.

Acute myocardial infarction continues to have a major impact on global health, and its management remains a crucial challenge for scientific advancement in medicine (Bhatt et al. 2013).

1.4 Endothelial cellular energy metabolism in EC

The endothelium is a dynamic organ consisting of a single layer of endothelial cells (ECs) lining the entire vascular system. Independently of their anatomic location (artery, arteriole, capillary, venule, vein), all endothelial share the common function of maintenance of vessel homeostasis (Sandoo et al. 2015). The control of vessel functions involves regulation of the blood flow, vascular tone, physical barrier, blood coagulation and the inflammatory response (Pober, Min, and Bradley 2009). A balanced production of various hormones, neurotransmitters, and vasoactive factors is crucial for maintaining

a homeostatic vessel function (Sandoo et al. 2015). An important vasoactive factor is eNOS-derived nitric oxide (NO) that promotes vasodilatation and inhibits important events that contribute to the development of vascular remodeling diseases, such as platelet aggregation, adhesion of leukocytes and oxidative stress (Förstermann and Sessa 2012). NO produced by the endothelium also plays an important role in mitochondrial respiration to maintain the oxygen gradient in oxygen limiting situations (Dromparis and Michelakis 2013)

When the NO precursor arginine and the eNOS cofactor tetrahydrobiopterin (BH_4) are not available, eNOS fails to produce NO and may promote the formation of reactive oxygen species (ROS), causing endothelial dysfunction and leading to atherosclerosis (Förstermann and Sessa 2012)

The importance of maintaining physiological and homeostatic EC functions is underlined by the development of major diseases like cardiovascular disease, diabetes, and cancer (Goveia, Stapor, and Carmeliet 2014). The endothelium can be disrupted by EC damage or apoptosis, which leads to a re-endothelialization response and in some cases, to the selection of ECs with an altered phenotype (Nogueira-Ferreira, Ferreira, and Henriques-Coelho 2014; Pober, Min, and Bradley 2009). Environmental stresses, such as oxidative stress and metabolic disturbances, are important sources of endothelial dysfunction, injury, and death (Pober, Min, and Bradley 2009).

1.4.1 Glycolysis in EC

When exposed to hypoxic conditions, mitochondrial alterations, or growth factors, ECs can rapidly shift from a quiescent cellular mode to an angiogenic state accompanied by changes in their cell metabolism. Under basal conditions, ECs rely mostly (> 80%) on glycolysis for generating their cellular energy and thus leaving the circulating oxygen available for underlying oxygen-requiring tissues (De Bock et al. 2013; Dromparis and Michelakis 2013; Goveia, Stapor, and Carmeliet 2014). In pathological conditions with sustained suppressed oxidative phosphorylation (OXPHOS), glycolytic flux is increased regardless of the oxygen supply as long as glucose is available (Warburg effect)

promoting the development of highly proliferative vascular disorders (Dromparis and Michelakis 2013; Parra-Bonilla et al. 2010). This predominant reliance on glycolysis over the use of more efficient mitochondrial oxidation is supported by the presence of fewer mitochondria when compared to cell types relying on mitochondrial respiration. The aerobic glycolytic flux quickly converts pyruvate to lactate, followed by an increase in glucose uptake (Parra-Bonilla et al. 2010).

The glycolytic enzyme phosphofructokinase-2/fructose-2,6-biphosphatase 3 (**PFKFB3**) is important for maintaining glycolysis, and it has been shown that PFKFB3 inactivation reduces EC proliferation (De Bock et al. 2013). PFKFB3 catalyzes the synthesis of fructose-2,6-biphosphate (Fru-2,6-P_2), an allosteric activator of phosphofructokinase 1 (PFK-1) and a potent stimulator of glycolysis. Partial reduction of the glycolytic flux by PFKFB3 inhibition was shown to be sufficient to impair EC proliferation without induction of cell death as caused by 2DG (2-deoxy-D-glucose) (De Bock et al. 2013; Schoors et al. 2014). PFKFB3 also displays an important role in the presence of stress stimuli like hypoxia, endothelial dysfunction, and cancer (Figure 1.2). Recent studies have shown that PFKFB3 plays a significant role in physiological as well as pathological glycolysis of ECs, with a major impact on endothelial migration and proliferation (Virmani et al. 2005). Thus, knockdown of PFKFB3 in ECs causes defects in the formation of filopodia and lamellipodia, suggesting that the inhibition of this enzyme could suppress features of pathological angiogenesis, such as that characterizing cardiovascular disease, cancer, or retinal angiogenesis (Van der Donckt et al. 2015). Another important glycolytic enzyme is the mitochondrial “gate-keeper” enzyme pyruvate dehydrogenase (PDH) that acts as a promoter of the entry of pyruvate in mitochondria (Cottrill and Chan 2013). PDH can be phosphorylated and inhibited through the activity of pyruvate dehydrogenase kinases (PDKs), resulting in a reduced mitochondrial contribution to energy production and concomitant promotion of aerobic glycolysis (Ryan et al. 2015). PDKs are induced by HIF1α and PDHs are additionally inhibited by altered mitochondrial Ca^{2+} signaling (Dromparis and Michelakis 2013). Upon PDH inhibition, pyruvate, rather than entering the mitochondrial respiratory chain, is converted to lactate by the enzyme lactate dehydrogenase A (LDH-A), allowing the transformation of NADH to NAD^+, which is crucial for maintaining further glycolysis.

Lactate is released to the extracellular microenvironment via monocarboxylate transporter 4 (MCT4). It can also enter the cells through monocarboxylate transporter 1 (MCT1) and used to feed the TCA cycle under low oxygen conditions, promoting the so-called “reverse Warburg effect”, a process that illustrates the symbiotic relationship between lactate-producing and lactate-consuming normal and pathological cells (Semenza 2008), an important adaptive mechanism to continuously changing micro-environmental conditions (N. Draoui and Feron 2011; Semenza 2008).

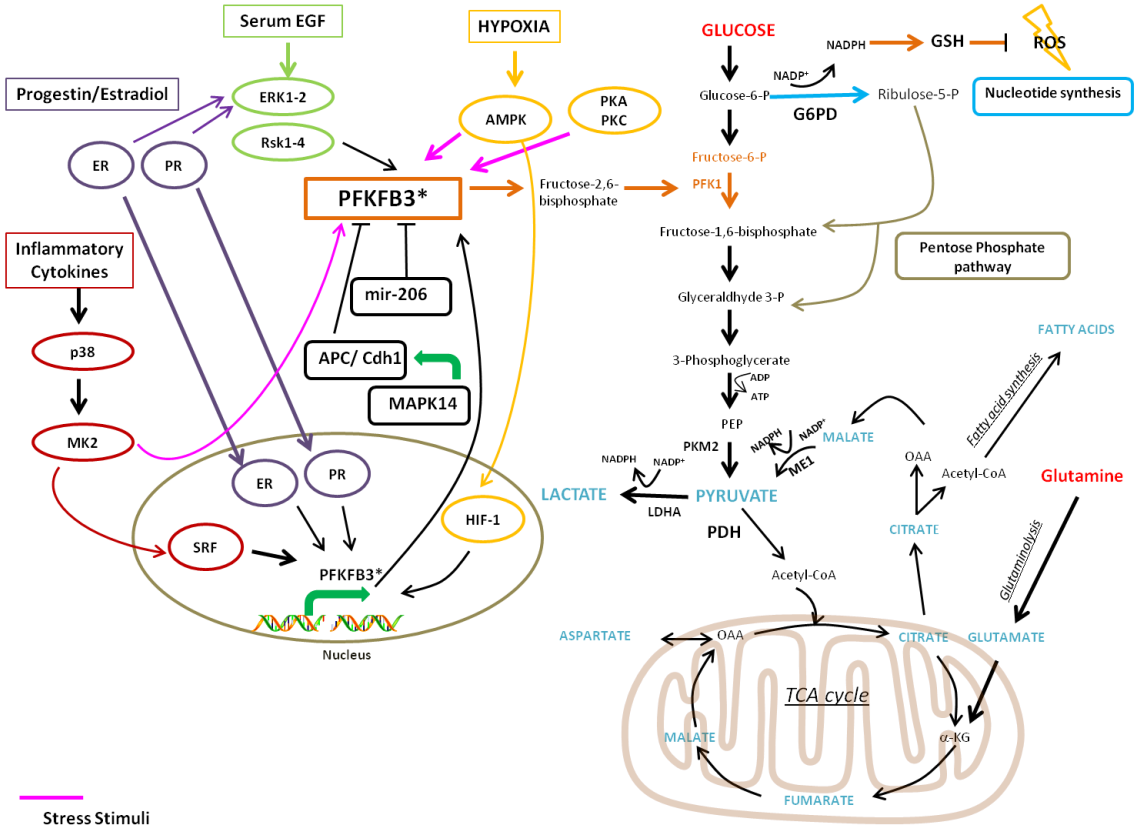

Figure 1.2: Signaling and metabolic pathways involving PFKFB3

Role PFKFB3 in physiological glycolysis, in normal endothelial cells, and in pathological glycolysis, in the presence of hypoxia and other stress stimuli. AMPK, 5'-AMP-activated protein kinase, APC anaphase-promoting complex, Cdh1, E-cadherin, ER estradiol, ERK1, serine/threonine kinase, MK2, mitogen-activated protein kinase-activated protein kinase-2, MAPK1, MAP kinase 14, OAA oxaloacetate, PDH, Pyruvate dehydrogenase, PFK1 Phosphofructokinase-1, PFKFB3 6-phosphofructo-2-kinase/fructose-2,6-biphosphatase 3, PKA protein kinase A, PKC protein kinase A, PKM2, pyruvate kinase muscle isozyme, PR, progesterone, RISK 1-4 ribosomal-S6-kinases, SRF subretinal fluid, VEGF, vascular endothelial growth factor, p38, mitogen-activated protein kinases.

Moreover, the increase in lactate production generates extracellular acidification of the microenvironment, which promotes the activity of certain metalloproteases that disrupt

the extracellular matrix, which also leads to an infiltration of the vascular wall with inflammatory cells and other cell types (Bonuccelli et al. 2010). The altered metabolic profile of mitochondrial suppression along with increased glycolytic rates causing a dysfunctional vasculature is similar to that of other rapidly proliferating healthy and malignant cell types, in which a shift occurs from mitochondrial respiration to lactate-producing aerobic glycolysis in order to sustain their rapid growth and to block apoptosis (De Bock et al. 2013; Heiden, Cantley, and Thompson 2009; Parra-Bonilla et al. 2010)

Glycolysis is also connected to the pentose phosphate pathway (PPP), a metabolic pathway that generates NADPH and ribose-5-phosphate, essential for the biosynthesis of lipids and nucleotides, respectively. NADPH moieties provide the reducing equivalents necessary for the synthesis of fatty acids and for the scavenging of ROS to promote cell survival (Patra and Hay 2014).

1.4.1.1 Role of PFKFB3 in endothelium metabolism and pathological angiogenesis

Angiogenesis, as discussed in section 1, is the growth of new blood vessels and when dysregulated, leads to the development of various malignant, ischaemic, inflammatory and immune diseases (De Bock et al. 2013; Schoors et al. 2014). ECs are critical in this process, and PFKFB3 driven glycolytic activity is very high reaching up to 85% of ATP from glycolysis, which is much higher than any other healthy cells, and it is similar to that of tumor cells. Recent studies showed that PFKFB3 plays a significant role in physiological as well as pathological ECs glycolysis, and the fundamental principles for the role of PFKFB3 derive from the effect of this enzyme on endothelial migration and proliferation (Virmani et al. 2005). PFKFB3 knockdown ECs exhibit defects in the formation of filopodia and lamellipodia, meaning that the inhibition of this enzyme can lead to a clear suppression of pathological angiogenesis. In addition to cardiovascular disease and cancer, also other diseases such as retina angiogenesis (Li, Kumar, and Carmeliet 2019a) are associated with pathological angiogenesis. Based on the reported implications of PFKFB3 in glycolysis and consequently, in pathological angiogenesis, this enzyme is considered an important starting point to understand the regulation of

glycolytic pathway in presence of an endothelial dysfunction and a key regulator in neovessels formation and atherogenic process in pathological condition (Van der Donckt et al. 2015; Li, Kumar, and Carmeliet 2019a)

1.4.2 Mitochondrial respiration in EC

Mitochondria are considered the quintessential cellular engine since its primary function is energy production in the form of adenosine triphosphate (ATP). ATP is essential to sustain cellular bioenergetic demands; glucose being the principal carbon substrate needed to generate ATP. OXPHOS is the mitochondrial metabolic pathway that enables cells to synthesize ATP from the oxidation of nutrients. For each glucose molecule that enters the glycolytic pathway, two pyruvate molecules are produced with a net energy of 2 ATP molecules. Subsequent pyruvate uptake into mitochondria results in 36 ATP molecules with minimal production of lactate under physiological conditions (Heiden, Cantley, and Thompson 2009; Parra-Bonilla et al. 2010). This process is oxygen-dependent, and, considering its high efficiency, it is the predominant source of energy in mammalian cells (Parra-Bonilla et al. 2010). Individual cell growth is controlled by environmental nutrient availability; therefore, cells only take up nutrients for cell division when stimulated by growth factors to avoid abnormal proliferation. In addition to ATP, active cell division requires nucleotides, amino acids, and lipids. To maintain cell growth and concomitant increase in biomass, part of the glucose must be redirected to the generation of critical macromolecular precursors such as acetyl-CoA, glycolytic intermediates, and ribose for the biosynthesis of, respectively, fatty acids, nonessential amino acids and nucleotides (Heiden, Cantley, and Thompson 2009). To promote this flow of carbon substrates towards biomass accumulation, rapidly growing cells are endowed with mechanisms that favor glycolysis over mitochondrial oxidation, as described above.

Although the major function of mitochondria is ATP production, these organelles are also important regulators of cell survival, ion homeostasis (H^+, Ca^{2+}), and cellular redox status (Collins et al. 2012). Tight regulation of the mitochondrial ion status is of great importance in tissues with limited oxygen consumption, like the vasculature and the

lung, which facilitate the diffusion of oxygen to more oxygen-requiring tissues. Disturbances in mitochondrial ion status have direct and indirect consequences on cell function, growth, and survival (Dromparis and Michelakis 2013). Altered mitochondrial morphology and function prompted by factors such as NO status have been associated with vascular endothelial dysfunction, and to diverse pathological conditions, including cardiovascular disorders, muscular degeneration and cancer (Collins et al. 2012; Dromparis and Michelakis 2013) Mitochondrial metabolism contributes actively to the production of reactive oxygen species (ROS). Mitochondria regulate redox signaling to and from mitochondria and initiate cellular apoptosis (Rizzuto et al. 2012). Oxidative stress is considered a major contributor to the destruction of well-balanced homeostatic mechanisms, causing cell injury either through direct oxidation of cellular proteins, lipids, and DNA or via cell death signaling pathways (Leopold and Loscalzo 2005; Sinha, Iyer, and Granata 2014). The sensitivity of cells to glycolytic and OXPHOS inhibitors (such as 2DG, and Oligomycin, respectively) can be used to help unveil the cell dependency on a specific energy-generating pathway (Suganuma et al. 2010). Such studies have shown that, in spite of the importance of the glycolytic pathway, especially under hypoxic conditions, the majority of cells use a combination of OXPHOS and glycolysis as a strategy for energy production, pointing out the importance of metabolic plasticity for cell survival under shifting environments and the complexity of metabolic adaptations in disease (Moreno-Sánchez et al. 2007).

1.4.3 ROS-Oxidative stress in EC

During OXPHOS, electrons from nicotinamide adenine dinucleotide, reduced form (NADH) and flavin adenine dinucleotide, reduced form ($FADH_2$) (electron donors) are transferred to electron acceptors, such as oxygen. These redox reactions are carried out by protein complexes located in the mitochondrial inner membrane and release energy, which is used to form ATP (Vega-Naredo et al. 2014). Small amounts of these electrons form mitochondria-derived reactive oxygen species (mROS), such as superoxide (O_2^-). ROS are oxygen-containing chemically reactive species that play important signaling roles to sustain fundamental cellular functions under various physiological conditions

(Förstermann 2008). High levels of oxygen and increased mitochondrial activity leads to excessive ROS production overcoming the buffer capacity of usable antioxidant systems, resulting in oxidative stress that can cause increased cell death and endothelial dysfunction (Dromparis and Michelakis 2013; Leopold and Loscalzo 2005; Li, Horke, and Förstermann 2014a). Mitochondria-based manganese superoxide dismutase (MnSOD, or SOD2) has an immediately anti-oxidative effect through the conversion of superoxide to the more stable and diffusible H_2O_2. After leaving mitochondria, physiological levels of hydrogen peroxide (H_2O_2) function as an important signaling system, acting on several redox-sensitive targets in the cytoplasm (HIF1α) and the cell membrane (K+ channels) and also with some proliferation-related enzymes (Dromparis and Michelakis 2013). Several other enzyme systems can produce ROS in the vascular wall, notably NADPH oxidase, xanthine oxidase, and eNOS, a dysfunctional endothelial NO synthase in which oxygen reduction is uncoupled from NO synthesis (Brandes and Kreuzer 2005; Förstermann 2008; Li, Horke, and Förstermann 2014a). These oxidases are multisubunit enzyme complexes that produce superoxide from molecular oxygen and NADPH as an electron donor (Drummond et al. 2011). Imbalances in the cellular oxidative status play significant roles in the pathophysiology of vascular diseases (Santos et al. 2011). Some cells might resort to a metabolic switch to glycolysis as a mechanism to reduce the production of ROS and thus to protect themselves from mitochondrial-mediated apoptosis (Ryan et al. 2015).

1.5 The importance of the endothelium in disease

1.5.1 Endothelial dysfunction in acute myocardial infarction

Acute myocardial infarction (AMI) is the development of myocardial necrosis caused by an unstable ischemic state. It remains one of the leading causes of death in both men and women worldwide, even if it men seem to have an increased risk of sudden death after ischemia (**Figure 1.3**) (Harvey and Chan 2017; Kovacic et al. 2019).

In response to acute coronary ischemia, women are more protected from apoptosis and present less adverse cardiac remodeling than men in the setting of the acute coronary syndrome (ACS) (Harvey and Chan 2017). Moreover, women develop acute coronary

syndrome at an older age than men, and earlier studies suggested that women's naturally occurring hormone levels might protect against heart disease before menopause when hormone levels drop (Dunlay et al. 2012).

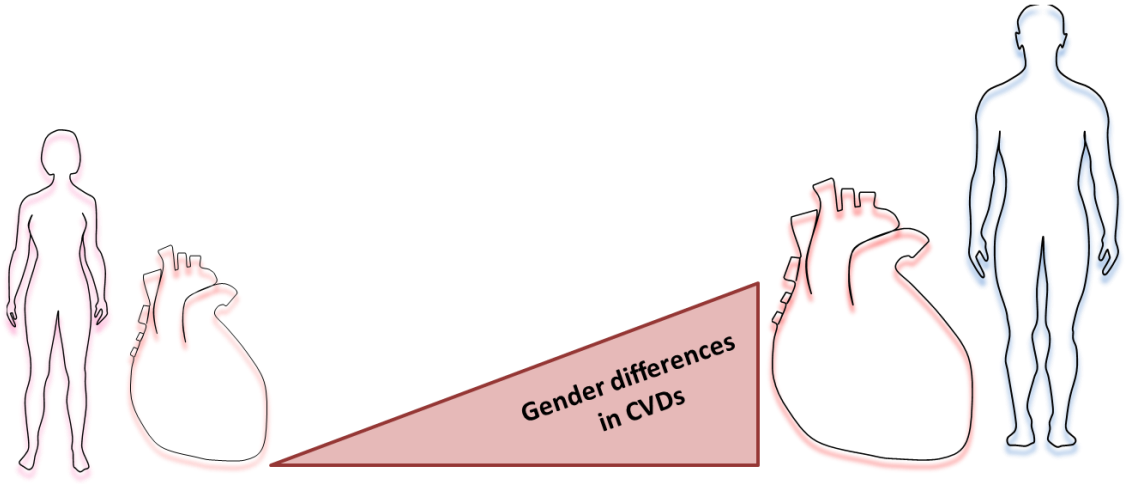

Figure 1.3: Men are about twice as likely as women to have a heart attack, mainly due to the gender's difference in hormone levels.

AMI is diagnosed and assessed based on clinical evaluation, electrocardiogram (ECG), biochemical testing, invasive and noninvasive imaging, and pathological evaluation. The usual triggering event of acute myocardial infarction is the rupture or erosion of a vulnerable, lipid-laden, atherosclerotic coronary plaque. This event results in the exposure of circulating blood to highly thrombogenic core and matrix materials in the plaque (Badimon, Padró, and Vilahur 2012a). In response to various stimuli, the normal endothelium endures phenotypic changes and variations, collectively known as endothelial dysfunction, characterized by a loss of the majority of the homeostatic mechanisms present in normal healthy endothelial cells. Usually, this dysfunction is associated with the upregulation of adhesion molecules, enhanced production of ROS, synthesis of pro-inflammatory factors and loss of vascular tone (**Figure 1.1**) (Sitia et al. 2010a). Recent studies suggest that this dysfunction contributes to the progression of the atherosclerotic plaque (Zardi and Afeltra 2010).

The pioneering role played by endothelial dysfunction in vascular pathology is supported by observations that individuals without any clinical sign of atherosclerosis but with high cardiovascular risk already present an endothelial dysfunction indicated by a diminished response to some vasodilators, such as acetylcholine (Zardi and Afeltra 2010). These findings suggest that endothelial dysfunction may precede and constitute a link between different vascular diseases and represents a good predictor of future cardiovascular events, including atherosclerotic diseases and AMI (Sitia et al. 2010a). Endothelial dysfunction is considered a systemic vascular process that not only leads to plaque formation but also determines the clinical course of atherosclerosis progression and associated coronary syndromes. Because several metabolic pathway abnormalities, such as the deregulation of the nitric oxide production and the excessive generation of ROS, are associated with atherosclerosis, the identification of key metabolic mechanisms underlying such alterations should provide fresh opportunities for the development of new strategies for the treatment of endothelial cell dysfunction in atherosclerosis and related vascular pathologies (Bierhansl et al. 2017).

1.5.1.1 Metabolic alterations and requirements in Acute Myocardial Infarction

Metabolically, atherosclerosis is characterized by the presence of an uncoupled and reduced eNOS, causing an imbalance between the production of NO, an anti-atherogenic molecule, and superoxide, a pro-atherogenic factor, thereby losing the atheroprotective function of eNOS (Eelen et al. 2015) (Eelen et al., 2015). As such, two general processes are largely responsible for the angiogenic growth observed in early atherogenesis: inflammation and oxidative stress. These metabolic alterations also affect, to a variable degree, vascular remodeling, and coagulation homeostasis (Nogueira-Ferreira, Ferreira, and Henriques-Coelho 2014). Beyond eNOS, a critical role in atherogenesis is also played by NADPH oxidase (NOX) enzymes, a large family of enzymes that are pivotal in the generation of ROS in the vasculature. NOX-4 is universally expressed in vascular smooth muscle cells (VSMCs), the primary components of the vascular wall and crucial determinants of vascular homeostasis and disease (Lu et

al. 2013). Its expression and activation during the angiogenic process promote a chain of events leading to vascular inflammation, cellular dysfunction, and atherosclerosis.

Additional metabolic mechanisms may contribute to the generation of a pro-inflammatory environment leading to atherogenesis. For example, the high glycolytic mode encountered in endothelial dysfunction implies a relative reduction in available ATP as compared to cells with OXPHOS-predominant metabolism. This results in diminished intracellular adenosine levels, which drive hydrolysis of S-adenosylhomocysteine (SAH) to adenosine and L-homocysteine (Hcy). Reduced SAH levels foster histone H3 lysine 4 hypomethylation and overexpression of a pro-inflammatory gene repertoire (Yiming Xu et al. 2017). A recent study (Ward-Caviness et al. 2017) identified three metabolic biomarkers, arginine, and two lysophosphatidylcholines (LPC 17:0 and LPC 18:2) associated with incident myocardial infarction (MI). This study also focuses on the association between these metabolites and the high-sensitivity C reactive protein (hsCRP), which is a measure for inflammation (Kaptoge et al. 2012). The three biomarkers correlated with each other and with hsCRP levels, suggesting that inflammation can represent a pathway through which these biomarkers are associated with MI (Cheng et al. 2012). As a consequence of these processes, increased rates of apoptosis are evident in more advanced atherosclerotic plaques, morphologically expressed as cellular contraction, condensation of chromatin and disruption of the cellular membrane. All cells existing in the atherosclerotic plaque, including lymphocytes, endothelial cells, smooth muscle cells, and macrophages, can undergo cellular apoptosis (Schrijvers et al. 2005).

1.5.1.2 AMI predictive biomarkers

Current conventional biomarkers predictive of CVD and AMI are essentially limited to the determination of blood high-density lipoprotein (HDL) cholesterol levels: low blood HDL cholesterol levels are associated to a very high cardiovascular risk, while high blood HDL cholesterol levels seem to be linked to cardiovascular protection(Rohatgi et al. 2014). It has been described that the key role of HDL is to promote the efflux of

cholesterol and to invert its transport from the periphery to the liver, which seems to correlate to a low incidence of cardiovascular events (Hoefer et al. 2015).

Several studies have approached the limitations of current vascular biomarkers, like hsCRPs (high sensitive C reactive proteins), through the discovery and validation of novel biomarkers with predictive value for CVD (Hoefer et al. 2015) and incident MI using emerging omics technologies, including metabolomics approaches (Shah et al. 2010b).

Metabolomic studies using general population-based cohorts have recently been performed using LC-MS/MS-based lipidomics and NMR-based approaches to identify species associated with incident CVD with a potential link to systemic inflammation and, in particular, pro-inflammatory lipid metabolites have generated great interest in the cardiovascular disease frame (Hoefer et al. 2015). Molecular lipid profiling by mass spectrometry and nuclear magnetic resonance spectroscopy, as well as proteomic identification and quantification of small metabolites, can improve individual cardiovascular risk prediction (Stegemann et al. 2014). The identification of potential metabolic targets for novel therapeutic approaches for acute myocardial infarction is, therefore, an interesting approach that should be investigated in earnest in the near future.

Other approaches are being explored in the quest for improved predictive biomarkers of CVD morbidity and mortality. For example, the detection of plasma-derived markers which include microparticles (MPs), microvesicles, and exosomes in human plasma, has spurred increasing interest in their potential as biomarkers. In particular, levels of MPs expressing CD31 or CD144 seem inversely correlated to endothelium-associated vasodilation, highlighting that MP levels might be good indicators of vascular lesions and acute endothelial dysfunction (Lacroix et al. 2010). Moreover, the complex composition of these microparticles which comprise proteins, lipids, and nucleic acids, represent an interesting material for omics-based analysis (Kanhai et al. 2013). Finally, recent studies have unveiled that micro-RNAs (miRNAs) not only present relevant intracellular functions, but also show potential value as cardiovascular disease biomarkers. miRNAs also circulate within microvesicles and may contribute to predict heart failure, early

atherosclerosis, and plaque vulnerability by targeting vascular and cardiac cells (Matsumoto et al. 2013).

1.5.1.3 Targeting endothelial cell metabolism as a treatment option in AMI

There is increasing evidence that endothelial dysfunction in cardiovascular disorders is associated with disease-specific metabolic alterations affecting ECs. Such metabolic reprogramming can function as a defense mechanism against disease-associated external insults, such as changes in glucose or oxygen availability, while, on the other hand, it can contribute to the generation of toxic end-products, anomalous accumulation of metabolic intermediates and alterations in energetic and redox metabolism that compromise physiological endothelial functions. The ability of ECs to readily switch between glycolysis and OXPHOS, as well as a highly plastic funneling of carbon and redox reactions through PPP and fatty acid oxidation (FAO) makes it a challenge to understand and target the altered EC metabolism in disease (Bujak et al. 2016; Lewis 2014).

Nevertheless, significant advances have fueled optimism for targeting endothelial cell metabolism to restore normal endothelial function. Thus, it has been shown that although a strong inhibition of PFKFB3 can result in vessel disintegration, moderate inhibition can block pathological angiogenesis and normalize EC dysfunction (Conradi et al. 2017). This suggests that restoration of physiological, metabolic networks in ECs may be subjected to strict inhibitor dosage within narrow therapeutic margins, which, in turn, requires a prior detailed quantitative knowledge of relevant enzymatic activities. This can be approached through the application of metabolic network modeling methods that employ data generated by metabolic flux analyses and transcriptomic profiling (Nilsson and Nielsen 2016; Ryu, Kim, and Lee 2015; Yilmaz and Walhout 2017; C. Zhang and Hua 2016).

In the present study, we have approached the identification of metabolic targets to improve endothelial dysfunction in CVDs through the study of metabolic functions as well as transcriptomics analysis of patient-derived endothelial cells.

1.6 CVDs and cancer

Although cardiology and oncology are considered separate medical fields, they are often interlaced (Mehta et al. 2018). Previous cardiovascular pathologies can affect the selection of cancer treatment and, at the same time cancer therapies can generate cardiovascular toxicities that could affect cancer treatment itself (Coviello 2018; Mehta et al. 2018; Mosca et al. 2013). Lots of the intersection between endothelial dysfunction and cancer, especially breast cancer (Mehta et al. 2018), refers to similarities in risk factors such as age, smoking, diet, obesity, and a sedentary lifestyle. CVDs risk factors increase in long-term cancer survivors (Coviello 2018) and, in female patients that have suffered breast cancer, are even higher than the risk of tumor recurrence. Besides, with advances in cancer therapy, some patients may develop cardiac side effects of cancer treatment, which include chemotherapy, radiation therapy, and targeted therapy (Mehta et al. 2018). For all these reasons, both pathologies have to be taken in careful consideration to choose the appropriate treatment for each patient with a particular medical history.

A deep study of new possible links between these two pathologies has been investigated in this thesis.

1.7 Cancer: a brief overview

Cancer is one of the most prevalent multifactorial diseases and one of the major causes of death worldwide. It is characterized by the malignant transformation of cells that acquire abnormal modification leading to tumor development and progression, and which may reach other tissues, through metastasis.

The origin of cancer is multifactorial and influenced by exogenous (tobacco, infectious organisms, chemicals, and radiation) and endogenous (inherited mutations, immune conditions, and metabolic alterations) factors (S. Wu et al. 2018). Moreover, the development and progression of cancer is a complex process that involves the acquisition of functional abnormalities like hyperproliferation, linked to an unbalanced homeostasis between cell growth and cell death, activation of oncogene and/or

inactivation of tumor suppressor which shunt to uncontrolled cell cycle and alteration of apoptotic process (Hanahan and Weinberg 2011).

As a consequence of this abnormal condition, cancer cells adapt their metabolism to reach the demand of energy and macromolecules; consequently, metabolic reprogramming is considered one of the hallmarks of cancer (Hanahan and Weinberg 2011). Moreover, alterations in oncogenes and tumor suppressor genes constrain the dependence of tumors on metabolic substrates, like glucose and glutamine (M. H. Kim and Kim 2013).

During the multistep progress of cancer, tumor cells adapt to suppress the defense mechanisms of the immune system (Gonzalez, Hagerling, and Werb 2018), and even if it is still unclear how tumor cells are able to escape the immune system recognition, some studies propose a direct interference with the cells of the adaptive immune response through alteration of the tumor microenvironment (Kareva and Hahnfeldt 2013; Palucka and Coussens 2016).

1.8 Endothelial cells and tumor microenvironment

The tumor microenvironment (TME) comprises a heterogeneous group of cell types, which includes immune cells, endothelial cells, and fibroblasts, apart from cancer cells (Denton, Roberts, and Fearon 2018). It is becoming increasingly clear that the interaction with the TME is crucial for tumor progression, as these cells support some factors like oxygen tension and blood pressure(Folkman 1990) or supply pro-invasive and/or immunosuppressive factors that help tumors in their growth and metastasis ability (Albini and Sporn 2007; Denton, Roberts, and Fearon 2018).

Endothelial cells associated with tumors are one of the principal components of the stromal cell population and fundamental for tumor angiogenesis (Sherwood, Parris, and Folkman 1971). Tumor vasculature, in fact, is principally composed of endothelial cells that cooperate with other stromal cells like mesenchymal cells, macrophages, and pericytes also releasing some pro-angiogenic factors, which are controlled by the tumor itself (Hanahan and Coussens 2012).

As described above, angiogenesis has long been known to play a crucial role in supporting cancer cell growth and development (Muthukkaruppan, Kubai, and Auerbach 1982; Nishida 2016). Tumor cells promote an angiogenic switch by providing angiogenesis inducing factors, such as VEGF and fibroblast growth factor (FGF), and by reducing the activity of angiogenesis inhibitor pathways (Rajabi and Mousa 2017). During tumor progression, the angiogenic process provides a route for invasive tumor cells to spread directly, via the blood circulatory system, or indirectly, via the lymphatic system (Martin et al. 2005) and allow the formation of metastasis to distant sites.

1.8.1 Signaling and metabolic commonalities shared between dysfunctional endothelial cells and cancer cells

In recent years, endothelial cell metabolism has been studied to find alternative targets to reduce endothelial proliferation and angiogenesis (Verdegem et al. 2014). Exploring the signaling pathways involved in blood vessel formation has driven nowadays to the identification of some targets (e.g. VEGF) able to reduce tumor angiogenesis and induce cancer regression (Bergers and Hanahan 2008; Comunanza and Bussolino 2017).

Several metabolic pathways have been reported to show similarities between endothelial and cancer cells (Fitzgerald, Soro-Arnaiz, and De Bock 2018a) (Figure 1.4). Cancer cells are known to be glycolytic, displaying Warburg effect and producing high lactate (Heiden, Cantley, and Thompson 2009), and they also show high expression of PFKFB3, inducing PFKFB3-driven glycolysis for proliferation (Ros and Schulze 2013) As already described, also endothelial cells are described to be glycolytic especially when activated for proliferation and migration; moreover VEGF stimulation has shown to increase the expression of glycolytic enzymes like LDH-A and PFKFB3, whose inhibition may cause a decrease in vessel sprouting and branching processes(De Bock et al. 2013; Schoors et al. 2014). In a highly glycolytic tumor environment, cancer cells use glucose producing a huge amount of exogenous lactate to be used by the stromal cells. Endothelial cells show higher expression of MCT1, which allows lactate entrance into the cells, or also reduced expression of MCT4, which reduces the exit of the lactate from the cells by tumor endothelial cells (Park et al. 2018).

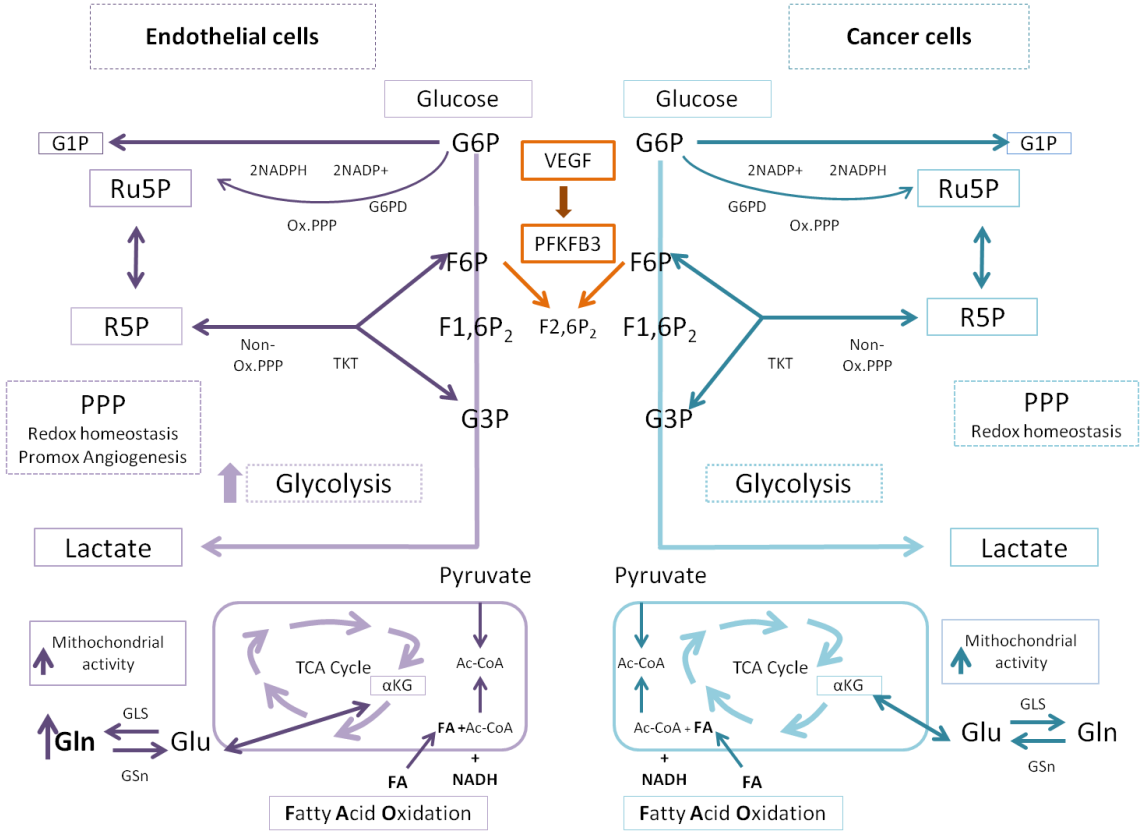

Figure 1.4: **Commonalities between metabolic pathways in CVDs (endothelial) and Cancer**
αKG – α-ketoglutarate, Ac-CoA – acetyl-CoA, F1,6P2 - fructose 1,6 bisphosphate, F2,6P2 - fructose 2,6 bisphosphate, F6P - fructose 6-phosphate, FA - fatty acid, FAO – fatty acid oxidation, G1P – glucose-1-phosphate, G3P – glyceraldehydes-3-phosphate, G6P – glucose-6-phosphate, G6PD -glucose-6-phosphate dehydrogenase, , GLS - glutaminase, NADH –nicotinamide adenine dinucleotide (reduced), NADP+/NADPH – nicotinamide adenine dinucleotide phosphate (oxidised/reduced), Non-Ox. PPP – a non-oxidative branch of PPP, Ox. PPP – oxidative branch of PPP, PFKFB3 - 6-phosphofructo-2-kinase/fructose-2,6-bisphosphatase-3, PPP - pentose phosphate pathway, R5P - ribose 5-phosphate, Ru5P - ribulose 5-phosphate, TCA - tricarboxylic acid.

Moreover, it has been observed in some tumors a pro-angiogenic effect of lactate, which induces angiogenesis through the endothelial MCT1 or MCT4, two classic lactate transporters (Van Beijnum et al. 2006). On the other hand, mitochondrial activity is upregulated in endothelial cells during mechanical stress like shear stress and compromised glycolysis and helps in endothelial apoptosis during vessel regression while low level of mitochondrial ROS induces angiogenesis (Cucullo et al. 2011; Mina et al. 2017). Regarding cancer cells, mitochondrial respiration is, in general, less active

even if it is found to change depending on the type of tumor and other linked pathological conditions (Aguilar et al. 2016). Glycogen degradation is also important for both endothelial and cancer cells, especially during hypoxia and low glucose conditions (Ormazabal et al. 2018). Oxidative PPP branch is important in both cell types for redox control during stressful conditions, and in endothelial cells, PPP is also used to promote angiogenesis (Riganti and Massaia 2013; Vizán et al. 2009). Fatty acid metabolism is important for endothelial cells for nucleotide synthesis, for cell proliferation and redox homeostasis (Hensley, Wasti, and DeBerardinis 2013), while in cancer cells, fatty acid oxidation helps for redox homeostasis and ATP generation for cancer survival under stressful conditions (Carracedo, Cantley, and Pandolfi 2013). The conversion of glutamine to glutamate is necessary for both endothelial and cancer cell survival and proliferation. Otherwise, the inhibition of this process induces senescence, especially in endothelial cells (Hensley, Wasti, and DeBerardinis 2013; Huang et al. 2017; Unterluggauer et al. 2008).

Briefly, lots of studies nowadays show that many metabolic pathways and cellular signaling pathways are common between endothelial cells and cancer cells, and have significant relevance in angiogenic functions and cancer cell survival, even if many of them are still uncharacterized. One of the main purposes of this study is to investigate these unexplored areas and characterize the most relevant pathways to depict a putative therapeutic strategy able to improve both these pathologies.

1.9 Invasion and metastasis

Metastasis is the process by which cancer cells spread to reach other tissues and is considered the leading cause of death by cancer.

Cancer cells are primed for metastatic behavior through many different possible strategies (Bogenrieder and Herlyn 2003). Once such processes are engaged, tumor cells invade and break the membrane and extracellular matrix to reach the bloodstream or the lymphatic circulation. Before tumor cells break the basement membrane to initiate invasion, they release angiogenic factors to stimulate endothelial cells in order to establish a vascular network (Hanahan and Coussens 2012; Hanahan and Weinberg

2011). Tumor-associated neoangiogenesis serves both to support tumor blood and oxygen supply and also to enable the escape of cancer cells from local environments, often potentiated by relative hypoxia owed to the abnormal tumor-associated vasculature.

The dissociation of cells from the primary tumor is enabled by the downregulation of cell adhesion molecules (CAMs) that mediate cell-cell contacts (Cavallaro and Christofori 2004) concomitant with the acquisition of a more motile phenotype (Bissell and Hines 2011), a process collectively known as epithelial-mesenchymal transition (EMT).

EMT is a major driver of intra-tumor heterogeneity which induces alterations in the cancer cell gene regulatory and metabolic networks (metabolic reprogramming) (Marín de Mas et al. 2018; Thomson, Balcells, and Cascante 2019).

EMT is a reversible physiological phenotypic shift in which epithelial cells break down cell-cell and cell-extracellular matrix connections and then migrate to other locations in the body (Radisky and LaBarge 2008). EMT is essential for the proper formation of the body plan and differentiation of many tissues and organs during embryonic development. During organ development, epithelia convert between epithelia and mesenchyme through multiple rounds of EMT and the reversible process mesenchymal-epithelial transition (MET). In adult tissue, the EMT program is reactivated during wound healing, organ fibrosis, and tumor progression. EMTs are classified into three main categories based upon involvement in different biological processes.

Epithelial cells exhibit an organized apical-basal polarity maintained by the arrangement of actin filaments and adhesive structures such as desmosomes, tight, and adherens junctions (Jordan et al. 2001; Müller and Bossinger 2003). Specific adhesive molecules, such as cadherins, integrins, and other cell-surface proteins, are essential for the maintenance of the epithelial phenotype by stabilizing cell-cell contacts. On the other hand, mesenchymal cells are characterized by a unique morphology defined by a front-back-end polarity and higher invasive potential (Zavadil et al. 2008).

Interestingly, the transient phenotypic changes associated with the acquisition of a mesenchymal state during EMT are often associated with the simultaneous acquisition of stem-like characteristics. Moreover, the molecular and phenotypic changes inherent

to EMT are also accompanied by a profound metabolic reprogramming through which cells shift carbon-source usage and predominant energy generation pathways (Thomson, Balcells, and Cascante 2019).

1.10 Epithelial-mesenchymal transition in cancer

Most human solid tumors are carcinomas that originate from epithelial cell types throughout the body. Cells from carcinoma break the basal membrane and start to invade other tissues losing cell-cell and cell-non-cellular adhesions and acquiring a motile phenotype (Thiery 2003).

In general, tumor cells achieve these changes by losing many features of their epithelial phenotype and acquiring the morphology and gene expression pattern of mesenchymal cells, with enhanced migratory and invasive capabilities (Thiery 2003). The activation of an EMT program is mainly encouraged by genetic and epigenetic changes and signals released by the reactive stroma that enable tumor cells to enter in an EMT state.

As mentioned above, EMT is characterized by the mutual loss of epithelial cell junction proteins, line E-cadherin, β-catenin and claudins, and increased expression of mesenchymal markers, such as N-cadherin, vimentin, and fibronectin (Chaw et al. 2012; Scanlon et al. 2013; Trimboli et al. 2008). The most frequent consequence of EMT in many invasive tumors is the functional defeat of E-cadherin and/or repression of the gene encoding this protein, commonly followed by a sort of switch of expression, by which the E-cadherin is replaced by the expression of N-cadherin (Gravdal et al. 2007)

The induction of an EMT program is often provoked by growth factors (like EGF and TGFβ) which induce downstream activation of EMT-inducing transcription factors including SNAIL (Zinc finger family), TWIST (basic helix-loop-helix family), ZEB1 and ZEB2 (zinc finger E-box binding homeobox family) (Garg 2013; Stemmler et al. 2019) that directly repress E-cadherin transcription. Moreover, the EMT process is characterized by wide differences in the splicing of specific RNAs, responsible for the generation of diverse proteins isoforms in mesenchymal cells as compared to epithelial cells.

During EMT, many of the changes at a splicing level result from the rapid downregulation of the expression of the Epithelial Splicing Regulatory Proteins 1 (ESRP1) and 2 (ESRP2), that promote splicing of the epithelial variant of some transcripts, resulting in mesenchymal protein isoforms that help to explain alterations in adhesion, motility and signaling pathways (Warzecha et al. 2009). The role of these protein ESRPs has been widely studied in this thesis as a crucial character in the EMT process in cancer and will be carefully described in this thesis.

Although EMT represents an important process necessary for tumor progression and metastatic spread of cancer cells, there is evidence suggesting that many invasive and metastatic tumors do not complete the transition to a mesenchymal phenotype remaining in an intermediate stage (Thiery 2003). This suggests that after their initial dissemination, the tumor cells that have acquired a mesenchymal phenotype need in some moment to reverse to an epithelial stage via a mesenchymal-epithelial transition (MET) to get back the ability to proliferate in distant organ sites. This agrees with the observations that E-cadherin is often detected in distant metastases, which may derive from cells that have previously undergone an EMT (Bukholm, Nesland, and Borresen-Dale 2000). Finally, although malignant cells may circulate from primary tumors mainly as individual mesenchymal-like cells, multicellular clusters are also found. This process, known as collective migration, is characterized by clusters of epithelial cells that detach from the site of the primary tumor and migrate as independent aggregates through the adjacent extracellular matrix.

Cells may exhibit dynamic behaviors, permitting reversion to an epithelial phenotype or maintaining a mesenchymal phenotype.

Lastly, lots of key factors involved in EMT and stem cell differentiation are regulated post-transcriptionally through RNA splicing mechanisms, and in particular through an alternative splicing system. This link between EMT and RNA splicing will be further discussed in the following section.

1.10.1 EMT and alternative splicing: Epithelial Splicing Regulatory Proteins

In addition to transcription factors that drive EMT, the expression of specific microRNAs, as well as the differential expression of alternative isoforms of a number of proteins, helps to establish and maintain the epithelial or mesenchymal states of cells. Members of the RBFOX, MBNL, CELF, hnRNP, or ESRP (Epithelial Splicing Regulatory Proteins) classes of splicing factors regulate alternative splicing events associated with EMT (Warzecha et al. 2009). Among these factors, ESRP1 and ESRP2 are the most studied as epithelial-specific RNA binding proteins that promote splicing of the epithelial variant of transcripts like FGFR2, ENAH, CD44 and CTNND1 (Jeong et al. 2017; Warzecha et al. 2009).

The ESRP regulated events include all known types of alternative splicing events and most of these regulated splicing events occur in transcripts that encode proteins with crucial roles in cytoskeleton organization, cell-cell adhesion and cell migration (Warzecha et al. 2009). Induction of an epithelial-to-mesenchymal transition (EMT) in a mammary epithelial cell line resulted in the downregulation of both ESRP1 and ESRP2 (Trimboli et al. 2008; Warzecha et al. 2009). It has been shown that these two splice factors are under transcriptional regulation by the EMT factor Snai1

Not only are ESRP1 and ESRP2 modulated during EMT, but they can directly participate in the phenotypic switch between mesenchymal and epithelial states. As such, it has been shown that ectopic expression of ESRP1 in a mesenchymal cell line induces and epithelial splicing pattern and an epithelial phenotype (Gökmen-Polar et al. 2019; Warzecha et al. 2009). These observations point to ESRP1 and ESRP2 as global regulators of an epithelial splicing regulatory network in different cellular models.

1.11 RNA splicing and alternative splicing: a brief overview

RNA splicing is a specific type of RNA processing through which a precursor messenger RNA transcript (pre-mRNA) is transformed into a mature messenger RNA (mRNA). During splicing, introns, segments of DNA located between two exons of a gene and that are defined as non-coding regions are removed, while the exons, that are those parts of

a gene that encode the final mature RNA, and for this called coding regions, are tied together (Black 2003; Sammeth, Foissac, and Guigó 2008). Splicing is usually required to generate an mRNA molecule to be translated into a functional protein. Normally, in mammalians, splicing is carried out by a series of reactions catalyzed by the spliceosome, a complex of small nuclear ribonucleoproteins (snRNPs), and this event is called Spliceosome Splicing (Sammeth, Foissac, and Guigó 2008). Sometimes it also occurs that some introns are able to form a ribozyme complex, a sort of spliceosome constituted by a complex of mRNA molecules, which enable the introns its-self to catalyze biochemical reactions (Black 2003).

There are several types of RNA splicing in nature and they principally differ in the structure of the spliced intron and the catalysts required for splicing to occur, among which the Alternative Splicing (AS) process has been disclosed as particularly relevant for this study.

AS is a biological process that occurs in eukaryotic cells, which results in a single gene coding for multiple proteins, increasing in this way the biodiversity of proteins that can be encoded by the genome. During this process, particular exons of a gene are included in the final messenger RNA (mRNA) produced from a single gene (Havens, Duelli, and Hastings 2013; Warzecha et al. 2009). It has already been described, analyzing mRNAs sequenced from different human tissues, that more than 90% of the human transcripts experience alternative splicing, indicating in this way that the regulation of splicing plays key roles in gene expression (Pan et al. 2008; Wang et al. 2008).

AS is regulated by RNA-binding proteins that link cis-regulatory elements that surround donor and acceptor splicing sites resulting in better or alternative use of the regulated splicing site. There are five different types of alternative splicing that have been found and studied in eukaryotes (Sammeth, Foissac, and Guigó 2008). The first and most common one (type I) is known as *exon skipping*, (or *cassette exon*), and it occurs when an exon is spliced out of, or retained in, the primary transcript. *Mutually exclusive exons* (type II) occur when splicing results in only one of two exons being retained in mRNAs. Other types of alternative splicing involve directly the donor (5' splice junction) or the acceptor (3' splice junction) sites, respectively, when an alternative 5' splice junction is used, changing the 3' boundary of the upstream exon (*alternative donor site*, type III) or,

vice-versa, when is 3' splice junction is used, changing the 5' boundary of the downstream exon (*alternative acceptor site*, type IV). Quite different from the other types of alternative splicing, the *intron retention* type occurs when a sequence is spliced out as an intron, or it is retained (Sammeth, Foissac, and Guigó 2008; Wong et al. 2016) (Figure 1.5).

In this case, the retained sequence is not flanked by introns, and if the retained intron is in a coding region it is forced to encode in-frame with the near exons, generating in this way a shift or a stop codon in the reading frame, thus producing a non-functional protein. The intro retention type is less common in mammalians, and it can provoke abnormalities and diseases, including cancer (Kim, Goren, and Ast 2008; El Marabti and Younis 2018).

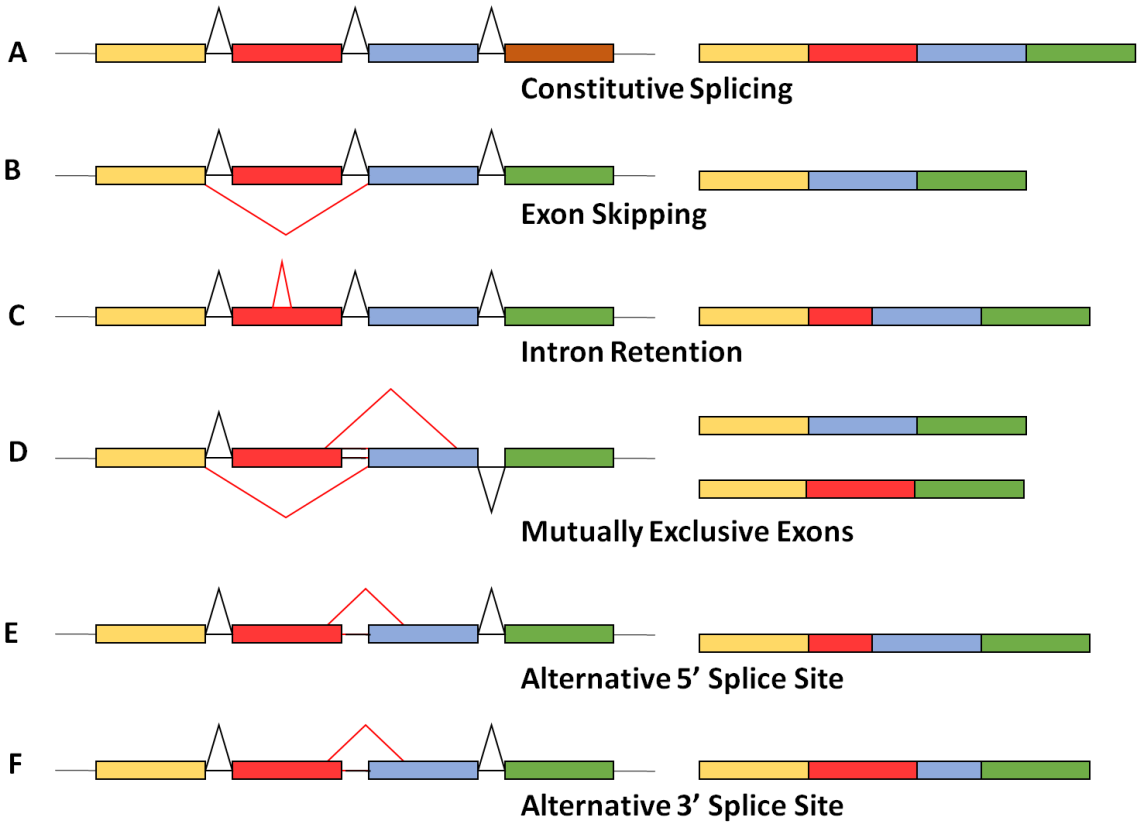

Figure 1.5: **Schematic illustration of alternative splicing events**
(**A**) constitutive splicing (**B**) exon skipping; (**C**) intron retention; (**D**) mutually exclusive exons; (**E**) alternative 5' splice site; (**F**) alternative 3' splice site.

It is still unclear if the aberrant splicing patterns play a driver or passenger role in a tumor's development and progression (El Marabti and Younis 2018). Eddo et al. have described that cancer cells exhibit aberrant transcript variants not found in normal cells, even if a clear reduction of alternative splicing events in cancer cells have been identified compared to normal cells. A possible explanation could be found in the higher incidence of *intron retention* and a lower frequency of *exon skipping* mechanisms in cancer cells relative to healthy ones (Wang, and Zhou 2013; Kim, Goren, and Ast 2008).

1.11.1 Splicing response to DNA damage

DNA damage affects splicing factors by altering the expression and activity (Shkreta and Chabot 2015). Moreover, DNA damage often disturbs splicing processes by interfering with its coupling to, having a strong impact on the splicing and alternative splicing of genes closely associated with machinery. In particular, DNA damages modulate the alternative splicing of the DNA repair gene, BRCA1 (Breast Cancer 1) (Rosen 2013; Wu, Lu, and Yu 2010).

1.11.1.1 BRCA1 /RAP80 in DNA damage

BRCA1 relocates to DNA damage sites and forms nuclear foci following DNA double-strand breaks (DSBs) (Scully et al. 1997), but despite of this, lots details about the signaling cascade that causes BRCA1's translocation remains largely unknown (Hu et al. 2011b; Wu, Lu, and Yu 2010; J. Zhang and Powell 2005). BRCA1 is first implicated in DNA damage repair also because it colocalizes with RAD51 (Figure1.6), an essential protein in homologous recombination repair (HR), one of the two repair pathways, together with non-homologous end-joining (NHEJ), for the most deleterious damage on the chromatin, the Double-strands breaks (DSBs) (Bernstein et al. 2002; Scully et al. 1997; J. Wu, Lu, and Yu 2010).

When DNA damage occurs, chromatin-associated histone γH2AX, which locates close to DNA break sites, is phosphorylated by ATM (ataxia telangiectasia mutated) and ATR

(ataxia telangiectasia mutated) (Weber and Ryan 2015). Subsequently, MDC1, a phospho-module binding mediator, and RNF8, an E3 ubiquitin ligase, are recruited to the DNA damage sites. BRCA1 colocalizes with them and with other DNA damage response (DDR) proteins, some of which interact with BRCA1 to execute key steps in the HR (Homologous recombination) process (Huen et al. 2007; Kolas et al. 2007; Wu, Lu, and Yu 2010). RNF8 cooperates with Ubc13, an E3 ubiquitin conjugase, to ubiquitinate histone H2A and H2B at chromatin lesions, which is in charge of the translocation of BRCA1 to the sites of genome breakage (Wu et al. 2009; Zhao et al. 2007).

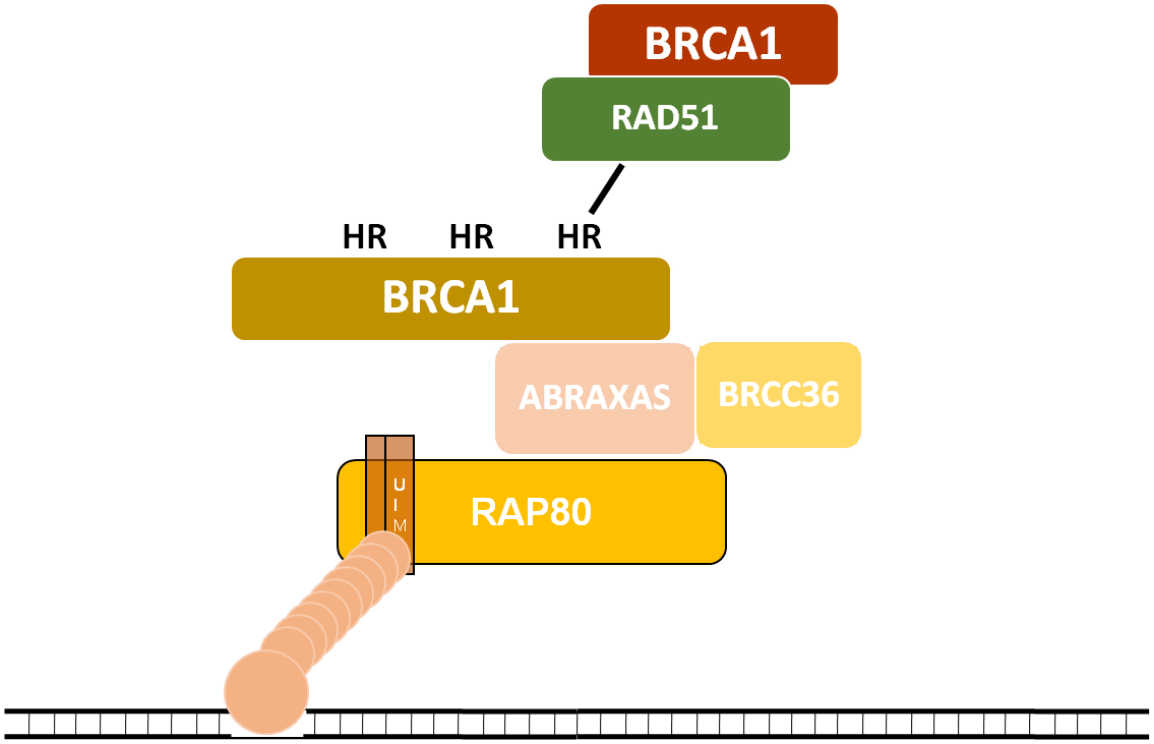

Figure 1.6: **Graphical representation of the main subunits of the RAP80 complex**
RAP80/BRCA1 complex is required to suppress double-strand breaks (DSB) and end processing. The main components of RAP80 complex. Abraxas, BRCC36, and BRCA1, with the homologous recombination(HR)-supporting BRCA1 complexes, RAD 51, RAP80 (UIMC1).

A number of studies have identified that RAP80/UIMC1, an ubiquitin-binding nuclear protein, favors the recruitment of BRCA1 to IRIF (ionizing radiation-induced foci) by binding to specific polyubiquitin structures at the site of double strands breaks (DBS) (Figure 1.6) (Hu et al. 2011b; Sobhian et al. 2007; Yan et al. 2007; Zhao et al. 2007). During DNA damage, RAP80 (Receptor Associated Protein 80) recognizes ubiquitinated histones at the site of DNA damage via its ubiquitin-interacting motif

(UIM) and recruits the big complex, including BRCA1 to DNA damage sites (Feng et al. 2009; Wu, Lu, and Yu 2010).

BRCA1 forms heterodimers with BARD1 (BRCA1 Associated RING Domain 1) and interact with RAP80 creating complexes that contain additional subunits, including Abraxas/CCDC98 complex, responsible of the junction between BRCA1 and RAP80 (Wu, Lu, and Yu 2010). It has also been reported that RAP80 depletion leads to a defective G2/M checkpoint and to increased cellular sensitivity to IR, which remarks on the importance of RAP80 in this DNA repair system (Hu et al. 2011a). As this multisubunit complex is involved in providing a proper response to DSB, the BRCA1/ RAP80 implication in this system have been widely described in this thesis.

1.11.1.2 RAP80 implication in DSB repair

In response to DNA double-strand breaks, BRCA1 forms complexes with other DNA-response proteins, among them RAP80, as discussed in the previous section (Wu, Lu, and Yu 2010). These complexes, located in nuclear focal points that mark sites of breakage of the genome, participate in homologous recombination (HR) repair process. The presence of RAP80 in this complex is crucial for BRCA1 to be recruited to the focus of damage to assure the maintenance of the genome's integrity. RAP80 promotes the recruitment of the BRCA1-Abraxas-BRCC36 complex to IRIF. Specifically, RAP80 contains a ubiquitin interaction domain (UIM) able to interact with ubiquitin strings linked to lysine 63 (K63) of the histones (H2A, H2B) located close to the DSBs; this domain is responsible for the translocation of the BRCA1-Abraxas-BRCC36 complex to the damage sites (Hu et al. 2011a; Yin et al. 2012).

It is further demonstrated that the RAP80/BRCA1 complex is required to suppress excessive DSB end processing, which is one of the principal causes of genetic abnormalities. Apart from the direct implication in DNA repair, the BRCA1/RAP80 complex has been studied for its involvement in several dysfunctions and diseases, and in particular in cancer.

1.11.1.2.1 BRCA1/RAP80 complex in diseases

BRCA1 has been extensively described as a suppressor of tumors in particular breast cancer, and when its activity has inhibited the risk of development and progression of breast and ovarian cancer increases (Hu et al. 2011a).

Breast cancer is the most common type of cancer in women and the second leading cause of cancer-related deaths, next to lung cancer (Bray et al. 2018; Wang et al. 2018) therefore, developing new therapeutic and preventive means in order to control this disease is a matter of vital importance. Breast cancer is the result of an imbalance in the complex regulatory agents to which the breast tissue is exposed, like hormones, epidermal growth factors and other agents that influence the normal growth and function (Wang et al. 2018), which make this disease a quite complex and heterogeneous syndrome.

Nowadays our understanding of this breast cancer has significantly improved at a molecular level thanks to basic measures, such as histological type, tumor grade, lymph node status and especially for the identification of predictive markers like estrogen receptor (ER) and human epidermal growth factor receptor 2 (HER2) which help in fast prediction at the initial stages of the tumor (Holliday and Speirs 2011; Yersal and Barutca 2014).

It has been reported that BRCA1 alterations and BRCA1-related mutations are good markers for the early detection of breast cancer progression (De Silva, Tennekoon, and Karunanayake 2019). As previously described, RAP80 is a subunit of the BRCA1 complex and targets BRCA1 to DNA damage sites in response to DBS break, an event that often occurs in cancerous cells (Wu, Lu, and Yu 2010).

In particular, a work published by Chunjing Bian et al., describes that in the absence of RAP80 the DNA damage-induced foci formation of the BRCA1 complex significantly decreases, and even the BRCA1-A complex itself seems to become less effective, suggesting that RAP80 is the scaffold subunit in the BRCA1 complex.

BRCA1 mutations are also associated with other types of cancer and pathologies (Bian et al. 2012).

Prostate cancer (PC) is the most commonly diagnosed non-cutaneous malignancy among western men and accounts for the second leading cause of cancer-related death

in the male gender. In the majority of cases, prostate cancer becomes independent of androgens, rescuing growth after androgen-deprivation therapies in a more aggressive form (Bray et al. 2018).

Although lots of common causes have been proposed as principal factors for a more predisposition to develop PC, the only well-established risk factors are age, ethnic background (African men have a higher risk), and a family history of the disease. (Castro and Eeles 2012; Crawford 2003). Interestingly, there is a recognized association between breast and prostate cancer, especially among relatives, and these observations base on common genes expressed in both pathologies and also on environmental factors that increase the risk to contract these diseases (Ghoussaini, Pharoah, and Easton 2013). The contribution of BRCA1 as a common factor of these disorders has also been broadly investigated; in fact, families with BRCA1 mutations show a tendency to develop prostate cancer in men compared with families without this genome alteration. BRCA1 relates to an enhanced risk of developing breast and ovarian cancer in women, but also of male prostate cancer in men of less than 65 years old (Castro and Eeles 2012). The implication of RAP80, as part of the BRCA1-A complex, to regulate DSB resection in breast and prostate cancer cells has been further investigated in this study.

2. OBJECTIVES

2.1 OBJECTIVES

The endothelium is the main participant in the pathophysiology of lots of diseases, like atherosclerosis and hypertension, and these anomalies are in turn, the major responsible for cardiovascular diseases. Nowadays, there is a great interest in finding an interconnection between cardiovascular diseases and other co-morbidities such as cancer. There are a lot of common risk factors like obesity, diabetes, hypertension, and tobacco smoking, and shared biological mechanisms, like oxidative stress, inflammation, and disrupted blood hemostasis, which can explain this tight relationship.

Accordingly, the main objective of this thesis is to explore the metabolic pathways behind a specific cardiovascular disease, the Acute Myocardial infarction, and how the ensuing endothelial dysfunction associated to this disease results not only in the alteration of the vascular homeostasis and integrity and in the development of a chronic inflammation, but also leads to genomic alteration, DNA damages and activation of alternative splicing mechanisms which promote the development of other pathological condition, among all an increased cancer risk. Not only metabolic but also signaling pathways have been investigated to shed light on the link between endothelial dysfunction and other pathologies.

Hence, to achieve this major aim, the specific objectives of the thesis are:

1. Development of an *in vitro* model of thrombus extracted-cells from patients of Acute Myocardial Infarction through a systematic evaluation in terms of morphology, antigen expression, proliferation, and angiogenic potential, focusing on the study of the central metabolism and of all the metabolic adaptations as a consequence of the endothelial dysfunction.

2. Identification of DNA damage as a result of endothelial anomalies occurring in patients, and investigation of alternative splicing mechanism as a common pathway among different pathologies.

3. MATERIALS AND METHODS

3.1 Cell culture

3.1.1 Endothelial cell culture and sample preparation

Human coronary artery endothelial cells (HCAECs) have been acquired from Lonza Clonetics (Walkersville, USA) and used as controls. Eight patients were isolated from coronary atherothrombotic specimens in patients undergoing percutaneous coronary intervention with thrombectomy for the treatment of acute ST-segment elevation myocardial infarction (STEMI) at the Royal Infirmary of Edinburgh, Scotland, UK.

Table 3.1: Clinical characteristics of patients providing coronary endothelial outgrowth following thrombectomy for ST-segment elevation myocardial infarction. Values are number (%) or mean ± standard deviation. ACE = angiotensin-converting enzyme; CABG = coronary artery bypass grafting; PCI = percutaneous coronary intervention.

	n=8
Age, years	60 ± 15
Gender, male	5 (66%)
Medical history and risk factors	
Previous myocardial infarction	1 (12%)
Previous PCI/CABG	1 (12 %)
Current smoker	3 (37%)
Ex-smoker	2 (25%)
Hypertension	1 (12%)
Hyperlipidaemia	4 (50%)
Family history of premature coronary heart disease	1 (12%)
Diabetes mellitus	0
Medication on admission	
Aspirin	2 (25%)
Clopidogrel	1 (12%)
B-Blockers	1 (12%)
ACE-Inhibitors	1 (12%)
Statins	3 (38%)
Myocardial injury	
Troponin I concentration, micrograms/L	27.9 ± 20.0
Culprit vessel	
Left anterior descending artery, n=12	1
Circumflex artery, n=2	1
Right coronary artery, n=23	4

The study protocol was approved by the Research Ethics Committee, and all subjects provided written informed consent. Specimens were washed with phosphate-buffered saline (PBS) and manually disaggregated. Tissue explants were seeded into collagen-I coated 6-well plates and maintained under standard cell culture conditions. After 24 hours, tissue explants, non-adherent cells, and debris were aspirated. The medium was changed every other day until the first passage of coronary endothelial outgrowth cells emerged and cells were cultured following the recommended instruction (Brittan et al. 2015; Padfield et al. 2013; Tura et al. 2013).

Briefly, both HCAECs and patient-derived cells were grown on 0.2% gelatin-coated plates with EGM™-2 bulletkit™ medium, which contains the EBM™-2 basal medium along with the EGM™-2 singlequots™ kit components, 10% FBS and 1% penicillin-streptomycin antibiotic. All the cell cultures were maintained in a 37°C humidified incubator at 5% CO2.

3.1.2 Cancer cell culture and sample preparation

PC-3/Mc and **PC-3/S** were clonally derived from the human cell line PC-3, isolated from the bone metastasis of prostate adenocarcinoma. The PC-3/Mc clone was selected by limiting dilution from PC-3 cells isolated from liver metastases produced in nude mice after intrasplenic injection of PC-3 cells. PC-3/S cells were selected by limiting dilution from parental PC-3 cells. Both cell subpopulations were cultured at 37°C in a 5% CO2 atmosphere in RPMI 1640 media (Sigma-Aldrich or Biowest) with 10 mM glucose and 2 mM glutamine supplemented with 10% Fetal Bovine Serum (FBS) (PAA Laboratories), 1% pyruvate (1 mM) (Biological Industries), 1% streptomycin (100 μg/mL)/penicillin (100 units/mL) (Gibco) and 1% nonessential amino acids (Biological Industries) (Celià-Terrassa et al. 2012).

MCF7, **T-47D** and **MDAMB 231** mammary gland, breast derived from metastatic sites cells were purchased from ATCC. All these cell lines were cultured in DMEM (Gibco, Thermo Fisher Scientific Inc., Waltham, MA, USA) containing 10% Fetal Bovine Serum (Gibco), 10mM D-Glucose (Sigma-Aldrich), 1mM Sodium Pyruvate (Biological Industries),

2mM Glutamine (Gi1bco), 0.1% antibiotic (Penicillin 10 Units/ml-Streptomycin 10 Units/ml, Gibco), 0.01 mg/ml Insulin (Sigma), and 1% Non-essential amino acids (Biological Industries).

Different types of cell variants have been used in several experiments and obtained as follows. The EMT factor ESRP1, ESRP2 and the DDR factor RAP80 (UIMC1 gene) were retrovirally transduced and overexpressed in PC-3/S cells (PC-3/S ESRP1/ PC-3/S RAP80). In the case of the cell variants with Knockdown (indicated as"-KD cells"), PC-3/Mc, MCF7, T-47D, and MDAMB 231 cells were subjected to ESRP1 and/or RAP80 knockdown by lentiviral transduction of shRNAs specific for these genes. Detailed experimental protocol and plasmid sequences are described in **Appendix 1**.

3.2 Cell proliferation and viability assay

To evaluate cell proliferation, cells were counted using a ScepterTM Handheld Automated Cell Counter (Merck Millipore, Billerica, MA, USA). Cells were seeded in 100-mm culture dishes, and the next day medium was replaced with fresh media (t = 0 h) and then proceed with cell counting every 24 h until 72 h. Proliferation and viability were also assessed by Hoechst staining (HO33342 probe, Sigma-Aldrich) (Aguilar et al. 2016). HO33342 (2'-[4-ethoxyphenyl)-5-[4-methyl-1-piperazinyl)-2,5'-bi-1H-benzimidazole trihydrochloride trihydrate) is a cell-permeable DNA stain that is excited by ultraviolet light and emits blue fluorescence at 460-490 nm. It binds preferentially to adenine-thymine (A-T) regions of DNA and it is used for specifically staining the nuclei of living or fixed cells. Cells were seeded in 96-well plates and media was replaced after 24 h with complete fresh media containing the drug under study or nutrient-deprived media. Finally, the media was removed, cells were washed with PBS, the supernatant was aspirated and 100 µL of 0.01% SDS was added to each well. Plates were then frozen at -20°C until analyzed. To analyze the samples, plates were thaw at 37°C and 100 µL of HO33342 stain solution was added to each well, in dark. HO33342 stain solution was prepared by diluting HO33342 stock solution (10 mg/mL in H2O) with Assay Buffer containing 1 M NaCl, 0.1 M EDTA, 1 M Tris, pH 7.4. Then plates were placed on a shaker

and incubated at 37°C for 1 h in the dark. Fluorescence was measured in a fluorescence plate reader (FluorStar) at 355 nm excitation and 460 nm emissions.

3.3 Cell cycle analysis

Cell cycle analysis was assessed by flow cytometry using a fluorescence-activated cell sorter (FACS). Cells were seeded in 6-well plates and after 24 h media was replaced with complete fresh media. Cells were collected 48 h later, fixed with 70% cold ethanol and stored in the ethanol fixative at -20°C. To prepare the samples for cell cycle analysis, cells were centrifuged, washed with PBS and resuspended in buffer consisted of PBS and 0.2 mg/mL RNAse A (REAL Laboratories) and incubated for 1 h at 37°C. Before analysis, 0.05 µg/mL PI was added (Aguilar et al. 2016). For cell cycle phase distribution analysis, the FlowJo®software (Tree Star, Inc.) was used, and the percentage of cells in G1, S and G2 phases was obtained.

3.4 Protein extraction

Confluent cells were trypsinized and collected by centrifugation at 1200 rpm for 5 min. Harvested cells were washed two times with cold PBS. The cell pellets were resuspended in the solubilization buffer (8 M urea in 50 mM Tris-HCl, 30 mM NaCl, pH: 8.5 and 1% protease inhibitor) and incubated on ice for 5-10 min. Cell lysates were further homogenized by sonication in an ice bath for three times each for 5sec with 30 sec intervals, using an ultra sonicator. Samples were centrifuged at 14000 rpm for 20 min at 4ºC. The protein supernatant was collected into the new eppendorf tube and pelleted cell debris was discarded.

Samples were stored at -80ºC until we use it for further experiments. The protein estimation and quantification was carried out by using the Lowry and bicinchoninic acid (BCA) Methods (Lowry et al. 1951; Smith et al. 1985).

3.5 Western blotting

Proteins obtained from control and pathological ECs were used to validate the expression pattern by western blot analysis, from either fresh cells or frozen plates using RIPA buffer (50 mM Tris pH 8.0, 150 mM NaCl, 0.1% SDS, 1% Triton X-100 and 0.5% sodium deoxycholate) supplemented with protease inhibitor cocktail (Sigma-Aldrich). The same procedure was followed to obtain cell protein extract were electrophoresed on 8% and 12% SDS-PAGE and transferred by a wet-transfer method. The membrane was blocked for 1h at room temperature using a blocking buffer (5% milk in PBS with 0.1% tween 20). Primary and secondary antibody dilutions and incubation times were maintained as per the manufacturer's instructions. Cell extracts were obtained Protein concentration from the supernatant was determined by the BCA assay (Smith et al. 1985). 30µg of protein were loaded and separated by 10% SDS-PAGE and proteins were transferred to a polyvinylidene fluoride (PVDF) membrane. Membranes were blocked by incubation with PBS-Tween (0.1% (v/v) containing 5% non-fat dried milk for 1-2 h at room temperature. Then, membranes were incubated with primary antibodies according to the conditions indicated below. In order to remove the excess of primary antibody, membranes were rinsed with PBS-Tween (0.1% (v/v) and incubated with the appropriate horseradish peroxidase-conjugated secondary antibody for 1 h at room temperature. Afterward, membranes were washed again with PBS-Tween (0.1% (v/v) before protein detection. Some blots were treated with the Immobilon ECL Western Blotting Detection Kit Reagent (Millipore) and developed after exposure to Fujifilm X-ray film in the darkroom with chemoluminescence system, other blots have been developed using the Odyssey infrared imaging system (Li-COR Biosciences) machine system after incubation with specific fluorescent dye-conjugated secondary antibodies for fluorescence system.

Expression of all target proteins was investigated against the β-actin or β -tubulin housekeeping proteins, as a loading control.

Table 3.2: Primary antibodies used for Western Blotting analysis

Protein	source	Brand	Dilution WB
CDH1	mouse	610181 BD Transduction laboratories	1/500
CD34			
CD105	mouse	MA5-17041 ThermoFisher Scientific	1/1000
CD44	mouse	sc-7297 SantaCruz	1/1000
FN1	rabbit	F3648 Sigma-Aldrich	1/2000
GAC	rabbit	19958-1-AP Proteintech	1/200
G6PD	rabbit	Ab993 Abcam	1/3000
HA-ESRP	mouse	3724S CellSignaling	1/1000
KGA	rabbit	20170-1-AP Proteintech	1/200
MCT1	rabbit	sc-50324 SantaCruz	1/1000
MCT4	mouse	sc-376140 SantaCruz	1/1000
PECAM1 (CD31)	mouse	PA5-24411 ThermoFisher Scientific	1/1000
PFKFB3	mouse	SAB1402305-100UG Sigma-Aldrich	1/500
PFKFB4	rabbit	Ab137785 Abcam	1/500
RAP80	rabbit	A300-763A BethylLaboratories	1/2000
VCAM1 (CD106)	mouse	MA5-15636 ThermoFisher Scientific	1/1000
ZEB-1	rabbit	GTX105278 Genetex	1/1000
β-ACTIN	mouse	69100 MP Biomedicals	1/100000
β-TUBULIN	mouse	T4026 Sigma-Aldrich	1/200

Table 3.3: Secondary antibodies used for Western Blotting analysis (first two antibodies have been used for chemoluminescence system, HRP-antibodies have been used for fluorescence method)

Secondary antibody	source	Brand	Dilution WB
anti-mouse	rabbit	PO260 Dako	1/10000
anti-rabbit	donkey	NA934V Amersham Biosciences	1/5000
anti-mouse HRP	goat	Pharmacia	1/2000
anti-rabbit- HRP	goat	Pharmacia	1/5000

3.6 RNA isolation and cDNA preparation

RNA isolation was performed from fresh or frozen pellets or cultured plates using Trizol® reagent (Invitrogen) following the manufacturer's instructions. Importantly, all pipette tips, tubes, and eppendorfs used along the isolation process were RNAse-free. Briefly, Trizol® was added to samples, and cell homogenates were mixed with chloroform and centrifuged, resulting in an upper aqueous phase, interphase, and a lower organic phase. RNA was precipitated from the aqueous phase by adding cold isopropanol and leaving the samples in the cold room overnight. Next, samples were centrifuged at 12000 xg for 15 min at 4°C and supernatant was removed and the pellet was washed three times with cold 75% ethanol. After ethanol evaporation at room temperature, RNA was resuspended in RNAse-free water for subsequent spectrophotometric quantification with a Nanodrop instrument (Thermo, Wilmington, DE).

3.7 Quantitative real-time PCR analysis

Quantitative RT-PCR analysis was performed for basal gene expression, and cDNA was amplified in triplicate and obtained from 1 μg of RNA using random hexamers (Roche) and M-MLV reverse transcriptase (Invitrogen) according to the manufacturer's indications. Gene expression analysis was performed by quantitative real-time RT-PCR (ABI Prism 7700 Sequence Detector System, Applied Biosystems), using either the

Universal Probe Library system (UPL; Roche) following the recommended protocol by the trading company.

In the case of the transcripts quantified with the UPL system (probes and sequences from Roche), RT-PCR assays were performed on a Light Cycler 480 instrument (Roche) The thermal cycling protocol includes different steps: 95°C for 10 minutes for enzyme activation, 40 cycles of amplification at 95°C for 15 seconds, followed by 60°C for 1 minute. RN18S1 was used as a housekeeping gene and its amplification levels as an internal standard to estimate the relative levels of specific transcripts.

Table 3.4: Primers and UPL probes used for RT-qPCR for gene expression analysis.

GENE	UPL probe	Primer forward	Primer reverse
RN18S1	#40	ggagagggagcctgagaaac	tcgggagtgggtaatttgc
CDH1	#35	cccgggacaacgtttattac	gctggctcaagtcaaagtcc
DSP	#49	gaatgtttggggtggatgag	ctgaggccaggtccacac
EpCam	#3	ccatgtgctggtgtgtgaa	tgtgttttagttcaatgatgatcca
ESRP1	#18	attcggatccatgacggcctctccggatac	gaatgtcgacttaggcgtagtcaggcacgtaaggataaaataccccattcttgggtag
ESRP2	#34	attcggatccatgactccgccgccgccgccg	aatgtcgacttaggcgtagtcaggcacgrcgtaaggacacacccattccttggggc
FN1	#43	gaactatgatgccgaccagaa	ggttgtgcagatttcctcgt
MYC	#34	caccagcagcgactctga	gatccagactctgacctttgc
SNAIL1	#11	gctgcaggactctaatccaga	atctccggaggtgggatg
SOX-2	#19	atgggttcggtggtcaagt	ggaggaagaggtaaccacagg
TWIST1	#35	aattctgttgaaactggaccaag	ggggaggggaaggaactc
UIMC-1	#41	ttcaactgtggaggggaagt	cttcactgtggcttttcc
ZEB-1	#3	gggaggagcagtgaaagaga	tttcttgcccttcctttctg

The results were analyzed with the Light Cycler 480 Software release 1.5.0. Relative expression of targeted genes was determined using the 2-ΔΔCT method for calculating the fold changes in gene expression. A p-value below 0.05 was considered as statistically significant (Livak and Schmittgen 2001).

3.8 Conventional PCR

PCR amplifications were set up in a final volume of 20 µl. The reaction mixture contained 5 µM each primer, 200 µM each dNTP, 5mM MgCl2, 0,5 ng/µl template DNA, DNA polymerase (5 U/µL), and filled up to the final volume with distilled water. The thermal cycling was done with the following protocol: 1 min at 95°C; followed by 34 cycles of 30 s denaturation at 95°C, 30 s annealing at 60°C, and 40 s extension at 72°C; and a final extension of 2 min at 72°C. All PCR reactions were performed on a T-Gradient Thermal device (Applied Biosystem thermal cycler). The PCR products were stained with 6xDNA loading buffer (0.25% bromophenol blue in water, 1:5 ratio buffer: DNA) and then separated on 1% agarose gel with 10% Sybr safe stain and visualized with a UV spectrophotometer, or in a 6% acrylamide gel and then incubated in TAE Buffer with 10% Sybr safe stain for 30 minutes, and visualized with using Electrophoresis image analysis system (Liuyi, Beijing, China).

3.9 Transcriptomic analysis

To identify differentially expressed genes in the AMI cells model, RNA-Sequencing (RNA-seq) analysis has been performed at the Genomic Platform of the CNIC institute in Madrid.

For the sample preparation, cells were grown to 70-80% confluence, lysed, and RNA isolated with the RNeasy Kit (Qiagen, Hilden, Germany), including a DNase digestion step and then sent to the CNAG Platform to be processed and analyzed.

RNA-seq is an efficient approach to identify gene expression, alternative isoforms regulation and differential splicing, among others (Mortazavi et al. 2008). It consists of poly(A) RNA sequenced by high throughput sequencing (HTS) technology, which is able to read several hundred million short (about 30 nucleotide long). These shorts are aligned to known mRNA sequences of genes, EST-based potential transcript variants, and all possible exon-exon combinations per gene. Predicted gene isoforms based on EST alignments and genomic sequence analyses are compiled in databases like the ASTD (Stamm 2006). Sequence reads over a splice junction of two exons allow determining which exons of a gene are spliced together and thus identify potential splice events (Sánchez-Cabo et al. 2011).

3.10 Measurement of media metabolites

Glucose, lactate, glutamate, and glutamine were determined by spectrophotometry (COBAS Mira Plus, Horiba ABX) from cell culture media by monitoring the production of NAD(P)H in specific reactions for each metabolite at 340 nm wavelength. Glucose concentration was measured using hexokinase (HK) and glucose-6-phosphate dehydrogenase (G6PDH) coupled with enzymatic reactions (commercial enzymatic kit). Lactate concentration was determined by lactate dehydrogenase (LDH) reaction, performed at 37°C by adding a media sample to a cuvette containing 1,55 mg/mL NAD^+ and 87,7 U/mL LDH in 0,2 M hydrazine, 12 mM EDTA buffer, pH 9. Glutamate concentration was determined by analyzing its conversion to α-ketoglutarate (α-KG) through glutamate dehydrogenase (GLDH) reaction in the presence of ADP. This reaction was prepared at 37°C by adding a media sample to a cuvette containing 2,41mM ADP, 3,9 mM NAD^+ and 39 U/mL GLDH in 0,5 M glycine, 0,5 M hydrazine, pH 9,0. Determination of Glutamine concentration was done by its conversion first to glutamate through glutaminase (GLS) reaction and then by the quantification of glutamate concentration obtained as a previous step. GLS reaction was performed for 30 min at 37°C and by adding a media sample to a cuvette containing a mixture of 125 mU/mL GLS in 125 mM acetate, pH 5,.0 (Aguilar et al. 2016). The metabolite consumption/production normalized rates resulted from the concentrations of the

measured metabolites and corrected according to cell proliferation under exponential growth conditions. All the values are expressed in micromol or nanomol of metabolite consumed or produced per hour and 10^6 cells (µmol/h·10^6 cells or nmol/h·10^6cells).

3.11 Analysis of polar intracellular metabolites (TCA cycle intermediates and amino acids)

Cells were grown to 70-80% confluence at the required condition for each cellular model and then media removed, and the plate washed with ice-cold PBS 1x. TCA cycle intermediates were extracted with addition of 100% methanol:H_2O (1:1) mixture and scrapping on ice; then, the extracts were sonicated using a titanium probe (VibraCell, Sonics & Materials Inc., 3 cycles of 5 seconds) and the chloroform was added to the lysates and tubes were placed in a shaker for vigorous agitation at 4°C for 30 min. After that, samples were centrifuged and the upper aqueous phase was separated and evaporated under airflow at room temperature, and then dichloromethane (CH_2Cl_2) was added to each tube to dehydrate completely the samples.

TCA cycle intermediates were derivatized by adding 2% (v/v) methoxyamine hidrochloride in pyriridine and shook vigorously at 37 °C for 90 min. Next, N-methyl-N-(tert-butyldimethylsilyl) trifluoroacetamide (MBTSTFA) + 1% tert-butyldimetheylchlorosilane (TBDMCS) was added and samples were incubated for 1 h at 55°C and finally transferred to GC/MS vials. GC/MS analysis was performed under an electron impact ionization model (Cascante and Marin 2008; Dettmer, Aronov, and Hammock 2007). The relative concentration of the polar intracellular metabolites is quantified using Norvaline (1mg/mL) as an internal standard.

3.12 Enzyme activities

Fresh cell culture plates were rinsed with phosphate-buffered saline (PBS) and scrapped with lysis buffer (20 mM Tris-HCl pH 7.5, 1 mM dithiothreitol, 1 mM EDTA, 0,2% Triton X-100, 0,02% sodium deoxycholate) supplemented with protease inhibitor cocktail

(Sigma-Aldrich). Cell lysates were disrupted by sonication using a titanium probe (VibraCell, Sonics & Materials Inc., 3 cycles of 5 seconds) and immediately centrifuged at 12000 xg for 20 min at 4°C. The supernatant was separated and used for the determination of specific enzyme activities determined by spectrophotometry (COBAS Mira Plus, Horiba ABX) by monitoring NAD(P)H production or disappearance at 340 nm wavelength. All enzymatic activities were normalized by protein content in the supernatant, determined by the BCA assay (Smith et al. 1985).

3.12.1 Glucose-6-phosphate dehydrogenase (G6PDH, EC 1.1.1.49)

G6PDH specific activity was measured by adding samples to a cuvette containing 0.5 mM $NADP^+$ in 50 mM Tris-HCl, pH 7.6, at 37°C. The reaction was initiated by the addition of glucose-6-phosphate at a final concentration of 2 mM (Aguilar et al. 2016).

3.13 Intracellular ROS assay

Total intracellular ROS levels were determined by means of flow cytometry using the H_2DCFDA probe (Invitrogen). Cells were incubated with incubation buffer (5.5 mM glucose in PBS containing 5 µM H_2DCFDA for 30 min at 37˚C and 5% CO_2. This first incubation allows cells to incorporate the probe. After that, this solution was replaced by warm culture media and cells were incubated for 45 min at 37˚C and 5% CO_2. This second incubation allows the activation of the probe by the action of intracellular esterases. Next, cells were trypsinized and resuspended in a PBS solution consisted of 50 µM H_2DCFDA and 20 µg/mL PI (Aguilar et al. 2016). The internalized and activated probe reacts with ROS and emits fluorescence when excited at 492 nm. Fluorescence emission was recorded by flow cytometry at 520 nm wavelength. For ROS analysis, only negative PI cells were considered.

3.14 GSH/GSSG analysis

Total glutathione content was determined by the glutathione reductase enzymatic method. Fresh cells were lysed with 5% 5-sulfosalicylic acid (Sigma-Aldrich) solution, vortexed and disrupted by two freezing/thawing cycles in liquid N_2 and 37˚C water bath. 50 µL of this solution was separated for subsequent protein quantification. Cell extracts were kept at 4˚C for 10 min and centrifuged at 10000 xg for 10 min. For glutathione quantification, a working solution consisted of 15 U/mL of glutathione reductase and 40 µg/mL of 5,5'-Dithiobis(2-nitrobenzoic acid) (Sigma-Aldrich) dissolved in assay buffer (100 mM K_2HPO_4/KH_2PO_4, 1 mM EDTA, pH 7.0) was prepared. Glutathione standards were prepared from a 50 mM oxidized glutathione (GSSG) stock solution. The reaction was initiated by mixing 150 µL of working solution with 10 µL of cell extract (diluted 1:5 or 1:10) or 10 µL of GSSG standard (final concentrations from 0 to 12.5 µM). Next, 50 µL of 0.16 mg/mL NADPH solution was added and the increase in absorbance was recorded at 340 nm wavelength. Total glutathione concentration was normalized by protein content determined by the BCA method (Smith et al. 1985).

3.15 *In vitro* invasiveness assay

Transwell chambers (96 wells plates Costar) with 8 µm diameter pore membranes coated with growth factor-reduced Matrigel (BD Biosciences) at 410 µg/mL and human umbilical cord hyaluronic acid (Sigma-Aldrich) at 100 µg/cm^2 have been used to perform this functional assay. Cells ($5 \cdot 10^4$/well in 96-well plates) were serum-deprived overnight, detached, resuspended in media supplemented with 0.5% FBS and then seeded onto the precoated. Transwell inserts, with the lower chamber containing media supplemented with 0.5% FBS. After 24 h, cells migrating to the lower chamber were collected (detachment with trypsin-EDTA and washes with PBS 1x) and then stained with propidium iodide (PI) (0.01 mg/mL) and counted by flow cytometry, using a known amount of calibration beads as an internal reference. Each experiment was performed in sextuplicate for a better statistical analysis.

3.16 *In vitro* migration assay (wound healing assay)

Cells were cultured on 12-well plates in complete medium (EGM-2 for AMI cells, RPMI for prostate cells and DMEM for breast cancer cells) supplemented with 10% FBS and antibiotics. After reaching confluence, cells starved for one hour in medium containing 0.5% FBS and Mitomycin C (1 mg/mL), a cytostatic drug that reacts covalently with DNA forming crosslinks between the complementary strands of DNA, preventing the separation of the complementary DNA strands and inhibiting DNA replication.

The use of mitomycin C guarantees that wound closure occurs because of the migration and not of cellular proliferation. Each well was marked below the plate surface by drawing a vertical line, and a scratch intercepting the marked line was done in each well using a 200-µl sterile tip. Pictures of scratches were taken at different times. Next, the mean closure of four different scratches was analyzed using ImageJ software (Schneider, Rasband, and Eliceiri 2012). EC migration was expressed as the percentage of scratch closure after 24 hours versus the initial area by using the formula: *% closure = [(scratched area at 0 hours–scratched area at 18 hours)/scratched area at 0 hours]×100.*

3.17 Spheroids formation assay

Cells were grown in DMEM or RPMI medium (depending on the cells) supplemented with B27, 20 ng/mL EGF, 20 ng/mL bFGF (LifeTechnologies), 4 µg/mL heparin, 5 µg/mL insulin and 0.5 mg/mL hydrocortisone (Sigma-Aldrich). Afterward, cells were plated in ultralow attachment 24 wells plates (Corning) (Aguilar et al. 2016). For serial passages, spheroids were centrifuged at 800 rpm, dissociated with 0.05% trypsin, 0.53 mM EDTA, sieved through a 70-µm sieve, analyzed microscopically for single-cellular and plated again (for secondary spheroids formation). Colonies were stained with MTT 5mg/mL in PBS 1X for 1-3 hours, images acquired and quantified by stained areas with Image J software (Schneider, Rasband, and Eliceiri 2012).

3.18 Soft-agar colony formation assay

The Soft Agar Assay for Colony Formation is another kind of anchorage-independent growth assay, and it is performed in soft agar to mimic the environment in which cell transformation takes place in the human body. For this assay, cells were plated in 24 wells plates in a mixture of 5% soft agar (which constitutes the base and the top layers in which the cells grow) and medium for 20 days incubated at 37°C at 5% CO_2. When it became big enough to be quantified, the colonies were fixed with glutaraldehyde 0, 5% for 30 minutes, and stained with MTT (5mg/mL in PBS1x) (Celià-Terrassa et al. 2012). Following this incubation period, formed colonies can be analyzed morphologically using cell stain and quantifying the number of colonies formed per well. The results were obtained quantifying the colonies number, using Image J software (Schneider, Rasband, and Eliceiri 2012).

3.19 Tubes formation assay

Endothelial tube formation was monitored using an in vitro angiogenesis assay kit (Merck Millipore ECM625) following the manufacturer's instructions. Briefly, EC cells were cultured in 96 wells plates coated with 5 % of matrigel (w/o growth factors Corning # 354230) in EGM2 medium without FBS and supplemented with 1% non-essential amino-acids and antibiotics and left in the incubator for 12 hours. Capillary tube branching points were counted in 5 random fields per concentration using the Angiogenesis plugging of Image J software(Schneider, Rasband, and Eliceiri 2012).

3.20 Immunofluorescence and confocal microscopy.

Cultured cells were seeded on sterile glass coverslips placed at the bottom of 24-well cell culture plates and allowed to attach for 24 h. Cells were washed with PBS, fixed with 4% paraformaldehyde/PBS for 15 min followed by cold methanol during 1 h at -20°C. After washing with PBS, the fixed cells were blocked with 3% Goat Serum/PBS, followed

by incubation with the appropriate primary antibodies diluted in blocking buffer during 1 h. Subsequently, three 5 min washes were made before incubation with the secondary antibody diluted in a blocking buffer containing 4,6-diamidino-2-phenylindole (DAPI, 1/10,000 dilution), during 1 h at room temperature (RT). Finally, 2 coverslips per slide were mounted with the mounting medium Mowiol (Mowiol 488 Sigma-Aldrich), which polymerizes at RT for 30 min. Images were captured with a Leica SP5 Confocal microscope. For nuclear foci counting the Volocity software (Perkin Elmer Corporation) was used.

Table 3.4: Primary antibodies used for Immunocytochemistry (nuclear fluorescent determinations)

Primary antibody	source	Brand	Dilution ICC
H2AX	rabbit	Cell Signalling technology	1/200
53bp1	mouse	BD Transduction laboratories	1/5000

Table3.5: Secondary antibodies used for Immunocytochemistry (nuclear fluorescent determinations)

Secondary antibody	source	Brand	Dilution ICC
Mouse Alexa488	goat	A28175 Invitrogen	1/600
Rabbit Alexa488	goat	A27034 Invitrogen	1/600

3.21 Mitochondrial potential membrane

Cationic cyanine dyes have been shown to accumulate in cells in response to potential membrane changes (Shapiro, Natale, and Kamentsky 1979). The MitoProbe™ $DiIC_1(5)$ Assay Kit provides a strong method for the study of mitochondrial membrane potential, supplying solutions of the cyanine dye DiIC1(5) (1,1',3,3,3',3'-hexamethylindodicarbo - cyanine iodide) and CCCP (carbonyl cyanide 3-chlorophenylhydrazone). $DiIC_1(5)$ penetrates the cytosol of eukaryotic cells, and the dye accumulates primarily in mitochondria with active membrane potentials (Holmes and Lantz 2001). $DiIC_1(5)$ stain intensity decreases when cells are treated with reagents that disrupt mitochondrial

membrane potential, such as CCCP. Cells were stained with $DiIC_1(5)$ and then by flow cytometry with red excitation and far-red emission, using 633 nm excitation and far-red emission. The approximate excitation and emission peaks of $DiIC_1(5)$ are 638 nm and 658 nm, respectively.

3.22 Statistical analysis:

For statistical analysis, the two-tailed Student's t-test for independent samples was applied. In figures, bars represent mean ± standard deviation (SD) and a number of replicates (n) are indicated in each case. Single asterisk indicates a significant difference at p-value < 0,05, double asterisks indicate a significant difference at p-value < 0,01 and triple asterisk indicate a significant difference at p-value < 0,001. Non-significant differences (p-value > 0,05) are indicated in some cases as ns. The log 2-fold changes of proteins were estimated by using the comparison of mean intensities between diseased and control groups (patients derived cell lines vs. HCAECs in the case of AMI; variant cells vs. respective control in cancer cells). The differentially regulated genes and proteins with an FDR adjusted p-value < 0,05 were considered as statistically significant.

4. RESULTS AND DISCUSSION

Chapter 4.1

Acute Myocardial Infarction pathology as a result of the endothelial dysfunction event: characterization of a unique *in vitro* model

4.1.1 Introduction

Vascular dysfunction is believed to be a primary factor in the onset and progression of atherosclerosis and other vascular-related disorders. Cardiovascular diseases (CVD) are the leading cause of death worldwide and comprise a range of syndromes affecting the functionality of the heart and blood vessels (Smolders et al. 2019; Townsend et al. 2016). The endothelium plays a pivotal role in the development of CVD, and emerging evidence indicates that pathological blood vessel responses and endothelial dysfunction are associated with metabolic alterations in ECs (Moreno-Viedma et al. 2016). As such, the study of endothelial metabolism and mitochondrial function may be central to unveiling fundamental mechanisms of cardiovascular pathogenesis and to identify novel critical metabolic biomarkers and therapeutic targets.

In this study, we focus our attention on a specific vascular disease, Acute Myocardial Infarction (AMI), a major cause of morbidity in the Western World (Smolders et al. 2019). AMI occurs when myocardial ischemia from diminished blood supply to the heart exceeds a critical threshold and overcomes myocardial cellular repair mechanisms designed to maintain normal operating function and homeostasis (Rathore 2018). The supply of myocardial oxygen and nutrients to heart tissues is interrupted when a

thrombus is superimposed on an ulcerated or unstable atherosclerotic plaque, leading to coronary occlusion (Badimon, Padró, and Vilahur 2012a; Smolders et al. 2019).

We have approached the study of endothelial metabolic adaptations associated with AMI through the establishment of an *in vitro* model of endothelial pathology from eight patients affected with AMI.

4.1.2 Results and Discussion

4.1.2.1 Characterization of a unique endothelial cell model of Acute Myocardial Infarction

4.1.2.1.1 Description of an Endothelial cell model of AMI: description

Human coronary artery endothelial cells (HCAECs) were attained from LonzaClonetics (Walkersville, USA) and used as controls. Pathological ECs were isolated from coronary atherothrombotic specimens from 8 patients undergoing percutaneous coronary intervention with thrombectomy for the treatment of acute ST-segment elevation myocardial infarction (STEMI) (Parsa et al. 2011b), as described in **3.1.1** section. The 8 patient-derived cell lines are designated throughout the text with two letters (CE) and two numbers (respectively 45, 46, 48, 51, 52, 53, 60, 61), maintaining in this way the exact nomenclature used by the Research Center which kindly provided us with this unique AMI model.

Both HCAECs (control-cells) and HCAEC-AMI cells (patient-derived cells) were grown on 0.2% gelatin-coated plates with EGM™-2 Bulletkit™ medium, 10% HyClone FBS and 100 U/mL penicillin, 100 µg/mL streptomycin. All cell cultures were maintained in a 37° C humidified incubator at 5% CO_2. In all experiments, cells were used at passage number 2-10. The medium was changed every other day and cells were cultured as detailed in 3.1.1 (Brittan et al. 2015; Tura et al. 2013).

4.1.2.1.2 Confirmation of the endothelial phenotype of our cell model

As a first step to ascertain the endothelial nature of our cell model, we assessed the morphology of our cells by optical microscopy. When maintained at high density and grown as a monolayer, endothelial cells have a uniform cobblestone appearance (Haudenschild et al. 1975), while, at low density, they adopt a more elongated shape. When they eventually become senescent, they tend to be more flattened and compacted (Adamson 1993). Thus, we explored from the outset the optimal confluence and the growth conditions of our *in vitro* model. As shown in Figure 4.1.1A, at 80% confluence, patient-derived cells presented the expected shape and appeared quite similar to the commercially available control endothelial cells, thus supporting the endothelial nature of the isolated cells.

We next assessed the expression of the *bona-fide* endothelial markers, V-CAM1, PECAM1, CD-34 and CD-105 in our cell models. VCAM-1, vascular cell adhesion protein 1, also known as CD-106, mediates the adhesion of lymphocytes to the vascular endothelium and it has been described to play a significant role in the development of atherosclerosis and rheumatoid arthritis (Ley and Huo 2001). PECAM-1, platelet endothelial cell adhesion molecule, also known as CD31, is an essential component of the endothelial cell intercellular junctions and is an immunoglobulin-like protein involved in angiogenesis and endothelial cell migration (Cao et al. 2002). CD-34, a transmembrane phosphoglycoprotein, is a cell-to-cell adhesion factor expressed in lymph node endothelium, required for T-cells to enter the lymph nodes (Valencia-Nuñez et al. 2017). CD105, also known as Endoglin, is a cell membrane glycoprotein expressed on cellular lineages of the vascular system, which is over-expressed on proliferating endothelial cells and thus considered a good marker of neovascularization and blood vessel development (Fonsatti et al. 2003). The protein levels of these endothelial markers, assessed by Western blotting (Figure 4.1.1 B, C), confirmed the endothelial nature of both patient-derived and control cells.

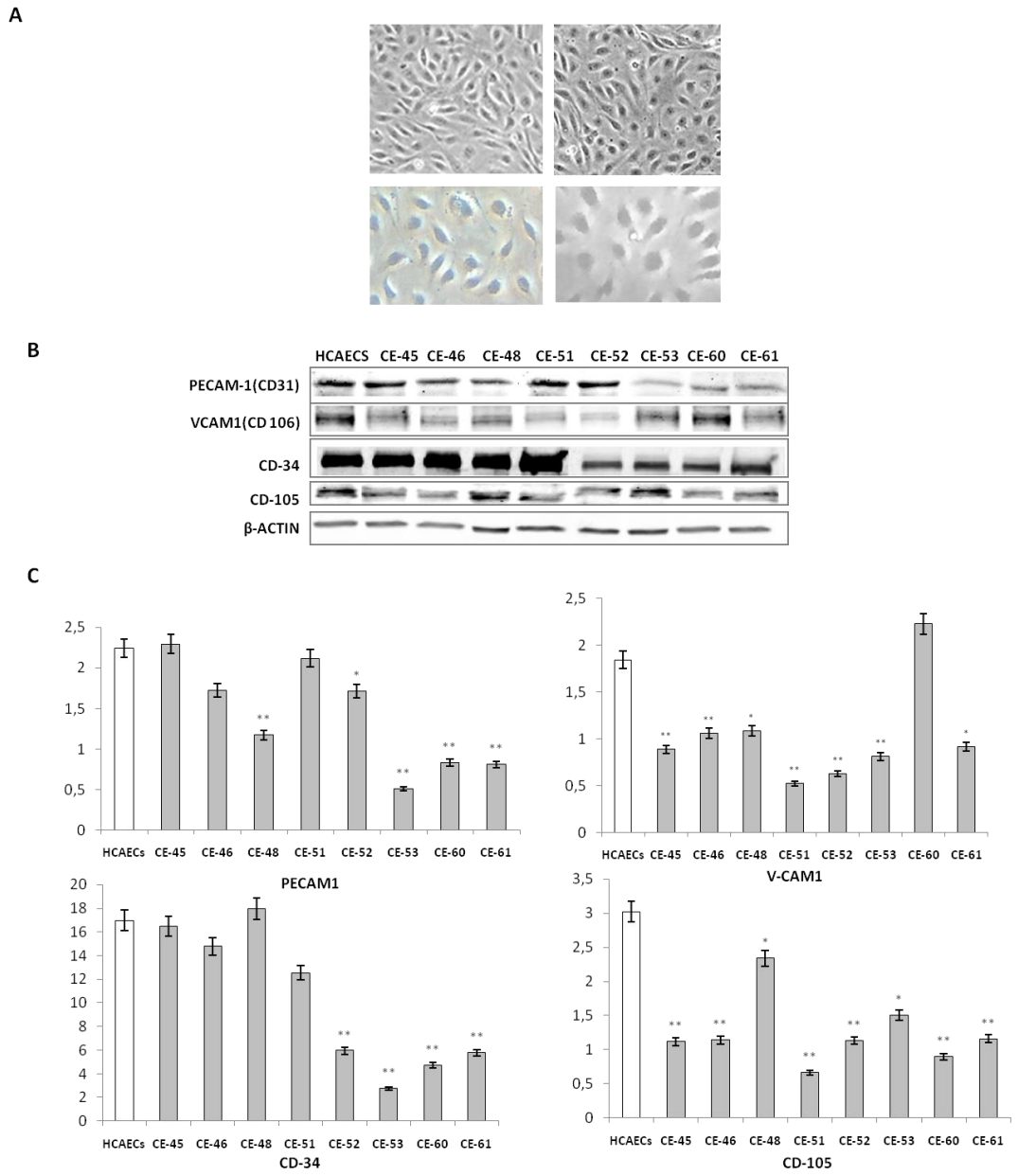

Figure 4.1.1: **Validation of the endothelial phenotype of AMI patients-derived cells**
(A) Bright-field images of HCAECs (on the left) vs. patients (on the right) cell line, 10x, and 20x objectives Leica microscope. (B) Protein levels of endothelial markers (PECAM-1, V-CAM1, CD-34, CD-105) to confirm the endothelial phenotype of the patients- derived cells (C)Proteins bands quantification by Image-J program. Each band has been quantified and compared to β-actin as a loading control Significance was determined for patient-derived cells vs. HCAECs control cells, *p < 0,05, **p < 0,01 and ***p < 0,001.

4.1.2.1.3 AMI patient-derived endothelial cells show impaired growth

Next, we addressed the proliferation and viability features of our patient-derived cells compared to control cells. Because optimal growth conditions for endothelial cells

entails maintaining them at a relatively high confluence, they cannot be kept in culture for prolonged periods at an optimal confluence (70-80%), as overgrowth will cause cells to pile up and lose their “physiological” monolayer growth pattern. Therefore, cell growth monitoring was limited to 168 hours. Under these conditions, all patient-derived cells consistently displayed slower growth rates as compared to control HCAECs (Figure 4.1.2 A). Indeed, after 168 hours, while control cells had reached a plateau in their growth, patient-derived cells continued to proliferate exponentially, albeit at slow rates, without reaching saturation

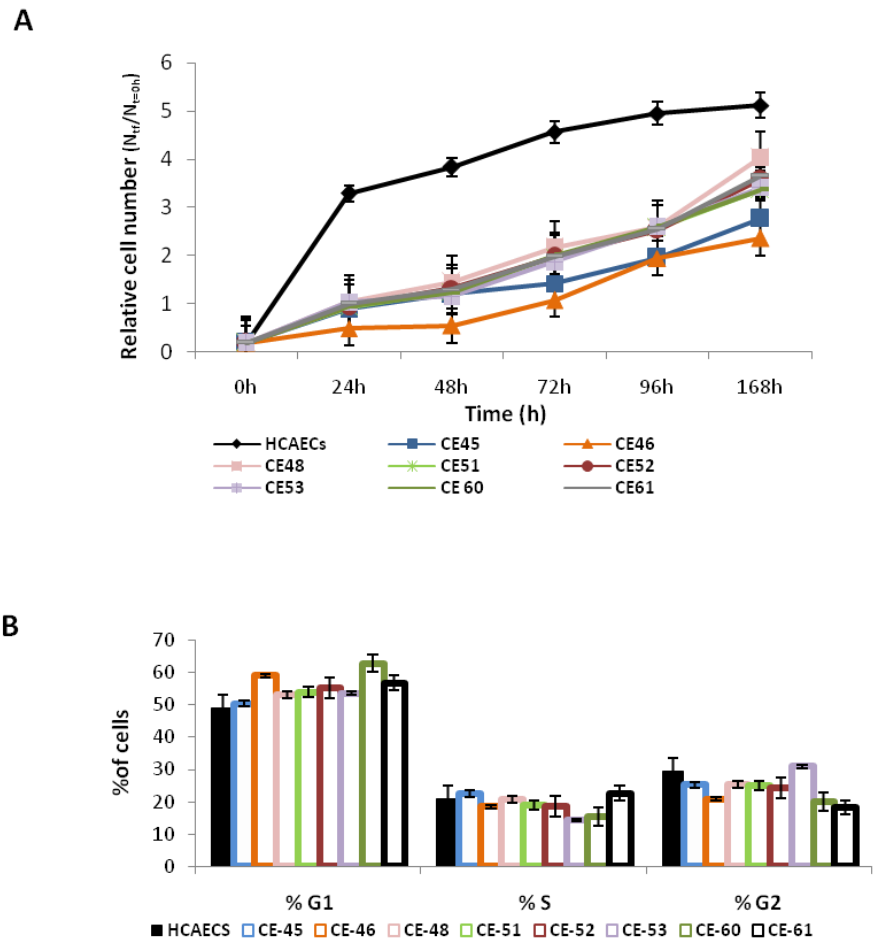

Figure 4.1.2: **Proliferation rate and cellular cycle measurement of patients-derived cells compared to control cells**

(A) Growth rate and proliferation ability of patients-derived cells vs. control. Proliferation rates of patients-derived cells and control cells in full EGM™-2 bulletkit™medium , expressed as relative cell number ($N_{tf}/N_{t=0h}$), where N_{tf} and $N_{t=0h}$ corresponds to the final and initial number of cells, respectively (B) Cellular Cycle assay showing a slight tendency of patients-derived cell lines distribution in G1 phase. The harvested cells stained with PI and their DNA content analyzed by flow cytometry. This graph shows the variation in the percentage of cells in each phase of the cell cycle. Data are representative of an experiment repeated 3 times and conducted in triplicate.

Given these results, we determine the cell cycle distribution of these cells by flow cytometry at 24 hours after seeding, the point of maximum growth in the healthy control cells. Somewhat contrary to our expectations, we observed no significant differences in the distribution of cell cycle phases between patient-derived and control cells (Figure 4.1.2 B), except for a modest tendency, without reaching statistical significance, of patient-derived cells to accumulate in the G1 phase relative to HCAECs. These experiments allow us to observe the distribution of cell populations among the different phases of the cell cycle, but not the relative dynamics and kinetics of cell cycle transitions, for which other approaches are needed. Nevertheless, the slow growth rate in conjunction with unaltered cell cycle phase distribution of patient-derived cells suggests an overall slowing down of growth that affects equally all phases of the cell cycle.

These observations suggest that endothelial cells from AMI patients manifest abnormal cell-autonomous traits independently of additional influences that they are undoubtedly subjected to *in vivo*. The specific trait described above is a dramatic impairment in proliferative ability. This straightforward initial result encouraged us in our subsequent pursuit of cell-autonomous signs and mechanisms of metabolic dysfunction associated with AMI.

4.1.2.1.4 AMI patient-derived endothelial cells display impaired migration

The impaired rate of proliferation observed for patient-derived endothelial cells pointed to dysfunction in the fundamental properties of these cells. Thus, we studied a second major biological features, namely their migration ability. A commonly used *in vitro* procedure to test the migration ability of cells is the scratch or wound-healing assay, which entails monitoring the migration of the cells from the edge of a scratch produced on a confluent monolayer. After 24 hours of seeding and migration of proliferation-arrested cells (with Mitomicyn C), control endothelial cells achieved a complete closure of the wound (Figure 4.1.3). In contrast, three patient-derived cell lines displayed wound closures below 50%, four other about 60%, and only one about 80% after 24 h of migration under the same conditions (Figure 4.1.3).

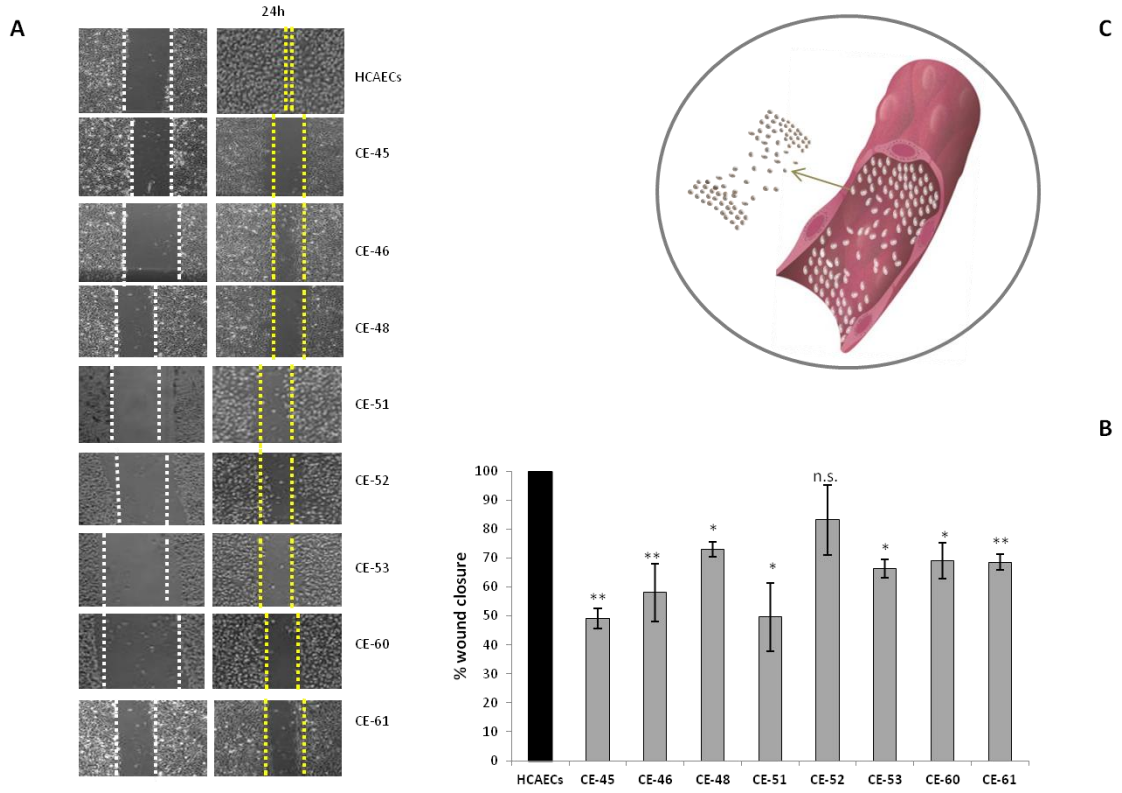

Figure 4.1.3: **Migration ability of cells derived from patients with AMI pathology**
(A) Representative images of MitoC-treated EC migration in scratch wound assays showing reduced migration in AMI cells compared to the control (B) Quantification of EC migration in scratch wound assay showing reduced migration after 24h in the presence of MitoC. The results are represented as % of wound closure, as described in section 3.15. (C) Graphical representation of Endothelial cells migration in human vessels. Data are representative of an experiment repeated 3 times and conducted in triplicate. Significance was determined for patients derived cells vs. HCAECs, *p < 0,05, **p < 0,01 and ***p < 0,001.

These results lend further support to the notion that AMI patient-derived coronary endothelial cells are dysfunctional in major cell-autonomous processes, namely growth, and migration. The ability to migrate is one of the most critical functions of healthy endothelial cells, which can migrate while branching from existing blood vessels towards sources of angiogenic stimuli, guided by tip cells (De Bock et al. 2013). Impairment in this fundamental endothelial function is considered a hallmark of vascular diseases.

4.1.2.1.5 Defective tubulogenesis in AMI patient-derived endothelial cells

A major feature of healthy endothelium is its ability to generate new vessels, known as vasculogenesis or tubulogenesis. Tubulogenesis, or formation of tubes, is a

fundamental morphogenetic process in multicellular organisms by which organs and structures constituted by interconnected tubes play essential roles in the delivery of nutrients, in the removal of waste products and the formation of physiological barriers between the organs and the outside environment (Andrew and Ewald 2010; Lubarsky and Krasnow 2003). In healthy endothelium, the generation and sprouting of new tubes is a frequent event which occurs through the proliferation and migration of endothelial cells under the stimulus of different growth factors, resulting in the generation of new vascular structures that favor the development of the organs and the exchange of oxygen, CO_2, nutrients, growth factors and other molecules in the entire organism (Traore and George 2017). Vascular pathologies that affect endothelial cell proliferation or migration may lead to either abnormally enhanced or reduced vasculogenesis. Control and patient-derived endothelial cells were cultured under conditions that favor tubulogenesis, and branching points scored after 12 h of switching to tubulogenic medium containing VEGF (Figure 4.1.4).

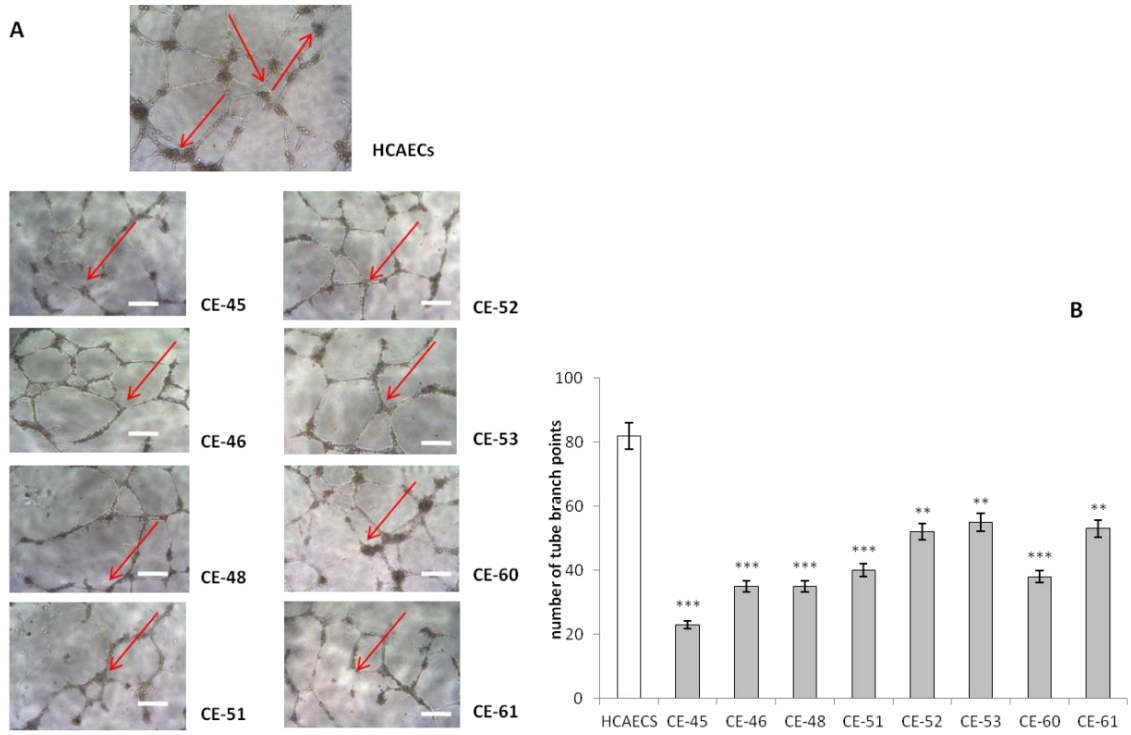

Figure 4.1.4a: AMI **patient-derived cells ability to generate new tubes networks under VEGF stimulation after 12 hours**

(A) The bright-field images are an example of an experiment of triplicate for each cellular line. Scale bar = 100 µm. (B) The progression of angiogenesis is quantified by counting the amount of tubes branch points at the same time point. Data are the mean ± SD from n=3. Significance was determined for patient-derived cells vs. HCAECs, *p < 0,05 **p < 0,01 and ***p < 0,001.

While control HCAECs averaged 80 branching points (Figure 4.1.4). AMI patient-derived endothelial cells displayed a significantly reduced tubulogenic potential, evident both as a diminished number of branching points Figure 4.1.4a panel B) and as shorter and fragmented tubes as compared to control cells (Figure 4.1.4a panel A).

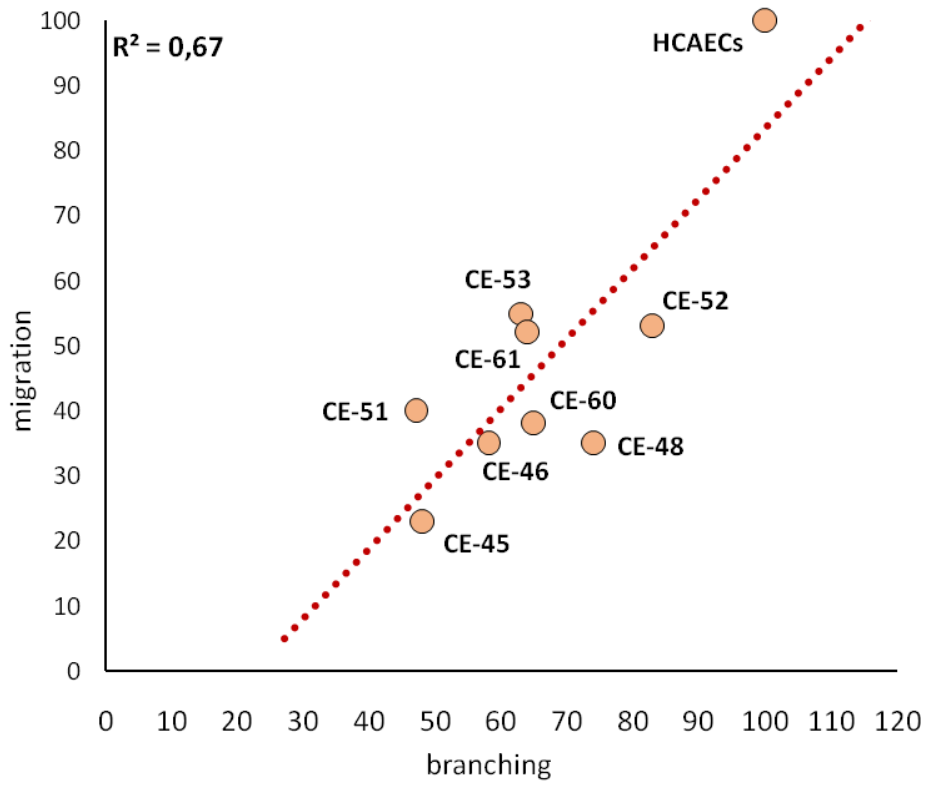

Figure 4.1.4b: **Correlation between migration and branching in control and AIM patient-derived endothelial cells**

Relative values from migration (Figure 4.1.3) and tubulogenesis assays (Figure 4.1.4a) were plotted, and linear regression performed.

The branching capacity of the different AMI patient-derived endothelial cell lines was linearly correlated (R^2 = 0.67) with their ability to migrate (Figure 4.1.4b) regardless of their growth rates (Figure 4.12) suggesting that the deficient tubulogenesis or sprouting of these cells is linked to a defect in their migration properties, rather than to abnormal proliferation or survival.

4.1.2.1.6 AMI patient-derived endothelial cells display abnormal glucose and lactate consumption and production patterns

The above characterization points to cell-autonomous defects in AMI patient-derived endothelial cells that compromise their ability to proliferate, migrate and form branched tubular structures. We next tackled the hypothesis that the metabolic features of these cells might be associated with at least part of the observed phenotypes.

To assess nutrient and metabolite consumption and production rates, the concentration of selected metabolites in culture media was determined. We focused on glucose as the major carbon source of the glycolytic pathway, lactate as the main metabolic end-product of glycolysis, and glutamine/glutamate as alternative sources of carbon metabolism and major providers of mitochondrial anaplerosis. We found that 6 out of the 8 patient-derived endothelial cell lines consumed glucose at significantly lower rates than control HCAECs cells (Figure 4.1.5), which may reconcile with the lower growth rates of patient-derived cells, while 2 patient-derived cell lines consumed more glucose than control cells. Remarkably, all patient-derived cell lines displayed a strong production of lactate, comparable or superior to control cells, regardless of their levels of glucose uptake (Figure 4.1.5).

High lactate production is frequently linked to strong glycolytic activity, as the glycolytic end-product, pyruvate, can be converted to lactate catalyzed by the enzymatic activity of lactate dehydrogenase-A (LDH-A). Indeed, in highly proliferating cells, such as cancer or progenitor cells, a high rate of glycolysis can be accompanied with an inhibition of the mitochondrial entry of pyruvate, which, instead, is diverted towards the generation of lactate, a metabolic rewiring designated the Warburg effect, or aerobic glycolysis (Burns and Manda 2017). Strong glycolysis coupled to high lactate production and mitochondrial shutdown is also characteristic of hypoxia, through transcriptional regulation by HIF-1α of key regulators of these three processes, and has been observed in dysfunctional endothelial cells associated with atherosclerosis and vascular diseases (Fitzgerald, Soro-Arnaiz, and De Bock 2018a; Theodorou and Boon 2018).

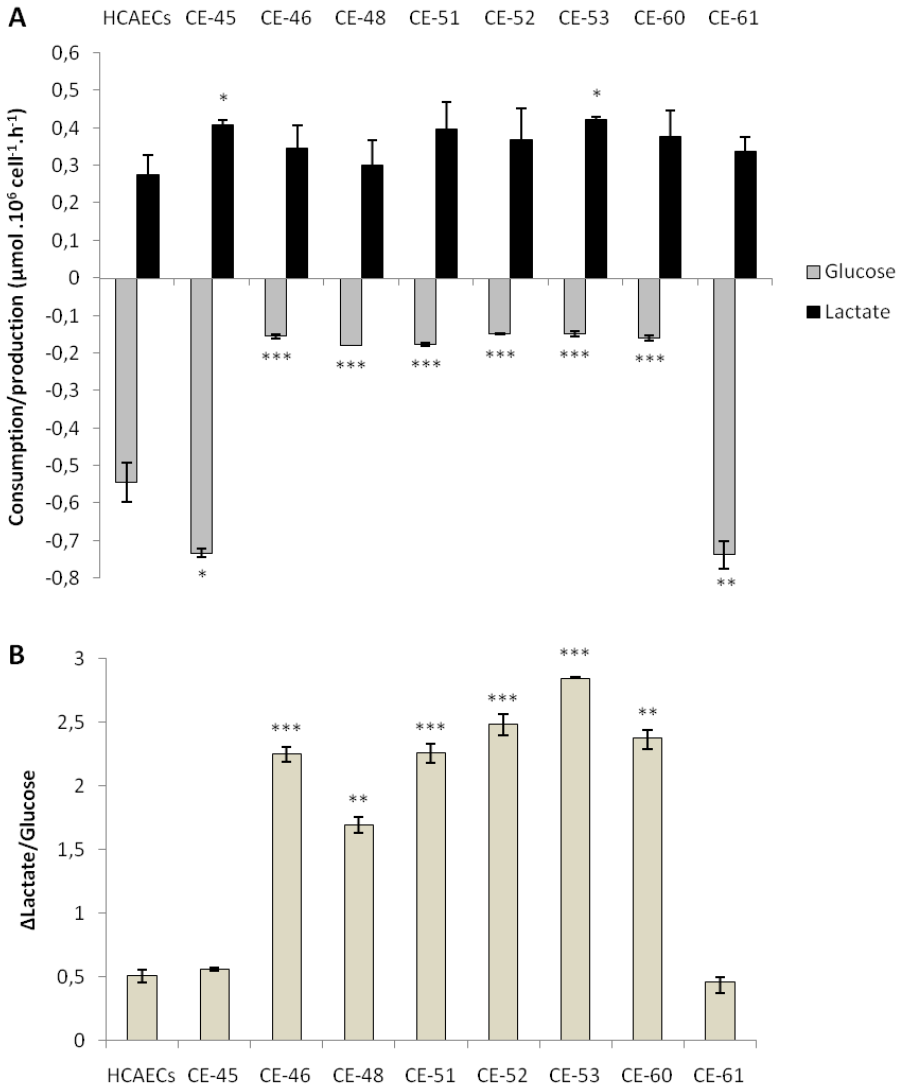

Figure 4.1.5: **Determination of AMI patient-derived cells metabolism**
(A) Glucose consumption and Lactate production have been measured after 48 h (B)Conversion rate of glucose to lactate. The bars correspond to the mean ± SD of n = 3. Statistically significant differences between patient-derived cells and HCAECs control cells were indicated by Student's t-test * $p < 0,05$, **$p < 0,01$ and ***$p < 0,001$.

Two of the patient-derived endothelial cell lines, CE-45 and CE-61, consumed high levels of glucose and displayed robust lactate production (Figure 4.1.5), and thus, it may be assumed that lactate is produced through glycolysis. The cells may also be hypothesized to be under a Warburg effect. However, their slow rates of proliferation stand in contrast to the rapid proliferation phenotypes seen in other cell types displaying a Warburg effect, such as cancer cells.

On the other hand, the remaining 6 patient-derived endothelial cell lines, also slow growers, showed high levels of lactate production in spite of low glucose consumption (Figure 4.1.5). This uncoupling of lactate production from glycolysis suggests the existence of an alternative source of lactate in these cells. In this regard, it is worth noting that glutaminolysis also produces lactate, in a pathway that involves oxidation of glutamine to malate and then to pyruvate by the malic enzyme (ME), followed by conversion to lactate by the action of LDH-A (Brooks 2018).

As pointed out above, the greatly augmented lactate production/glucose consumption ratios observed in AMI patient-derived cells is reminiscent of the Warburg effect, as some authors define this effect as a lactate production/glucose consumption ratio ≥ 2. We caution, though, that the observed scenario may not correspond to a "standard" Warburg effect, as we lack evidence for a shutdown of the entry of pyruvate to mitochondria, and glucose consumption is diminished in 6 out of the 8 pathological cell lines. Production of lactate from pyruvate, catalyzed by LDHA, has the important function of recycling NADH to NAD+. The resulting lactate is transported outside the cell by the monocarboxylate transporter MCT4. However, lactate can also serve as a fuel source. Extracellular lactate is uptaken through a second monocarboxylate transporter, MCT1, in a passive down-gradient manner (Dimmer et al. 2000; Nihed Draoui and Feron 2011), and converted to pyruvate by LDHB, a reaction that reduces NAD+ to NADH, and pyruvate then enters the TCA cycle or used for gluconeogenesis (Cori cycle). There are many examples of the so-called lactate shuttle, e.g., the astrocyte-neuron lactate shuttle and the reverse-Warburg effect in tumors, by which lactate produced by highly glycolytic cells is taken up and consumed by neighboring cells. However, lactate-producing glycolytic cells can use their own lactate through transport into mitochondria and subsequent oxidation to pyruvate (catalyzed by mitochondrial LDHB), which then enters the TCA (Y. J. Chen et al. 2016). The mitochondrial conversion of lactate to pyruvate entails the reduction of NAD+ to NADH, which is then available for complex I of the electron transport chain and initiate respiration. Both MCT4 and MCT1 have been described to localize in mitochondria and presumably act as mitochondrial lactate transporters (Brooks 2018; Nihed Draoui and Feron 2011; Hertz and Dienel 2005). In addition to its functions in redox balance through the NAD+ - NADH recycling during lactate production, the lactate import/export balance by MCT1 and MCT4 plays a key

role in maintaining a functional intracellular pH, providing the necessary homeostatic stability for cellular proliferation and fitness (S. J. Park et al. 2018). With this backdrop, we determined by Western blotting the levels of expression of MCT1 and MCT4 in our endothelial cell model. We found that MCT1 was expressed in patient-derived cells at levels not significantly different from control cells (Figure 4.16).

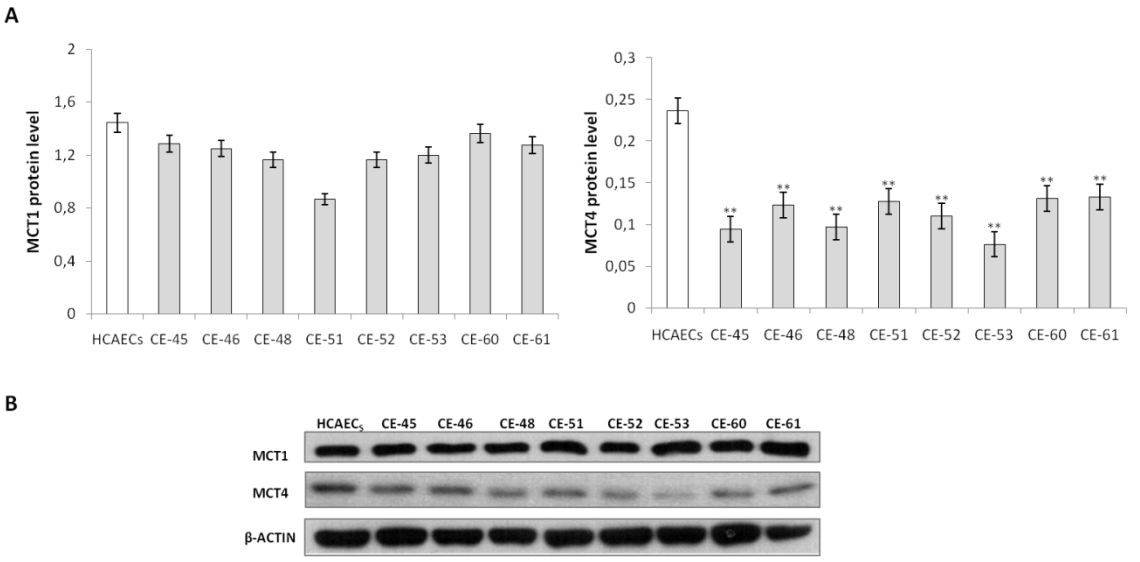

Figure 4.1.6: **Identification of MCT1 and MCT4 transporter in patients-derived cells compared to control** (A) Determination of the protein level by western blot of two lactate transporters MCT1 (importer) and MCT4 (exporter) compared to β-actin as a loading control and quantified by Image-J program (B). Results showed a lower signal for MCT4 in all patient-derived cells when compared to HCAECs control. Significance was determined for patient-derived cells vs. HCAECs control cells, *p < 0,05, **p < 0,01 and ***p < 0,001. Data are the mean ± SD from n=3.

That control cells, with a lower net export of lactate into the extracellular medium, express higher levels of the lactate exporter MCT4 than patient-derived cells, may be explained by considering that, in control cells, the MCT4 transporter may be located both in the plasma membrane and in mitochondria. A fraction of the produced lactate would be transported into mitochondria, and the remaining fraction exported to the extracellular milieu. Patient-derived cells, on the other hand, may have low mitochondrial localization, and would thus export most or all of the lactate to the extracellular medium. This scenario would imply that total lactate production in both types of cells, patient-derived, and control, may not differ significantly, and that differ in

the distribution of lactate, into mitochondria or the extracellular space. This hypothesis would require further experimental substantiation.

4.1.2.1.7 Aberrant expression of 6-phosphofructo-2-kinase/fructose-2,6-bisphosphatases (PFKFBs) in AMI-derived endothelial cells

The low glucose uptake observed in 6 out of the 8 patient-derived endothelial cell lines prompted us to explore the expression of key enzymes in the glycolytic pathway.

Under normal conditions, endothelial cells rely mainly on glycolysis to generate the energy required for their functions (De Bock et al. 2013; Dromparis and Michelakis 2013; Goveia, Stapor, and Carmeliet 2014).

As such, this essential anaerobic bioenergetic pathway provides most of the total intracellular ATP and initiates with the uptake of glucose, which is converted through ten steps into pyruvate, which can either enter mitochondria or be converted to lactate. A rate-limiting enzyme in this pathway is phosphofructokinase 1 (PFK1), responsible for the phosphorylation of fructose-6-phosphate (F-6-P) to fructose-1,6-phosphate (F-1,6-P) in an ATP-dependent reaction. PFK1 is allosterically activated by fructose-2,6-bisphosphate (F-2,6-BP), produced from F-6-P through the catalytic activity of 6-phosphofructo-2-kinase/fructose-2,6-bisphosphatases (encoded in mammals by paralogs PFKFB1, PFKFB2, PFKFB3, PFKFB4 and TP53-induced glycolysis and apoptosis regulator (TIGAR) (Bensaad et al. 2006; Eelen et al. 2018). These are bifunctional enzymes bearing, on the same polypeptide, an N-terminal 6-phosphofructo-2-kinase domain, and a C-terminal fructose 2,6-bisphosphatase domain. By producing F-2,6-BP through their kinase activity, PFKFB enzymes allow glycolysis to proceed, while by degrading F-2,6-BP through their bisphosphatase activity, they block glycolysis. PFKFB1 and PFKFB2 have similar relative kinase and bisphosphatase activities, while PFKFB4 exhibits a stronger bisphosphatase activity (Chesney et al. 2014; Yi et al. 2019). In contrast, PFKFB3 has substantially higher kinase activity and thus strongly favors the formation of F-2,6-P2, resulting in an enhanced glycolytic rate. Finally, TIGAR has bisphosphatase activity but no kinase activity. Nevertheless, the different PFKFB enzymes are also regulated by post-translational

modifications which modulate their relative kinase and bisphosphatase activities (De Bock et al. 2013; Van Schaftingen et al. 1982).

Given its relative kinase and bisphosphatase activities, PFKFB3 is a preferred target to inhibit glycolysis over other isoforms in this family of enzymes. PFKFB3 has been described to play a significant role in the glycolytic activity of pathological ECs, and its inhibition dramatically abrogates their proliferation and migration (Li, Kumar, and Carmeliet 2019a; Schoors et al. 2014).

We determined PFKFB3 protein levels by Western blotting, finding significantly lower levels in 7 out of the 8 patient-derived endothelial cells, as compared to control HCAECs (Figure 4.1.7) consistent with their lower glucose uptake. In fact, one of the two patient-derived cell lines with high glucose uptake, CE-45, expressed PFKFB3 at levels close to those of control cells (Figure 4.1.7), thus reinforcing the notion that cell lines with low glucose uptake have low rates of glycolysis.

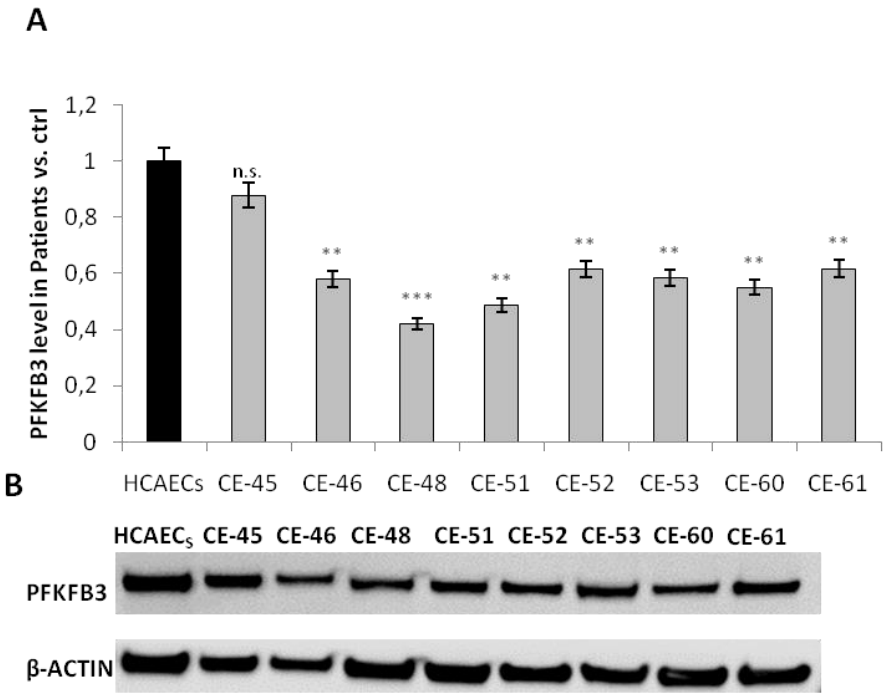

Figure 4.1.7: **PFKFB3 measurement in AMI patients derived cells compared to control**
(A) Protein levels determination of PFKFB3 in AMI patients -derived cells vs. control by western blot, quantified by Image-J program, and compared to β-actin as a loading control (B). Data are the mean ± SD from n=3. Significance was determined for patient-derived cell vs. HCAECs *p < 0,05 **p < 0,01 and ***p < 0,001.

This may also help explain, at least in part, the low proliferation rates, migration capacity and tubulogenic activity of these cells, as these processes require robust glycolysis.

We also determined PFKFB4 protein levels, finding significantly higher levels of expression in patient-derived cells compared to control cells (Figure 4.1.8).

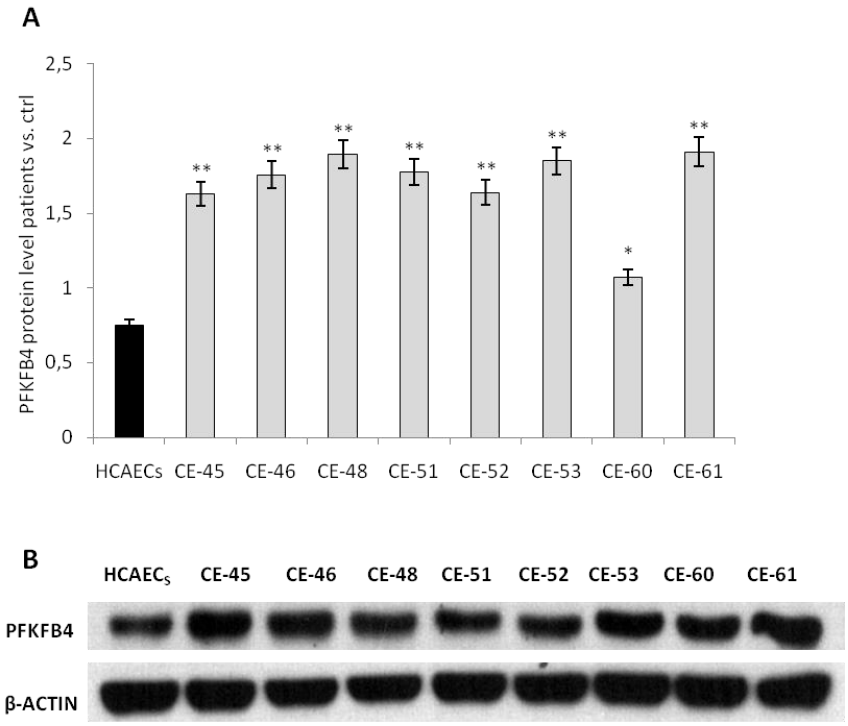

Figure 4.1.8: **Determination of PFKFB4 level in patients derived cells vs. control cells**

Protein levels determination of PFKFB4 in AMI patients derived cells vs. control by western blot (A), quantified by Image-J program and compared to β-actin as loading control (B) Data are the mean ± SD from n=3 .Significance was determined for patients-derived vs. HCAECs *p < 0,05, **p < 0,01 and ***p < 0,001.

Both PFKFB4 and PFKFB3 are upregulated in hypoxia through transcriptional activation by HIF-1α (Minchenko et al. 2014) by activation of the mTOR pathway (Y. Feng and Wu 2017) and peroxisome proliferator-activating receptor γ (PPARγ) (Shu et al. 2016). On the other hand, although wild-type p53 transcriptionally represses both PFKFB3 (Franklin et al. 2016) and PFKFB4 (Ros et al. 2017) activated in response to DNA damage, only PFKFB4, but not PFKFB3, has been described as strongly upregulated in the absence of p53 (Ros et al. 2017).

As HIF-1α, mTOR and PPARγ drive glycolysis, while our patient-derived endothelial cells show evidence of diminished glycolysis accompanied with low expression levels

of PFKFB3, it seems unlikely that the high levels of PFKFB4 observed in these cells is a downstream outcome of the activation of these pathways.

The hypothesis of a blunted function of p53 as a driver of PFKFB4 upregulation in these cells could merit further investigation. Interestingly, the malic enzyme isoforms, ME1, and ME2 are also under negative regulation by p53 and are upregulated in the absence of p53 (Ros et al. 2017).

Regardless of the mechanisms underlying PFKFB3 over-expression along with PFKFB4 over-expression in AIM patient-derived endothelial cells, predicted downstream consequences are (1) decreased levels of F-2,6-P2 resulting in low PFK1 activity and diminished glycolytic flux, which is consistent with the observed phenotypes, and (2) shunting of G6P towards the pentose phosphate pathway (PPP), reinforced by the activation by PFKFB4 of steroid receptor coactivator-3 (SRC-3), enhancing its transcriptional activity and stimulating the expression of transketolase (TKT) (Dasgupta et al. 2018).

Low levels of PFKFB3 expression coupled to high levels of PFKFB4 expression in AMI patient-derived cells predict a redirection of glucose-6-phosphate (G6P) towards the PPP (Yamamoto et al. 2014). As a consequence, we would expect (1) increased production of NADPH reducing equivalents through the oxidative branch of the PPP (Dasgupta et al. 2018; S Ros et al. 2017; Yi et al. 2019) and (2) increased production of ribose-5-phosphate through the non-oxidative branch, for *de novo* synthesis of nucleotides as well as acetyl-CoA carboxylase 1 activation and lipogenesis (by inhibiting activation of liver kinase B1/AMPK signaling). The NADPH reducing equivalents produced through the non-oxidative branch afford the maintenance of redox homeostasis by scavenging reactive oxygen species (ROS) (Benito et al. 2017; Li, Horke, and Förstermann 2014a; Sun et al. 2017; Xia et al. 2017).

The nucleotides supplied through the non-oxidative branch of the PPP can be used for DNA synthesis in proliferating cells, and also in DNA damage repair (Bester et al. 2011).

In light of these predictions, we determined the expression level and activity of glucose-6-phosphate dehydrogenase (G6PD), the rate-limiting enzyme of the oxidative branch of the PPP. Consistently, we found significantly higher levels of G6PD in AMI patient-

derived cells than control cells (Figure 4.1.9 A). Likewise, patient-derived cells displayed higher levels of G6PD enzyme activity than control cells (Figure 4.1.9B).

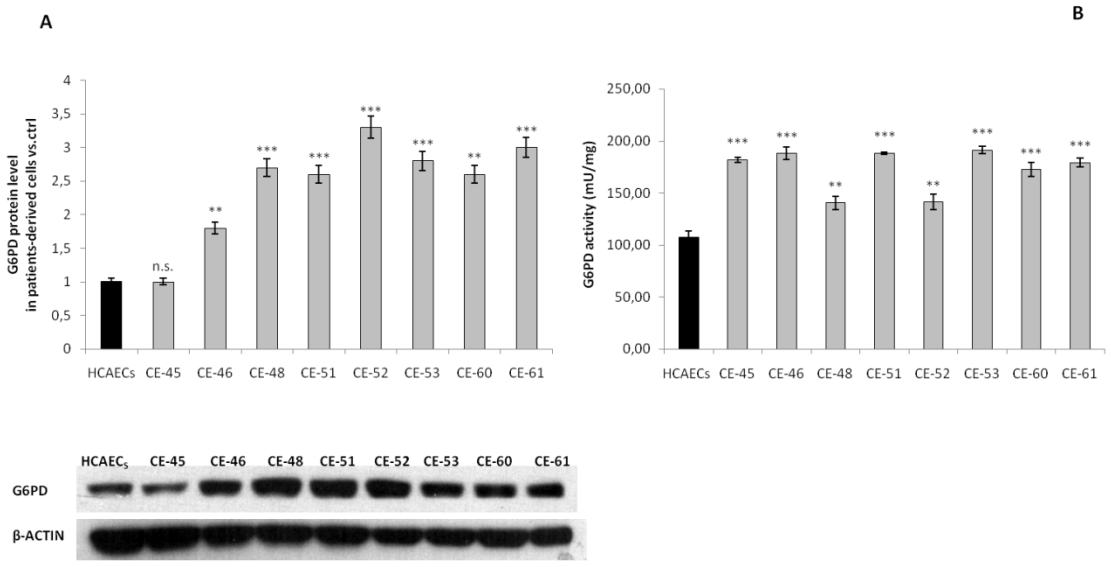

Figure 4.1.9: **Determination of the protein level and the activity of G6PD, a rate-limiting enzyme of the oxidative branch of the PPP**

(A) Protein level determination of G6PD in AMI patient-derived cells vs. control by western blot compared to β-actin as a loading control and quantification performed by Image-J program (B) G6PD enzyme activities normalized to intracellular protein content. Data are representative of an experiment repeated 3 times. Significance was determined for patient-derived cells vs HCAECs *p < 0,05, **p < 0,01 and ***p < 0,001.

These results support an enhanced activity of the oxidative branch of the PPP. This is expected to generate higher levels of NADPH, which, in turn, should contribute to improving ROS scavenging by maintaining glutathione in its reduced state. We thus determined ROS and glutathione levels in our cell model. Seven out of the 8 patient-derived cell lines contained ROS at significantly higher levels than control cells (Figure 4.1.10A). The one cell line with near-normal ROS levels, CE-45, was the same with normal levels of G6PD protein (Figure 4.1.9A). Similarly, the intracellular concentration of reduced glutathione was increased in all 8 patient-derived cell lines (Figure 4.1.10B). Therefore, glutathione levels are upregulated to counter the excess ROS levels in these cells.

.

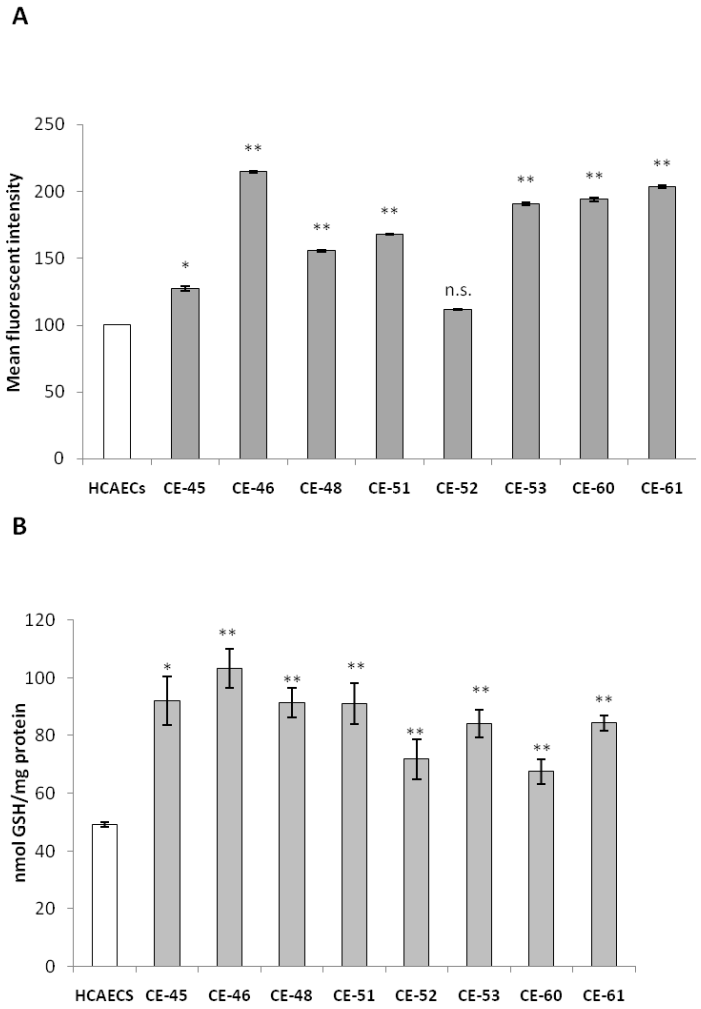

Figure 4.1.10: **Intracellular glutathione and ROS levels measurements in patients-derived cells vs. control cells**

(A) ROS levels determined by flow cytometry. Results are expressed as the mean fluorescent intensity (MnX). (B) Total intracellular glutathione content. Values are normalized to the protein concentration of the cell extract used for the analysis of glutathione. Bars represent the mean ± SD of n=3. Significant differences compared to HCAECs were assessed by Student's t-test * $p < 0,05$, **$p < 0,01$ and ***$p < 0,001$.

In vivo, endothelial cells in AMI patients are under numerous physiological and pathological stresses, including mechanical and inflammatory, which may generate excess ROS and oxidative stress (Dasgupta et al. 2018; Seo and Lee 2014). However, our patient-derived cells are no longer in an *in vivo* environment and are rather in an *in vitro* environment identical to that of control endothelial cells, and therefore their increased ROS levels cannot be directly attributed to environmental factors. Absent maintenance of long-term epigenetic memory of past stress responses *in vivo*, it is reasonable to assume that the high levels of ROS in AIM patient-derived cells may be elicited by

endogenous damage signals impinging upon mitochondria (Murphy 2009), or through NAD(P)H oxidases.

Glutathione is a natural endogenous antioxidant that counters the oxidative power of ROS. Its biosynthesis involves two ATP-dependent steps: first, in a rate-limiting step, gamma-glutamylcysteine is synthesized from L-glutamate and cysteine; second, glycine and gamma-glutamylcysteine undergo glutathione synthetase (GSS)-catalyzed condensation, to form glutathione (Kojima et al. 2018a).

Given the likely relevance of glutathione in the observed phenotypes and the possibility of a glutamine origin of the excess lactate produced in the AMI patient-derived endothelial cells (section 4.2.1.5), we next tackled the study of glutamate and cysteine contents in these cells.

4.1.2.1.8 AMI patient-derived endothelial cells exhibit a strong glutamine metabolism

The complexity of metabolic dependencies in pathological cells goes beyond the Warburg effect, as cells depend on glutaminolysis, the PPP, and fatty acid oxidation in addition to glycolysis (Yi et al. 2019). Glutaminolysisis the process by which glutamine is converted into TCA cycle metabolites, glutamate, aspartate, CO_2, pyruvate, lactate, alanine, and citrate, through the activity of multiple enzymes (L. Yang, Venneti, and Nagrath 2017). These pathways have been further investigated in our AMI model.

Determination of the extracellular fluxes of glutamine showed that the consumption of glutamine in patient-derived cells is higher than in control cells (Figure 4.1.11A) The latter consumed more glucose than patient-derived cells (see also above), and thus the glutamine to glucose consumption ratio is far greater in patient-derived cells than in control cells (Figure 4.1.11B).

This suggests that AMI patient-derived cells mainly resort to glutamine, rather than glucose, as their carbon source.

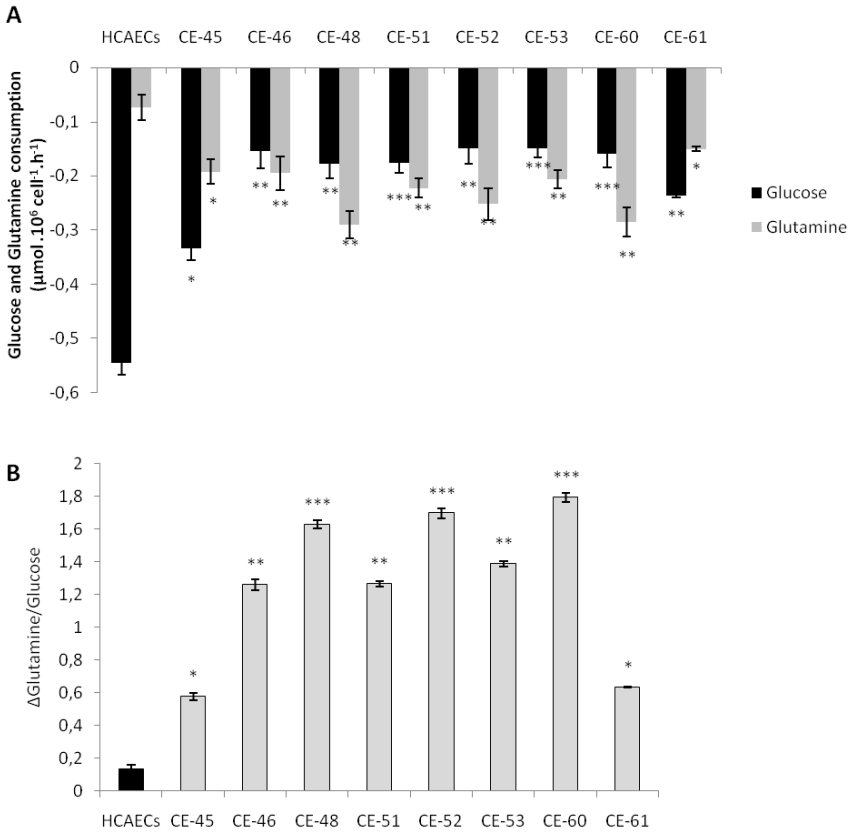

Figure 4.1.11: **Study of glutamine metabolism in AMI patients derived cells in comparison with the control**

(A) Glutamine and Glucose consumption have been measured by Cobas Mira collecting cellular media after 48h (B) Consumption rate of glutamine over glucose, which displays the preferential glutamine consumption of patients-derived cells. The bars correspond to the mean ± SD of n = 3. Statistically significant differences between patient-derived cells and HCAECs control cells were indicated by Student's t-test * $p < 0,05$ **$p < 0,01$ and ***$p < 0,001$.

Glutamine is the most abundant free amino acid in circulation and in intracellular pools, and it is used by cells for both bioenergetics and biosynthetic needs; it can act as a carbon source or nitrogen donor and is consequently used as a precursor for the synthesis of amino acids, proteins, nucleotides and lipids, and represents the main substrate for TCA cycle anaplerosis (DeBeradinis and Cheng 2010; Nihed Draoui, De Zeeuw, and Carmeliet 2017b; Fitzgerald, Soro-Arnaiz, and De Bock 2018a; Laplante and Sabatini 2012).

Moreover, glutamine participates in redox homeostasis, a process that has a close connection with the PPP, as one of its main functions is to generate glutathione to counter the oxidative stress generated by ROS (see above). Thus, the increased

glutamine consumption observed in AMI patient-derived cells is consistent with the increased glutathione levels observed in these cells (Figure 4.1.10).

The anaplerotic role of glutamine requires its conversion to glutamate, in a reaction catalyzed by glutaminase (GLS). There are three isoforms of human GLS: the kidney-type (KGA) and its splice variant glutaminase C (GAC) encoded by the GLS1 gene, and the liver-type (LGA) encoded by the GLS2 gene (Van Den Heuvel et al. 2012; Thangavelu et al. 2014). Relevant to our above observations, the GAC isoform of GLS1 is crucial for cell growth under acidic pH, as would be expected in the presence of high levels of lactate (Aguilar et al. 2016). In endothelial-related diseases, the capacity of the glutaminase reaction to counterbalance acidic conditions by the release of ammonia, after glutamine is metabolized to glutamate, is still poorly explored.

Given the high levels of consumption of glutamine observed in patient-derived cells, we determined the expression of glutaminase by Western blotting, using isoform-specific antibodies (Figure 4.1.12). Consistently, both isoforms of GLS1, KGA, and GAC, are expressed at significantly higher levels in patient-derived cells than control cells (Figure 4.1.12).

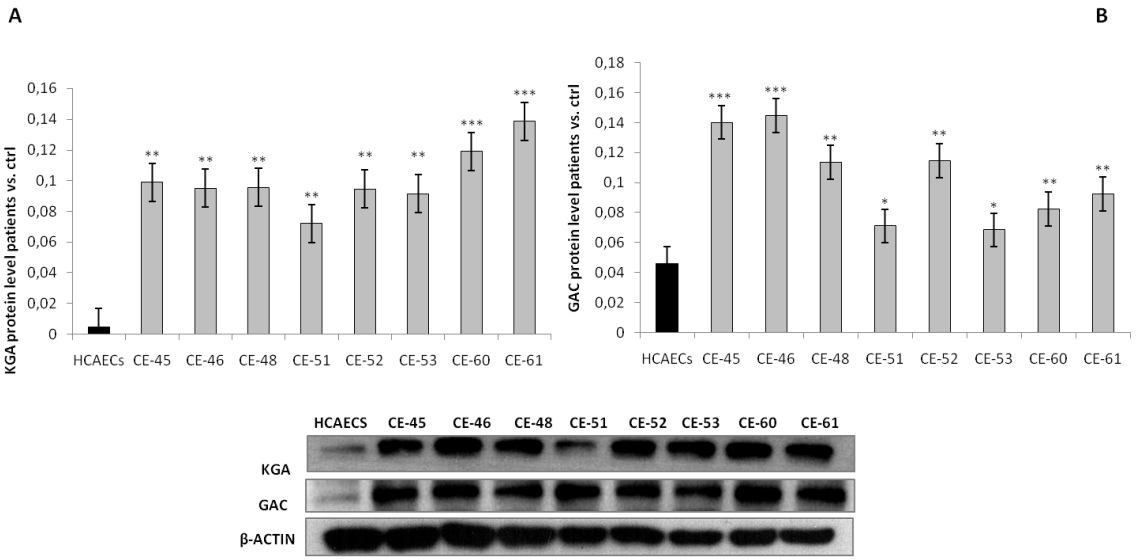

Figure 4.1.12: **Protein determination of GLS1 isoforms in patients-derived cells vs. control cells**
The protein level of two isoforms of GLS1, KGA (A) and GAC (B) has been determined in patients-derived cells vs. control cells, by Western Blotting compared to β-actin as a loading control and the bands quantified by Image-J program. Data are representative of 3 independent experiments. Significance was determined for patient-derived cells vs. HCAECs controls, *p < 0,05, **p < 0,01 and ***p < 0,001.

Although glutamine can be synthesized endogenously from α-ketoglutarate, converted to glutamate by glutamate dehydrogenase using NADPH, and then to glutamine by glutamine synthase, using NH_3 (Bhutia and Ganapathy 2016), the endogenous biosynthetic pathway does not satisfy the cellular demand, which makes cells often depend on extracellular glutamine. Being hydrophilic, extracellular glutamine cannot simply diffuse into cells across the plasma membrane and need the intervention of active transporters (Van Geldermalsen et al. 2016). Transcriptional profiling by RNA-Seq was performed, allowing us to ascertain the expression of two classical glutamine transporters: the Alanine, Serine, Cysteine Transporter **ASCT2** (encoded by the **SLC1A5** gene) and the cystine/glutamate antiporter Xc^- system (encoded by the SLC7A11/ SLC3A2 genes).

ASCT2 is a sodium-dependent carrier of neutral amino acids, belonging to the SLC1 family and localized in the plasma membrane of several cell types. The preferred substrate of ASCT2 is glutamine, with cysteine acting as a modulator more than a substrate (Schulte et al. 2018). High levels of ASCT2 expression are associated with poor prognosis in a number of human cancers, including lung, breast, and colon (Osanai-Sasakawa et al. 2018). Consistent with the high consumption of glutamine, all of the patient-derived cells expressed significantly higher levels of the SLC1A5 than control cells (Figure 4.1.13). Like the other members of the SLC1 family of transporters, ASCT2 is an obligatory exchanger, cooperating with the LAT1 transporter to transfer leucine into the cell in exchange for glutamine, followed by glutamine being transported back in by ASCT2 (Figure 4.1.13B). This transport process is electroneutral, involving the influx of Na^+/amino acid coupled to the efflux of Na^+/amino acid, maintaining the homeostasis of neutral amino acids inside the cells. Collectively, our data suggest that AMI patient-derived cells rely heavily on glutamine both as an alternative to glucose as a carbon source and in order to maintain redox homeostasis in these cells. Related to our observations, a link between glutamine metabolism and clinical manifestations of atherosclerosis, such as intima-media thickness and plaques development, has been described (Grajeda-Iglesias and Aviram 2018; Würtz et al. 2012).

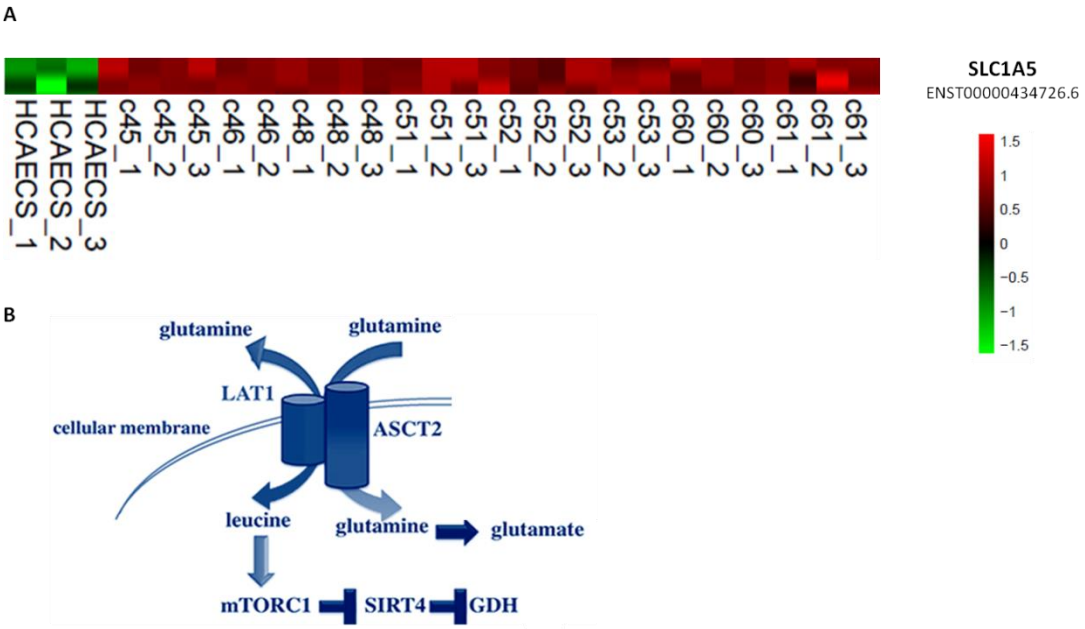

Figure 4.1.13: **Role of ASCT2 transporter in AMI patients -derived cells**
(A) Heatmap of differential expression of the gene SLC1A5 encoding for ASCT2 transporter by Rna-Seq transcriptomic analysis of patients-derived cells vs. HCAECs control cells. (B) Graphical representation of the ASCT2 transporter of glutamine inside the cell reproduced under the **Creative Commons Attribution 4.0 International License 4.0** from G. J. Yoshida, *J. Exp. Clin. Cancer Res.*, (2015) 34, 111.

4.1.2.1.9 The Cystine/Glutamate antiporter Xc^- system

A second transporter coupled to ASCT2 is the cystine /glutamate antiporter Xc^- system. The Xc- system is a cystine-glutamate exchanger that functions always in the import of cystine into cells under physiologic conditions, and the imported cystine is immediately reduced, by intracellular GSH (through the formation of a mixed disulfide intermediate) or by thioredoxin reductase 1 (TRR1), to cysteine then used in the synthesis of glutathione (Mandal et al. 2010).

This transporter is constituted by two subunits: the xCTsubunit (light chain), encoded by the SLC7A11 gene, and the CD98hc subunit (heavy chain), encoded by the SLC3A2 gene (Nihed Draoui, De Zeeuw, and Carmeliet 2017b; Ishimoto et al. 2011). These two genes are expressed at higher levels in patient-derived cells than control cells (Figure 4.1.14 A). This suggests that, in addition to glutamine, cystine import is higher in patient-derived cells than control cells.

Cysteine (Cys), one of the least abundant amino acids, contains a thiol side chain, derived from methionine, susceptible to oxidation to give the disulfide derivative cystine (L-dicysteine). Because of the ability of thiols to undergo redox reactions, cysteine has antioxidant properties, and it is one of the main substrates for the synthesis of glutathione (Estrela, Ortega, and Obrador 2006). Cystine is abundant in human blood and plays an important structural role in many proteins (Chawla et al. 1984; Marino and Gladyshev 2010).

To investigate if increased expression of this antiporter results in a higher concentration of glutamate and cysteine in patient-derived cells, polar intracellular metabolites (TCA cycle intermediates and amino acids) were determined by GC/MS.

The results disclosed a higher intracellular content of both cysteine and glutamate in all of the AMI patient-derived cells when compared to control cells (Figure 4.1.14B,C) Expression of xCT at the cell surface is essential for the uptake of cysteine, required for GSH synthesis to maintain the intracellular redox balance (Figure 4.1.14D) (Lo, Wang, and Gout 2008). Cysteine can be synthesized from methionine, and also converted to homocysteine through the intermediate S-adenosylmethionine (Figure 4.1.14E) (Kumar et al. 2017). We thus determined the intracellular content of methionine by GC/MS, finding a higher content in patient-derived cells compared to the control cells (Figure 4.1.14 F).

All these findings are consistent with the higher intracellular content of GSH detected in AMI patients cells (Figure 4.1.10 B), which on the other hand, constitute the antioxidant response to the increased oxidative stress caused by a big accumulation of ROS level found in AMI patients (Figure 4.1.10A).

Xc^{-}system has been described to be over-expressed in cancer and other diseases, but little is still known about its task in endothelial dysfunction and in particular, in cardiovascular disease (Lo, Wang, and Gout 2008; Seib, Patel, and Bridges 2011).

Our observations suggest that the Xc^{-} antiporter, along with other factors, forms part of the antioxidant defense mechanisms engaged in AMI patient-derived endothelial cells.

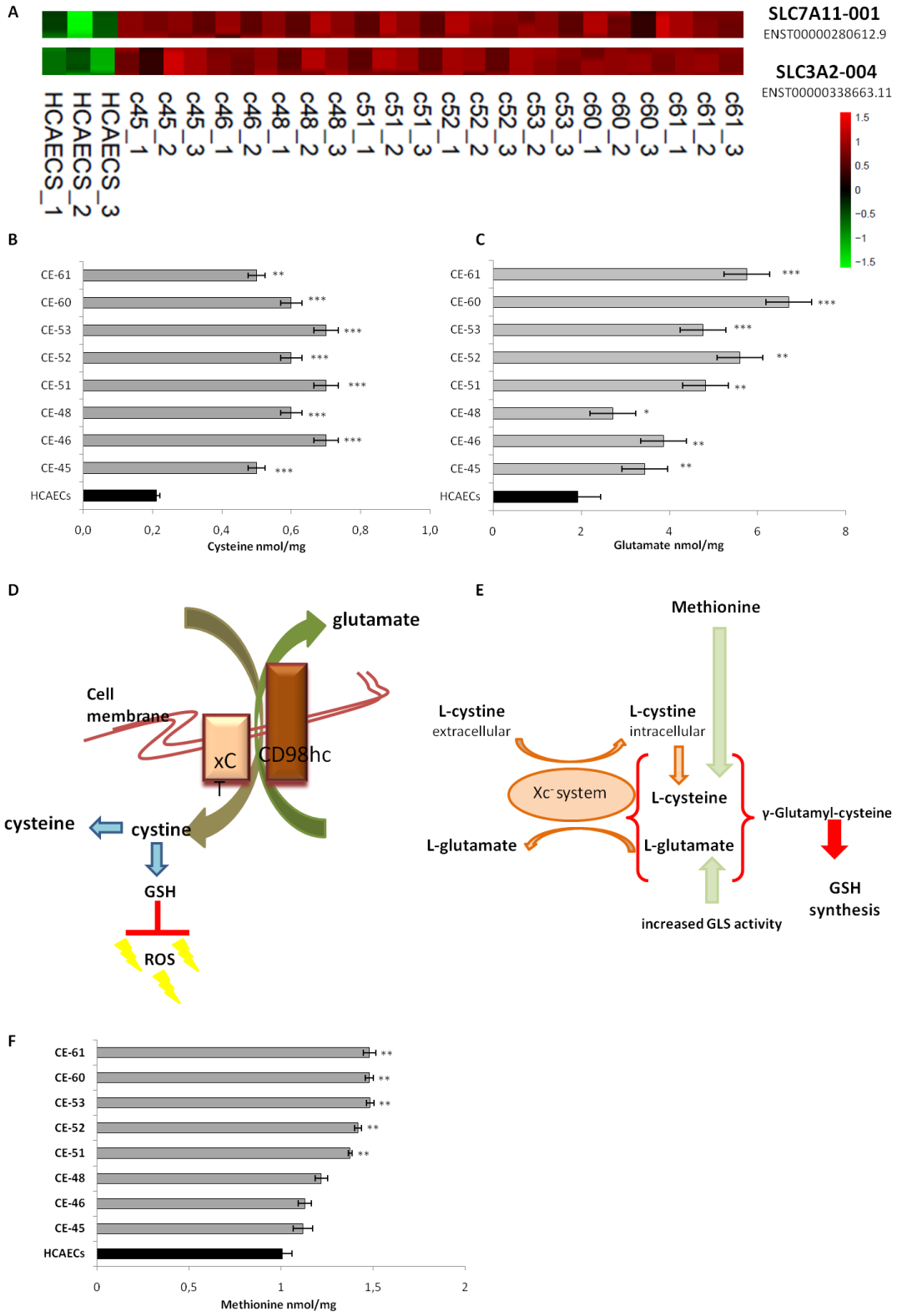

Figure 4.1.14: **Role of the Cystine/Glutamate antiporter system Xc⁻ in AMI patients derived cells**

(A) Heatmap of differential expression of the SLC7A11 and SLC3A2 by Rna-Seq transcriptomic analysis of patients-derived cells vs. control cells. SLC7A11 and SLC3A2 genes codify respectively for the xCT (light chain), and the CD98hc sub-unity (heavy chain) of the Cystine/Glutamate antiporter system Xc⁻, its expression on the cells surface is crucial for the uptake of cystine required for intracellular GSH synthesis to maintain the intracellular redox balance. (B, C) Intracellular amino acid contents of patient-derived cells (nmol/mg). Results are represented as nmol/mg protein using Norvaline (1mg/mL) as an

4.1.2.1.10 Glutamate as a substrate for GSH synthesis against oxidative stress in AMI

Although the synthesis of glutathione (GSH) is especially dependent on cysteine (Estrela J.M. et al., 2016), glutamate is also important.

Enhanced expression of the cystine/glutamate transporter could help to maintain high concentrations of this amino acid and contribute to the intracellular levels of GSH (Ishimoto et al. 2011).

As discussed above, most of the glutamine transported into the cell is converted to glutamate by glutaminase, which is then converted to α-ketoglutarate (αKG) by glutamate dehydrogenase (GLDH). αKG is used as a carbon source for the anaplerotic replenishment of the TCA cycle, while glutamate, which normally accumulates in the cells, is a precursor of GSH (DeBeradinis and Cheng 2010; Nihed Draoui, De Zeeuw, and Carmeliet 2017b; Son et al. 2013). Thus, glutamate also contributes to redox homeostasis and ROS detoxification, along with the PPP.

We thus determined glutamate in culture media, finding lower levels of production in 6 out of the 8 patient-derived cells as compared to control cells (Figure 4.1.15 A). Moreover, the ratio between glutamate production and glutamine consumption is considerably lower in patient-derived cells (Figure 4.1.15B). Because of the high levels of glutaminase in patient-derived cells, implying a strong conversion of glutamine to glutamate, the lower levels of extracellular export of glutamate is suggestive of a robust consumption of glutamate in the production of GSH in these cells.

internal standard. Data are expressed as mean ± SEM n=3 for patient-derived cells vs. the control HCAECs. The higher intracellular concentration of cysteine (Cys) (B) and glutamate (Glu) (C) in patients-derived cells correlates with the bigger demand of GSH to contrast the oxidative stress generated by the endothelial dysfunction, and the subsequent increase of ROS species. (D) Schematic representation of the Xc^- antiporter system composed of the two subunits xCT and CD98hc. (E) Graphical representation of cysteine and glutathione metabolism in AMI patients-derived cells. The big demand for cysteine availability as a substrate for GSH synthesis is supported by methionine (Met) the other sulphur-containing amino acid from which cysteine can be also produced. The intracellular content of methionine has also been measured by GC/MS. *p < 0,05 **p < 0,01 and ***p < 0,001.

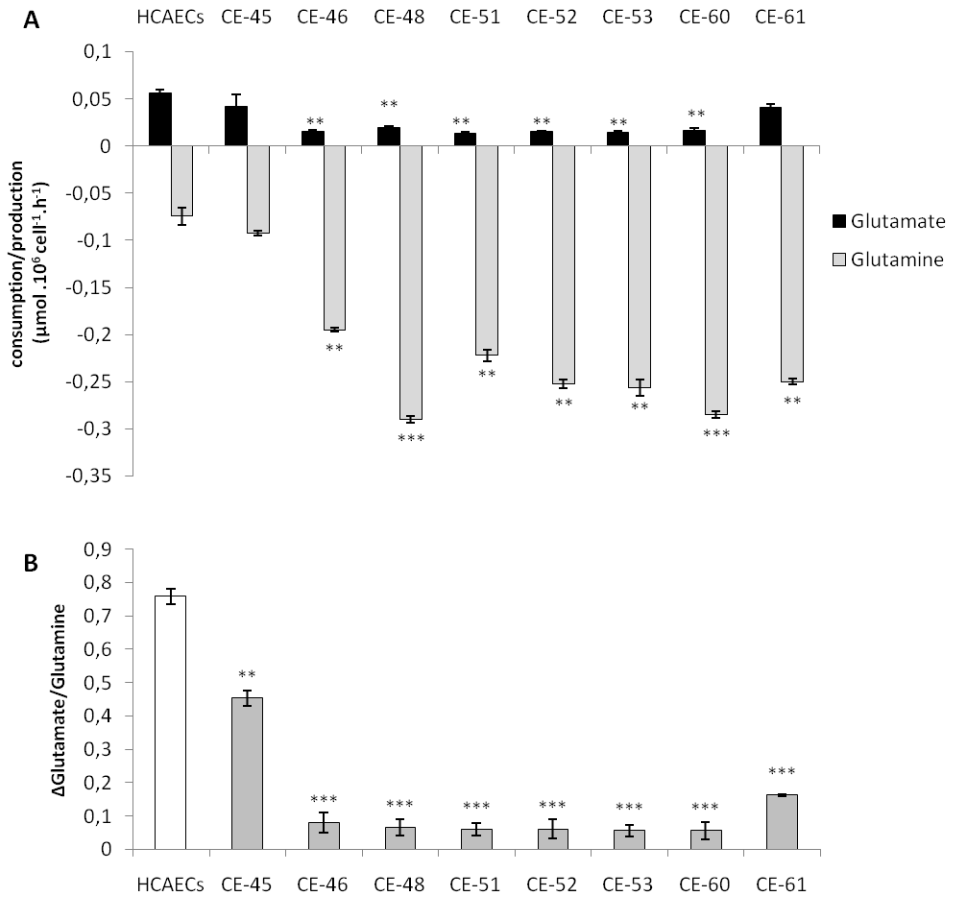

Figure 4.1.15: **Glutamate production and glutamine consumption by patient-derived cells compared to control cells**

(A) Glutamine consumption and glutamate production have been measured after 48 h. (B) The ratio between glutamate production respect to glutamine consumption The bars correspond to mean ± SD of n = 3. Statistically significant differences between patient-derived cells and HCAECs control cells were indicated by Student's t-test * $p < 0,05$, ** $p < 0,01$ and *** $p < 0,001$.

Interestingly, the two pathological cell lines with the highest levels of glutamine efflux, CE-45, and CE-61, are also those with the highest consumption of glucose (Figure 4.1.5). Our evidence supports the notion that these two cell lines display robust glycolysis and, hence, subsequent entry of pyruvate to mitochondria, which would make them less dependent on glutamate for anaplerotic replenishment for the TCA cycle (DeBeradinis and Cheng 2010; Son et al. 2013).

One of these two cell lines, CE-45, is also one with the lowest content of ROS (Figure 4.1.10), which would also entail a diminished need for glutamate for the synthesis of glutathione as a ROS scavenger.

4.1.2.1.11 The mitochondria of AMI patient-derived endothelial cells have higher levels of membrane potential

A possible source of the high levels of ROS observed in patient-derived cells is increased mitochondrial respiration in these cells. On the other hand, high levels of glutaminase glutamine and consumption suggest a strong activation of glutaminolysis in patient-derived cells. Once in the internal space of the mitochondria, glutamate is converted into α-ketoglutarate and ammonia by glutamate dehydrogenase, together with the reduction of $NAD(P)^+$ into NADPH. NADH is the substrate of complex I of the mitochondrial respiratory chain, and its oxidation results in the translocation of H^+ across the membrane, thus producing a proton gradient.

Together, our evidence predict an increased mitochondrial membrane potential in these cells.

High membrane potential simply large negative potentials in the mitochondrial matrix, leading to glutamate expulsion and high glutaminase activity. Maintenance of the mitochondrial membrane potential (Δψm) is an essential component in the process of energy storage during oxidative phosphorylation, as it reflects the pumping of H^+ across the inner membrane during the process of electron transport and oxidative phosphorylation (Zorova et al. 2018).

We thus determined the status of the mitochondrial membrane potential in our cells. For this, we used the fluorescent probe $DiIC_1(5)$ (MitoProbe), a positively charged, cell-permeant dye that accumulates within the mitochondrial matrix, which is negatively charged. In consequence, hyperpolarized mitochondrial membranes sequester higher levels of the probe, whereas, depolarization results in the release of the dye. As shown in Figure 4.1.16, $DiIC_1(5)$ accumulated at significantly higher levels in all patient-derived cells relative to control cells, indicating a mitochondrial hyperpolarization due to increased membrane potentials.

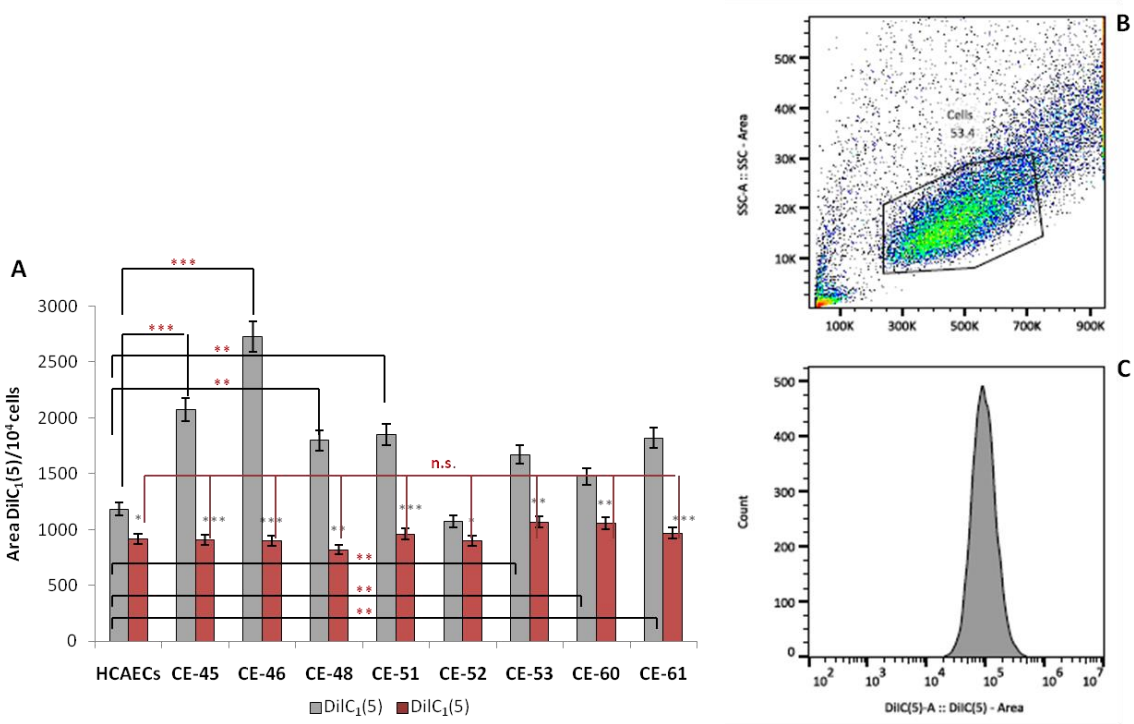

Figure 4.1.16: **Measurement of the mitochondrial metabolic potential of control cells (HCAECs) and patients-derived cells using MitoProbe™ DiIC$_1$(5) Assay Kit**

Cells were stained with DiIC$_1$(5) and then analyzed by flow cytometry with red excitation and far-red emission, using 633 nm excitation and far-red emission. The approximate excitation and emission peaks of DiIC$_1$(5) are 638 nm and 658 nm, respectively. The MitoProbe™ DiIC$_1$(5) Assay Kit provides solutions of the cyanine dye DiIC$_1$(5) and CCCP (carbonyl cyanide 3-chlorophenylhydrazone), for the study of mitochondrial membrane potential. The dye accumulates primarily in mitochondria with active membrane potentials. DiIC$_1$(5) stain intensity decreases when cells are treated with reagents that disrupt mitochondrial membrane potential, such as CCCP. In panel **A**, the grey bars represent the fluorescence of the cells stained with 50nM of DiIC$_1$(5), and the red bars the fluorescence in the presence of 50µM of CCCP. In all the cell lines, a significant decrease in DiIC$_1$(5) fluorescence after the addition of CCCP has been detected. B and C images depict how the method works for the detection of the colorant fluorescence by flow cytometry. Results are expressed as stained area respect to the number of cells analyzed by the cytometer. Samples have been compared separately (each cell line vs. w/o CCCP) and then patient-derived cells vs. HCAECs stained just with DiIC$_1$(5) and in the presence of CCCP. *p < 0,05 **p < 0,01 and ***p < 0,001.

The subsequent addition of the uncoupling agent carbonyl cyanide m-chlorophenylhydrazone (CCCP) (50 µM) resulted in a rapid depolarization, reflecting the proton gradient dissipation. A higher mitochondrial membrane potential implies a higher mitochondrial activity and consequent participation of the TCA cycle in cellular metabolism.

These observations are consistent with higher levels of mitochondrial respiration and higher anaplerotic use of glutamate. The latter requires the transport of glutamate

into mitochondria, which is accomplished by specific glutamate transporters belonging to the **SLC25** family of transporters. The mitochondrial solute carrier (SLC) family 25 is composed of 53 members that transport metabolites across the inner mitochondrial membrane (IMM), of which four are responsible for the transport of glutamate: the aspartate-glutamate antiporters SLC25A12 and SLC25A13, and the glutamate-protons importers SLC25A18 (GC1, glutamate carrier 1) and SLC25A22 (GC2, Glutamate carrier 2) (Palmieri 2004; Palmieri and Monné 2016). These transporters are essential for several metabolic pathways, including the Krebs cycle and the β-oxidation of fatty acids, and apart from the simultaneous transport of glutamate/protons through the IMM, they are also able to transfer glutamate against OH^-gradients in the antiporter system (Fiermonte et al. 2002).

Consistent with the observed hyperpolarization of the mitochondrial membranes, transcriptional profiling unveiled increased levels of expression of the glutamate/H+ symporter, SLC25A22, in patient-derived cells (Figure 4.1.17).

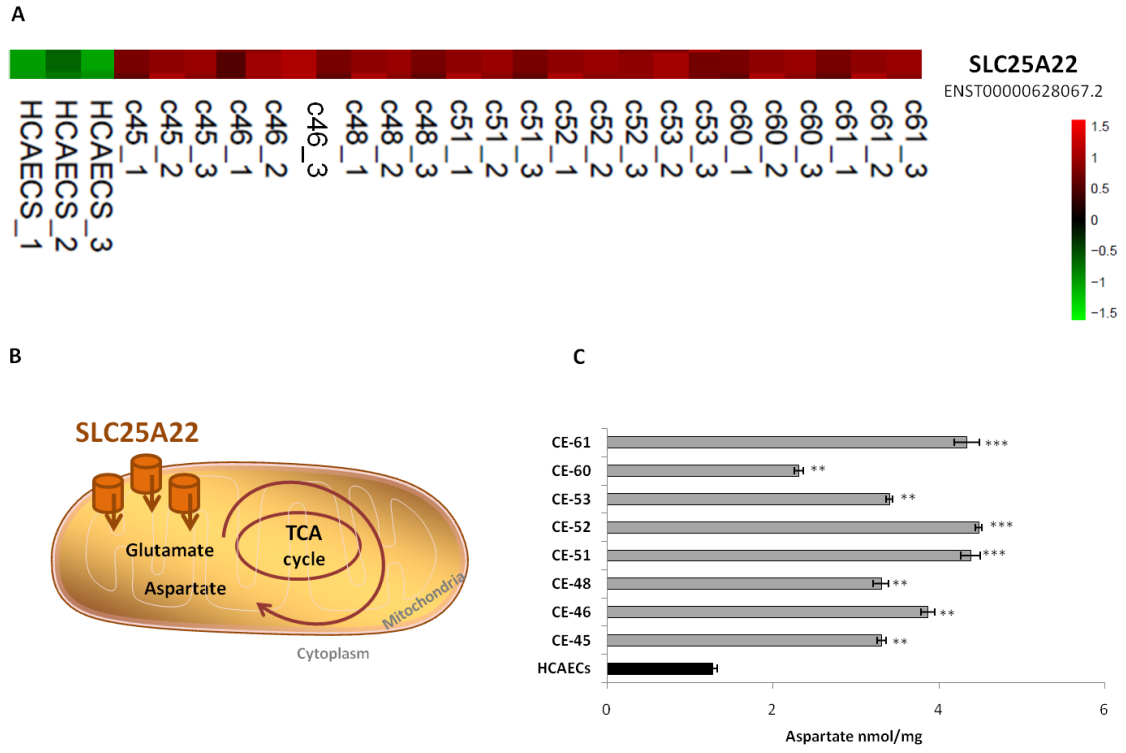

Figure 4.1.17: **Differential expression of SLC25A22 gene, codifying for the GC2 transport, in AMI patient-derived cells vs. control**

(A) Schematic diagram showing the mechanism of action of SLC25A22, which is essential for the transport of glutamate inside the mitochondria. SLC25A22 is also essential for the synthesis of aspartate via glutaminolysis. Aspartate derived from oxaloacetate and is catabolisis produce NAD^+ and NADPH, which are required for glycolysis and redox balance, respectively (B) Intracellular Aspartate content (nm/mg) by GC/MS measurements (C). $p < 0,05$, $^{**}p < 0,01$ and $^{***}p < 0,001$.

Because the transport of glutamate into mitochondria through SLC25A22 is also essential for the biosynthesis of aspartate (Wong et al. 2016) we determined the intracellular content of aspartate, finding increased levels in patient-derived cells (Figure 4.1.17). Aspartate derived from oxaloacetate, via glutaminolysis, produces NAD+, required for glycolysis and NADPH, needed for redox balance (C. C. Wong et al. 2016). Therefore, this pathway also contributes to offset the high levels of ROS in these cells.

Aspartate derived from oxaloacetate, via glutaminolysis, produces NAD+, required for glycolysis and NADPH, needed for redox balance (C. C. Wong et al. 2016). Therefore, this pathway also contributes to offset the high levels of ROS in these cells.

4.1.2.1.12 Diminished intron retention suggests a broad shift in post-transcriptional gene regulation in AMI patient-derived endothelial cells

The foregoing observations indicate a profound metabolic reprogramming in AMI patient-derived endothelial cells, affecting glycolysis, glutamine metabolism, mitochondrial function, and redox state. This suggests the occurrence of a broad systemic dysfunction in these cells.

As an unbiased approach to address the possible nature of these alterations, we performed transcriptomic profiling by RNAseq of 7 patient-derived and control cell lines (technical issues forced us to exclude from the analysis one of the 8 pathological cell lines). Perhaps as a reflection of the individual variability between the patient-derived cell lines, relatively small numbers of genes were found coordinately expressed among all cell lines with statistically significant differences in expression levels relative to control cells. For example, a set of 30 genes were significantly ($P \leq 0.05$) up-regulated or down-regulated in cell lines CE-48, CE-51, CE-52, CE-53, and CE-60, but not CE-45, relative to HCAECs (Figure 4.1.18). At lower levels of significance, additional genes were found differentially expressed (see below).

That CE-45 cells fail to share some of the most significant genes profiled with the rest of the cell lines is in line with the distinct phenotype displayed by this particular cell line (see above).

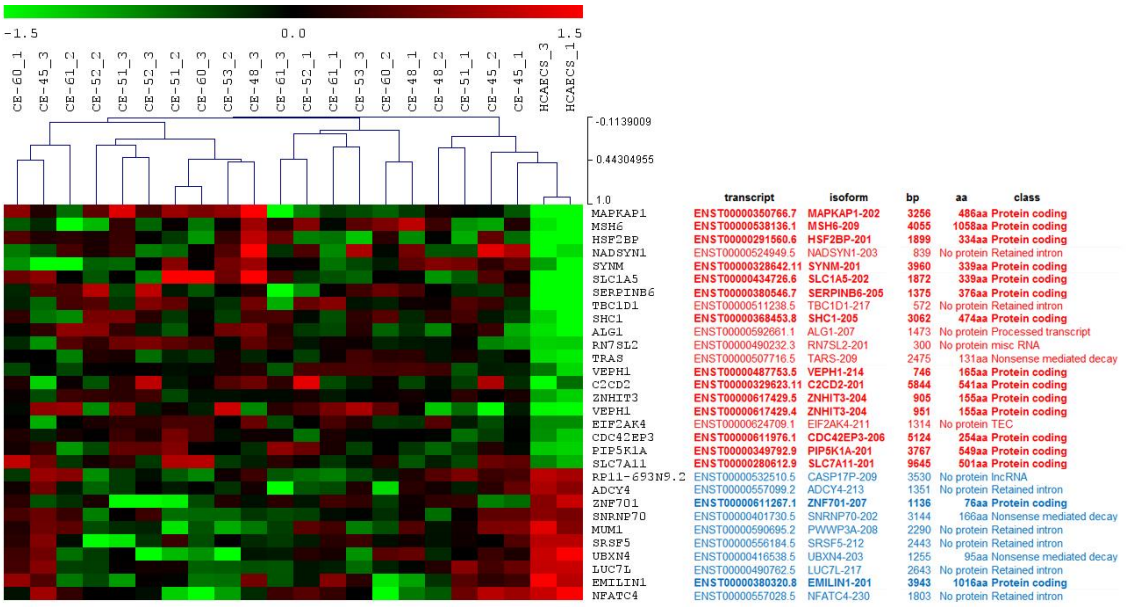

Figure 4.1.18: **Differentially expressed genes in AMI patient-derived endothelial cells vs. control cells**
Only isoforms with significantly different expression levels ($p \leq 0.05$) are shown. Normalized log-transformed values were used for hierarchical clustering. Information is provided as to the specific transcripts represented, their ENSEMBL isoforms nomenclature, their size in bp (cDNA) and predicted aa length (protein), and whether they are coding or not.

We noted that many of the down-regulated transcripts, but much fewer of those upregulated, in patient-derived cells corresponded to non-coding forms (Figure 4.1.18), in particular as retained introns (RI) (the analysis included many more transcripts than illustrated in (Figure 4.1.18) data not shown). To determine the extent of this phenomenon, we resorted to an overall search for RI in the entire analyzed transcriptomes using IRFinder (https://github.com/williamritchie/IRFinder; Middleton et al. Genome Biol2017; 18: 51). As can be seen, the transcripts in patient-derived cell lines vs. control cells fall into 3 discreet clusters, with RI scores considerably higher, considerably lower, and closer to control cells (Figure 4.1.19).

Except for CE-45 cells, the median IR ratios were significantly lower in all other patient-derived endothelial cells ($p < 0.001$, Wilcoxon Signed Rank Test). Therefore, patient-derived cells have clearly different alternative splicing activities as compared to control cells, specifically those that result in retained introns. A low IR ratio for a particular transcript indicates more efficient splicing for that transcript. The observed trend for a significant number of transcripts in patient-derived to have lower IR ratios

suggests that the splicing machinery is generally more efficient in patient-derived cells than in control cells.

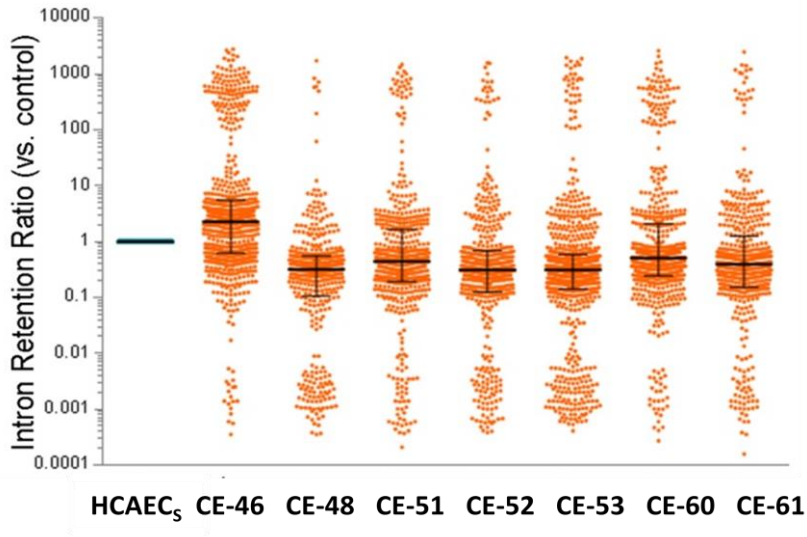

Figure 4.1.19: **Intron retention ratios in control vs. AMI patient-derived endothelial cells**
Normalized RNAseqcounts were submitted to analysis for IR scores and the resulting scores for each individual transcript in patient-derived cells were normalized relative to the IR scores for the corresponding transcripts in control cells. Each dot on the graph represents the IR ratio for an individual transcript. Horizontal lines mark the median values, and vertical bars denote the corresponding interquartile ranges. All pairwise comparisons of median values for IR ratios between control and patients-derived samples were significant ($p < 0,0001$, Wilcoxon Signed Rank Test).

Intron retention is a mode of posttranscriptional gene regulation conserved through phylogeny (Braunschweig et al. 2014) with important functions in development, lineage differentiation and responses to environmental stress(Jacob and Smith 2017). Transcripts with retained introns are “non-productive”, as they are not translated, and they may be degraded through nonsense-mediated decay or retained in the nucleus. Depending on the particular lineage, IR can be increased or decreased during differentiation. In cancer, IR is frequently, although not invariably, enhanced in malignant *vs*. normal cells, and along with malignant progression (Jung et al. 2015; Koh et al. 2015). Very few examples of differential intron retention have been described in association with endothelial cell physiology of pathology (Blanco and Bernabeu 2011). Our finding of global shifts in IR frequency in AMI patient-derived endothelial cells is unprecedented and warrants further investigation, as it suggests a

hitherto an unknown abnormality in a fundamental biochemical process in association with endothelial dysfunction in AMI.

4.1.2.1.13 Transcriptional profiling unveils additional factors potentially involved in the phenotypes of AMI patient-derived endothelial cells

Among the list of genes with an increase in expression detected in all patients, **Adenylate kinase 4** (**AK4**) (Figure 4.1.20) stands out because of its relationship to the different pathways studied in this work and its implication in oxidative stress.

During metabolic stress, AMP-activated protein kinase (AMPK) is activated by detecting a decrease in the ratio of ATP to AMP, leading to the inhibition of ATP-consuming metabolic pathways and activation of energy-producing pathways (Hardie 2011). The adenylate kinases (AKs) are nucleotide phosphotransferases, which catalyze the generation of two molecules of ADP by transferring a phosphate group from one molecule of ATP (or GTP) to AMP, to maintain energy homeostasis (Jan et al. 2019). AK4, in particular, is localized in the mitochondrial matrix (Noma et al. 2001) and binds to mitochondrial ADP/ATP translocase (ANT) as a mechanism to maintain cell survival in response to stress (Liu et al. 2009). Overexpression of AK4 inactivates metabolic adaptation toward increased intracellular oxidative stress and antioxidant capacity at the same time, and, in endothelial cells, subsequently promotes endothelial-to-mesenchymal transition in a HIF-1α-dependent manner (as AK4 stabilizes HIF 1 α) (Jan et al. 2019).

Based on our observations and considering the evidence found in literature, we speculate that upregulation of AK4 in AMI patient-derived endothelial cells (Figure 4.1.20) may play a role in the phenotypes observed in our cells, as its expression correlates with genes that regulate glycolysis, gluconeogenesis, and glutathione metabolism, and oxidative stress responses.

STK25 is a serine/threonine kinase that is activated in response to environmental stress, including oxidative stress and endoplasmic reticulum stress (or unfolded protein response, UPR) (Cansby et al. 2018). It localizes in the Golgi apparatus, where it regulates protein transport events and at the plasma membrane, where it regulates

cell adhesion and polarity complexes important for cell migration. Its overexpression in patient-derived endothelial cells (Figure 4.1.20) could be associated with the observed impairment in tubulogenesis and migration. Additionally, STK25 has been recently identified as a critical regulator of ectopic lipid storage in non-adipose tissue and systemic insulin resistance (Cansby et al. 2018). We speculate that this may be linked to low glucose uptake, i.e., similar to insulin resistance, observed in the majority of our patient-derived cells.

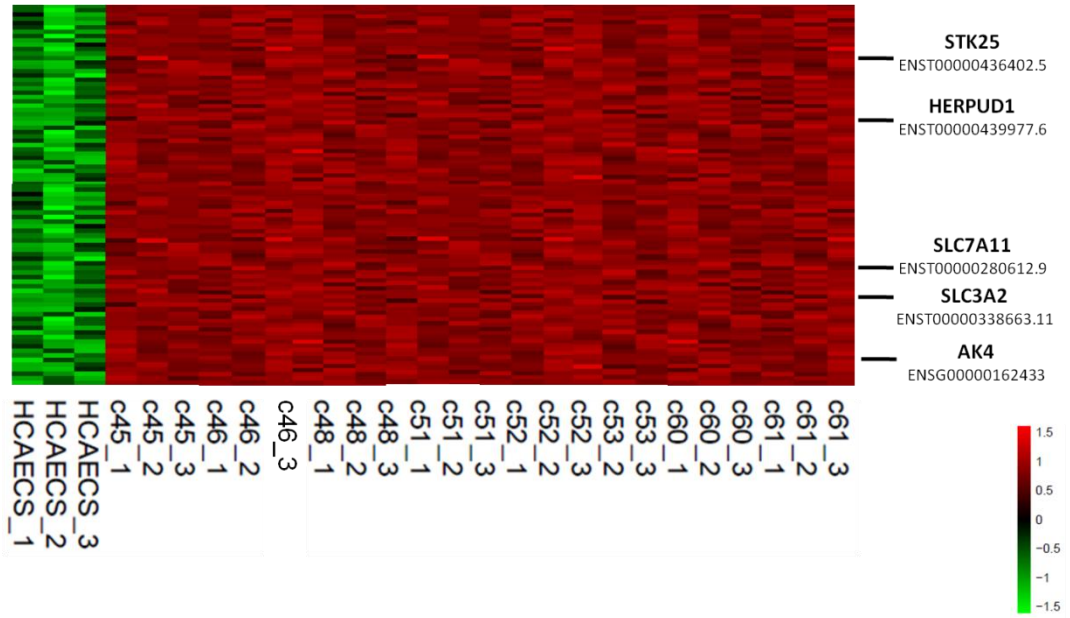

Figure 4.1.20: **Transcriptomic analysis by Rna-Seq of patients-derived cells vs. control cells**
Heatmap of differential gene expression. Relative positions of the selected genes are indicated on the right.

HERPUD1 (homocysteine and ER stress-induced protein with a ubiquitin domain 1), also overexpressed in patient-derived cells (Figure 4.1.20), is an ER-localized protein that contributes to ER homeostasis by participating in the ER-associated protein degradation pathway (ERAD) (Ho and Chan 2015). The expression of HERPUD 1 is induced by increased levels of homocysteine and in response to ER stress. This response is dependent on NRF1, an isoform of NRF2, implicated in homocystinuria-associated atherogenesis. Homocystinuria is a disorder of methionine metabolism that leads to an abnormal accumulation of homocysteine and its metabolites,

homocystine and homocysteine-cysteine complexes. The coordinated overexpression of HERPUD 1 and STK25 might be proposed as a future biomarker for the early identification of the AMI.

Of note, the overexpression of HERPUD1 in our patient cells is concomitant with the overexpression of **SLC7A11** and **SLC3A2**, encoding the two chains of the cystine/glutamate antiporter Xc^- system (see section 4.1.2.1.9), and also with the increased levels of intracellular cysteine (Figure 4.1.14, section 4.1.2.1.9).

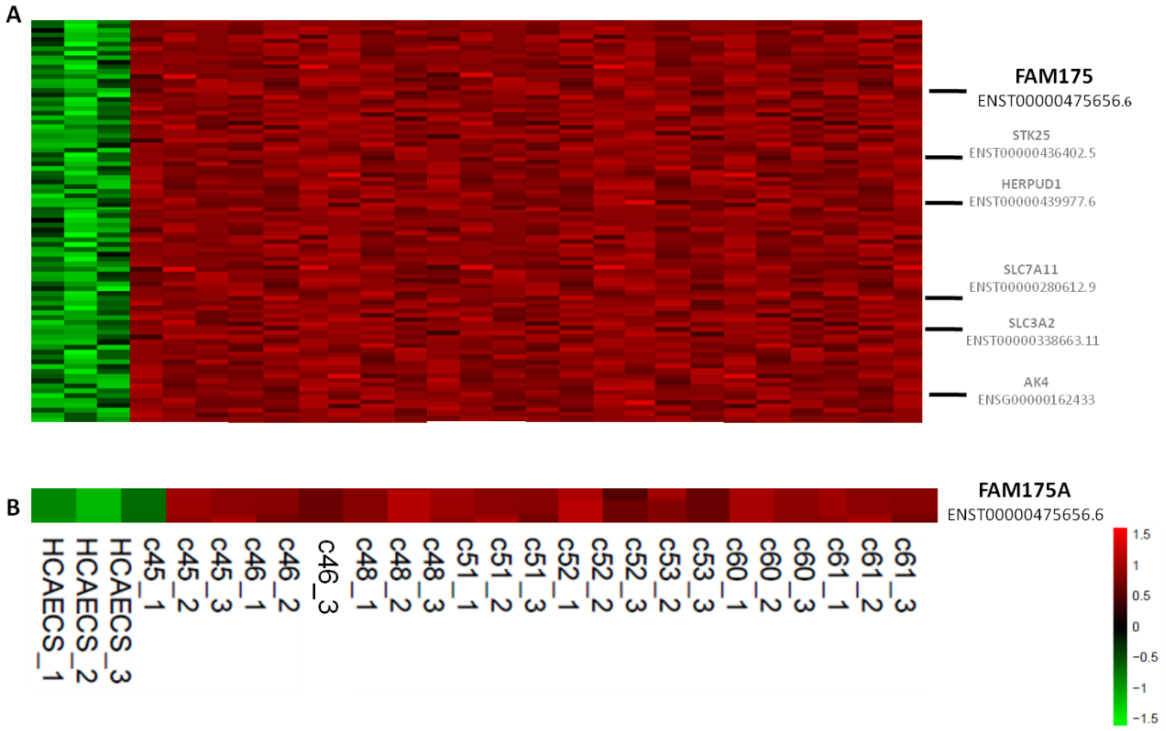

Figure 4.1.21: **Heatmap of differential gene expression of AMI patients versus HCAECs control cells**
(A) Over-expression of some genes related to alternative splicing and EMT (or Endo-MT) processes. Relative positions of selected genes are indicated on the right. (B) FAM175 gene expression (encoding for ABRAXAS).

In consonance with the shift in alternative splicing observed in patient-derived cells, as described in the preceding section 4.1.2.1.12, we found differential expression of alternatively spliced isoforms between patient-derived and control cells, that may have also participated in the observed phenotypes. We will discuss one example, namely FAM175A (Figure 4.1.21).

Isoforms of **FAM175A** are differentially expressed between patient-derived and control cells. This gene encodes ABRAXAS-1, a protein that binds to the C-terminal repeats of breast cancer 1 (BRCA1) through a phospho-SXXF motif, and is a core component of the BRCA1-A complex. This complex is recruited to DNA damage sites by Ubiquitin interaction motif containing 1 (UIMC1, or RAP80) and it is a major executor of homology-directed DNA repair (HDR) (Pellagatti et al. 2018).

Patient-derived cells express an isoform of FAM175A expected to encode a functional ABRAXAS-1 protein, whereas control cells express a non-coding isoform. This suggests that the BRCA1-A complex is more abundant in patient-derived cells than in control cells. Since this complex is induced upon DNA damage, it is plausible that patient-derived cells may be undergoing endogenous processes that lead to DNA damage, such as replication or transcriptional stress.

We have shown in a previous section (4.1.2.1.6) that patient-derived cells have a more active PPP than control cells, which should lead to higher levels of reducing equivalents and also nucleotide precursors. However, patient-derived cells grow significantly slower than control cells, and thus there is no apparent need for increased synthesis of nucleotides for growth. Nucleotide synthesis, however, is also required for DNA repair under different modalities. DNA can be damaged by ROS, as has been shown in atherosclerosis (Shah and Mahmoudi 2015). Our AMI patient-derived endothelial cells are under oxidative stress, are slow growers, and have very active oxidative PPP. The combined phenotype is compatible with ongoing DNA damage and thus with the expression of DNA repair systems. Based on these considerations, we are keen to explore in the future the DNA damage and repair status of our AMI patient-derived endothelial cells.

Chapter 4.2

Alternative splicing in cell models of epithelial-mesenchymal transition

4.1.3 Introduction

The previous observations, described in Chapter 4.1, indicate a profound metabolic reprogramming in AMI patient-derived endothelial cells. This suggests the occurrence of a broad and complex dysfunction in these cells, that should be reflected in global processes. We thus proceeded to study this event, by means of transcriptomic profiling by RNAseq finding an anomalous transcriptional pattern common to all patient-derived cells displaying shared phenotypes.

This finding indicates a broad shift in AS, which is a major mechanism governing differentiation, development or responses to environmental cues in many cell types and tissues (Nakka et al. 2018). That alternative splicing reprogramming may also be associated with endothelial dysfunction was not previously known, while it has been already described to be linked to cancer progression and metastasis development. For this reason, in Chapter 4.2 we focused on the relevance of AS in the regulation of specific phenotypes in cancer cell models, to unveil possible shared events among different pathologies like endothelial dysfunction and cancer.

Alternative splicing (AS) governs cell-type, lineage-specific, or environmentally regulated expression of variant forms of mRNAs and their encoded proteins that exert differential functions specifically and exquisitely adapted to a particular cellular context. During alternative splicing, non-coding sequences are removed, through a combination of events (splicing sites, exonic or intronic sequences, mutually exclusive exons or retained introns) to create different mature messenger RNAs or isoforms, and generate a diversity of protein products (Martinez-Montiel, Hilda Rosas-Murrieta, et al. 2018). In recent years, numerous genomic and transcriptomic studies have allowed collecting a wealth of information about the general implications of alternative splicing events in cell physiology and different pathologies (Jurica and Moore 2003).

Because 90% of human gene expression is regulated by alternative splicing, coordinately affecting the expression of specific sets of proteins and thus biochemical pathways and biological functions, disease-associated isoform patterns have gained attention as drivers, hallmarks and potential therapeutic targets for several diseases, in particular for cancers (Martinez-Montiel, Rosas-Murrieta, et al. 2018). In the present study, we have identified alternatively spliced mRNAs with potential impact on the self-renewal capacities of cancer cell subpopulations by employing a prostate cancer cell model in which distinct tumor cell subpopulations display clearly differentiated epithelial or mesenchymal phenotypes and gene programs.

These cellular subpopulations cooperate in order to make a solid tumor more aggressive and malignant. The first cell line (PC-3/Mc) is highly proliferative, presenting a marked glycolytic Warburg effect and a strong metastatic potential. The second cell line (PC-3/S) displays an opposite phenotype: a robust invasive capacity with low metastatic potential and a low rate of growth, deriving its ATP mainly from oxidative phosphorylation (Aguilar et al. 2016; Celià-Terrassa et al. 2012).

We set out to search for factors regulated by the AS regulator ESRP1/2 (Fici et al. 2017; Warzecha et al. 2009) that may determine the growth characteristics of these cells. This was approached by applying RNA-seq followed by an analysis of mRNA isoforms differentially expressed between the two subpopulations, modified by expression of ESRP1 and/or ESRP2. This has led us to discover that mRNAs for RAP80 (gene symbol

UIMC1), an adaptor protein that recruits BRCA1 to sites of DNA damage, are expressed as either predominantly epithelial or predominantly mesenchymal isoforms and that these isoforms switch their expression in epithelial or mesenchymal cells as a function of expression of ESRP1/2.Given the importance of BRCA1 in breast cancer, we also performed extensive analyses to determine the relevance of these specific alternatively spliced RAP80 isoforms in breast cancer progression.

4.1.4 Results and Discussion:

4.1.4.1 ESRP1/2 expression confers epithelial traits and growth advantage to prostate cancer cells

The dual cellular model constituted by the clonal subpopulations PC-3/Mc and PC-3/S, derived from the prostate cancer cell line PC-3, display two opposite phenotypes in which PC-3/Mc cells are strongly epithelial, highly proliferative and metastatic while PC-3/S cells present traits of a stable epithelial-mesenchymal transition, proliferate at a low rate and are poorly metastatic (Celià-Terrassa et al. 2012). We noted, through previous results obtained in our lab, that the AS regulator ESRP1 and its paralog ESRP2 were among the most strongly differentially expressed genes distinguishing these two cell types (Figure 4.2.1).

ESRP1/2 regulates AS of target transcripts that are differentially expressed in epithelial or mesenchymal plastic states and play a significant role in epithelial-mesenchymal transition (Dittmar et al. 2012; Warzecha et al. 2009). As previously introduced, alternative splicing regulates gene programs through the expression of variant forms of genes and proteins that display different functions depending on the inclusion or exclusion of functional protein domains in the various forms resulting from this splicing event (Warzecha et al. 2009). In order to explore phenotypes of interest regulated by ESRP1/2 in our cell model, we over-expressed these splicing regulators in PC-3/S cells (see protocol details in Appendix1) which express low endogenous levels of these genes (Figure. 4.2.2 A, B).

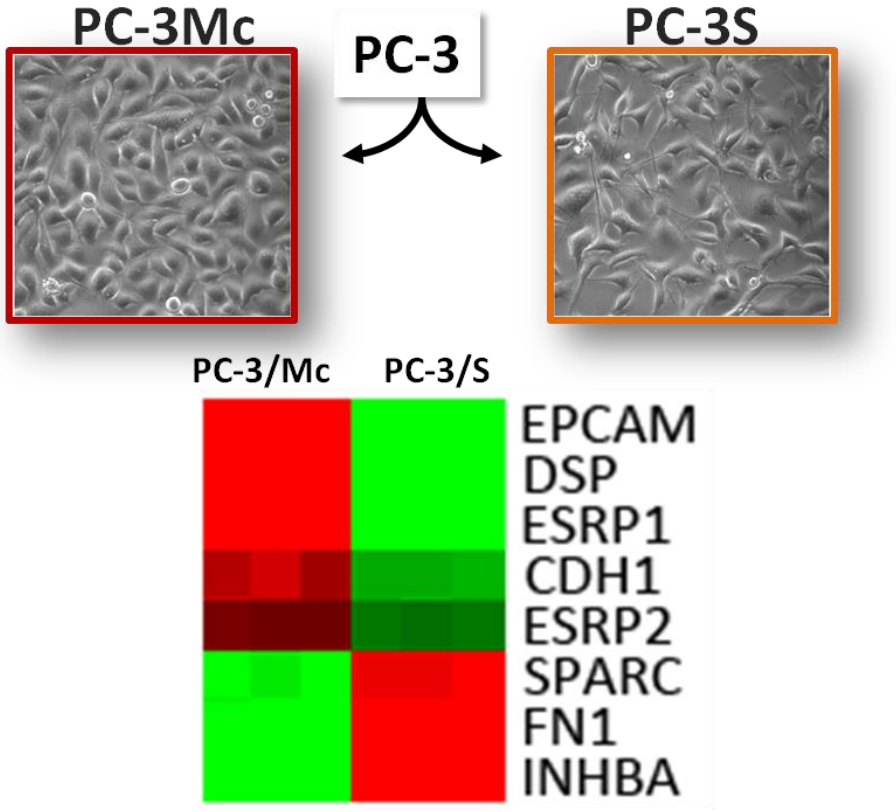

Figure 4.2.1: **A dual cellular model constituted by two clonal subpopulations PC-3/Mc and PC-3/S**
(A) Bright field images (microscope 10x) showing PC-3/Mc (on left) and PC-3/S (on right) phenotype ,(B) Differential expression of ESRP1/2 in epithelial (PC-3/Mc) *vs*. mesenchymal (PC-3/S) clonal PC-3 subpopulations.

PCR-amplified ESRP1 and 2 cDNAs were cloned into the retroviral vector pBABE-puro and the resulting constructs (pBabe-ESRP1 and pBabe ESRP2) used to produce retroviral particles to be tranduced into PC-3/S cells, generating PC-3/S.oeESRP1 and PC-3/S.oeESRP2 variant cell lines (Figure 4.2.2C-F).

In parallel, expression of ESRP1 or ESPR2 was stably silenced in PC-3/Mc cells by means of lentiviral transduction of specific shRNAs, generating the PC-3/Mc.kdESRP1 and PC-3/Mc.kdESRP2 variants (Figure 4.2.2D-F) (see protocol details in Appendix1). All the PC-3/Mc and PC-3/S cells variants produced were selected with puromycin (1µg/mL), as both vectors used contains a puromycin resistance gene.

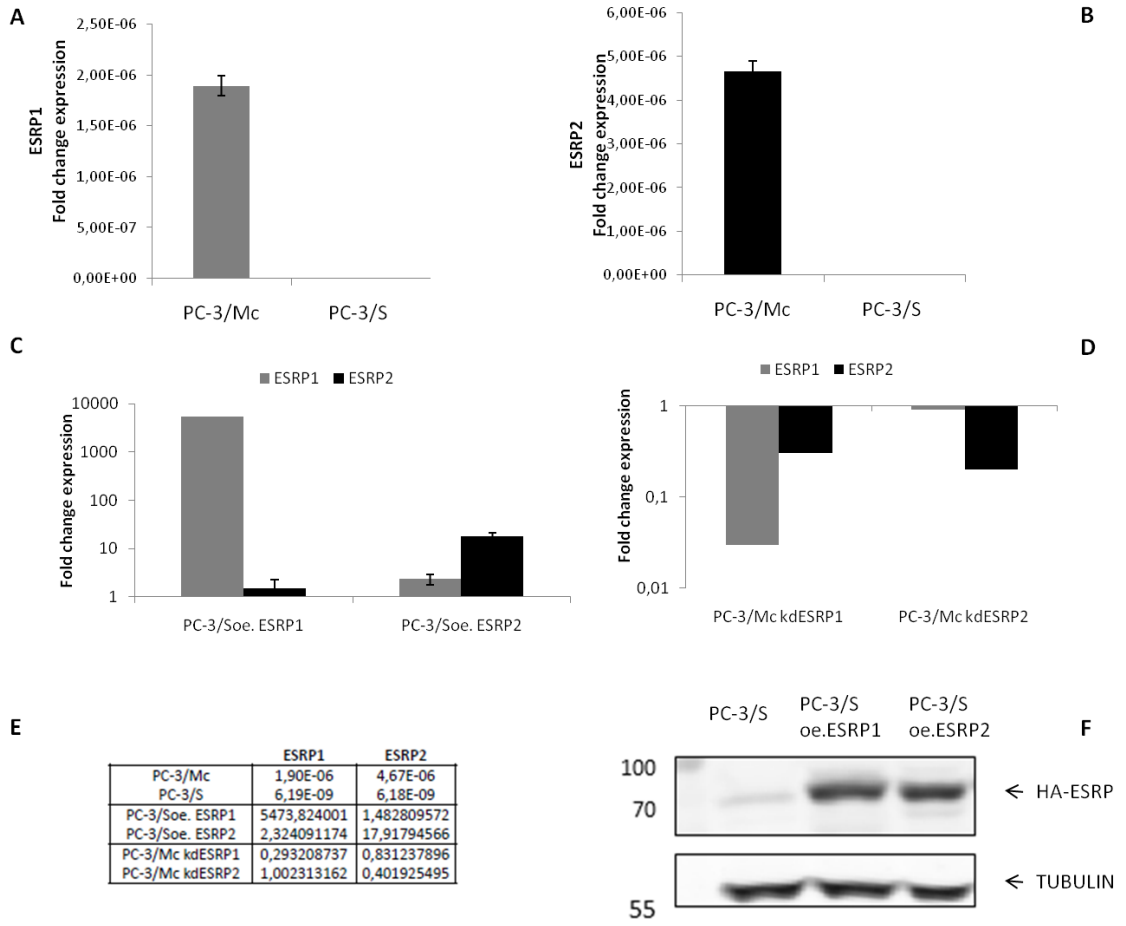

	ESRP1	ESRP2
PC-3/Mc	1,90E-06	4,67E-06
PC-3/S	6,19E-09	6,18E-09
PC-3/Soe. ESRP1	5473,824001	1,482809572
PC-3/Soe. ESRP2	2,324091174	17,91794566
PC-3/Mc kdESRP1	0,293208737	0,831237896
PC-3/Mc kdESRP2	1,002313162	0,401925495

Figure 4.2.2: **Identification of the intrinsic level of ESRP1 and ESRP2 genes in PC-3/M and PC-3S**
(A) Gene expression levels of ESRP1 and ESRP2 through qPCR in PC-3/Mc and in (B) PC-3/S. (C) Determination of ESRP1 and ESRP1 gene-level after over-expression in PC/3S, to generate PC-3/Soe.ESRP1 and PC-3/Soe.ESRP2. (D) ESRP1 and ESRP2 stable silencing produced in PC-3/MckdESRP1 and PC-3/MckdESRP2 has been measured through qPCR. (E) 2exp level gene expression level in PC-3/Mc and PC-/3S and variants. (F) ESRP1 and ESRP2 overexpression in PC-3/Soe ESRP1 and in PC-3/Soe.ESRP2 has also been confirmed by Western Blotting. The bars correspond to mean ±SD of n =3.

Seeking to determine if the expression of ESRP1/2 contributes to a shift to a more epithelial-like phenotype, the expression levels of epithelial and mesenchymal markers were determined by qPCR. Indeed, over-expression of ESRP1 or ESRP2 in PC-3/S cells caused a modest but significant upregulation of the epithelial hallmark genes E-cadherin (CDH1), EpCAM and desmoplakin (DSP) (Figure 4.2.3B, C). Conversely, knockdown of the same target transcripts in PC-3/Mc cells was accompanied by the downregulation of these three genes (Figure 4.2.3 A, B).

A

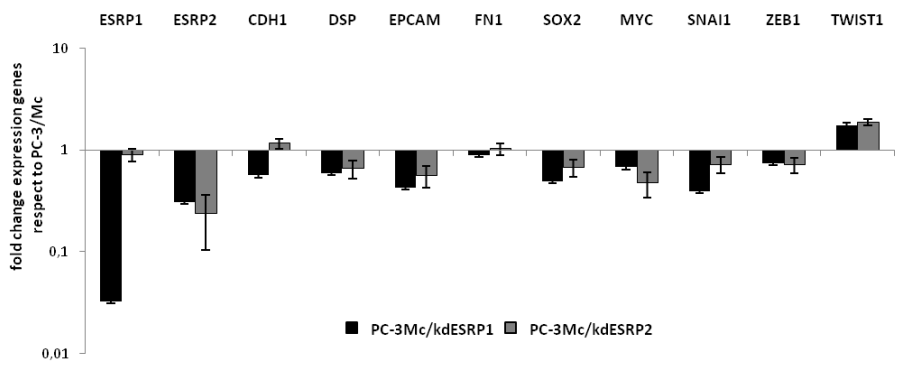

B

	ESRP1	ESRP2	CDH1	DSP	EPCAM	FN1	SOX2	MYC	SNAI1	ZEB1	TWIST1
PC-3/MckdESRP1	0,03272	0,30992	0,56644	0,60151	0,42928	0,89502	0,49540	0,68223	0,39868	0,74742	1,77358
PC-3/MckdESRP2	0,90125	0,23542	1,16204	0,66051	0,56252	1,02574	0,67595	0,47521	0,72196	0,71863	1,87470
PC-3/S oe.ESRP1	6368,18	1,64338	3,44220	6,53566	1,82344	0,75873	1,26137	1,23684	1,38991	0,95594	0,31864
PC-3/S oe.ESRP2	1,32868	30,09948	2,48802	2,29209	1,31950	0,79922	1,36288	0,81507	0,82169	0,66128	0,62778

C

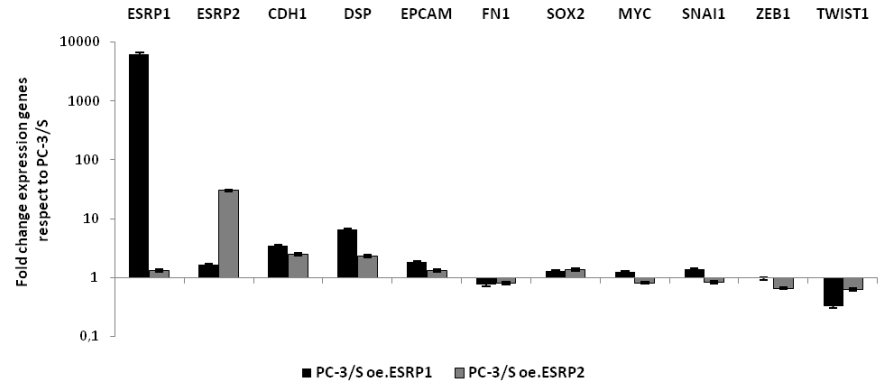

Figure 4.2.3: **Study of the expression level of selected genes in PC-3/MkdESRP1 PC-3/MckdESRP1 respect to PC-3/M, and PC-3/S oe.ESRP1, PC-3/Soe.ESRP2 respect to PC-3/S**

(A) A study by qPCR of the change in expression of EMT markers (ESRP1/2, SNAI1, ZEB1, TWIST1), Self-renewal gene (SOX-2, MYC), Epithelial markers (CDH-1, EPCAM, DSP), Mesenchymal marker (FN1) in PC-3/Mc stable knock-down variants for ESRP1-2 vs. PC- 3/M. (**B**) The expression level of the same genes has been identified for PC-3/Soe.ESRP1 and PC-3/Soe.ESRP2 vs. PC-3/S. Results are expressed as 2exp level gene expression values of the variants respect to PC-3/M and PC-3/S. The bars correspond to mean ±SD of n = 3.

CDH1 is a gene that encodes for the subtype of the cadherin protein of adhesion expressed by cells with an epithelial phenotype. It is involved in regulating cell polarity, differentiation, and migration and behaves as a tumor suppressor gene (Serrano-Gomez, Maziveyi, and Alahari 2016). The extracellular E-cadherin binds to cadherins of the contiguous cells creating a connection among the cytoskeletons (Baranwal and Alahari 2009). **Desmoplakin** is another cell-cell contact protein considered an epithelial marker that is downregulated upon EMT (Serrano-Gomez, Maziveyi, and Alahari 2016). The epithelial cell adhesion molecule (**EpCam** or CD326), another hallmark of epithelial

phenotypes, is involved in cell-to-cell adhesion, cell differentiation and migration (Trzpis et al. 2007).

Fibronectin (FN1) is one of the most representative mesenchymal markers, consistently up-regulated during EMT. FN1 is a component of the mammary mesenchymal compartment, and it is associated with an invasive and metastatic cancer phenotype (Li et al. 2017).

Zinc finger E-Box-binding homeobox 1 (**ZEB1**) is a major effector of EMT, through which it promotes invasive properties and tumor progression (Orellana-Serradell et al. 2018). **CD44** is a transmembrane glycoprotein expressed as multiple isoforms regulated by the splicing activities of ESRP1 and 2. Cells with an epithelial phenotype express the epithelial splice isoform of CD44v (variant CD44), while the cells with a mesenchymal-like phenotype express the mesenchymal isoform of CD44s (standard CD44) (Chen et al. 2018).

Western blotting analyses indicated an upregulation of E-cadherin and downregulation of FN1 and the EMT factor ZEB1 in PC-3/S upon expression of ESRP1 or ESRP2 (Figure. 4.2.4). We also observed the appearance of CD44v, the epithelial isoform of CD44, in addition to the CD44s mesenchymal isoform (Figure.4.2.4), thus confirming the expected function of ESRP1/2 as a splicing regulator for CD44. These data also indicate that the expression of ESRP1 or ESRP2 in our cell model sustains an epithelial gene program.

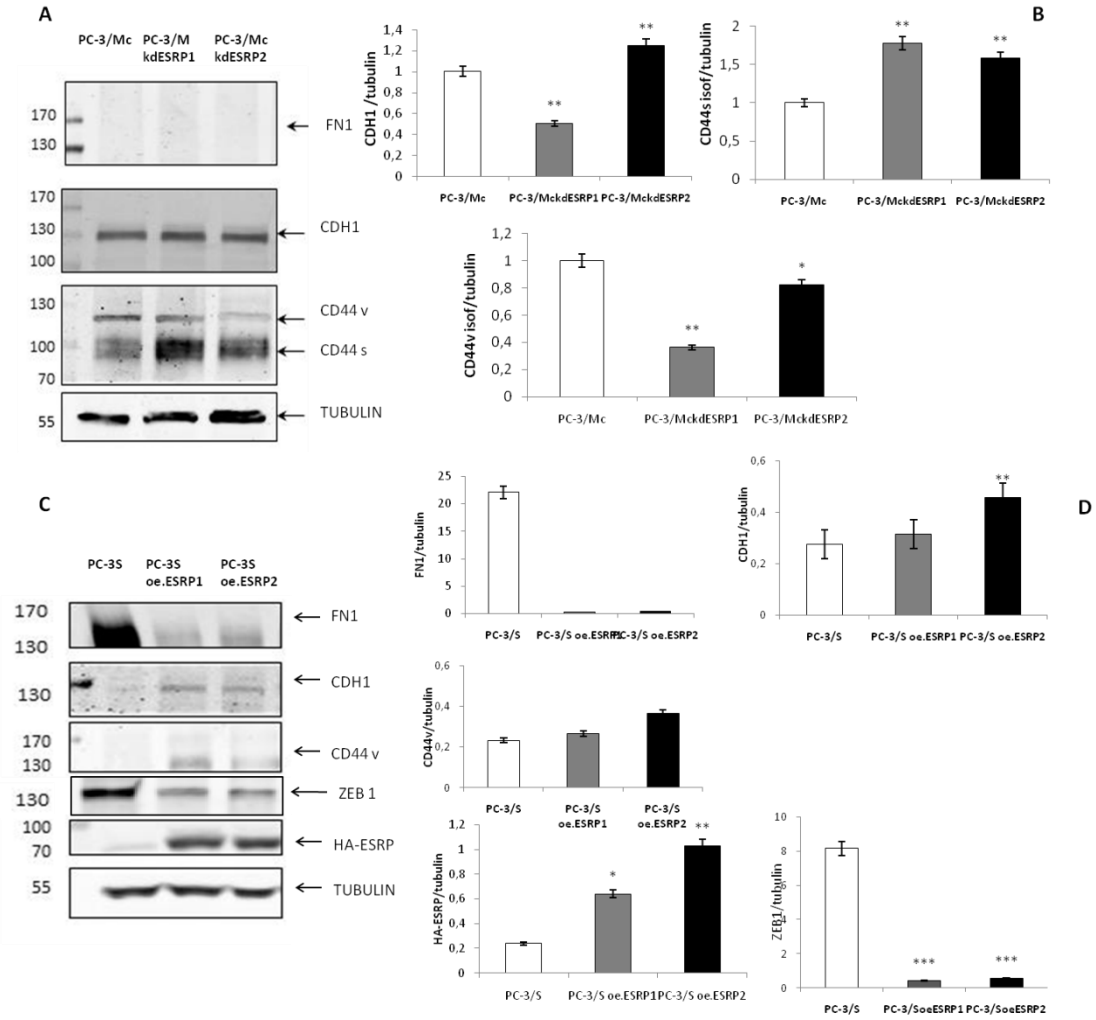

Figure 4.2.4: **Phonotypical characterization of ESRP1 and ESRP2 knockdown and over-expression variants**

(A, C) Determination by Western Blotting of protein levels of EMT markers (ESRP1/2, CD44 v/s, ZEB1), epithelial markers (CDH-1), mesenchymal marker (FN1) in PC-3/Mc stable knock-down variants and in PC/3S over-expressed variants. (B, D) Proteins bands have been quantified by the Image-J program and compared to tubulin as a loading control. The bars correspond to mean ±SD of n =3 Significance was determined for PC-3/MkdESRP1 PC-3/MckdESRP1 versus PC-3/M, and PC-3/S oe.ESRP1, PC-3/SoeESRP2 vs. PC-3/S *$p < 0,05$, **$p < 0,01$ and ***$p < 0,001$.

Phenotypically, knockdown of ESRP1/2 in PC-3/Mc cells did not affect their invasive potential in Matrigel-Transwell assays, while overexpression of ESRP1 or ESRP2 significantly diminished the invasiveness of PC-3/S cells (Figure 4.2.5 A and B), supporting that the expression of ESRP1/2 imparts a mesenchymal-to-epithelial switch in these cells. Likewise, knockdown of ESRP1 or ESRP2 in PC-3/Mc cells did not significantly affect their growth in either adherent or non-adherent conditions (Figure 4.2.5 C and E).

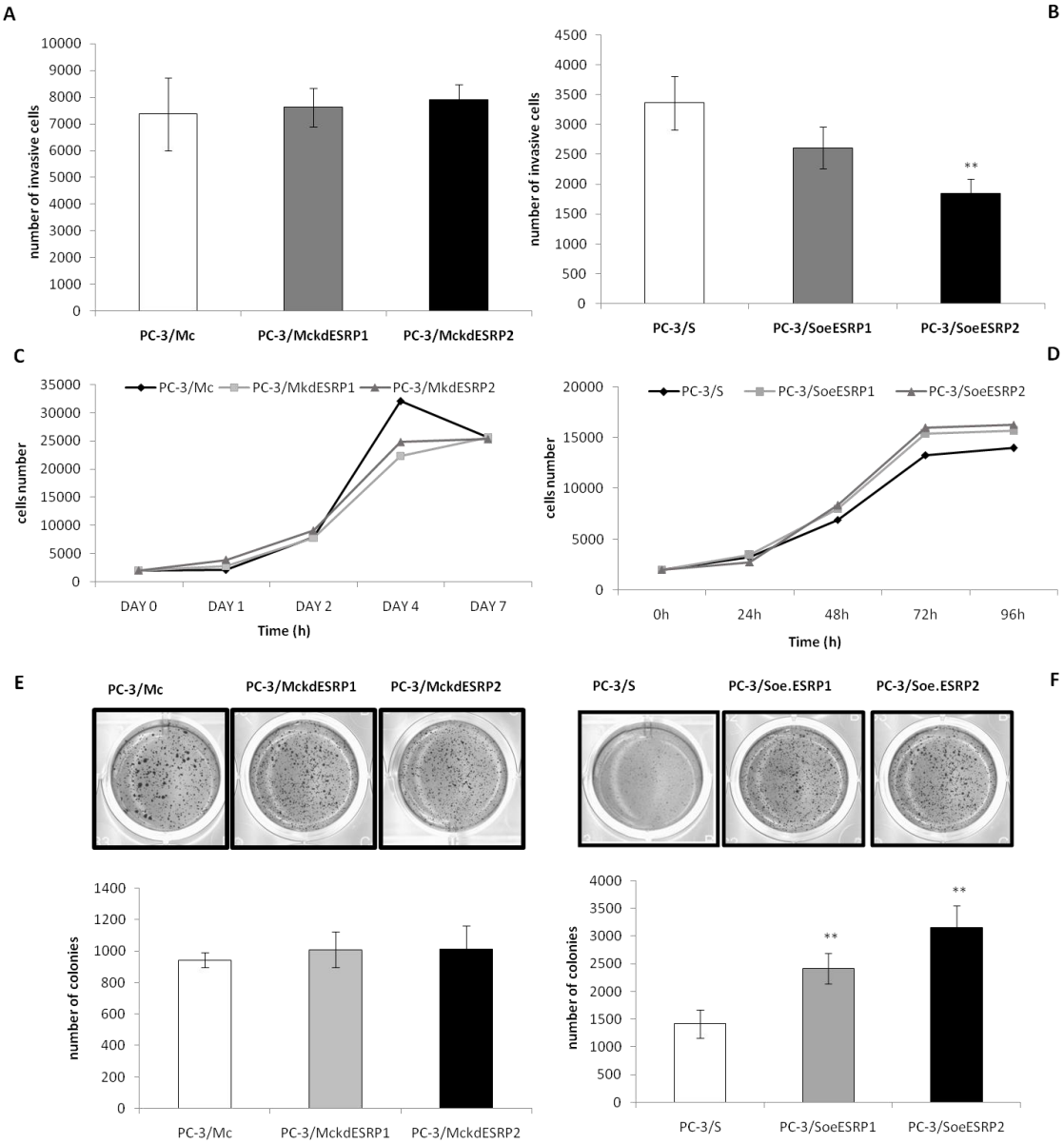

Figure 4.2.5: **ESRP1/2 silencing effects on invasion ability and growth capacity, in adherent and anchorage-independent condition, of PC-3/MkdESRP1 and PC-3/MkdESRP2 vs. PC-3/M and PC-3/Soe.ESRP1 and PC-3/Soe.ESRP2 vs. PC-3/S**

(A) Invasion ability of PC-3/Mc and (B) PC-3/S variants respect to PC-3/Mc, and PC-3/S has been measured by transwell assay showing impairment in the presence of ESRP1/2 deletion and an increase when ESRP1/2 are overexpressed. (C) No changes in proliferation ability have been identified in PC-3/McshESRP1 and 2 (D) while an increase in the proliferation of PC-3/S ESRP1 and 2 variants has been detected. (E) The knockdown of ESRP1/2 does not affect the growth of PC-3/Mc variants in non-adherent conditions, studied through the soft agar method. (F) Overexpression of ESRPs genes in PC-3/S variants enhanced this ability. Significance was determined for PC-3/Mc variants vs. PC-3/Mc, and variant cell lines vs. PC-3/S vs. PC-3/S The bars correspond to mean ±SD of n = 4.*p < 0,05 **p < 0,01 and ***p < 0,001.

In contrast, expression of ESRP1 or ESRP2 strongly promoted the growth of PC-3/S cells in adherent conditions (Figure 4.2.5D) and also significantly enhanced the growth of PC-

3/S cells under non-adherent conditions, determined by the soft agar method (Figure. 4.2.5 F).

4.1.4.2 Differentially expressed isoforms associated with ESRP1/2 expression

Prior studies in our lab have shown that PC-3/Mc cells owe their robust *in vitro* and *in vivo* growth properties to the expression of an epithelial gene program (Celià-Terrassa et al. 2012; Mateo et al. 2014). The above results suggested that part of the gain in anchorage-independent growth conferred to PC-3/S through an epithelial gene program is exerted by ESRP1/2, subsequently resulting in the expression of epithelial-preferred isoforms of regulators of anchorage-independent growth.

To test this hypothesis, we performed RNA-seq analysis to identify transcript isoforms associated with the expression of ESRP1 or ESRP2 in PC-3/Mc, PC-3/S, PC-3/S.oeESRP1, and PC-3/S.oeESRP2 cells. The following pairwise comparisons: PC-3/Mc.pBabe *vs*. PC-3/S.pBabe; PC-3/S.pBabe *vs*. PC-3/S.oeESRP1; and PC-3/S.pBabe *vs*. PC-3/S.oeESRP2 (pBabe being the "empty" control vector) were analyzed to identify genes showing differential expression of isoforms, such that a set of isoforms were up-regulated in one cell and the second set of isoforms of the same gene were down-regulated in that cell, as compared to the matched control cell.

In the PC-3/Mc.pBabe *vs*. PC-3/S.pBabe comparison, 2,210 genes fulfilled the differential isoform expression patterns as defined above, 2,017 in the PC-3/S.oeESRP1 *vs*. PC-3/S.pBabe comparison and 2,058 in the PC-3/S.oeESRP2 *vs*. PC-3/S.pBabe comparison. Of these, a set of 764 genes was common to all three pairwise comparisons, including the well-characterized ESRP1/2 AS substrates CD44 and FGFR1. FGFR1 is a fibroblast growth factor receptor, involved in cell division, cell growth, and maturation, wound healing process and formation of blood vessels (Tomlinson et al. 2012). FGF signaling is known to regulate EMT during development and in models of breast and prostate cancer, to control migration and to manage the EMT of the mesoderm by regulating E-cadherin expression (Ciruna and Rossant 2001). All modes of AS were observed in the common 764 geneset (alternative 5' donor site, alternative 3' acceptor site, retained intron, exon skipping, and mutually exclusive exons) (Figure 4.2.6).

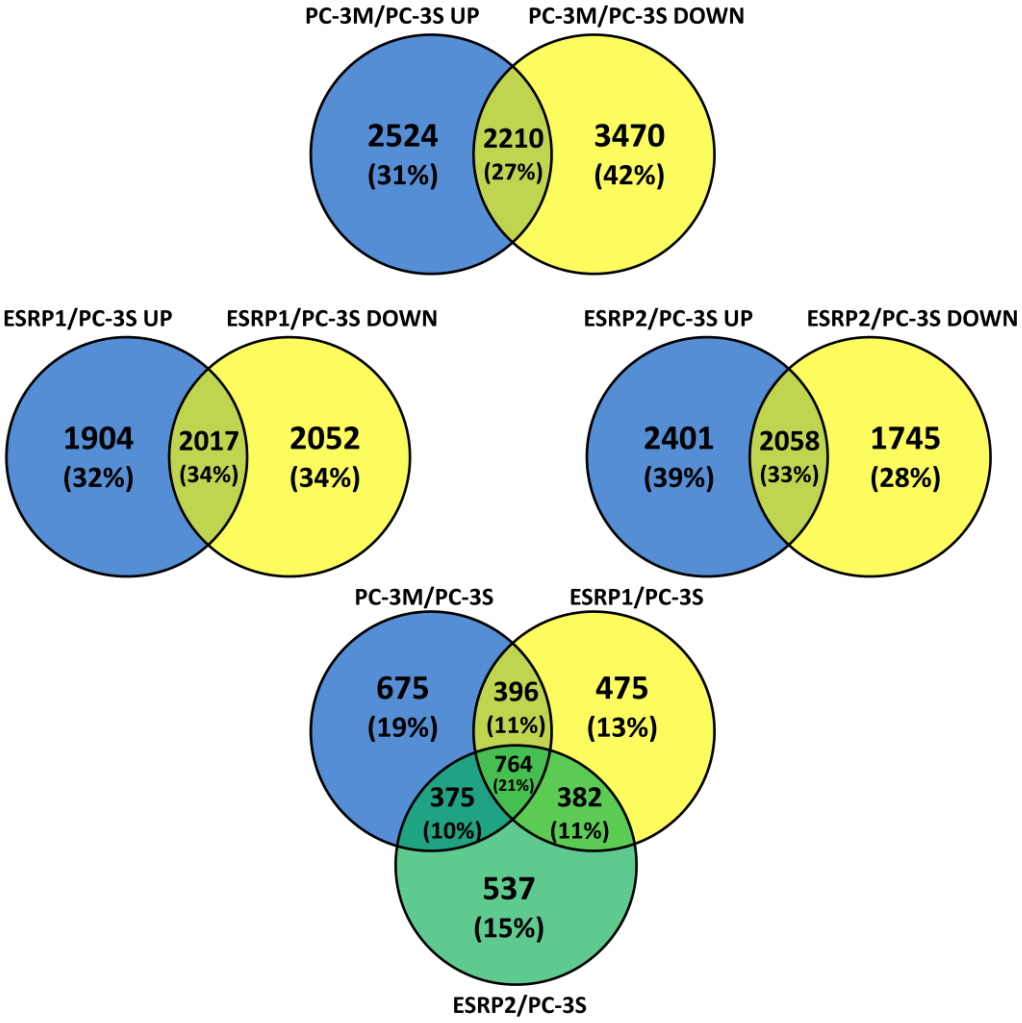

Figure 4.2.6: **Differential isoform expression patterns found in PC-3/Mc.pBabe vs. PC-3/S.pBabe, PC-3/S.oeESRP1 vs. PC-3/S.pBabe and PC-3/S.oeESRP2 vs. PC-3/S.pBabe**
Of the 764 common geneset identified, 199 presented a strong differential expression of alternative splicing isoforms (-2 ≥ $\log_2$FC ≥ 2) in the three pairwise comparisons PC-3/Mc vs PC-3/S, PC-3/SoeESRP1 vs. PC-3/S, PC-3/SoeESRP2 vs. PC-3/S of which186 (93.5%) had exon skipping events.

Of these, the most frequent were exon skipping events (see Table A2, Appendix 1). We focused our attention on the latter because they are more likely to generate protein isoforms with gains or losses of functional domains encoded by the alternatively spliced exons. At this point, we hypothesized that the differential expression of functionally distinct isoforms regulated by ESRP1/2could explains the gain in anchorage-independent growth conferred by this AS regulator in the PC-3/Mc vs. PC-3/S model. Of the 764 common geneset, 199 presented a strong differential expression of AS isoforms (-2 ≥ $\log_2$FC ≥ 2) in the three pairwise comparisons (Figure 4.2.6), of which 186 (93.5%) had exon skipping events (Figure 4.2.6).

4.1.4.3 Pathways associated with differentially expressed isoforms under ESRP1/2 regulation

In order to infer predominant pathways associated with the 764 differentially expressed isoforms, this geneset was analyzed by Gene Set Enrichment Analysis (GSEA) (Subramanian et al. 2005). Although no KEGG pathways were significantly enriched as measured by FDR, several pathways showed enrichment as per their P values and enrichment ratios. As such, the phosphonate and phosphinate metabolism had an enrichment ratio of 15.1 (P = 0,06) with only 1 gene, Phosphate Cytidylyltransferase 1, Choline, Alpha (PCYT1A), represented in the gene set; the glyoxylate and dicarboxylate pathway had an enrichment ratio of 9.0 (P = 0,004) with 3 genes, Acyl-CoA Synthetase Short chain 2 (ACSS2) one isoform of the acetyl-CoA synthetase family which has been described to be negatively correlated to metastatic processes, Propionyl CoA carboxylase β (PCCB) and Serine HydroxyMethylTransferase 2 (SHMT2), which has been recently described to be implicated in regulating BRISC complex function inDNA double-strand break repair; and the homologous recombination pathway, with an enrichment ratio of 6,6 (P = 0,01) with three genes represented in the gene set, the DNA repair/recombination protein 54L (RAD54L), which cooperates with RAD51 to promote recombinational DNA repair in multiple types of cancer, DNA topoisomerase III α (TOP3A), associated with DNA repair, cell-cycle checkpoints regulation and genomic stability, and UIMC1 (Hou et al. 2017; Li et al. 2018; Rabl et al. 2019a; Sun et al. 2017; Xu et al. 2018).

Two isoforms of ACSS2 (acyl-CoA synthetase short-chain 2) are differentially expressed in our model: ENST00000481284 (coding for a 37 aa form, predicted to undergo non-sense mediated decay), expressed at higher levels in ESPR1/2-expressing (epithelial) cells, and ENST00000484354 (147 aa), expressed in their mesenchymal counterparts. While the full-length ACCS2 contains an N-terminal acetyl-CoA synthetase activity, an AMP-dependent synthetase/ligase activity, and a C-terminal AMP-binding domain, the *mesenchymal isoform* of ACCS2 only harbors the acetyl-CoA synthetase activity, suggesting that it is not regulated by AMP.

Three isoforms of PCCB (propionyl CoA carboxylase β) are differentially expressed: ENST00000469217 (559 aa) and ENST00000478469 (303 aa) with higher levels in

epithelial cells, and ENST00000462542 (163 aa) with higher levels in mesenchymal cells. Both the 303 aa *epithelial* and the 163 aa *mesenchymal* forms contain N-terminal segments of the carboxylase domain, with different length C-terminal extensions, present in the full-length 559 aa epithelial form.

Seven isoforms of SHMT2 (serine hydroxymethyltransferase 2) are differentially expressed: ENST00000553474 (483 aa), ENST00000554975 (215 aa), ENST00000553529 (147 aa) and ENST00000553949 (non-coding) with higher levels in epithelial cells, and ENST00000555563 (86 aa, subjected to non-sense mediated decay), ENST00000553324 (non-coding), and ENST00000557740 (non-coding) with higher levels in mesenchymal cells. While the 483 aa epithelial isoform is near full-length and contains the entire pyridoxal phosphate-dependent hydroxymethyl transferase domain, the other two epithelial forms harbor partial fragments of the active domain. The mesenchymal cells in our model are not predicted to express the SHMT2 protein.

Three isoforms of RAD54L are differentially expressed: ENST00000488942 (321 aa) and ENST00000463715 (30 aa) with higher levels in epithelial cells, and ENST00000476687 (63 aa, subjected to non-sense mediated decay) with higher levels in mesenchymal cells. The 321 aa epithelial isoform is predicted to contain the C-terminal, but not the N-terminal, helicase domain of full-length RAD54L.

Three isoforms of TOP3A (DNA topoisomerase III α) are differentially expressed: ENST00000585031 (95 aa, subjected to non-sense mediated decay) with higher levels in epithelial cells, and ENST00000321105 (1001 aa, full-length) and ENST00000469739 (non-coding) with higher levels in mesenchymal cells. Thus, TOP3A is predicted to be expressed as a full-length isoform in mesenchymal, but not epithelial, cells in our model.

Three isoforms of UIMC1 (ubiquitin interaction motif containing 1, also called RAP80) are differentially expressed: UIMC1-201, ENST00000377227 (719 aa, full-length) and UIMC1-213 ENST00000512031 (161 aa, subjected to non-sense mediated decay) with higher levels in epithelial cells, and UIMC1-207, ENST00000506128 (553 aa) with higher levels in mesenchymal cells. The 719 aa full-length epithelial isoform of UIMC1 (RAP80) contains an N-terminal bipartite ubiquitin-interaction motif and a more distal Abraxas-

interaction region (AIR). The 553 aa mesenchymal isoform differs from the full-length isoform in that it contains the bipartite UIM, but lacks the AIR (Figure 4.2.7).

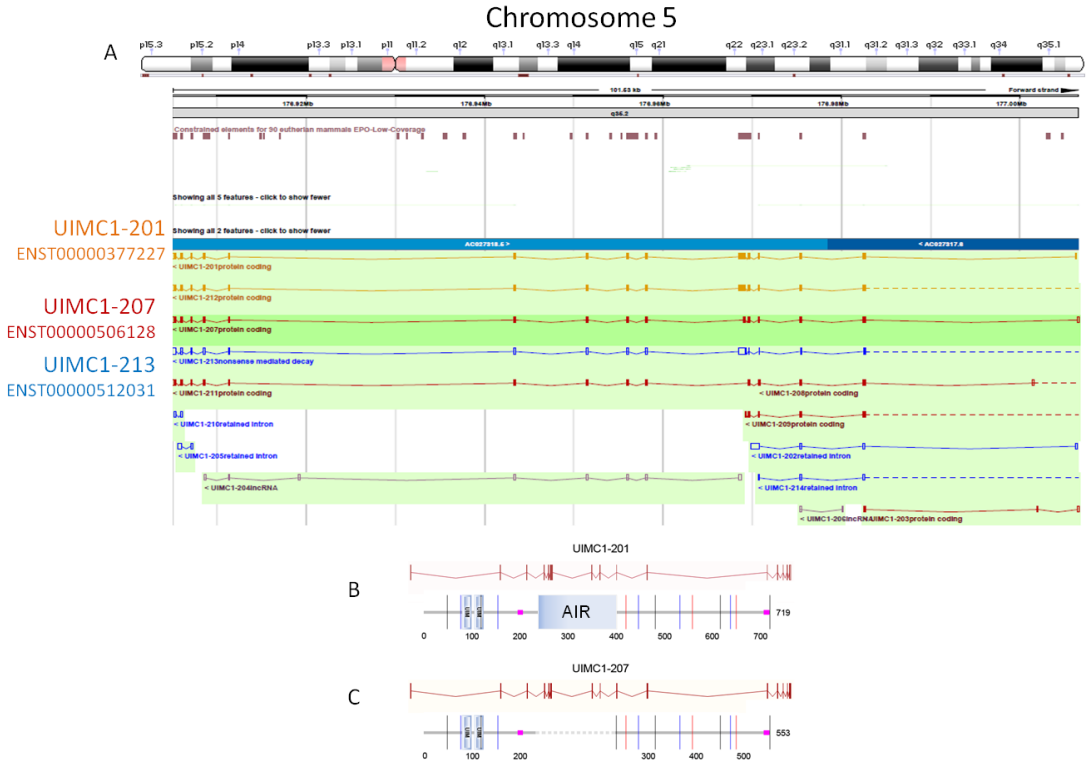

Figure 4.2.7: **UIMC1 transcript isoforms**
(A) 3 out of the 10 major UIMC1 (RAP80) transcript isoforms are differentially expressed as a function of ESRP1/2 in our cell models and represented in the figure: UIMC1-201, UIMC1-213, UIMC1-207 (B) In detail, UIMC1-201, ENST00000377227 (719 aa) full-length form, bears the functionally essential UIM (Ubiquitin Interaction Motif) and a more distal Abraxas interaction region (AIR) (C) In detail, UIMC1-207, ENST00000506128 (553 aa) encodes for the shorter version, and contains UIM but not the AIR region, and presented in higher levels in mesenchymal cells.

The RAP80 UIM serves to recognize K63-linked di-ubiquitins, notably as these chains build-up at DNA damage sites, and the AIR recruits Abraxas and the BRCA1-A complex to damage sites. Therefore, while the *epithelial isoform* of RAP80 is predicted to recruit the BRCA1-A complex to DNA damage sites, the *mesenchymal isoform* is predicted to be deficient in this function. To sum up, of the genes described above, only UIMC1 (RAP80) is differentially expressed in our model such that epithelial and mesenchymal isoforms differ by one functional domain encoded by alternatively spliced exons putatively regulated by ESRP1/2. We thus set out to interrogate RAP80 in the context of our model and other cellular models, as well as the relevance of its alternatively spliced isoforms in cancer progression.

4.1.4.4 RAP80 (UIMC1) regulates self-renewal in prostate and breast cancer cells downstream of ESRP1/2

First, we verified the differential expression of RAP80 isoforms in the PC-3/Mc vs. PC-3/S model by conventional PCR, which showed that PC-3/Mc cells express higher levels than PC-3/S cells of the long RAP80 isoform (UIMC1-201 in Ensembl nomenclature ensembl.org), with a higher relative abundance than the short isoform (UIMC1-207) (Figure 4.2.8).

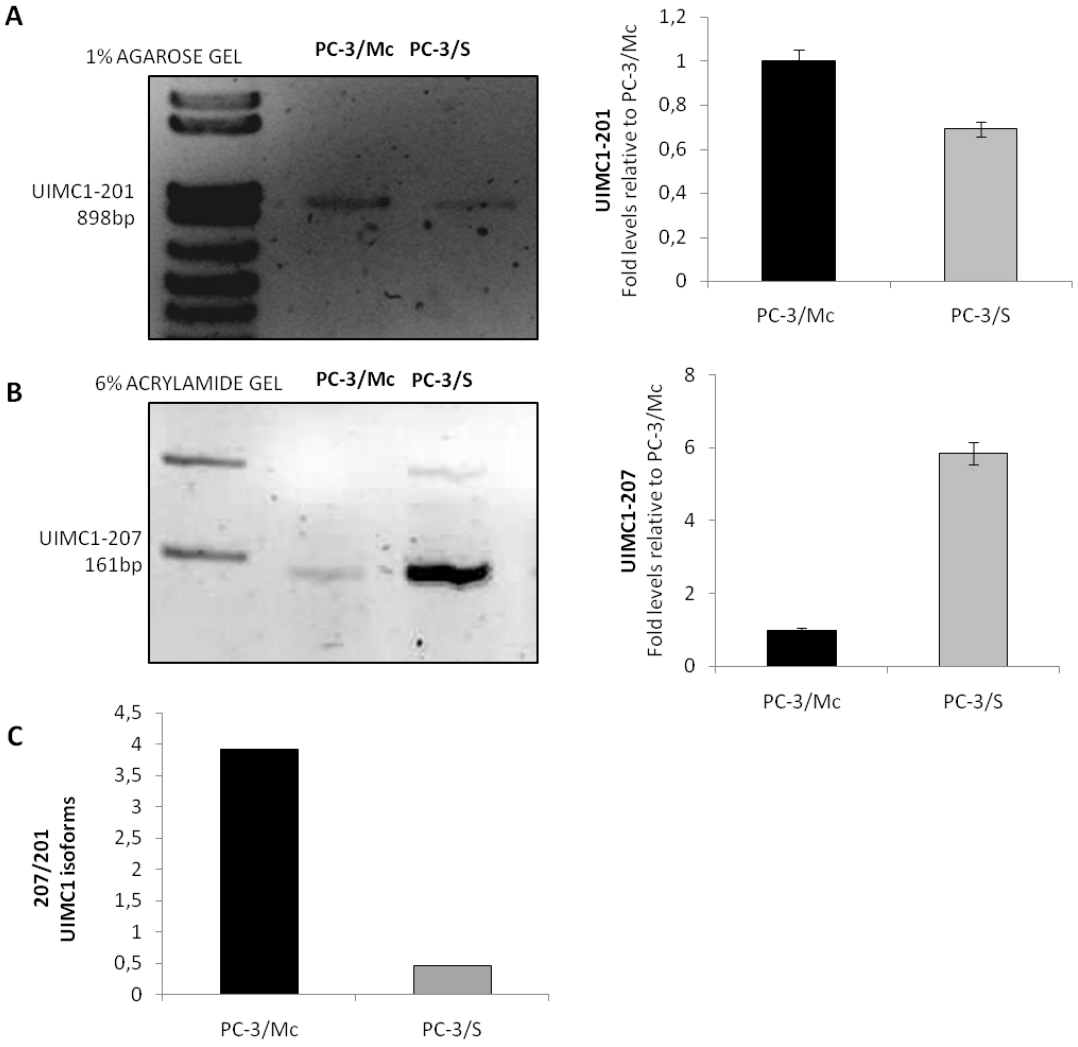

Figure 4.2.8: **Identification of the expression of the UIMC1 isoforms in PC-3/Mc and PC-3/S**
Conventional PCR to determine the UIMC1 isoforms intrinsic expression in PC-3/Mc and PC-3/S (A) UIMC1-201 isoform has been identified through conventional PCR performed in 1% agarose gel (B)UIMC1-207 has been identified through conventional PCR running a 6% acrylamide gel, due to the short length of this isoform. Resulting bands have been quantified using the Image J program. (C) UIMC1-201/207 isoforms ratio was calculated and resulted higher in PC-3/Mc than in PC-3/S. The bars correspond to mean ±SD of n = 3.

This was confirmed by Western blotting with an antibody that recognizes both major isoforms, p80 and p60, corresponding to UIMC1-201 and UIMC1-207, respectively (Figure 4.2.9).

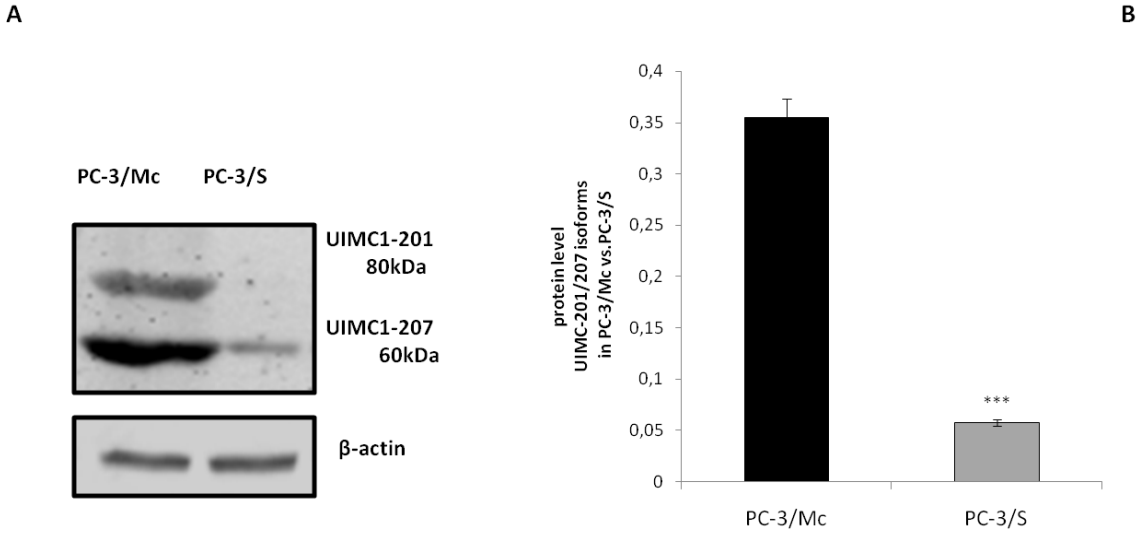

Figure 4.2.9: **Determination of protein level by Western Blotting of the two isoforms UIMC1-201 and UIMC-207 in PC-3/Mc and PC-3/S and quantification by Image J program**
(A). UIMC1-201/207 ratio is higher in the epithelial-like cells PC-3/Mc (B) The bars correspond to mean ±SD of n = 3 *p < 0,05, **p < 0,01 and ***p < 0,001.

Because of the importance of BRCA1 in breast cancer, we also studied the relevance of RAP80 isoforms in breast cancer cell models. In non-neoplastic breast epithelial cell lines with opposing mesenchymal (MCF10CA1h.Hygro) or epithelial (MCF10CA1h.miR200-C2) phenotypes (Sánchez-Cid et al. 2017), the p80/p60 RAP80 isoform ratio was higher in the epithelial cells (Figure.4.2.10), in agreement with the differential epithelial-mesenchymal isoform expression observed in the prostate cancer model. Next, we analyzed the expression of RAP80 isoforms in two breast cancer cell lines with strong epithelial (MCF-7 and T-47D) or mesenchymal (MDA-MB-231) phenotypes. In contrast to the previous findings, the basal-like MDA-MB-231 cells, with strong mesenchymal traits, expressed high levels of p80 with high p80/60 ratios, as compared to the strongly epithelial luminal-A type T-47D and MCF-7 cells (Figure.4.2.10).

As MDA-MB-231 cells display a stronger growth rate and are highly metastatic, the latter result may suggest that the epithelial-mesenchymal RAP80 switch, which may be a default physiological regulatory mode, maybe co-opted towards the epithelial isoforms

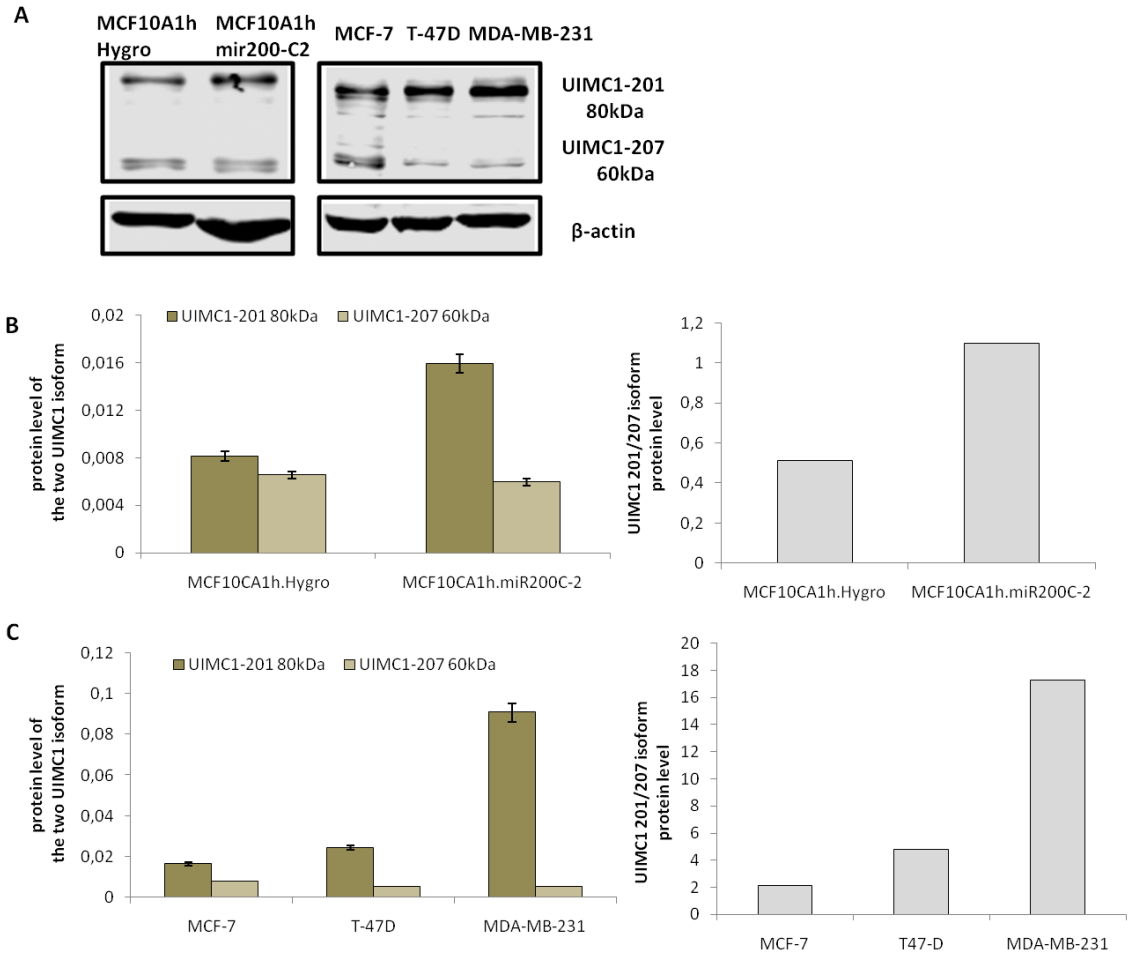

Figure 4.2.10: **Identification of RAP80 isoforms intrinsic levels in different breast cancer cell lines**
(A) Determination of protein level by Western Blotting of the two isoforms UIMC1-201 and UIMC-207 in breast cancer cells MCF10CA1h.Hygro (mesenchymal) compared to MCF10CA1h.miR200-C2 (epithelial) and in epithelial luminal-A breast cells MCF-7 and T-47D in comparison to the mesenchymal-like MDA-MB-231. β-actin is used as a loading control. (B, C) Results have been quantified by the Image J program and expressed as the relative level of each isoform and as ratio UIMC1-201/207. The bars correspond to mean ±SD of n = 3.

in cancer, to impart aggressive phenotypes also in tumor cells with mesenchymal phenotypes. Because the p80 RAP80 isoform is predicted to be fully functional in BRCA1-A recruitment, while the p60 isoform is predicted as non-functional in this activity, we approached the problem as cells expressing different levels of functional RAP80 in BRCA1-A-regulated DNA damage repair (a homologous recombination-mediated repair pathway). To this end, we stably silenced RAP80 by means of lentiviral transduction of specific shRNAs in the following cell lines: PC-3/Mc, PC-3/S, PC-3/S.oeESRP1 and PC-3/S.oeESRP2 (prostate cancer model), MCF-7, T-47D and MDA-MB-

231 (breast cancer cells). The specific knockdown of RAP80was verified by qPCR and Western blotting (Figure 4.2.11 A and B). Subsequently, the expression of RAP80isoforms was analyzed by Western blotting (Figure 4.2.11C-F). The results showed that a significant RAP80 silencing was achieved (Figure 4.2.11).

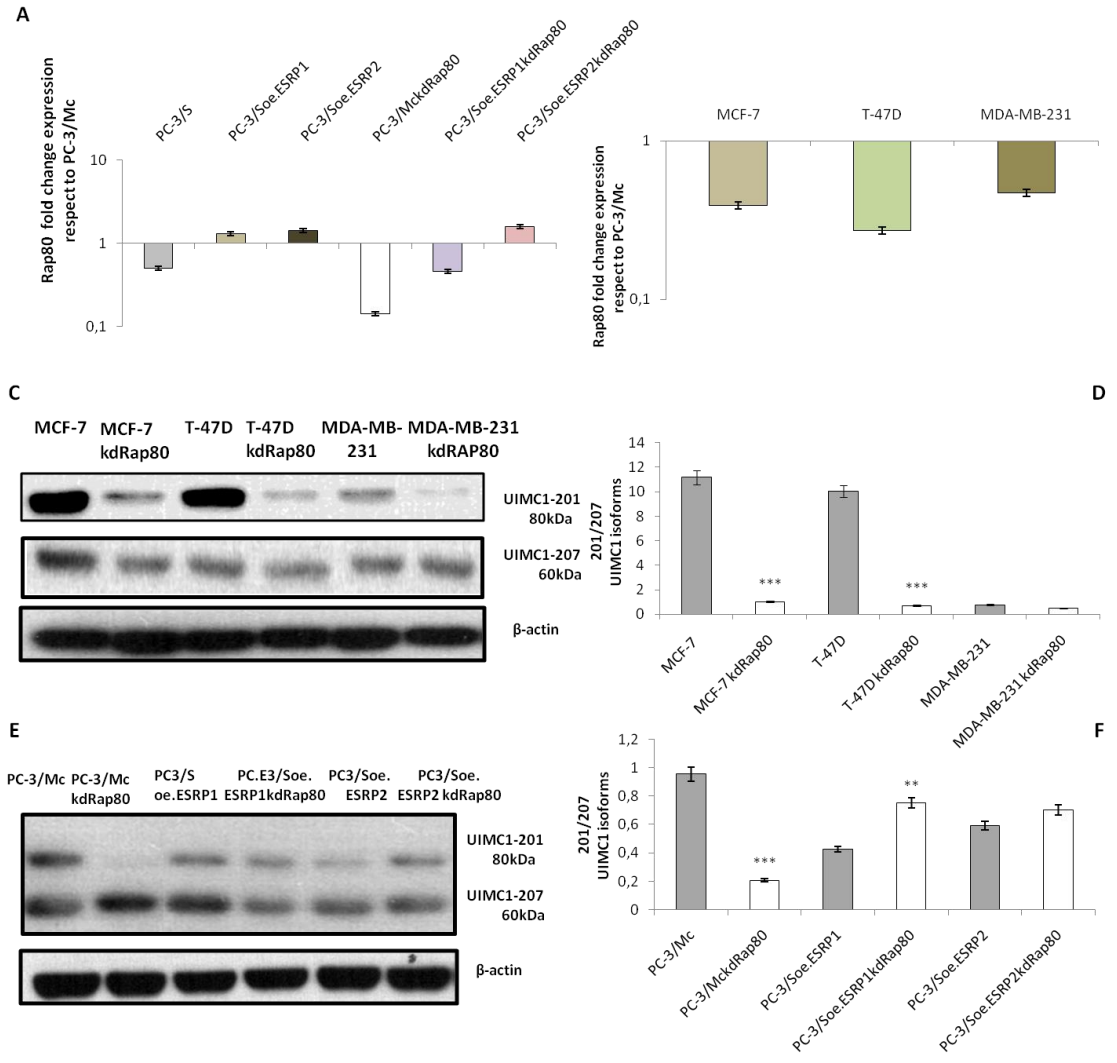

Figure 4.2.11: **Stable silencing of RAP80 gene in prostate cancer cells (PC-3/Mc, PC-3/S, PC 3/Soe.ESRP1, PC-3/Soe.ESRP2) and breast cancer cells (MCF-7, T-47D, and MDA-MB-231)**

(A, B) Gene expression level by qPCR to measure the efficiency of RAP80 silencing in the prostate (A) and breast cancer cell variants (B). Results are expressed as $2^{-\Delta\Delta CT}$RAP80 compared to PC-3/Mc. (C, D) Western Blotting assay, using β-actin as a loading control, to confirm RAP80 knockdown of the two isoforms UIMC1-201 (80kDa) and UIMC-207 (60kDa). The results are expressed as ratio of the longer isoform (UIMC1-201) respect to the shorter one (UIMC1-207) of MCF-7 vs. MCF-7kdRAP80; T-47D vs. T-47D kdRAP80 and MDA-MB-231 vs. MDA-MB-231 kdRAP80 (D) PC7-3/Mc vs. PC-3/Mc kdRAP80, PC-3/Soe.ESRP1 vs. PC-3/Soe.ESRP1kdRAP80 and PC-3/Soe.ESRP2 vs. PC-3/Soe.ESRP2 kdRAP80 (F). *p < 0,05, **p < 0,01 and ***p < 0,001.

The knockdown of RAP80 in PC-3/Mc cells caused a marked impairment of cell growth under standard attachment conditions and a near abrogation of spheroid growth in anchorage-independent conditions (Figure.4.2.12 A and B).

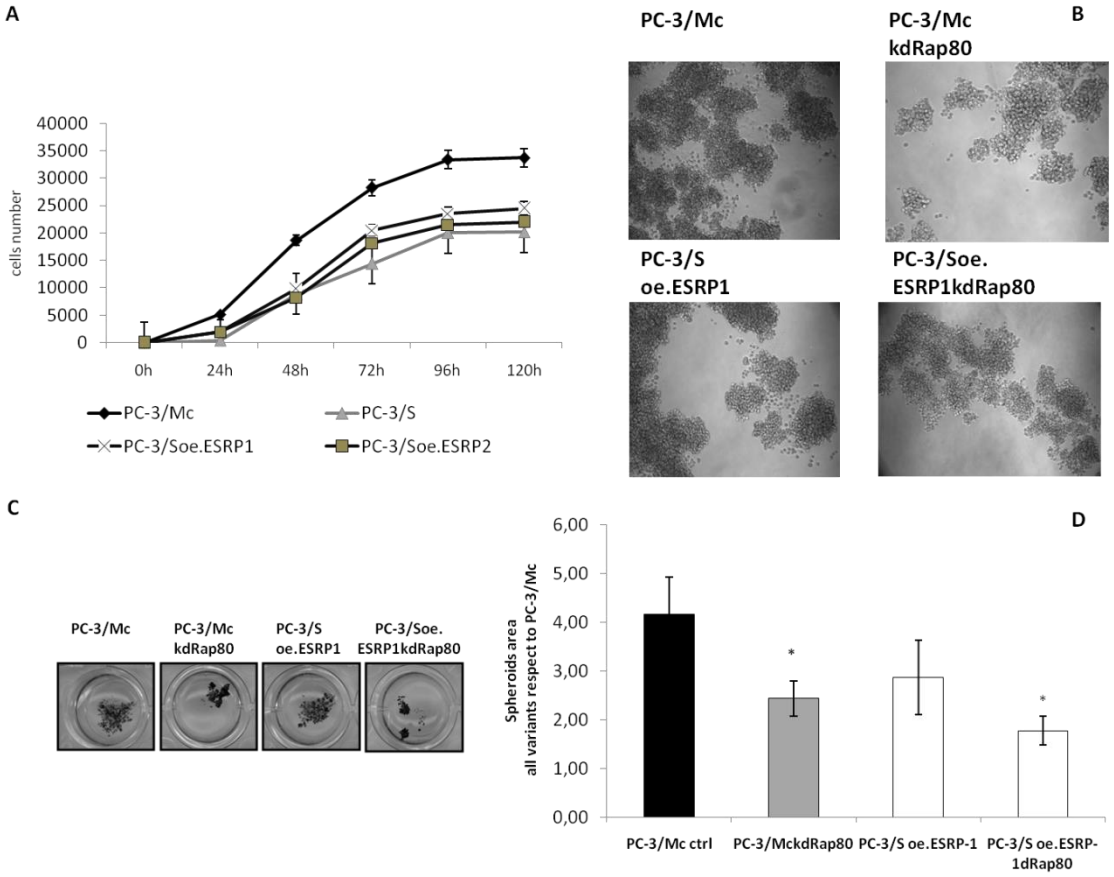

Figure 4.2.12: **Studies of the effect of RAP80 gene silencing on growth properties (in adherent and in anchorage-independent condition) in PC-3/MckdRAP80 vs. PC-3/Mc and PC-3/Soe.ESRP1kdRAP80 vs. PC-3/S**

(A) Growth curve of PC-3/Mc, PC-3/Mc kdRAP80 PC-3/Soe.ESRP1 and PC-3/Soe.ESRP1 kdRAP80. Results showed impairment in proliferation in adherent condition for PC-3/MckdRAP80 when compared to PC-3/Mc(B-D) RAP80 silencing decreased anchorage-independent growth, measured by spheroids assay, in both in PC-3/Mc kdRAP80 and PC-3/Soe.ESRP1 kdRAP80. (B) Bright-field images of the spheroids. (C, D) MTT staining to count the colonies formation and quantification by Image J. Results are represented as spheroids area. The bars correspond to mean ±SD of n = 4. *p < 0,05, **p < 0,01 and ***p < 0,001.

It also abolished the growth advantage conferred to PC-3/S cells by overexpression of ESRP1 or ESRP2 (Figure 4.2.12 C and D). In contrast to the remarkable effects on growth observed in the prostate cancer cell model, knockdown of RAP80 in the three breast cancer cell lines tested had little effect on their growth in attachment conditions (Figure 4.2.13A).

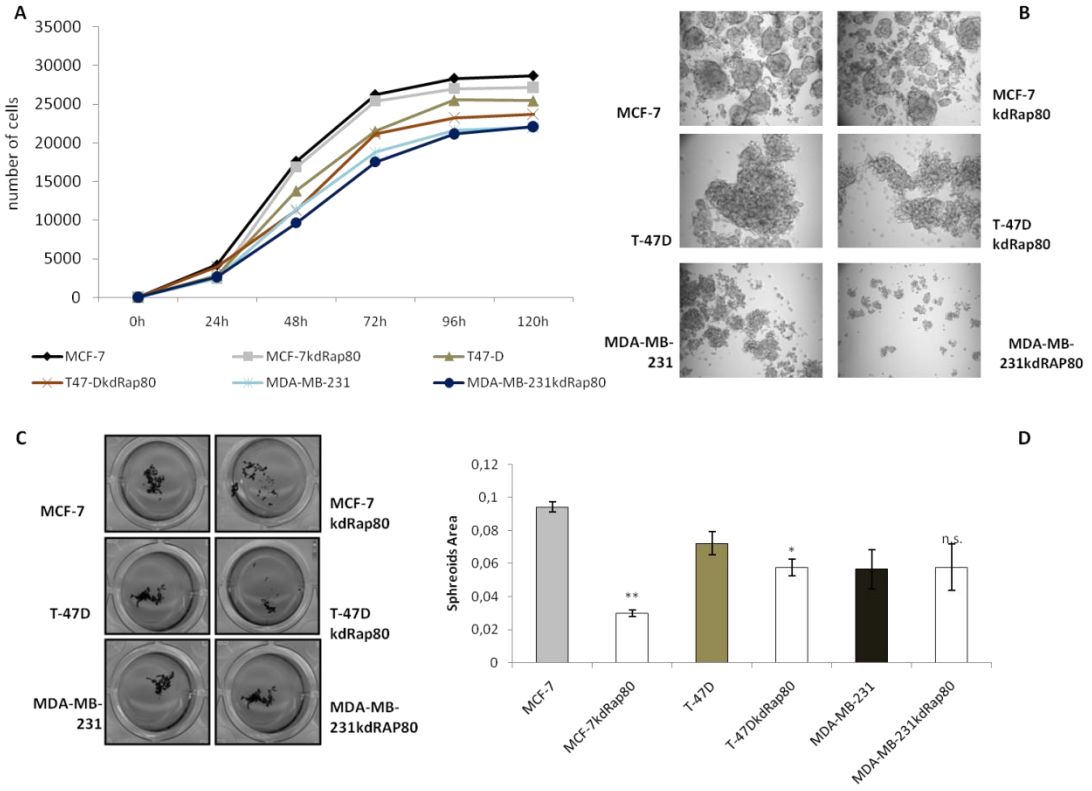

Figure 4.2.13: **Studies of the effect of RAP80 gene silencing on growth properties (both in adherent and in anchorage-independent condition) of the selected breast cancer cells, displaying an epithelial (MCF-7, T-47D) or a mesenchymal phenotype (MDA-MB-231)**

(A) Growth curve of MCF-7, T-47D, MDA-MB-231 cells versus the respective kdRAP80 variants. RAP80 silencing doesn't show a significant effect on breast cancer variants' growth in adherent conditions. (B, C) Studies of growth ability in anchorage-independent condition, through spheroids assay, showed a decrease in MCF-7kdRAP80 and T-47DkdRAP80 variants' ability to grow in anchorage-independent condition respect to MCF-7 and T-47D. (B) Bright-field image of spheroids formation in MCF-7 vs. MCF-7kdRAP80; T-47D vs. T-47D kdRAP80 and MDA-MB-231 vs. MDA-MB-231 kdRAP80. (C) MTT staining of spheroids to perform quantification by Image J program (D) Results are expressed as spheroids area, each variant compared to the respective control (MCF-7 kdRAP80 vs. MCF-7, T-47D kdRAP80 vs.T-47D, MDA-MB-231kdRAP80 vs. MDA-MB-231). The bars correspond to mean ±SD of n = 4. *p < 0,05, **p < 0,01 and ***p < 0,001.

However, knockdown of RAP80 in the epithelial cell lines MCF-7 and T-47D, but not in the mesenchymal-like MDA-MB-231, strongly inhibited mammosphere growth (Figure 4.2.13 B-D). These observations suggest that RAP80 is necessary for prostate and breast cancer cell growth under anchorage-independent conditions, a reflection of self-renewal, especially in cells displaying epithelial phenotypes, and that it is a key downstream factor responsible for the growth advantage associated with ESRP1/2.

4.1.4.5 RAP80 is required for homologous recombination and cancer cell survival in response to DNA damage

Self-renewal in rapidly dividing cells is accompanied by genomic instability, resolved predominantly through homologous recombination and homology-directed repair (HDR) (Choi et al. 2017; Park et al. 2018). The extent of DNA damage can be monitored through scoring of immunofluorescent foci revealed with antibodies to proteins recruited to damage sites, including 53BP1 (Figure 4.2.14).

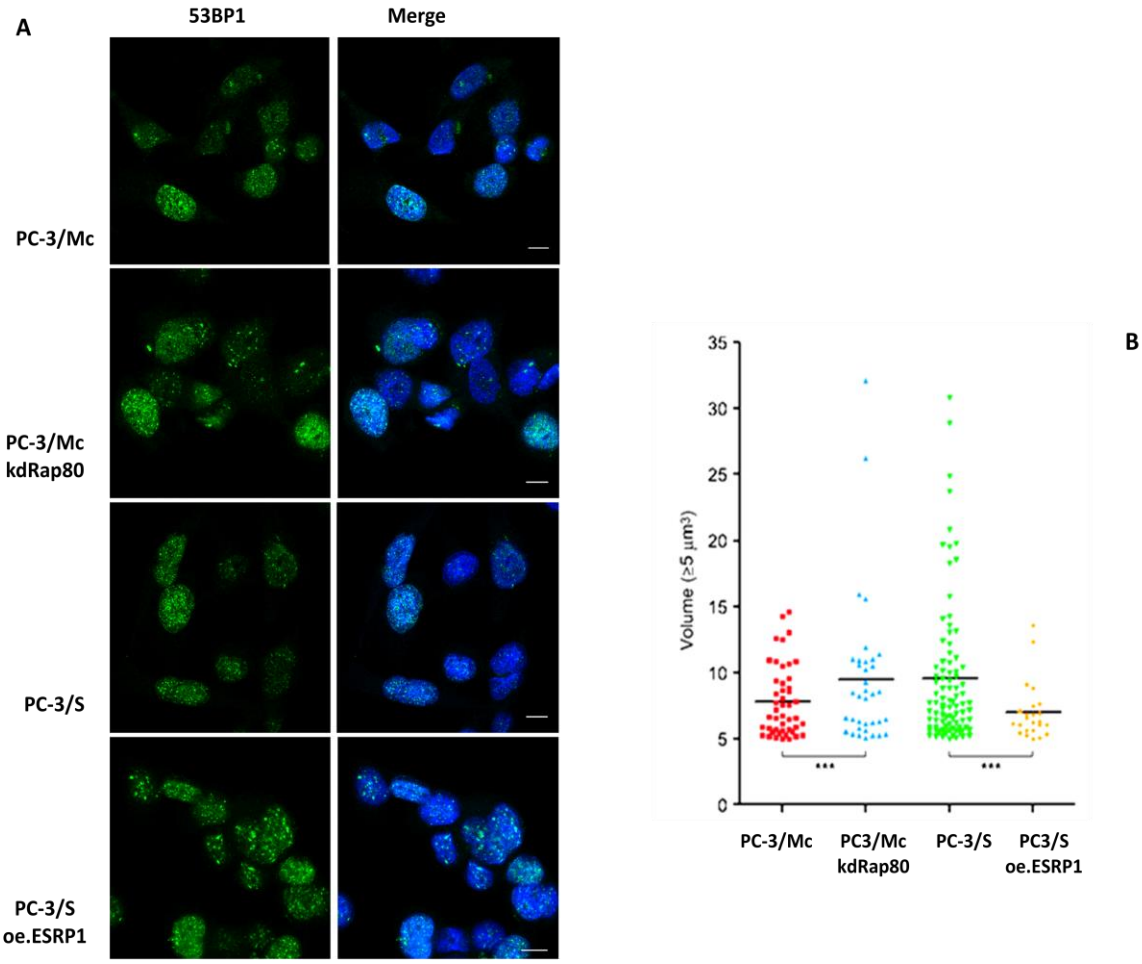

Figure 4.2.14: **DNA damage quantification through scoring of immunofluorescent foci revealed with antibodies to 53BP1 in PC-3/Mc and PC-3/S and respective variants PC-3/Mc kdRAP80 and PC-3/Soe.ESRP1**

(A) The depletion of RAP80 in PC-3/M cells causes an increment in intrinsic 53BP1 foci. On the other hand, forced expression of ESRP1 in PC-3/S cells also causes a decrease in 53BP1 foci. (B) Quantification of foci by the Volocity software, represented as foci volume (μm^3) for PC-3/Mc, PC-3/MckdRAP80, PC-3/S and PC-3/S.oeESRP1.

We thus performed such immunofluorescent analyses as a relative measure of the efficiency of HDR in control and RAP80 knockdown cells, in the absence of exogenous damage. In the prostate cancer model, PC-3/Mc cells had formed fewer intrinsic 53BP1 foci as compared to PC-3/S cells (Figure 4.2.14). The knockdown of RAP80 in PC-3/Mc cells caused an increase in intrinsic 53BP1foci formation to levels comparable to PC-3/S cells. Importantly, over-expression of ESRP1 in PC-3/S cells significantly reduced intrinsic 53BP1 foci formation, which was reversed by knockdown of RAP80 (Figure 4.2.14). These results support that, in the prostate cancer cell model, the formation of intrinsic 53BP1 foci is partly regulated by RAP80 and that ESRP1 exerts a similar regulation through RAP80. We thus performed such immunofluorescent analyses as a relative measure of the efficiency of HDR in control and RAP80 knockdown cells, in the absence of exogenous damage. In the prostate cancer model, PC-3/Mc cells had formed fewer intrinsic 53BP1 foci as compared to PC-3/S cells (Figure 4.2.14). The knockdown of RAP80 in PC-3/Mc cells caused an increase in intrinsic 53BP1foci formation to levels comparable to PC-3/S cells.

Importantly, over-expression of ESRP1 in PC-3/S cells significantly reduced intrinsic 53BP1 foci formation, which was reversed by knockdown of RAP80 (Figure. 4.2.14). These results support that, in the prostate cancer cell model, the formation of intrinsic 53BP1 foci is partly regulated by RAP80 and that ESRP1 exerts a similar regulation through RAP80.

In breast cancer cells, the levels of intrinsic 53BP1 foci formation also correlated with expression levels of the long isoform of RAP80 (Figure. 4.2.15). However, in contrast to the prostate cancer cell model, knockdown of RAP80 in breast cancer cells did not cause significant effects in intrinsic 53BP1 foci formation (Figure 4.2.15), suggesting that additional factors regulate the formation of 53BP1 foci in these cells.

Prompted by the observed association of intrinsic 53BP1 foci with RAP80 levels, we assayed the relative sensitivity of control and RAP80 kd cells to drugs that lead to DNA double-strand breaks, preferentially repaired by HDR, namely, Etoposide, a potent inhibitor of topoisomerase II and Olaparib, an inhibitor of poly (ADP-ribose) polymerase (PARP). Etoposide is used therapeutically in aggressive forms of several solid tumors,

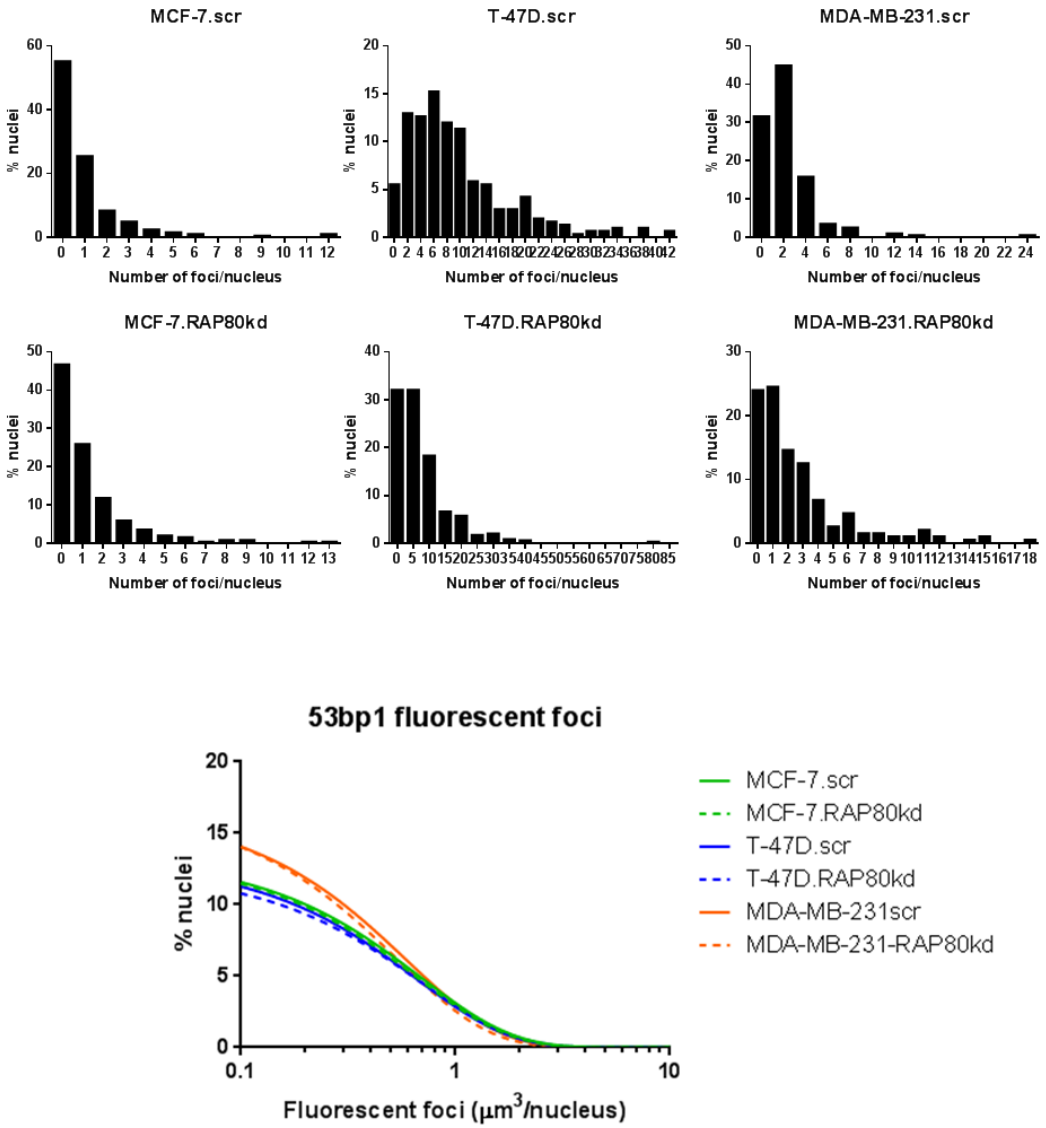

Figure 4.2.15: **DNA damage quantification through scoring of immunofluorescent foci revealed with antibodies to 53BP1 in breast cancer cells MCF-7, T-47D and MDA-MB-231, and respective RAP80kd variants**

(A) Quantification of the number of foci/nucleus for each breast cancer cell lines vs. respective kdRAP80 variant. (B) The number of foci identified in each nucleus respect to the % of nuclei with DNA damage identified in each breast cell line. Results are represented as MCF-7kdRAP80 vs. MCF-7kdRAP80, T-47D vs. T-47DkdRAP80, and MDA-MB-231 vs. MDA-MB-231kdRAP80.

including breast cancer, and Olaparib is particularly effective for the treatment of cancers with loss-of-function mutations in HDR pathway components, such as BRCA1 and BRCA2. While control PC-3/Mc cells were relatively resistant to the cytotoxic effects of Etoposide, knockdown of RAP80 sensitized them nearly 14-fold (Figure.4.2.16).

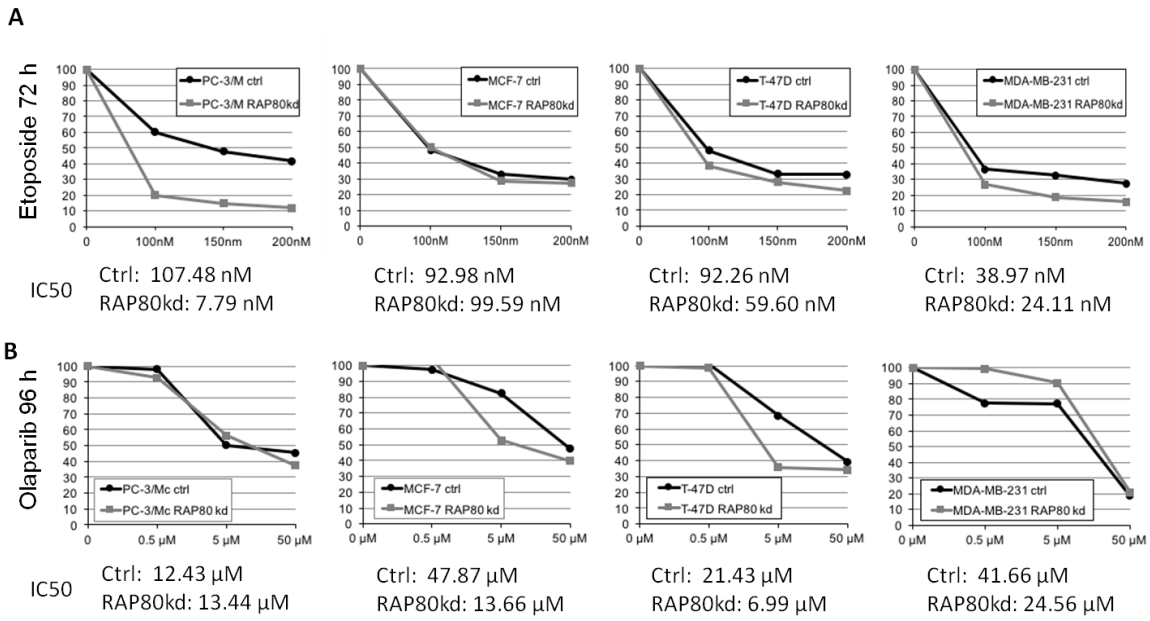

Figure 4.2.16: **Determination of the cytotoxic effect of DNA double-strand breaks- inducer drugs on PC-3/Mc, MCF-7, T-47D, MDA-MB-231 cells, and respective RAP80kd cells variants**
Graphs of the viability of the PC-3/Mc and PC-3/S, MCF7, T-47D, MDA-MB-231 cells and respective kdRAP80 variants at different (A) Etoposide and (B) Olaparib concentrations of the values of IC50 and the difference of these Values (Fold-change) in the different cellular variants with respect to their controls The fold-change values of PC-3/S show that these cells have a higher sensitivity to Etoposide than the PC-3/Mc cells. At the same time, the cell variants PC-3/Mc kd RAP80 are more sensitive to Etoposide than the PC-3/Mc cells. All the breast cancer cells variants apart from MDA-MB231 kdRAP80 displayed higher sensitivity to Olaparib when compared to the respective c MCF-7 and T-47D, MDA-MB-231.

On the other hand, knockdown of RAP80 only modestly sensitized breast cancer cells to Etoposide (Figure 4.2.16A). Intriguingly, knockdown of RAP80 did not sensitize PC-3/Mc cells to Olaparib, while it sensitized MCF-7 and T-47D, but not MDA-MB-231, breast cancer cells about 3-fold (Figure 4.2.16B).

The results suggest that, in our PC-3-derived prostate cancer cells, RAP80 is critical for homology-directed repair of Etoposide-induced DSBs. On the other hand, RAP80 does not appear to be involved in damage repair upon PARP1 inhibition in PC-3-derived cells or in MDA-MB-231 breast cancer cells.

Given the increase in intrinsic 53BP1 foci formation in prostate cancer cells with stable knock down of RAP80 (Figure 4.2.14) and the higher sensitivity to Etoposide treatment, focus formation in PC-3/Mc kdRAP80, PC-3/S.oeESRP1 exposed to Etoposide [37 nM] for

24h were also performed (Figure 4.2.17). However, we did not observe significant differences in focus formation between these variant cells and their controls.

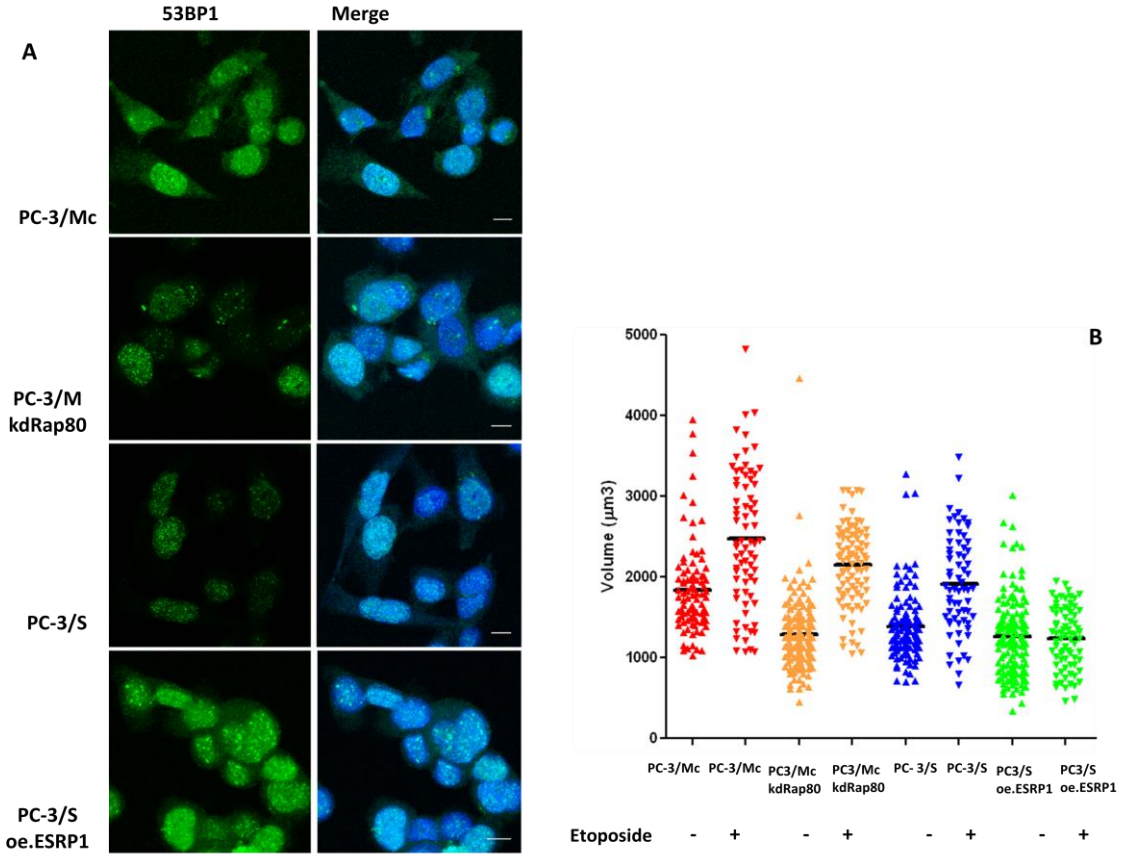

Figure 4.2.17: **DNA damage quantification after Etoposide incubation through scoring of immunofluorescent foci revealed with antibodies to 53BP1 in PC-3/Mc and PC-3/S and respective variants PC-3/Mc kdRAP80 and PC-3/Soe.ESRP1**

(A) The depletion of RAP80 together with Etoposide administration in PC-3/Mc cells results in a strong increment in 53BP1 fluorescent foci. ESRPs overexpression decreases the number of foci when compared to PC-3/S both in the presence and in the absence of Etoposide [37nM] for 24h. (B) Quantification of foci, performed using the Volocity program. Results are represented as foci volume (µm3) for PC-3/MckdRAP80 and PC-3/S.oeESRP1 variants relative to control.

4.1.4.6 RAP80 isoform expression ratio is an independent prognostic factor in breast cancer

In light of the above observations, we explored the TCGA databases (https://bioinformatics.mdanderson.org/TCGASpliceSeq/) for expression levels in cancer of the two RAP80 isoforms (UIMC1-201 and UIMC1-201) differentially expressed in our cell models. The exon exclusion AS responsible for the differential expression of the AIR

can be the consequence of several AS events affecting the inclusion of exons 7.1 and 7.2, coding for the AIR (Figure 4. 2.18).

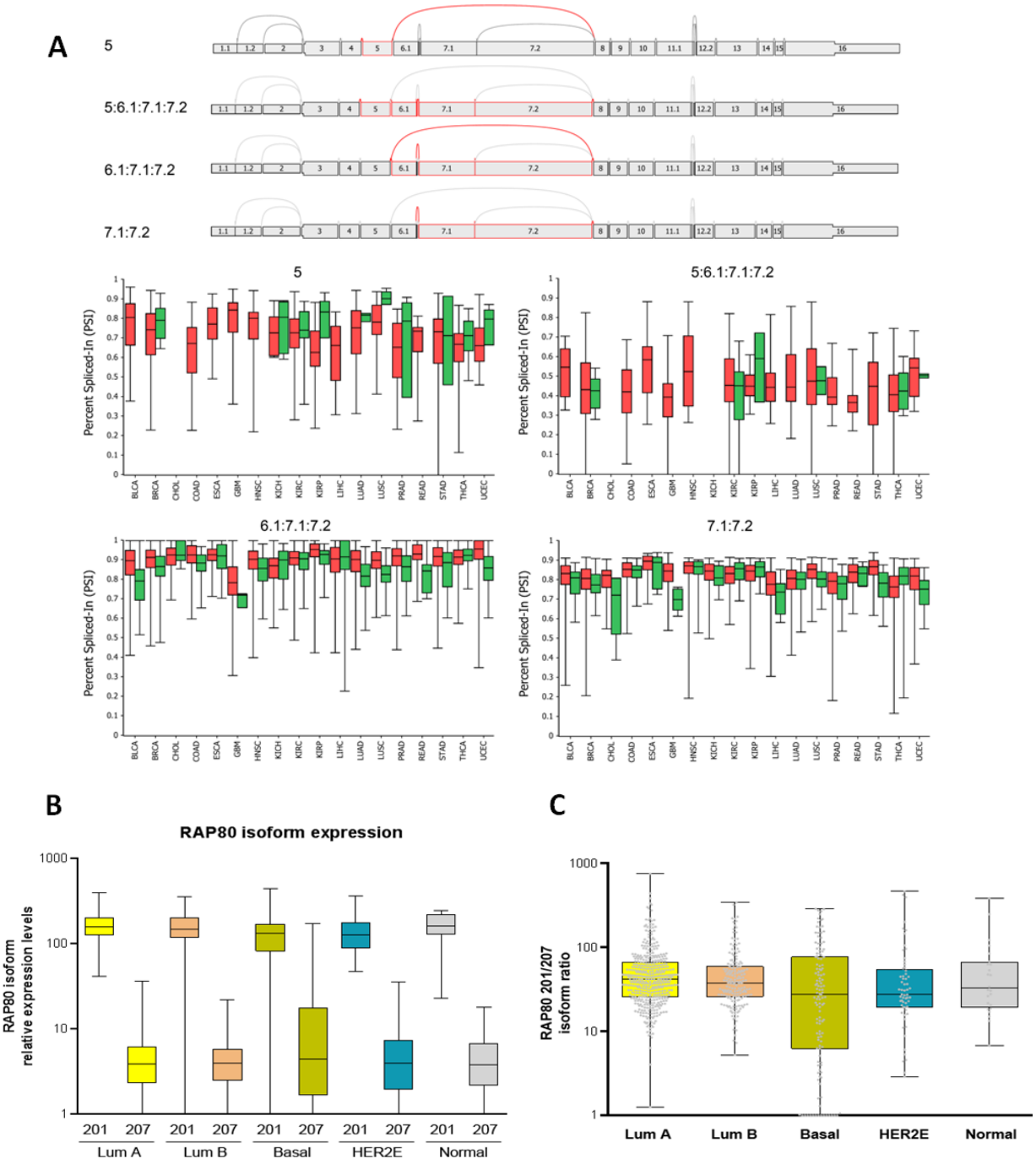

Figure 4.2.18: **Differential UIMC1 (RAP80) isoform expression in cancer**
(A) The percent spliced-in (PSI) score reflects the average percentage of isoforms in a given tumor class including the exons under consideration. In those tumors for which information on the corresponding normal (non-tumor) samples is available (green boxes), PSI for exons 7.1 and 7.2 is significantly higher in tumors vs. normal tissues. (B, C) RAP80 isoform expression in breast cancer, scored as isoform score (see text), stratified according to molecular subtype.

Inclusion of exons 7.1 and 7.2 will result in isoform UIMC1-201, while their exclusion will result in isoform UIMC1-207. The percent spliced-in (PSI) score reflects the average percentage of isoforms in a given tumor class including the exons under consideration. In those tumors for which information on the corresponding normal (non-tumor) samples is available (green boxes), PSI for the 6.1:7.1:7.2 splicing event is significantly higher in tumors *vs*. normal tissues in bladder carcinoma (BLCA), breast carcinoma (BRCA), colon adenocarcinoma (COAD), glioblastoma (GBM), head and neck squamous carcinoma (HNSC), lung adenocarcinoma (LUAD), lung squamous carcinoma (LUSC), prostate adenocarcinoma (PRAD) and rectum adenocarcinoma (READ). For the 7.1:7.2 splicing event, PSI is significantly higher in tumor *vs*. normal tissues in BRCA, cholangiocarcinoma (CHOL), GBM, liver hepatocellular carcinoma (LIHC) and LUSC (Figure 4.2.18 A).

Focusing on breast cancer, we extracted isoform expression data, which we stratified according to molecular subtype. It can be seen that UIMC1 isoform 201 is expressed at higher levels than isoform 207 in all subtypes (Figure 4.2.18B), although basal-like tumors express, in average, higher levels of the 207 isoforms as compared to the other subtypes, highlighted when applying a UIMC1 isoform ratio (201/207) (Figure.4.2.18C).

This ratio, stratified as high or low and used as a parameter to study association with patient overall survival (OS), provided significant discriminant power between good and poor prognosis, with high UIMC1 201/207 ratios being a poor prognostic factor (Figure 4.2.19).

For comparison, the same dataset was analyzed for OS in association with genomic BRCA1 alterations. While BRCA1 deletions were not prognostic of OS, gains and amplification of this gene were associated with poor prognosis (Figure 4.2.19). These observations suggest that higher levels of full-length RAP80 and BRCA1, driving more effective HDR, are associated with more aggressive breast cancers.

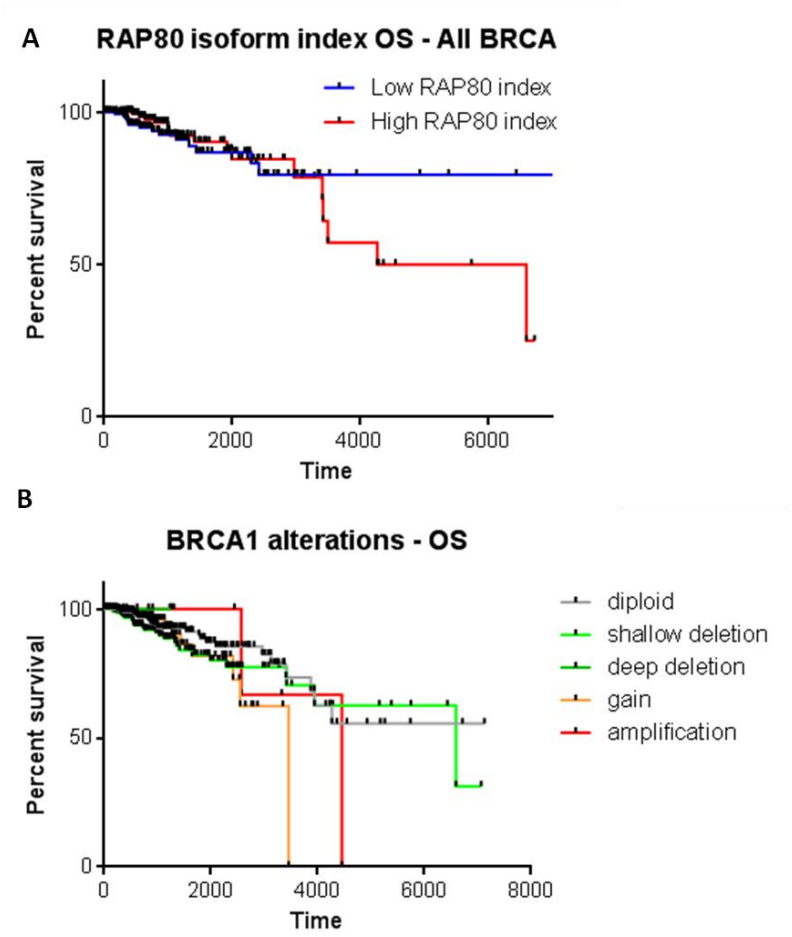

Figure 4.2.19: **UIMC1 (RAP80) isoform score and BRCA1 alteration to predict breast cancer**
Kaplan-Meier survival curves of patients with breast cancer. (A) Higher UIMC1 201/207 ratio is associated with more aggressive breast cancers. (B) Gains and amplification of the BRCA1 gene are associated with poor prognosis.

4.1.4.7 RAP80 as a new target to reduce aggressive phenotypes in breast and prostate cancer models

Alternative splicing is used as a strategy in evolution and development to reversibly increase the functional diversity of genomes (Barash, Blencowe, and Frey 2010). Specific AS regulators, expressed in lineage- or developmental-stage limited manner, favor the inclusion or exclusion of exons in target RNAs that may encode domains critical for particular activities of the resulting proteins. The developmentally critical process co-opted during cancer progression, epithelial-mesenchymal transition (EMT), is regulated by AS mainly through ESRP1/2 (RBM35A/B), RBM47 and QKI, which favor an epithelial transcript isoform program (Yang et al. 2016), and hnRNPM, which favors a

mesenchymal isoform program (Harvey et al. 2018; Xu et al. 2014). Although past studies have provided targets and mechanisms accounting for the effects of these AS regulators on EMT (or the reverse process, mesenchymal-to-epithelial transition, MET), whether they also contribute to additional traits relevant to cancer stem cells, such as self-renewal and resistance to genotoxic insult, has been less studied.

In this study, we provide evidence that RAP80 (UIMC1), an adaptor protein with critical functions in homology-dependent DNA repair (HDR), is expressed as alternatively spliced isoforms in epithelial and mesenchymal cells, as a function of ESRP1/2 expression. More specifically, we have found that the ratio of expression of a full-length isoform to a short isoform of RAP80 is significantly higher in epithelial cells than mesenchymal cells in a prostate cancer cell model for EMT. Full-length RAP80 contains a SUMO-interacting motif juxtaposed to a bipartite ubiquitin-interaction motif (SIM-UIM_2) that binds mixed SUMO and K63-Ub chains and tether RAP80 to DNA damage sites populated by these tags through the activity of RNF4/RNF8/RNF168 (Guzzo et al. 2012; Typas et al. 2015). In close proximity and carboxy-terminal to the SIM-UIM_2 domain, RAP80 contains a region required for interaction with Abraxas (Abraxas interaction region, AIR), a core component of the BRCA1-A complex (Wang et al. 2007). The short RAP80 isoform found here is predicted to lack the AIR, and thus to be deficient in the recruitment of the BRCA1-A complex to DNA damage sites.

The BRCA1-A complex contains, in addition to RAP80 and Abraxas, the K63-specific deubiquitinase BRCC36 and the scaffolding protein MERIT40 (Kim, Chen, and Yu 2007; Sobhian et al. 2007; Wang et al. 2007). Phosphorylation of Abraxas at its carboxy terminus is recognized by the BRCT domain of BRCA1, which, by virtue of its entry into the BRCA1-A complex, is positioned ~2–10 kb distal from DNA break sites, thus limiting its DNA resection activity as part of homology-directed repair (HDR) (Goldstein and Kastan 2015; Kakarougkas et al. 2013). Therefore, BRCA1-A limits HDR by restraining resection (Coleman and Greenberg 2011; Hu et al. 2011a). As such, failure to recruit BRCA1-A to damage sites (e.g., by mutations in RAP80 UIM_2or Abraxas) (NikkiÏ et al. 2009; Solyom et al. 2012) leads to unhinged hyper-resection by BRCA1, while the loss of BRCA1 causes defective HDR and also to unresolved DSBs (Dever et al. 2011). This

explains the increased formation of intrinsic 53BP1 foci observed in PC-3/Mc cells upon knockdown of RAP80.

We propose that the ratio of full-length (fully functional) RAP80 to the short isoform lacking AIR is a new mechanism for the regulation of HDR mediated by BRCA1. A higher long/short RAP80 isoform ratio will favor, and lower ratios will counter, the recruitment of BRCA1-A complexes to DSBs. Shifts in this ratio through ESRP1/2-regulated alternative splicing is expected to dynamically fine-tune the access of BRCA1 to damage sites, thus potentiating or limiting resection and HDR.

The physiological and pathological importance of these proposed mechanisms is supported by our findings that the long/short RAP80 isoform ratio is an independent predictor of overall survival in breast cancer patients. Interestingly, we found higher ratios as predictive of poor outcome, suggesting that HDR through the RAP80 pathway is associated with more aggressive tumors. In consonance with this hypothesis, we found that BRCA1 amplification, but not the loss, was also predictive of poor prognosis in breast cancer patients (Figure 4.2.19).

In addition to the nuclear BRCA1-A complex, BRCA1 participates in a second multiprotein complex, BRISC, located in the cytoplasm and which modulates cellular stress response and immune signaling (Wu, Lu, and Yu 2010; Yin et al. 2012; Zheng et al. 2013).

BRCA1 enters BRISC through interaction with an Abraxas-related protein, ABRO1 (also designated ABRAXAS2) (Yiduo Hu et al. 2011b; B. Wang et al. 2007). The substrates of BRISC include ATF4, THAP5, NLRP3, and the cytosolic domain of IFNAR1, an interferon receptor (Py et al. 2013; Zheng et al. 2013). BRISC also interacts with serine hydroxymethyl transferase 2 (SHMT2), a metabolic enzyme that converts serine to glycine and a tetrahydrofolate-bound one-carbon unit, and occurs in cytosolic (SHMT2α) and mitochondrial (mSHMT2) forms (Figure 4.2.21) (Rabl et al. 2019a; Yin et al. 2012; Zheng et al. 2013).

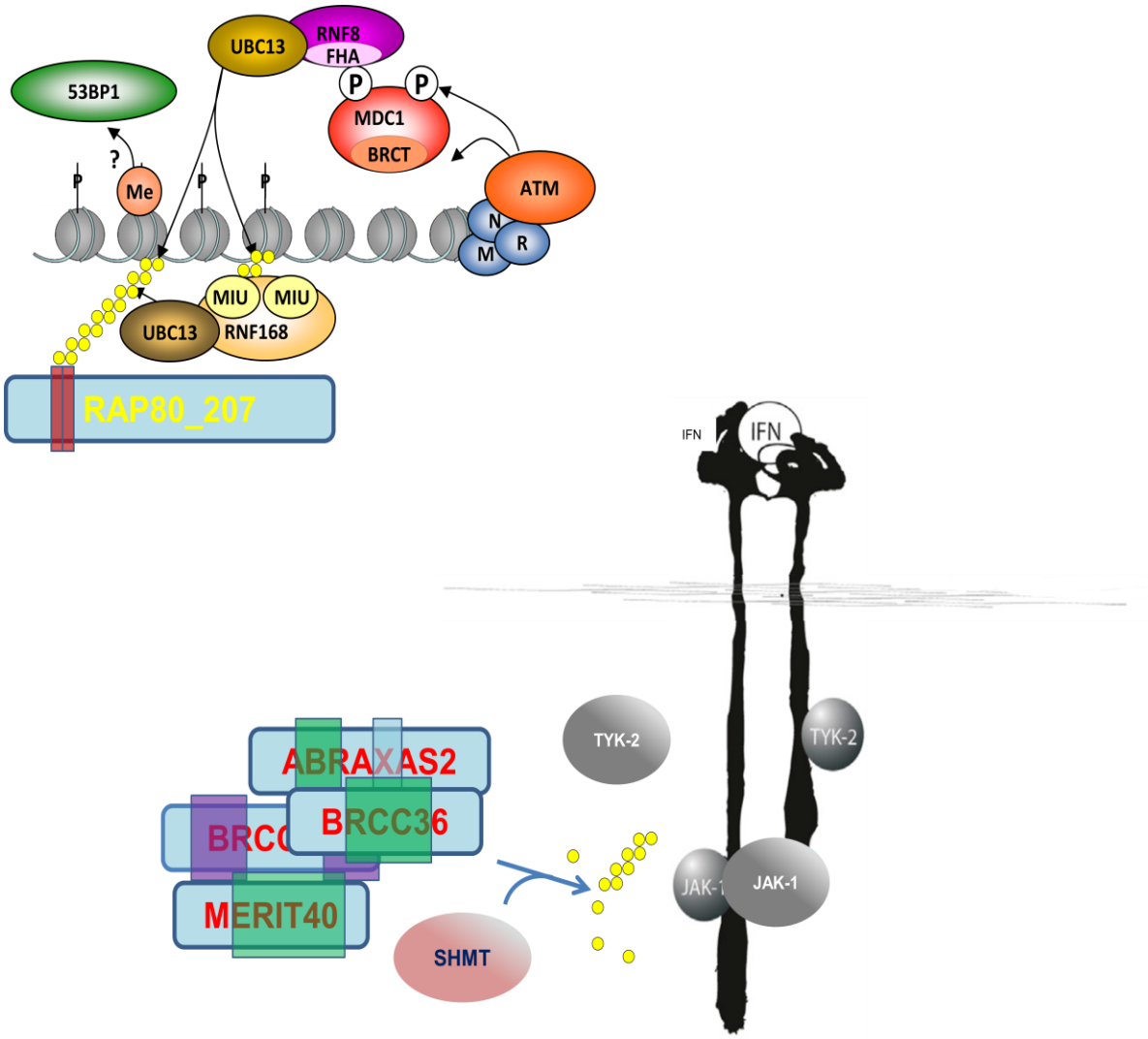

Figure 4.2.20: **Proposal of the effects of differential RAP80 isoform expression onSHMT-BRISC complex regulation of the interferon (IFN) response**
High levels of the short RAP80 isoform (207), lacking the Abraxas-interaction region (AIR), are expected to be defective in the recruitment of the BRCA1-A complex, making it available for its cytoplasmic functions in deubiquitinating K63-linked polyubiquitin chains (through the BRCC36 deubiquitinase) on the type I IFN receptor encoded by IFNAR1. Diminished K63 ubiquitination of this receptor reduces its endocytosis and inactivation, and thus more abundant BRCA1-A complexes will dampen type I IFN responses. SHMT2 inhibits the deubiquitinase activity of BRCC36, and thus high levels of this enzyme promote K63-ubiquitination of IFNAR1, with consequent enhanced endocytosis and termination of the IFN signal.

Expression of high levels of SHMT2 plays important role in the metabolic adaptation of cancer cells to hypoxia (Amelio et al. 2014; Kim et al. 2015; Lee et al. 2014; Zheng et al. 2013). Interestingly, SHMT2 regulates the interferon signaling function of BRISC by inhibiting the deubiquitinase activity of BRCC36 on interferon αβ receptor (the product of IFNAR1) (Rabl et al. 2019a; Zheng et al. 2013).

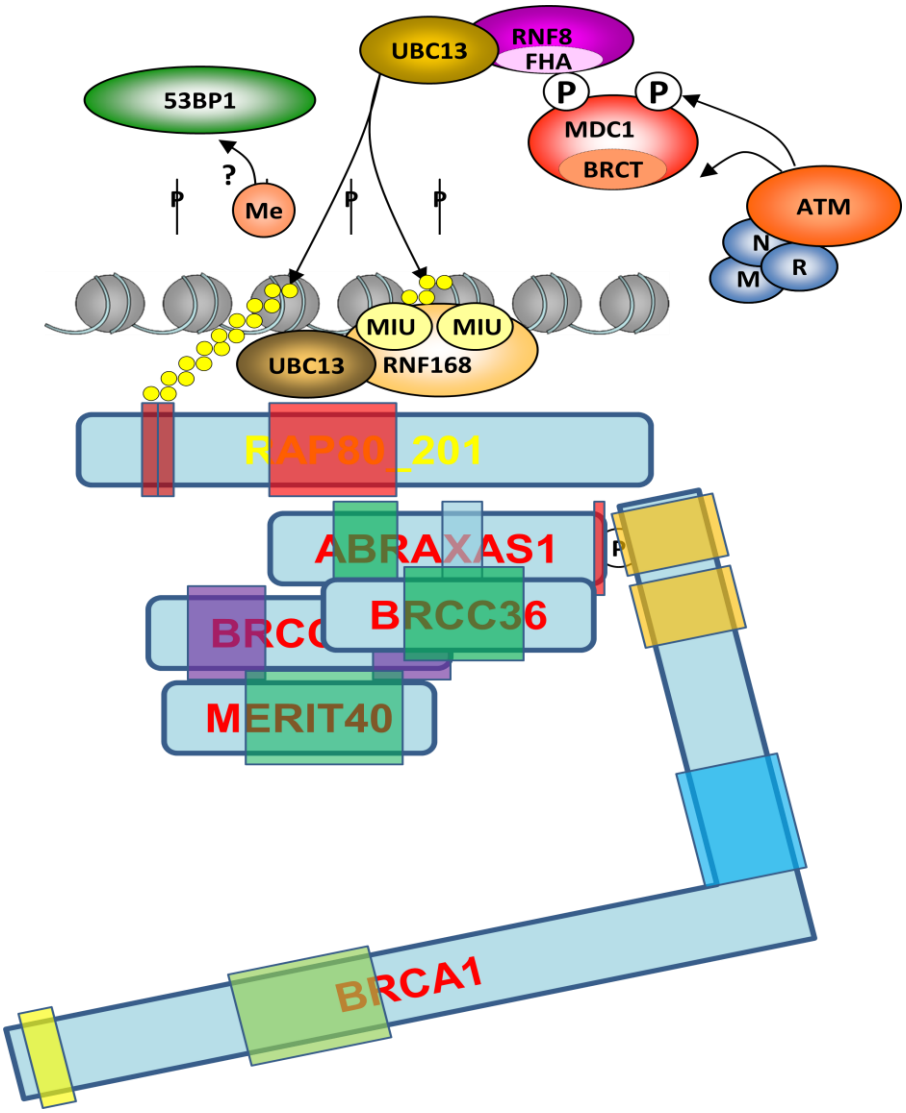

Figure 4.2.21: **Schematic representation of BRCA1 ABRAXAS RAP80 cooperation to the DNA damage sites**

Upon DNA damage, the E3 ligase RNF8 promotes K63-ubiquitination of histone H3 through the E2 ligase activity of UBC13-UEV. K63-linked diubiquitins are recognized by RAP80 through its UIM2 domain. Abraxas is also recruited via its interaction with RAP80 at its Abraxas-interaction region (AIR), tethering the BRCA1-A complex, which includes the K63-ubiquitin de-ubiquitinase BRCC36 and the scaffolding protein MERIT40. Phosphorylation at the C-terminus of Abraxas is recognized by the BRCA1 CTD, which is also recruited near (albeit at a distance of) the DNA damage site. For the sake of simplicity, SUMOylation reactions and additional interactions are omitted from this scheme.

We speculate that RAP80 isoform ratios may also fine-tune the availability of BRISC, and hence interferon signaling (Figure 4.2.21). At high long/short RAP80 isoform ratios, the recruitment of BRCA1 to damage sites will be favored upon DNA damage, thus reducing the availability of BRISC to de-ubiquitinate K63-Ub modified IFNAR1. This will counter the endocytosis of this receptor, enhancing interferon and immune responses. At low

long/short RAP80 ratios, more BRCA1 molecules will be available to assemble into BRISC, favoring de-ubiquitination of IFNAR1 through BRCC36, receptor endocytosis and dampening of cytokine signaling. SHMT2 should also be considered in this scenario, such that high levels will dampen cytokine signaling by inhibiting BRCC36 (Zheng et al. 2013).

In conclusion, our observations warrant the exploration of RAP80 as a target to curtail aggressive phenotypes in breast and prostate cancers, and the intricate cross-talk between DNA damage, cytokine signaling, and metabolism.

5. GENERAL DISCUSSION

5.1 GENERAL DISCUSSION

Endothelial cells are the main components of blood vessels, and they play an important role in vasculogenesis in normal and pathological situations.

In this study, we have generated and characterized a unique model consisting of endothelial cells derived from patients undergoing treatment for Acute Myocardial Infarction. The drivers for this effort have been the assumption that endothelial dysfunction is a major factor in the onset of this pathology and the hypothesis that this entails cell-autonomous metabolic reprogramming.

Slow growth, poor migration, and defective tubulogenesis are associated with less glucose consumption and higher lactate efflux in AMI patient-derived endothelial cells

The first sign of cell-autonomous anomalies affecting AMI patient-derived endothelial signs was the observation of clearly abnormal growth and migration patterns, as well as tubulogenesis potential when compared to control (healthy) coronary artery endothelial cells. These findings encouraged us in the subsequent search for cell-autonomous signs and mechanisms of metabolic dysfunction associated with AMI endothelial cells.

Indeed, we did find striking shifts in metabolic patterns in our pathological cells, relative to control cells. Thus, all except 2 patient-derived endothelial cell lines consumed significantly less glucose and, yet, effluxed significantly higher levels of lactate to the cell culture medium than control cells. This intriguing result represents a conundrum, as in most cells and conditions, lactate has been proposed to be produced mainly by glycolysis, and higher lactate efflux is expected to reflect more active glycolysis accompanied with more, not less, glucose consumption. To further explore this issue, we determined the expression levels of the two main lactate transporters, MCT1 (SLC16A1) and MCT4 (SLC16A3), whose main activities are lactate import and export, respectively. The results were, once again, unexpected, as patient-derived endothelial cells that effluxed more lactate expressed significantly lower levels of the lactate exporter, MCT4, than control cells or the patient-derived cell lines with lower levels of lactate efflux. As such, we face a double conundrum affecting the same metabolic pathway in patient-derived cells, namely a higher lactate efflux associated with (1) lower

glucose consumption and (2) lower levels of expression of the major lactate exporter, MCT4.

We provide two possible explanations, which are not mutually exclusive to this intriguing metabolic phenotype. First, in addition to its production by glycolysis, lactate can also be produced by glutaminolysis, in a pathway that involves oxidation of glutamine to malate and then to pyruvate by the malic enzyme (ME), followed by conversion to lactate by the action of LDHA (Brooks 2018). This conversion also promotes the recycling of NADH to NAD+. The resulting lactate may be transported outside the cell by MCT4, and later taken up through MCT1 and converted by mitochondrial LDHB to pyruvate which enters the TCA cycle or used for gluconeogenesis through the conversion to oxaloacetate catalyzed by pyruvate carboxylase (Cori cycle) (Chen et al. 2016; Dimmer et al. 2000). Indeed, AMI patient-derived cells consume significantly more glutamine than control cells (as discussed in more detail below). However, this explanation, while possibly pinpointing a non-glucose source of lactate, does not explain the relatively high lactate efflux associated with low levels of expression of its main exporter, MCT4.

Both MCT4 and MCT1 have been described to localize in mitochondria, where they presumably act as mitochondrial lactate transporters (Draoui and Feron 2011; Draoui, De Zeeuw, and Carmeliet 2017a). We speculate that, in control endothelial cells, MCT4 localized in mitochondria mediates the import of lactate into mitochondria, and thus the produced lactate will follow two paths out of the cytoplasm, into mitochondria and the extracellular milieu. On the other hand, if patient-derived cells have low levels of mitochondria-located MCT4, lactate will be mainly effluxed from the cell, and not transported into mitochondria. This scenario would explain both the low levels of MCT4 and the higher extracellular efflux of lactate in patient-derived cells as compared to control cells. Were this the case, the total lactate production in both patient-derived and control cells do would not need to differ significantly, the observed difference in efflux being attributable to the distribution of lactate into mitochondria or the extracellular space. This hypothesis would require further experimental validation.

Compromised glycolysis favors enhanced pentose phosphate pathway in AMI patient-derived endothelial cells

Under normal conditions, endothelial cells mainly rely on glycolysis to generate the energy required for their functions, which is a bioenergetic pathway providing most of the total intracellular ATP in these cells (De Bock et al. 2013; Dromparis and Michelakis 2013). A rate-limiting enzyme in this pathway is phosphofructokinase 1 (PFK1), responsible for the phosphorylation of fructose-6-phosphate (F-6-P) to fructose-1,6-phosphate (F-1,6-P) in an ATP-dependent reaction. PFK1 is allosterically activated by fructose-2,6-bisphosphate (F-2,6-BP), produced from F-6-P through the catalytic activity of 6-phosphofructo-2-kinase/fructose-2,6-bisphosphatases, encoded in mammals by paralogs PFKFB1, PFKFB2, PFKFB3, PFKFB4. These are bifunctional enzymes bearing, a kinase and a bisphosphatase domains (Dromparis and Michelakis 2013). PFKFB3 has a substantially higher kinase activity, which promotes the formation of F-2,6-P2, resulting in an enhanced glycolytic rate. On the other hand, PFKFB4 exhibits a stronger bisphosphatase activity (De Bock et al. 2013). PFKFB3 has been described to play a significant role in the glycolytic activity of pathological ECs, and its inhibition dramatically abrogates their proliferation and migration (Burke and Virmani 2000; Li, Kumar, and Carmeliet 2019a; Schoors et al. 2014).

Consistent with their low glucose consumption, PFKFB3 levels in patient-derived cells were expressed at lower levels than control cells. This suggests less active glycolysis in the pathological cells, which would explain their low proliferation rates, migration capacity and tubulogenic activity of these cells, as these processes normally require robust glycolysis (Fitzgerald, Soro-Arnaiz, and De Bock 2018a). In contrast, patient-derived cells expressed significantly higher levels of PFKFB4 than control cells. This finding is also consistent with low glycolytic activity, as the bisphosphatase activity of PFKFB4 prevails over its kinase activity, leading to the conversion of whatever fructose-2,6-bisphosphate (F-2,6-P) is formed by PFKFB3 back to fructose-6-phosphate (F-6-P), effectively dampening the activation of PFK1 and thus slowing down the glycolytic flux. PFK1 is allosterically inhibited by high levels of ATP. Low pH (as associated with high lactate production and efflux) and citrate augment, while AMP reverts, the inhibitory activity of ATP on PFK1.

The hydrolysis of F-2,6-P catalyzed by PFKFB4 (or other bisphosphatases) to yield F-6-P is accompanied by the release of one phosphate moiety (Figure5.1)

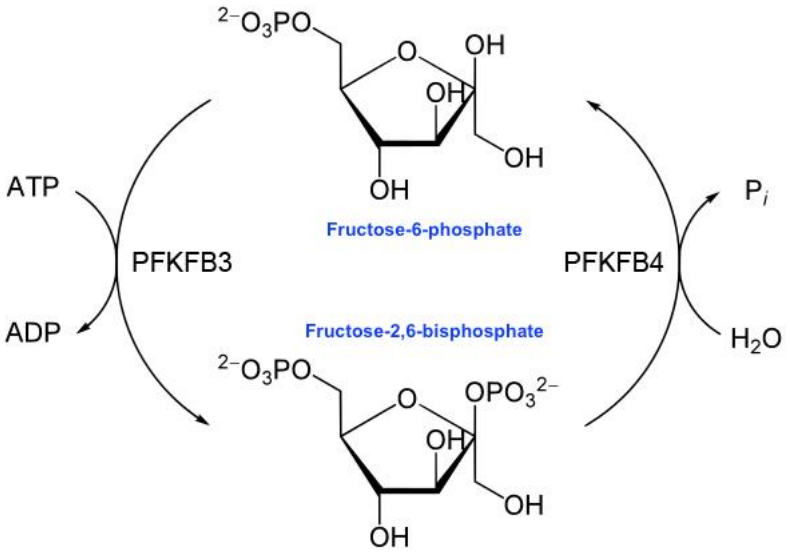

This Pi can be used to recycle ATP from ADP:

ATP + β-D-fructose 6-phosphate ⇔ ADP + β-D-fructose 2,6-bisphosphate

Therefore, lower levels of F-2,6-P due to low PFKFB3 and high PFKFB4 levels would lead to inhibition of PFK1 because of (1) loss of allosteric activation by F-2,6-P and (2)inhibition by higher levels of ATP. Adding to this, the high levels of lactate production in the pathological cells, causing a decrease in intracellular pH, would further contribute to the inactivation of PFK1. This is expected to result in an accumulation of PFK1's substrate, glucose-6-phosphate (G-6-P), which would be redirected to the pentose phosphate pathway (PPP) and to gluconeogenesis (see next section).

What mechanisms may explain the relatively low levels of PFKFB3 and high levels of PFKFB4 observed in AMI patient-derived endothelial cells?

Both PFKFB4 and PFKFB3 are up-regulated in hypoxia through transcriptional activation by HIF-1α, and both are transcriptionally repressed by wild-type p53 activated in

response to DNA damage. However, only PFKFB4, but not PFKFB3, has been reported as strongly up-regulated in the absence of p53 (Franklin et al. 2016; S Ros et al. 2017). As such, one may hypothesize a blunted function of p53 as a driver of PFKFB4 up-regulation. This possibility needs further investigation.

Oxidative stress and enhanced mitochondrial activity characterize AMI patient-derived endothelial cells

The hypothesis of increased shunting of G-6-P towards the PPP was supported by our observations of increased levels of expression and activity of the key enzyme of the oxidative branch of the PPP, glucose-6-phosphate dehydrogenase (G6PD). This is expected to produce higher levels of NADPH, which contribute to ROS scavenging by maintaining glutathione in its reduced state. Indeed, we found that patient-derived cells contained intracellular concentrations of reduced glutathione at levels significantly higher than control cells. Glutathione synthesis is induced in response to oxidative stress (Kojima et al. 2018a). That patient-derived cells were under oxidative stress was also confirmed, as they contained ROS at significantly higher levels than control cells.

These findings prompted our next question: Do patient-derived cells consume higher levels of glutathione precursors in order to meet its increased synthetic demand?

The two major precursor amino acids in the synthesis of glutathione are glutamate and cysteine. Although glutamate can be synthesized through more than one pathway or transported into cells, it is mostly derived from glutamine. Glutamine is the most abundant circulating amino acids in organisms, and we found that glutamine consumption is significantly higher in patient-derived cells than in control cells. In fact, the glutamine *vs.* glucose consumption ratios were greater in patient-derived cells than in control cells, suggesting that AMI patient-derived cells mainly resort to glutamine, rather than glucose, as their preferred carbon source.

The conversion of glutamine to glutamate is catalyzed by glutaminases, encoded in humans by two genes, GLS1 and GLS2. Consistently, we found significantly higher levels of expression of the two GLS1 isozymes, KGA and GAC, in patient-derived cells as compared to control cells. Moreover, we found increased levels of expression of the

major glutamine transporter, SLC1A5 (ACT2), as well as higher levels in patient-derived cells of the Xc- system (formed by two components encoded by SLC7A11/SLC3A2), a cystine-glutamate exchanger that imports cystine into cells which is then reduced by GSH and/or TRR1 to cysteine, crucial in the synthesis of glutathione(Draoui, De Zeeuw, and Carmeliet 2017b; Ishimoto et al. 2011). In further support of the use of glutamate in the biosynthesis of glutathione and other catabolic pathways (mainly the TCA cycle), patient-derived cells exported less glutamate into the extracellular medium than control cells.

The observed increased levels of ROS in patients-derived cells suggested increased mitochondrial respiration in these cells, as a possible source of ROS. Once in the mitochondrial matrix, glutamate is converted into α-ketoglutarate and ammonia by glutamate dehydrogenase, together with the reduction of $NAD(P)^+$ into NADPH (Bhutia et al. 2015). NADH is the substrate of complex I of the mitochondrial respiratory chain and its oxidation results in the translocation of H^+ across the membrane, thus causing a proton gradient and producing a mitochondrial membrane potential (Zorova et al. 2018). Accordingly, we found higher levels of mitochondrial respiration and higher anaplerotic use of glutamate in patient-derived cells relative to control cells. This outcome is consistent with the increased transcriptional levels of expression of the glutamate/H+ symporter, SLC25A22, found in patient-derived cells, required for the transport of glutamate into the mitochondria (Palmieri and Monné 2016).

Collectively, these data provide multiple evidences that AMI patient-derived cells display a strong mitochondrial activity with consequent enhanced ROS levels that, in turn, induce high levels of glutathione, whose synthesis is facilitated by augmented intake of glutamine and conversion to glutamate through glutaminolysis, as well as the enhanced import of cystine (Figure 5.2).

The synthesized glutathione is maintained in its reduced state thanks to the reducing equivalents produced through the oxidative branch of the PPP, and is thus functionally effective for neutralization of the excess ROS in these cells.

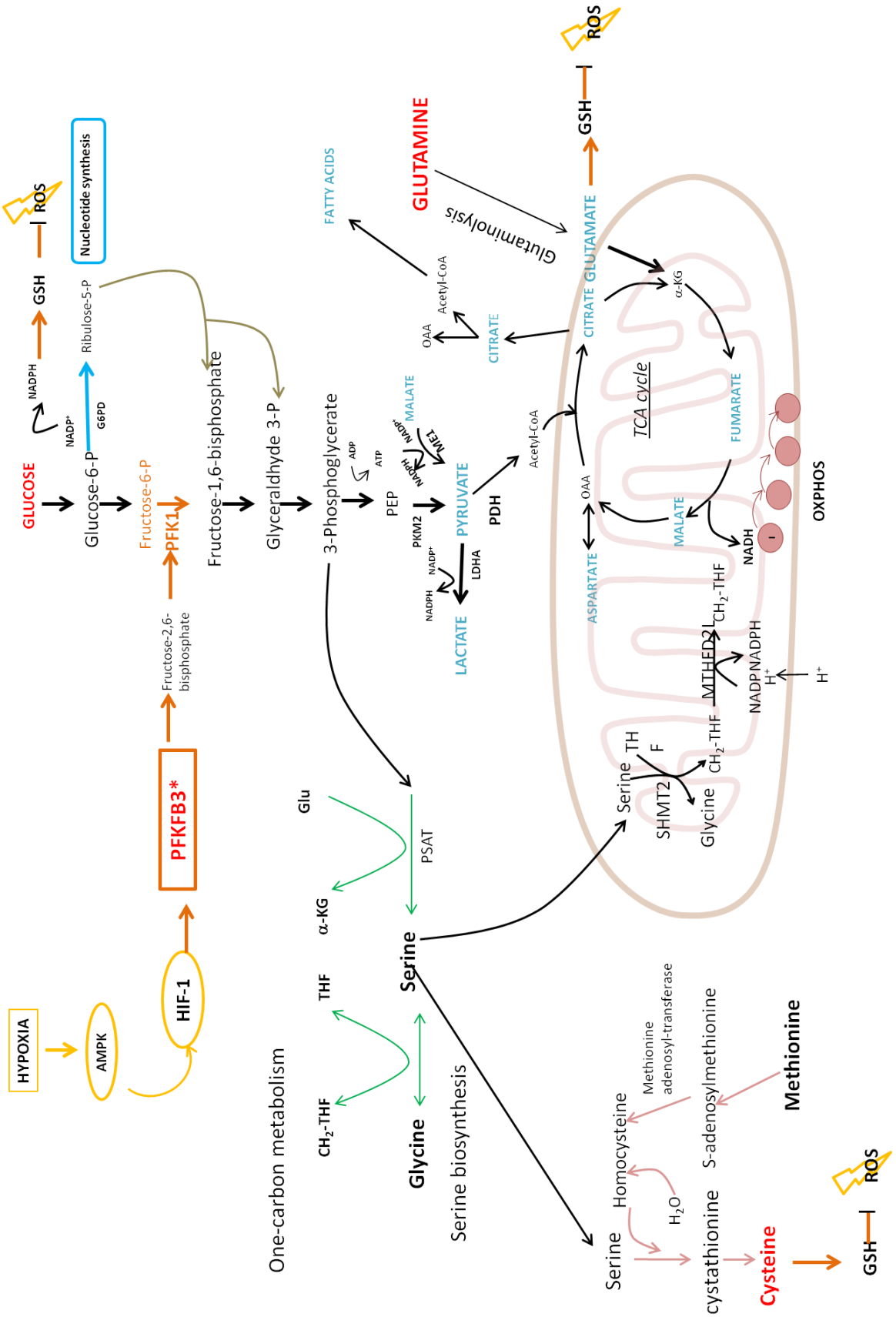
HYPOXIA
AMPK
HIF-1
PFKFB3*
Fructose-2,6-bisphosphate
PFK1
Fructose-6-P
Fructose-1,6-bisphosphate
Glyceraldhyde 3-P
3-Phosphoglycerate
PEP
PKM2
PYRUVATE
LACTATE
LDHA
PDH
Acetyl-CoA
OAA
CITRATE
Acetyl-CoA
FATTY ACIDS
GLUTAMINE
Glutaminolysis
CITRATE
GLUTAMATE
α-KG
TCA cycle
FUMARATE
MALATE
ASPARTATE
OAA
NADH
I
OXPHOS
ROS
GSH
MALATE
ME1
NADPH
NADP+
NADPH
NADP+
ADP
ATP
GLUCOSE
Glucose-6-P
G6PD
NADPH
NADP+
Ribulose-5-P
Nucleotide synthesis
GSH
ROS
Glu
α-KG
PSAT
Serine
THF
CH2-THF
Glycine
Serine biosynthesis
One-carbon metabolism
Serine
SHMT2
TH
F
Glycine
CH2-THF
MTHFD2L
CH2-THF
NADPNADPH
H+
H+
Serine
Homocysteine
Methionine adenosyl-transferase
S-adenosylmethionine
Methionine
cystathionine
H2O
Cysteine
GSH
ROS

Figure 5.2: **Schematic representation of AMI patient-derived cells metabolism**
These cells display a strong mitochondrial activity with enhanced ROS levels, inducing high levels of glutathione, whose synthesis is promoted by increased uptake of glutamine and conversion to glutamate through glutaminolysis, as well as the enhanced import of cystine.
α-KG, α-ketoglutarate, AMPK, 5'-AMP-activated protein kinase, G6PD, glucose 6 phosphate dehydrogenase, LDHA, Lactate dehydrogenase A, ME1, NADP-dependent malic enzyme, MTHFD2L, methylenetetrahydrofolate dehydrogenase, NADPH, Nicotinamide Adenine Dinucleotide Phosphate Hydrogen, OAA, oxalacetate, OXPHOS, oxidative phosphorylationPDH, Pyruvate dehydrogenase, PFK1 Phosphofructokinase-1, PFKFB3 6-phosphofructo-2-kinase/fructose-2,6-biphosphatase 3, PKA protein kinase A, PKC protein kinase A, PKM2, pyruvate kinase muscle isozyme, PPP, pentose phosphate pathway; PSAT, phosphoserine aminotransferase; ROS, reactive species of oxygen, SHMT1, serine hydroxymethyltransferase (cytosol); SHMT2, serine hydroxymethyltransferase (mitochondria) THF, tetrahydrofolate.

Our evidence also supports that and increased PPP activity is fed through an increased derivation of G-6-P secondary to a stalling of glycolysis at the level of the conversion of F-6-P to F-1,6-P because of an inhibition of PFK1, in turn owed to lower levels of the PFK1 allosteric activator F-2,6-P caused by increased ratios of PFKFB4/PFKFB3 (Figure 5.3).

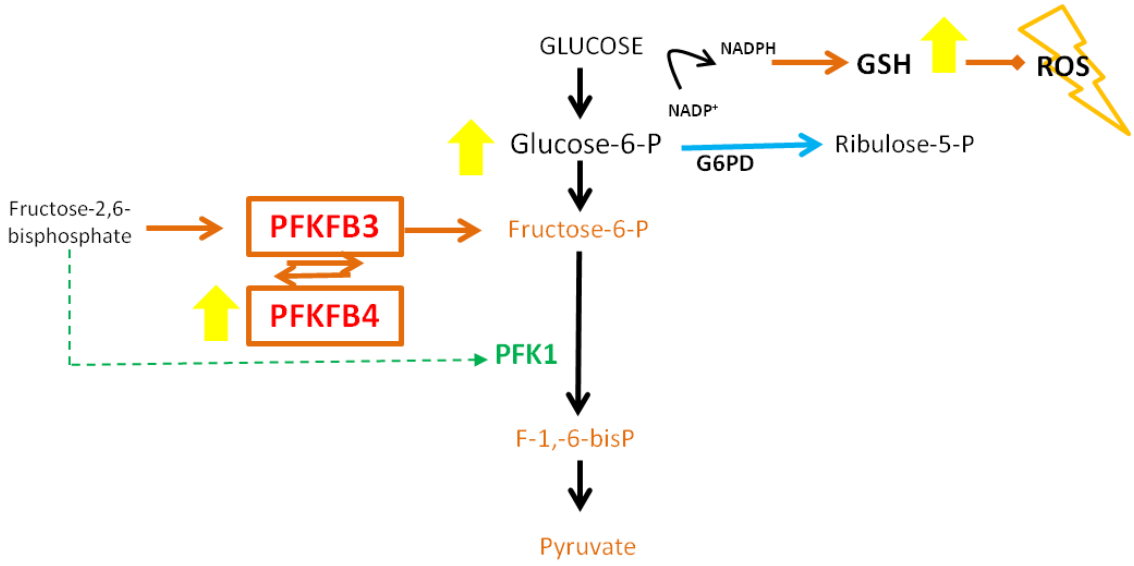

Figure 5.3: **The high ratio PFKFB4/PFKFB3 impairs PFK1 activity in patients-derived cells**
An augmented PPP activity in patients derived cells have been found, due to an increased derivation of G-6-P secondary to a impasse of glycolysis at the level of the conversion of F-6-P to F-1,6-P because of an inhibition of PFK1, in turn related to lower levels of the PFK1 allosteric activator F-2,6-P caused by increased ratios of PFKFB4/PFKFB3.
F-1,6-bisP Fructose 1,6-bisphosphate, F-2,6-bisP, Fructose 2,6-bisphosphate, G6PD, glucose-6-phosphate dehydrogenase, GSH, glutathione, NADPH, Nicotinamide Adenine Dinucleotide Phosphate Hydrogen, PFK1, Phosphofructokinase-1, PFKFB3, 6-phosphofructo-2-kinase/fructose-2,6-biphosphatase, PFKFB4, 6-phosphofructo-2-kinase/fructose-2,6-biphosphatase 4, ROS, reactive species of oxygen.

Alternative splicing reprogramming as a new indicator of endothelial dysfunction in AMI

The previous observations indicate a profound metabolic reprogramming in AMI patient-derived endothelial cells. This suggests the occurrence of a broad and complex dysfunction in these cells, that should be reflected in global processes. We thus proceeded to an unbiased approached to study this, by means of transcriptomic profiling by RNAseq.

Although relatively small numbers of genes were found coordinately expressed between all cell lines with statistically significant differences in expression levels relative to control cells, possibly attributable to individual variability between the different patient-derived cell lines, we found an anomalous transcriptional pattern common to all patient-derived cells displaying shared phenotypes. Specifically, when analyzed for differentially expressed alternatively spliced (AS) isoforms, patient-derived cells had a significantly lower frequency of retained intron (IR) isoforms than control cells. This has two main implications: First, as low IR ratios for a particular transcript indicates more efficient splicing for that transcript, patient-derived cells are predicted to display more efficient AS for entire classes of transcripts than control healthy cells. Because RI isoforms are not productive, as they are not translated and tend to be degraded by nonsense-mediated decay (Jung et al. 2015), this implies that patient-derived cells express proteins not expressed in control cells, through this mechanism, that may not be detected as differentially expressed productive transcripts.

Second, this finding indicates a broad shift in AS, which is a major mechanism governing differentiation, development or responses to environmental cues in many cell types and tissues (Nakka et al. 2018). That AS reprogramming may also be associated with endothelial dysfunction was not previously known. Importantly, we have observed lower IR frequency only in those patient-derived cells that share a common growth, migration and metabolic phenotype, but not in the outlier cell line, CE-45, that does not share these characteristics. As such, decreased IR frequency is a new cell-autonomous molecular indicator of endothelial dysfunction in AMI. Further work is warranted to unveil the mechanisms underlying AS reprogramming in these cells and to identify and functionally characterize the specific classes of transcripts under this mode of

regulation, that may help identify fundamental molecular mechanisms of endothelial dysfunction in AMI.

Alternative splicing regulates self-renewal and DNA damage repair in cellular models of epithelial-mesenchymal transition

Alternative splicing (AS) is a process that takes place during gene expression and results in a single gene coding for multiple proteins and also non-coding transcripts with little known functions (Black 2003). Shifts in AS have been found associated with a number of pathologies, including atherosclerosis, CVDs, dysfunctional endothelium, and especially cancer (Chen et al. 2015).

AS regulators favor the inclusion or exclusion of exons in target RNAs that may encode domains critical for particular activities of the resulting proteins (Barash, Blencowe, and Frey 2010). Among others processes, epithelial-mesenchymal transition (EMT) is regulated by AS mainly through ESRP1/2 (RBM35A/B), which favor an epithelial isoform program (Yang et al. 2016) and hnRNPM, which favors a mesenchymal isoform program (Harvey et al. 2018; Hu et al. 2011a; Hu et al. 2017).

In this second part of this thesis, and inspired by our findings of altered AS, in our endothelial cell model of AMI, we explored the relevance of AS in the regulation of specific phenotypes in a different cell model, in the hope that it might shed light into events shared among different pathologies. The cell model chosen for these studies is a well-defined dual-cell model that permits clear-cut comparisons between two distinct cell phenotypes and transcriptional programs: one clonal cell line, PC-3/Mc, displays a strong epithelial phenotype, and is highly proliferative and metastatic, while a second clonal cell line, PC-3/S, displays a strong mesenchymal phenotype and is highly invasive but poorly proliferative and non-metastatic (Celià-Terrassa et al. 2012). As our focus on AS regulation, we directed our attention to ESRP1 and ESRP2, major regulators of EMT through AS.

A systematic analysis led us to discover that the adaptor protein RAP80 (encoded by UIMC1), a critical factor in homology-directed repair (HDR), is regulated by ESRP1/2, and, in turn, regulates cell growth and response to genotoxic stress. The most significant

discovery of this study, though, is that RAP80 can be expressed as two major productive isoforms, one preferentially expressed in cells with epithelial phenotypes, and one expressed preferentially in cells with mesenchymal phenotypes. The *epithelial isoform* of RAP80 is the full-length protein, containing the critical domains necessary to perform its cognate functions in HDR, namely a SIM-UIM_2 (SUMO-interaction motif and bipartite ubiquitin-interaction motif) domain, and an AIR (Abraxas-interaction region) (Hu, Paul, and Wangs 2012).

The *mesenchymal isoform* of RAP80, on the other hand, is predicted to contain the SIM-UIM_2 domain but lacks the AIR (RAP80 *short isoform*). Full length RAP80 is recruited to sites of DNA damage through its SIM-UIM_2 domain, that binds to SUMO and K63-linked bi-ubiquitin moieties that decorate histone H3 at damage sites, and tethers the BRCA1-A complex (ABRAXAS1, BRE, MERIT4, BRCCC36, BRCA1) through its interaction with ABRAXAS1 (Kim, Chen, and Yu 2007; Sobhian et al. 2007; Wang et al. 2007). A consequence of this process is that RAP80 positions BRCA1 at a distance from the damage site, thus limiting its excision activity on the target double-strand breaks (Goldstein and Kastan 2015). The *short isoform* of RAP80 is also predicted to be recruited to DNA damage sites through its SIM-UIM_2domain, but not to tether the BRCA1-A complex because it lacks AIR and thus would fail to interact with ABRAXAS1.

This is a novel scenario of regulation of DNA damage response, through alternative splicing of RAP80. A high expression ratio of full-length to short RAP80 isoforms is predicted to result in diminished excision by BRCA1. Conversely, a high level of expression of the short isoform of RAP80 (or low overall levels of RAP80) is predicted, on one hand, to result in high levels of DNA excision at damage sites owed to unhinged BRCA1 activity (NikkiÏ et al. 2009) and, on the other, to relieve the BRCA1-A complex from its nuclear functions and travel to the cytoplasm, where it performs a totally unrelated function.

Our analysis of the expression of these two RAP80 AS isoforms in breast cancer demonstrates the clinical relevance of these AS events, as we have found that the long/short RAP80 isoform ratio is an independent prognostic predictor in breast cancer, that clearly overperforms the predictive power of BRCA1 deletions or amplifications.

The cytoplasmic function of the BRCA1-A complex regulates the type-I interferon signaling and interacts with serine metabolism through serine hydroxymethyl transferase 2 (SHMT2). SHMT2 converts serine to glycine and is critical for one-carbon metabolism (Walden et al. 2019). Therefore, the differential expression of the two major alternatively spliced RAP80 isoforms discovered in our study is predicted to have unforeseen connections between DNA damage, cytokine signaling, and metabolism.

We hypothesize an involvement of this new mechanism in a broad range of physiological and pathological conditions, including endothelial dysfunction, for which there is a wealth of evidence for an important role of DNA damage. Interestingly, as described in Chapter 4.1, we observed differential AS of ABRAXAS1 in our AMI patient-derived endothelial model, with a productive isoform predicted to be preferentially expressed in the pathological cell lines, suggestive of a response to ongoing DNA damage in these cells.

6. CONCLUSIONS

6.1 CONCLUSIONS

- Shifts in metabolic patterns in patient-derived cells, relative to control cells have been found, indicating that most of the patient-derived endothelial cell lines consumed significantly less glucose and effluxed significantly higher levels of lactate to than control cells. We provide two possible explanations: on the one hand, lactate can also be produced by glutaminolysis, in a pathway that involves oxidation of glutamine to malate and then to pyruvate followed by conversion to lactate by the action of LDHA; on the other hand, we speculated that patient-derived cells have low levels of mitochondria-located MCT4 transport. So, lactate is mainly effluxed from the cells, and not transported into mitochondria, which explains both the low levels of MCT4 and the higher extracellular efflux of lactate in patient-derived cells as compared to control cells.

- PFKFB3 levels in patient-derived cells were expressed at lower levels than control cells which suggests a less active glycolysis in the pathological cells, consistent to the low glucose consumption. Lower levels of F-2,6-P due to low PFKFB3 and high PFKFB4 levels leads to inhibition of PFK1 because of (1) loss of allosteric activation by F-2,6-P and (2) inhibition by higher levels of ATP. Moreover, the high levels of lactate production in the pathological cells, which causes a decrease in intracellular pH, further contribute to the inactivation of PFK1. In addition, while both PFKFB3 and PFKFB4 are up-regulated in hypoxia through transcriptional activation by HIF-1α, only PFKFB4 has been reported as strongly up-regulated in the absence of p53 in response to DNA damage. So a blunted function of p53 as a driver of PFKFB4 up-regulation has been hypothesized.

- We observed increased levels of ROS in patients-derived cells which suggests an augmented mitochondrial respiration in these cells, as a possible source of ROS. The enhanced ROS levels inducts high levels of glutathione, whose synthesis is promoted by augmented intake of glutamine and conversion to glutamate (through glutaminolysis), as well as enhanced import of cystine. The synthesized glutathione is maintained in its reduced state thanks to the reducing equivalents produced through the oxidative branch of the PPP, and is thus functionally effective for neutralization of the excess ROS. Our evidence supports that and increased PPP activity is fed through an increased derivation of G-6-P secondary to a stalling of glycolysis at the level of the conversion of

F-6-P to F-1,6-P because of an inhibition of PFK1, in turn due to lower levels of the PFK1 allosteric activator F-2,6-P caused by increased ratios of PFKFB4/PFKFB3.

- Apart from a profound metabolic reprogramming we found an anomalous transcriptional pattern common to all patient-derived cells displaying shared phenotypes: when analyzed for differentially expressed alternatively spliced (AS) isoforms, patient-derived cells had significantly lower frequency of retained intron (IR) isoforms than control cells. Shifts in AS have been found associated to a number of pathologies, including dysfunctional endothelium and cancer; furthermore, among others processes, epithelial-mesenchymal transition (EMT) is regulated by AS mainly through ESRP1/2 (RBM35A/B), which favor an epithelial isoform program and hnRNPM, which favors a mesenchymal isoform program. A systematic analysis led to the discovery that RAP80, an adaptor protein encoded by UIMC1, with critical role in homology-directed repair (HDR) is regulated by ESRP1/2 and can be expressed as two major productive isoforms, one preferentially expressed in cells with epithelial phenotypes (long isoform UIMC1-201), and one expressed preferentially in cells with mesenchymal phenotypes (short isoform UIMC1-207). Analysis of the expression of these two RAP80 AS isoforms in breast cancer demonstrates the clinical relevance of these AS events, as we have found that the long/short RAP80 isoform ratio is an independent prognostic predictor in breast cancer. So we propose RAP80 as a target to reduce aggressive phenotypes in breast and prostate cancers, and we hypothesize a direct implication of this gene in the DNA-damage associated with the endothelial dysfunction.

7. REFERENCES

Adams, Stephen P, Sarpreet S Sekhon, and James M Wright. 2014. “Rosuvastatin for Lowering Lipids (Review).” *Cochrane Database of Systematic Reviews* 11: 1–262.

Adamson, R H. 1993. “Microvascular Endothelial Cell Shape and Size in Situ.” *Microvascular research* 46(1): 77–88.

Aguilar, Esther et al. 2016. “Metabolic Reprogramming and Dependencies Associated with Epithelial Cancer Stem Cells Independent of the Epithelial-Mesenchymal Transition Program.” *Stem Cells* 34(5): 1163–76.

Albini, Adriana, and Michael B. Sporn. 2007. “The Tumour Microenvironment as a Target for Chemoprevention.” *Nature Reviews Cancer* 7(2): 139–47.

Amelio, Ivano et al. 2014. “Serine and Glycine Metabolism in Cancer.” *Trends in biochemical sciences* 39(4): 191–98.

Anderson, Jeffrey L., and David A. Morrow. 2017. “Acute Myocardial Infarction.” *New England Journal of Medicine* 376(21): 2053–64.

Andrew, Deborah J., and Andrew J. Ewald. 2010. “Morphogenesis of Epithelial Tubes: Insights into Tube Formation, Elongation, and Elaboration.” *Developmental Biology* 341(1): 34–55.

Badimon, Lina, Teresa Padró, and Gemma Vilahur. 2012a. “Atherosclerosis, Platelets and Thrombosis in Acute Ischaemic Heart Disease.” *European Heart Journal: Acute Cardiovascular Care* 1(1): 60–74.

Baranwal, Somesh, and Suresh K Alahari. 2009. “Molecular Mechanisms Controlling E-Cadherin Expression in Breast Cancer.” *Biochemical and biophysical research communications* 384(1): 6–11.

Barash, Yoseph, Benjamin J Blencowe, and Brendan J Frey. 2010. “Model-Based Detection of Alternative Splicing Signals.” *Bioinformatics (Oxford, England)* 26(12): i325-33.

Van Beijnum, Judy R. et al. 2006. “Gene Expression of Tumor Angiogenesis Dissected: Specific Targeting of Colon Cancer Angiogenic Vasculature.” *Blood* 108(7): 2339–48.

Benito, Adrián et al. 2017. “Glucose-6-Phosphate Dehydrogenase and Transketolase Modulate Breast Cancer Cell Metabolic Reprogramming and Correlate with Poor Patient Outcome.” *Oncotarget* 8(63): 106693–706.

Bensaad, Karim et al. 2006. “TIGAR, a P53-Inducible Regulator of Glycolysis and Apoptosis.” *Cell* 126(1): 107–20.

Bergers, Gabriele, and Douglas Hanahan. 2008. “Modes of Resistance to Anti-Angiogenic Therapy.” *Nature Reviews Cancer* 8(8): 592–603.

Bergheanu, S. C., M. C. Bodde, and J. W. Jukema. 2017. “Pathophysiology and Treatment of Atherosclerosis: Current View and Future Perspective on Lipoprotein Modification Treatment.” *Netherlands Heart Journal* 25(4): 231–42.

Bernstein, Carol, Harris Bernstein, Claire M. Payne, and Harinder Garewal. 2002. “DNA Repair/pro-Apoptotic Dual-Role Proteins in Five Major DNA Repair Pathways: Fail-Safe Protection against Carcinogenesis.” *Mutation Research - Reviews in Mutation Research* 511(2): 145–78.

Bester, Assaf C. et al. 2011. “Nucleotide Deficiency Promotes Genomic Instability in Early Stages of Cancer Development.” *Cell* 145(3): 435–46.

Bhatt, Deepak L, Gregg W Stone, kenneth W Mahaffey, and C Michael Gibson. 2013. “Effect of Platelet Inhibition with Cangrelor during PCI on Ischemic Events.” *The New England Journal of Medicine* 368(14): 1303–13.

Bhutia, Yangzom D., and Vadivel Ganapathy. 2016. “Glutamine Transporters in Mammalian Cells and Their Functions in Physiology and Cancer.” *Biochimica et Biophysica Acta - Molecular Cell Research* 1863(10): 2531–39. http://dx.doi.org/10.1016/j.bbamcr.2015.12.017.

Bhutia, Yangzom D, Ellappan Babu, Sabarish Ramachandran, and Vadivel Ganapathy. 2015. “Amino Acid Transporters in Cancer and Their Relevance to ‘Glutamine Addiction’: Novel Targets for the Design of a New Class of Anticancer Drugs.” *Cancer research* 75(9): 1782–88.

Bian, Chunjing, Rong Wu, Kathleen Cho, and Xiaochun Yu. 2012. “Loss of BRCA1-A Complex

Function in RAP80 Null Tumor Cells." *PLoS ONE* 7(7).
Bierhansl, Laura et al. 2017. "Central Role of Metabolism in Endothelial Cell Function and Vascular Disease." *Physiology* 32(2): 126–40. http://physiologyonline.physiology.org/lookup/doi/10.1152/physiol.00031.2016.
Bissell, Mina J., and William C. Hines. 2011. "Why Don't We Get More Cancer? A Proposed Role of the Microenvironment in Restraining Cancer Progression." *Nature Medicine* 17(3): 320–29.
Black, Douglas L. 2003. "Mechanisms of Alternative Pre-Messenger RNA Splicing." *Annual Review of Biochemistry* 72(1): 291–336.
Blanco, Francisco J., and Carmelo Bernabeu. 2011. "Alternative Splicing Factor or Splicing Factor-2 Plays a Key Role in Intron Retention of the Endoglin Gene during Endothelial Senescence." *Aging Cell* 10(5): 896–907.
De Bock, Katrien et al. 2013. "Role of PFKFB3-Driven Glycolysis in Vessel Sprouting." *Cell* 154(3): 651–63.
Bogenrieder, Thomas, and Meenhard Herlyn. 2003. "Axis of Evil: Molecular Mechanisms of Cancer Metastasis." *Oncogene* 22(42): 6524–36.
Bonuccelli, Gloria et al. 2010. "Ketones and Lactate 'Fuel' Tumor Growth and Metastasis: Evidence That Epithelial Cancer Cells Use Oxidative Mitochondrial Metabolism." *Cell Cycle* 9(17): 3506–14.
Brandes, Ralf P., and Jörg Kreuzer. 2005. "Vascular NADPH Oxidases: Molecular Mechanisms of Activation." *Cardiovascular Research*.
Braunschweig, Ulrich et al. 2014. "Widespread Intron Retention in Mammals Functionally Tunes Transcriptomes." *Genome Research* 24(11): 1774–86.
Bray, Freddie et al. 2018. "Global Cancer Statistics 2018: GLOBOCAN Estimates of Incidence and Mortality Worldwide for 36 Cancers in 185 Countries." *CA: A Cancer Journal for Clinicians* 68(6): 394–424.
Brittan, Mairi et al. 2015. "Impaired Vascular Function and Repair in Patients with Premature Coronary Artery Disease." *European journal of preventive cardiology* 22(12): 1557–66.
Brooks, George A. 2018. "The Science and Translation of Lactate Shuttle Theory." *Cell Metabolism* 27(4): 757–85.
Bujak, Renata et al. 2016. "New Biochemical Insights into the Mechanisms of Pulmonary Arterial Hypertension in Humans." *PLoS ONE* 11(8).
Bukholm, I K, J M Nesland, and A L Borresen-Dale. 2000. "Re-Expression of E-Cadherin, Alpha-Catenin and Beta-Catenin, but Not of Gamma-Catenin, in Metastatic Tissue from Breast Cancer Patients [Seecomments]." *J Pathol* 190(1): 15–19.
Burke, A, and R Virmani. 2000. "Significance of Multiple Coronary Artery Thrombi. A Consequence of Diffuse Atherosclerotic Disease?" *Italian heart journal : official journal of the Italian Federation of Cardiology* 1(12): 832–34.
Burns, Jorge S, and Gina Manda. 2017. "Metabolic Pathways of the Warburg Effect in Health and Disease: Perspectives of Choice, Chain or Chance." *International journal of molecular sciences* 18(12).
Cansby, Emmelie et al. 2018. "STK25 Regulates Cardiovascular Disease Progression in a Mouse Model of Hypercholesterolemia." *Arteriosclerosis, Thrombosis, and Vascular Biology* 38(8): 1723–37.
Cao, Gaoyuan et al. 2002. "Involvement of Human PECAM-1 in Angiogenesis and in Vitro Endothelial Cell Migration." *American Journal of Physiology - Cell Physiology* 282(5 51-5).
Carracedo, Arkaitz, Lewis C. Cantley, and Pier Paolo Pandolfi. 2013. "Cancer Metabolism: Fatty Acid Oxidation in the Limelight." *Nature Reviews Cancer* 13(4): 227–32.
Cascante, Marta, and Silvia Marin. 2008. "Metabolomics and Fluxomics Approaches." *Essays in biochemistry* 45: 67–81.
Castro, Elena, and Rosalind Eeles. 2012. "The Role of BRCA1 and BRCA2 in Prostate Cancer." *Asian Journal of Andrology* 14(3): 409–14.

Catapano, Alberico L. et al. 2016. “2016 ESC/EAS Guidelines for the Management of Dyslipidaemias.” *European Heart Journal* 37(39): 2999-3058l.

Cavallaro, Ugo, and Gerhard Christofori. 2004. “Multitasking in Tumor Progression: Signaling Functions of Cell Adhesion Molecules.” *Annals of the New York Academy of Sciences* 1014: 58–66.

Celià-Terrassa, Toni et al. 2012. “Epithelial-Mesenchymal Transition Can Suppress Major Attributes of Human Epithelial Tumor-Initiating Cells.” *The Journal of Clinical Investigation* 122..

Chaw, S. Y. et al. 2012. “Epithelial to Mesenchymal Transition (EMT) Biomarkers - E-Cadherin, Beta-Catenin, APC and Vimentin - In Oral Squamous Cell Carcinogenesis and Transformation.” *Oral Oncology* 48(10): 997–1006.

Chawla, Rajender K. et al. 1984. “Plasma Cysteine, Cystine, and Glutathione in Cirrhosis.” *Gastroenterology* 87(4): 770–76. http://dx.doi.org/10.1016/0016-5085(84)90069-6.

Chen, Chen, Shujie Zhao, Anand Karnad, and James W. Freeman. 2018. “The Biology and Role of CD44 in Cancer Progression: Therapeutic Implications.” *Journal of Hematology and Oncology* 11(1).

Chen, Pei Yu et al. 2015. “Endothelial-to-Mesenchymal Transition Drives Atherosclerosis Progression.” *Journal of Clinical Investigation* 125(12): 4514–28.

Chen, Ying Jr et al. 2016. “Lactate Metabolism Is Associated with Mammalian Mitochondria.” *Nature Chemical Biology* 12(11): 937–43.

Cheng, Susan et al. 2012. “Metabolite Profiling Identifies Pathways Associated with Metabolic Risk in Humans.” *Circulation* 125(18): 2222–31.

Chesney, Jason et al. 2014. “Fructose-2,6-Bisphosphate Synthesis by 6-Phosphofructo-2-Kinase/Fructose-2,6-Bisphosphatase 4 (PFKFB4) Is Required for the Glycolytic Response to Hypoxia and Tumor Growth.” *Oncotarget* 5(16): 6670–86.

Choi, Eui Hwan, Seobin Yoon, Kyung Soon Park, and Keun P. Kim. 2017. “The Homologous Recombination Machinery Orchestrates Post-Replication DNA Repair during Self-Renewal of Mouse Embryonic Stem Cells.” *Scientific Reports* 7(1).

Ciruna, Brian, and Janet Rossant. 2001. “FGF Signaling Regulates Mesoderm Cell Fate Specification and Morphogenetic Movement at the Primitive Streak.” *Developmental Cell* 1(1): 37–49.

Coleman, Kara A., and Roger A. Greenberg. 2011. “The BRCA1-RAP80 Complex Regulates DNA Repair Mechanism Utilization by Restricting End Resection.” *Journal of Biological Chemistry* 286(15): 13669–80.

Collins, Y. et al. 2012. “Mitochondrial Redox Signalling at a Glance.” *Journal of Cell Science*.

Comunanza, Valentina, and Federico Bussolino. 2017. “Therapy for Cancer: Strategy of Combining Anti-Angiogenic and Target Therapies.” *Frontiers in cell and developmental biology* 5: 101.

Conradi, Lena-Christin et al. 2017. “Tumor Vessel Disintegration by Maximum Tolerable PFKFB3 Blockade.” *Angiogenesis*.

Cottrill, Katherine A., and Stephen Y. Chan. 2013. “Metabolic Dysfunction in Pulmonary Hypertension: The Expanding Relevance of the Warburg Effect.” *European Journal of Clinical Investigation* 43(8): 855–65.

Coviello, Jessica Shank. 2018. “Cardiovascular and Cancer Risk: The Role of Cardio-Oncology.” *Journal of the advanced practitioner in oncology* 9(2): 160–76.

Crawford, E David. 2003. “Complementary Medicine, Chemoprevention, and Staging of Prostate Cancer.” *Reviews in urology* 5 Suppl 6: S23-32.

Cucullo, Luca et al. 2011. “The Role of Shear Stress in Blood-Brain Barrier Endothelial Physiology.” *BMC Neuroscience* 12.

Dasgupta, Subhamoy et al. 2018. “Metabolic Enzyme PFKFB4 Activates Transcriptional Coactivator SRC-3 to Drive Breast Cancer.” *Nature* 556(7700): 249–54.

DeBeradinis, Ralph, and Tzuling Cheng. 2010. “Q’s next: The Diverse Function of Glutamine

Metabolism in Cancer." *Oncogene* 29(3): 313–24.
Denton, Alice E., Edward W. Roberts, and Douglas T. Fearon. 2018. "Stromal Cells in the Tumor Microenvironment." In *Advances in Experimental Medicine and Biology*, Springer New York LLC, 99–114.
Dettmer, Katja, Pavel A. Aronov, and Bruce D. Hammock. 2007. "Mass Spectrometry-Based Metabolomics." *Mass Spectrometry Reviews* 26(1): 51–78.
Dever, Seth M. et al. 2011. "Mutations in the BRCT Binding Site of BRCA1 Result in Hyperrecombination." *Aging* 3(5): 515–32.
Dimmer, K. S. et al. 2000. "The Low-Affinity Monocarboxylate Transporter MCT4 Is Adapted to the Export of Lactate in Highly Glycolytic Cells." *Biochemical Journal* 350(1): 219–27.
Dittmar, Kimberly A et al. 2012. "Genome-Wide Determination of a Broad ESRP-Regulated Posttranscriptional Network by High-Throughput Sequencing." *Molecular and cellular biology* 32(8): 1468–82.
Van der Donckt, Carole et al. 2015. "Elastin Fragmentation in Atherosclerotic Mice Leads to Intraplaque Neovascularization, Plaque Rupture, Myocardial Infarction, Stroke, and Sudden Death." *European heart journal* 36(17): 1049–58.
Draoui, N., and O. Feron. 2011. "Lactate Shuttles at a Glance: From Physiological Paradigms to Anti-Cancer Treatments." *Disease Models & Mechanisms* 4(6): 727–32. http://dmm.biologists.org/cgi/doi/10.1242/dmm.007724.
Draoui, Nihed, and Olivier Feron. 2011. "Lactate Shuttles at a Glance: From Physiological Paradigms to Anti-Cancer Treatments." *Disease models & mechanisms* 4(6): 727–32.
Draoui, Nihed, Pauline De Zeeuw, and Peter Carmeliet. 2017a. "Angiogenesis Revisited from a Metabolic Perspective: Role and Therapeutic Implications of Endothelial Cell Metabolism." *Open Biology* 7(12).
Dromparis, Peter, and Evangelos D. Michelakis. 2013. "Mitochondria in Vascular Health and Disease." *Annual Review of Physiology* 75(1): 95–126.
Drummond, Grant R., Stavros Selemidis, Kathy K. Griendling, and Christopher G. Sobey. 2011. "Combating Oxidative Stress in Vascular Disease: NADPH Oxidases as Therapeutic Targets." *Nature Reviews Drug Discovery*.
Dunlay, Shannon M. et al. 2012. "Longitudinal Changes in Ejection Fraction in Heart Failure Patients with Preserved and Reduced Ejection Fraction." *Circulation: Heart Failure* 5(6): 720–26.
Eelen, Guy et al. 2018. "Endothelial Cell Metabolism." *Physiological Reviews* 98(1): 3–58.
Eelen, Guy, Pauline De Zeeuw, Michael Simons, and Peter Carmeliet. 2015. "Endothelial Cell Metabolism in Normal and Diseased Vasculature." *Circulation Research*.
Estrela, José M., Angel Ortega, and Elena Obrador. 2006. "Glutathione in Cancer Biology and Therapy." *Critical Reviews in Clinical Laboratory Sciences* 43(2): 143–81.
Feng, Jing et al. 2009. "[Diagnostic Value of BRCA1 and P16 Gene Methylation in Sporadic Breast Cancer]." *Ai zheng = Aizheng = Chinese journal of cancer* 28(4): 436–40.
Feng, Yonghuai, and Liusong Wu. 2017. "MTOR Up-Regulation of PFKFB3 Is Essential for Acute Myeloid Leukemia Cell Survival." *Biochemical and Biophysical Research Communications* 483(2): 897–903.
Fici, Pietro et al. 2017. "Splicing Factor Ratio as an Index of Epithelial-Mesenchymal Transition and Tumor Aggressiveness in Breast Cancer." *Oncotarget* 8(2): 2423–36.
Fiermonte, Giuseppe et al. 2002. "Identification of the Mitochondrial Glutamate Transporter. Bacterial Expression, Reconstitution, Functional Characterization, and Tissue Distribution of Two Human Isoforms." *Journal of Biological Chemistry* 277(22): 19289–94.
Fitzgerald, Gillian, Inés Soro-Arnaiz, and Katrien De Bock. 2018a. "The Warburg Effect in Endothelial Cells and Its Potential as an Anti-Angiogenic Target in Cancer." *Frontiers in Cell and Developmental Biology* 6(SEP): 1–17.
Folkman, Judah. 1990. "How the Field of Controlled-Release Technology Began, and Its Central Role in the Development of Angiogenesis Research." *Biomaterials* 11(9): 615–18.

Fonsatti, E et al. 2003. “Emerging Role of Endoglin (CD105) as a Marker of Angiogenesis with Clinical Potential in Human Malignancies.” *Current cancer drug targets* 3(6): 427–32.

Förstermann, Ulrich. 2008. “Oxidative Stress in Vascular Disease: Causes, Defense Mechanisms and Potential Therapies.” *Nature Clinical Practice Cardiovascular Medicine*.

Förstermann, Ulrich, and William C. Sessa. 2012. “Nitric Oxide Synthases: Regulation and Function.” *European Heart Journal*.

Franklin, Derek A. et al. 2016. “P53 Coordinates DNA Repair with Nucleotide Synthesis by Suppressing PFKFB3 Expression and Promoting the Pentose Phosphate Pathway.” *Scientific Reports* 6.

French, John K et al. 2010. “Mechanical Complications After Percutaneous Coronary Intervention in ST-Elevation Myocardial Infarction (from APEX-AMI).” *The American Journal of Cardiology* 105(1): 59–63.

Garg, Minal. 2013. “Epithelial-Mesenchymal Transition - Activating Transcription Factors - Multifunctional Regulators in Cancer.” *World Journal of Stem Cells* 5(4): 188.

Van Geldermalsen, M. et al. 2016. “ASCT2/SLC1A5 Controls Glutamine Uptake and Tumour Growth in Triple-Negative Basal-like Breast Cancer.” *Oncogene* 35(24): 3201–8.

Ghoussaini, Maya, Paul D.P. Pharoah, and Douglas F. Easton. 2013. “Inherited Genetic Susceptibility to Breast Cancer: The Beginning of the End or the End of the Beginning?” *American Journal of Pathology* 183(4): 1038–51.

Gökmen-Polar, Yesim, Yuan Gu, Xiaoping Gu, and Sunil S. Badve. 2019. “Abstract 2109: A Novel Role for *ESRP1* in Regulating Proliferation in Therapy-Resistant ER-Positive Breast Cancer.” In *Experimental and Molecular Therapeutics*, American Association for Cancer Research, 2109–2109.

Goldstein, Michael, and Michael B. Kastan. 2015. “Repair versus Checkpoint Functions of BRCA1 Are Differentially Regulated by Site of Chromatin Binding.” *Cancer Research* 75(13): 2699–2707.

Gonzalez, Hugo, Catharina Hagerling, and Zena Werb. 2018. “Roles of the Immune System in Cancer: From Tumor Initiation to Metastatic Progression.” *Genes and Development* 32(19–20): 1267–84.

Goveia, Jermaine, Peter Stapor, and Peter Carmeliet. 2014. “Principles of Targeting Endothelial Cell Metabolism to Treat Angiogenesis and Endothelial Cell Dysfunction in Disease.” *EMBO molecular medicine* 6(9): 1–16.

Grajeda-Iglesias, Claudia, and Michael Aviram. 2018. “Specific Amino Acids Affect Cardiovascular Diseases and Atherogenesis via Protection against Macrophage Foam Cell Formation: Review Article.” *Rambam Maimonides medical journal* 9(3)..

Gravdal, Karsten, Ole J Halvorsen, Svein A Haukaas, and Lars A Akslen. 2007. “A Switch from E-Cadherin to N-Cadherin Expression Indicates Epithelial to Mesenchymal Transition and Is of Strong and Independent Importance for the Progress of Prostate Cancer.” *Clinical cancer research : an official journal of the American Association for Cancer Research* 13(23): 7003–11.

Grootaert, Mandy O.J. et al. 2015. “Defective Autophagy in Vascular Smooth Muscle Cells Accelerates Senescence and Promotes Neointima Formation and Atherogenesis.” *Autophagy*.

Guzzo, Catherine M. et al. 2012. “RNF4-Dependent Hybrid SUMO-Ubiquitin Chains Are Signals for RAP80 and Thereby Mediate the Recruitment of BRCA1 to Sites of DNA Damage.” *Science Signaling* 5(253).

Hanahan, Douglas, and Lisa M. Coussens. 2012. “Accessories to the Crime: Functions of Cells Recruited to the Tumor Microenvironment.” *Cancer Cell* 21(3): 309–22.

Hanahan, Douglas, and Robert A. Weinberg. 2011. “Hallmarks of Cancer: The next Generation.” *Cell* 144(5): 646–74.

Hansson, Göran K. 2005. “Inflammation, Atherosclerosis, and Coronary Artery Disease.” *n engl j med* 35216(21).

Hardie, D. Grahame. 2011. “AMP-Activated Protein Kinase-an Energy Sensor That Regulates All Aspects of Cell Function.” *Genes and Development* 25(18): 1895–1908.

Harvey, Lloyd, and Stephen Chan. 2017. “Emerging Metabolic Therapies in Pulmonary Arterial Hypertension.” *Journal of Clinical Medicine* 6(4): 43.

Harvey, Samuel E. et al. 2018. “Coregulation of Alternative Splicing by HnRNPM and ESRP1 during EMT.” *RNA* 24(10): 1326–38.

Haudenschild, Christian C., Ramzi S. Cotran, Michael A. Gimbrone, and Judah Folkman. 1975. “Fine Structure of Vascular Endothelium in Culture.” *Journal of Ultrasructure Research* 50(1): 22–32.

Havens, Mallory A., Dominik M. Duelli, and Michelle L. Hastings. 2013. “Targeting RNA Splicing for Disease Therapy.” *Wiley Interdisciplinary Reviews: RNA* 4(3): 247–66.

Heiden, Matthew G Vander, Lewis C. Cantley, and Craig B. Thompson. 2009. “Understanding the Warburg Effect: The Metabolic Requirements of Cell Proliferation.” *Science* 324(5930): 1029–33.

Hensley, Christopher T, Ajla T Wasti, and Ralph J DeBerardinis. 2013. “Glutamine and Cancer: Cell Biology, Physiology, and Clinical Opportunities.” *The Journal of clinical investigation* 123(9): 3678–84.

Hertz, Leif, and Gerald A. Dienel. 2005. “Lactate Transport and Transporters: General Principles and Functional Roles in Brains Cells.” In *Journal of Neuroscience Research*, , 11–18.

Van Den Heuvel, A. Pieter J., Junping Jing, Richard F. Wooster, and Kurtis E. Bachman. 2012. “Analysis of Glutamine Dependency in Non-Small Cell Lung Cancer: GLS1 Splice Variant GAC Is Essential for Cancer Cell Growth.” *Cancer Biology and Therapy* 13(12): 1185–94.

Hida, Kyoko, Nako Maishi, Dorcas A. Annan, and Yasuhiro Hida. 2018. “Contribution of Tumor Endothelial Cells in Cancer Progression.” *International Journal of Molecular Sciences* 19(5).

Ho, Daniel V., and Jefferson Y. Chan. 2015. “Induction of Herpud1 Expression by ER Stress Is Regulated by Nrf1.” *FEBS Letters* 589(5): 615–20.

Hoefer, Imo E. et al. 2015. “Novel Methodologies for Biomarker Discovery in Atherosclerosis.” *European Heart Journal*.

Holliday, Deborah L., and Valerie Speirs. 2011. “Choosing the Right Cell Line for Breast Cancer Research.” *Breast Cancer Research* 13(4).

Holmes, Kevin L., and Larry M. Lantz. 2001. “Protein Labeling with Fluorescent Probes.” *Methods in Cell Biology* (63): 185–204.

Hou, Guo Xin, Panpan Liu, Jing Yang, and Shijun Wen. 2017. “Mining Expression and Prognosis of Topoisomerase Isoforms in Non-Small-Cell Lung Cancer by Using Oncomine and Kaplan-Meier Plotter.” *PLoS ONE* 12(3): 1–16.

Hu, Xin, Atanu Paul, and Bin Wangs. 2012. “Rap80 Protein Recruitment to DNA Double-Strand Breaks Requires Binding to Both Small Ubiquitin-like Modifier (SUMO) and Ubiquitin Conjugates.” *Journal of Biological Chemistry* 287(30): 25510–19.

Hu, Yiduo et al. 2011a. “RAP80-Directed Tuning of BRCA1 Homologous Recombination Function at Ionizing Radiation-Induced Nuclear Foci.” *Genes & development* 25(7): 685–700.

Hu, Ying et al. 2017. “Splicing Factor HnRNPA2B1 Contributes to Tumorigenic Potential of Breast Cancer Cells through STAT3 and ERK1/2 Signaling Pathway.” *Tumour biology : the journal of the International Society for Oncodevelopmental Biology and Medicine* 39(3): 1010428317694318.

Huang, Hongling et al. 2017. “Role of Glutamine and Interlinked Asparagine Metabolism in Vessel Formation.” *The EMBO Journal* 36(16): 2334–52.

Huen, Michael S Y et al. 2007. “RNF8 Transduces the DNA-Damage Signal via Histone Ubiquitylation and Checkpoint Protein Assembly.” *Cell* 131(5): 901–14.

Husted, Steen et al. 2014. “Non-Vitamin K Antagonist Oral Anticoagulants (NOACs): No Longer New or Novel.” *Thrombosis and Haemostasis* 111(5): 781–82.

Hyder, J. A., M. A. Allison, M. H. Criqui, and C. M. Wright. 2007. “Association between Systemic Calcified Atherosclerosis and Bone Density.” *Calcified Tissue International*.

Ibanez, Borja et al. 2018. “2017 ESC Guidelines for the Management of Acute Myocardial Infarction in Patients Presenting with ST-Segment Elevation.” *European Heart Journal* 39(2): 119–77.

Ishimoto, Takatsugu et al. 2011. “CD44 Variant Regulates Redox Status in Cancer Cells by Stabilizing the XCT Subunit of System Xc- and Thereby Promotes Tumor Growth.” *Cancer Cell* 19(3): 387–400. http://dx.doi.org/10.1016/j.ccr.2011.01.038.

Jacob, Aishwarya G., and Christopher W.J. Smith. 2017. “Intron Retention as a Component of Regulated Gene Expression Programs.” *Human Genetics* 136(9): 1043–57.

Jan, Yi-Hua et al. 2019. “Adenylate Kinase 4 Modulates Oxidative Stress and Stabilizes HIF-1α to Drive Lung Adenocarcinoma Metastasis.” *Journal of hematology & oncology* 12(1): 12.

Jeong, H M et al. 2017. “ESRP1 Is Overexpressed in Ovarian Cancer and Promotes Switching from Mesenchymal to Epithelial Phenotype in Ovarian Cancer CellsThis Article Has Been Corrected since Advance Online Publication and an Erratum Is Also Printed in This Issue.” *Oncogenesis* 6(10): e389–e389.

Jordan, Karen, Rochelle Chodock, Art R. Hand, and Dale W. Laird. 2001. “The Origin of Annular Junctions: A Mechanism of Gap Junction Internalization.” *Journal of Cell Science* 114(4): 763–73.

Jung, Hyunchul et al. 2015. “Intron Retention Is a Widespread Mechanism of Tumor-Suppressor Inactivation.” *Nature Genetics* 47(11): 1242–48.

Jurica, Melissa S, and Melissa J Moore. 2003. 12 Molecular Cell *Review Pre-MRNA Splicing: Awash in a Sea of Proteins Purifying Any One Spliceosomal Subcomplex in Vitro, the Most Common Proteomics Approach to Date Has Been to Work with Mixtures of Assembly Intermediates (Neu*.

Kakarougkas, Andreas et al. 2013. “Opposing Roles for 53BP1 during Homologous Recombination.” *Nucleic acids research* 41(21): 9719–31.

Kalogeris, Theodore, Christopher P. Baines, Maike Krenz, and Ronald J. Korthuis. 2012. “Cell Biology of Ischemia/Reperfusion Injury.” In *International Review of Cell and Molecular Biology*, Elsevier Inc., 229–317.

Kanhai, Danny A. et al. 2013. “Microvesicle Protein Levels Are Associated with Increased Risk for Future Vascular Events and Mortality in Patients with Clinically Manifest Vascular Disease.” *International Journal of Cardiology* 168(3): 2358–63.

Kaptoge, S. et al. 2012. “C-Reactive Protein, Fibrinogen, and Cardiovascular Disease Prediction.” *New England Journal of Medicine* 367(14): 1310–20. http://www.nejm.org/doi/abs/10.1056/NEJMoa1107477.

Kareva, Irina, and Philip Hahnfeldt. 2013. “The Emerging ‘Hallmarks’ of Metabolic Reprogramming and Immune Evasion: Distinct or Linked?” *Cancer Research* 73(9): 2737–42.

Kim, Dohoon et al. 2015. “SHMT2 Drives Glioma Cell Survival in Ischaemia but Imposes a Dependence on Glycine Clearance.” *Nature* 520(7547): 363–67.

Kim, Eddo, Amir Goren, and Gil Ast. 2008. “Alternative Splicing: Current Perspectives.” *BioEssays* 30(1): 38–47.

Kim, Hongtae, Junjie Chen, and Xiaochun Yu. 2007. “Ubiquitin-Binding Protein RAP80 Mediates BRCA1-Dependent DNA Damage Response.” *Science (New York, N.Y.)* 316(5828): 1202–5.

Kim, Min Hyun, and Hyeyoung Kim. 2013. “Oncogenes and Tumor Suppressors Regulate Glutamine Metabolism in Cancer Cells.” *Journal of Cancer Prevention* 18(3): 221–26.

Kim, Seung-Jae et al. 2013. “Angiogenesis in Rheumatoid Arthritis Is Fostered Directly by Toll-like Receptor 5 Ligation and Indirectly through Interleukin-17 Induction.” *Arthritis and rheumatism* 65(8): 2024–36.

Koh, Cheryl M. et al. 2015. “MYC Regulates the Core Pre-MRNA Splicing Machinery as an Essential Step in Lymphomagenesis.” *Nature* 523(7558): 96–100.

Kojima, Keita et al. 2018a. “Cysteine Dioxygenase Type 1 (CDO1) Gene Promoter Methylation during the Adenoma-Carcinoma Sequence in Colorectal Cancer.” *PLoS ONE* 13(5).

Kolas, Nadine K et al. 2007. “Orchestration of the DNA-Damage Response by the RNF8 Ubiquitin Ligase.” *Science (New York, N.Y.)* 318(5856): 1637–40.

Kovacic, Jason C. et al. 2019. “Endothelial to Mesenchymal Transition in Cardiovascular Disease: JACC State-of-the-Art Review.” *Journal of the American College of Cardiology* 73(2): 190–209.

Kumar, Avinash et al. 2017. “The Metabolism and Significance of Homocysteine in Nutrition and Health.” *Nutrition & metabolism* 14: 78.

Lacroix, R. et al. 2010. “Standardization of Platelet-Derived Microparticle Enumeration by Flow Cytometry with Calibrated Beads: Results of the International Society on Thrombosis and Haemostasis SSC Collaborative Workshop.” *Journal of Thrombosis and Haemostasis* 8(11): 2571–74.

Laplante, Mathieu, and David M. Sabatini. 2012. “MTOR Signaling in Growth Control and Disease.” *Cell* 149(2): 274–93.

Lee, Genee Y. et al. 2014. “Comparative Oncogenomics Identifies Psmb4 and Shmt2 as Potential Cancer Driver Genes.” *Cancer Research* 74(11): 3114–26.

Leopold, Jane A., and Joseph Loscalzo. 2005. “Oxidative Enzymopathies and Vascular Disease - ATVB in Focus.” *Arteriosclerosis, Thrombosis, and Vascular Biology*.

Lewis, Gregory D. 2014. “The Emerging Role of Metabolomics in the Development of Biomarkers for Pulmonary Hypertension and Other Cardiovascular Diseases (2013 Grover Conference Series).” *Pulmonary Circulation* 4(3): 417–23.

Ley, K, and Y Huo. 2001. “VCAM-1 Is Critical in Atherosclerosis.” *The Journal of clinical investigation* 107(10): 1209–10.

Li, Cheng Lin et al. 2017. “Fibronectin Induces Epithelial-Mesenchymal Transition in Human Breast Cancer MCF-7 Cells via Activation of Calpain.” *Oncology Letters* 13(5): 3889–95.

Li, Huige, Sven Horke, and Ulrich Förstermann. 2014a. “Vascular Oxidative Stress, Nitric Oxide and Atherosclerosis.” *Atherosclerosis*.

Li, Qi et al. 2018. “CDC7-Dependent Transcriptional Regulation of RAD54L Is Essential for Tumorigenicity and Radio-Resistance of Glioblastoma.” *Translational oncology* 11(2): 300–306.

Li, Xuri, Anil Kumar, and Peter Carmeliet. 2019a. “Metabolic Pathways Fueling the Endothelial Cell Drive.” *Annual Review of Physiology* 81(1): 483–503.

Liu, Rujuan et al. 2009. “Enzymatically Inactive Adenylate Kinase 4 Interacts with Mitochondrial ADP/ATP Translocase.” *International Journal of Biochemistry and Cell Biology* 41(6): 1371–80.

Livak, Kenneth J., and Thomas D. Schmittgen. 2001. “Analysis of Relative Gene Expression Data Using Real-Time Quantitative PCR and the 2-ΔΔCT Method.” *Methods* 25(4): 402–8.

Lo, Maisie, Yu Zhuo Wang, and Peter W. Gout. 2008. “The Xc- Cystine/Glutamate Antiporter: A Potential Target for Therapy of Cancer and Other Diseases.” *Journal of Cellular Physiology* 215(3): 593–602.

LOWRY, O. H., N. J. ROSEBROUGH, A. L. FARR, and R. J. RANDALL. 1951. “Protein Measurement with the Folin Phenol Reagent.” *The Journal of biological chemistry* 193(1): 265–75.

Lu, Yuan et al. 2013. “Kruppel-like Factor 15 Is Critical for Vascular Infammation.” *Journal of Clinical Investigation*.

Lubarsky, Barry, and Mark A. Krasnow. 2003. “Tube Morphogenesis: Making and Shaping Biological Tubes.” *Cell* 112(1): 19–28.

Mandal, Pankaj Kumar et al. 2010. “System Xc- and Thioredoxin Reductase 1 Cooperatively Rescue Glutathione Deficiency.” *Journal of Biological Chemistry* 285(29): 22244–53.

El Marabti, Ettaib, and Ihab Younis. 2018. “The Cancer Spliceome: Reprograming of Alternative Splicing in Cancer.” *Frontiers in Molecular Biosciences* 5(SEP).

Marín de Mas, Igor et al. 2018. “Model-Driven Discovery of Long-Chain Fatty Acid Metabolic Reprogramming in Heterogeneous Prostate Cancer Cells.” *PLoS Computational Biology* 14(1): 1–20.

Marino, Stefano M., and Vadim N. Gladyshev. 2010. “Cysteine Function Governs Its Conservation and Degeneration and Restricts Its Utilization on Protein Surfaces.” *Journal of Molecular Biology* 404(5): 902–16.

Martin, T A, G Watkins, J Lane, and W G Jiang. 2005. “Assessing Microvessels and Angiogenesis in Human Breast Cancer, Using VE-Cadherin.” *Histopathology* 46(4): 422–30.

Martinez-Montiel, Nancy, Nora Hilda Rosas-Murrieta, et al. 2018. “Alternative Splicing as a Target for Cancer Treatment.” *International Journal of Molecular Sciences* 19(2): 1–28.

Martinez-Montiel, Nancy, Nora Hilda Rosas-Murrieta, et al. 2018. “Molecular Sciences

Mateo, Francesca et al. 2014. “SPARC Mediates Metastatic Cooperation between CSC and Non-CSC Prostate Cancer Cell Subpopulations.” *Molecular cancer* 13: 237.

Matsumoto, Sen et al. 2013. “Circulating P53-Responsive MicroRNAs Are Predictive Indicators of Heart Failure after Acute Myocardial Infarction.” *Circulation Research* 113(3): 322–26.

Mehta, Laxmi S. et al. 2018. “Cardiovascular Disease and Breast Cancer: Where These Entities Intersect: A Scientific Statement From the American Heart Association.” *Circulation* 137(8): e30–66.

Mina, Sara G., Peter Huang, Bruce T. Murray, and Gretchen J. Mahler. 2017. “The Role of Shear Stress and Altered Tissue Properties on Endothelial to Mesenchymal Transformation and Tumor-Endothelial Cell Interaction.” *Biomicrofluidics* 11(4).

Minchenko, Oleksandr H et al. 2014. “Mechanisms of Regulation of PFKFB Expression in Pancreatic and Gastric Cancer Cells.” *World journal of gastroenterology* 20(38): 13705–17.

Moreno-Sánchez, Rafael, Sara Rodríguez-Enríquez, Alvaro Marín-Hernández, and Emma Saavedra. 2007. “Energy Metabolism in Tumor Cells.” *The FEBS Journal* 274(6): 1393–1418.

Moreno-Viedma, V. et al. 2016. “Common Dysregulated Pathways in Obese Adipose Tissue and Atherosclerosis.” *Cardiovascular Diabetology* 15(1): 120.

Mortazavi, Ali et al. 2008. “Mapping and Quantifying Mammalian Transcriptomes by RNA-Seq.” *Nature Methods* 5(7): 621–28.

Mosca, Lori et al. 2013. “Fifteen-Year Trends in Awareness of Heart Disease in Women: Results of a 2012 American Heart Association National Survey.” *Circulation* 127(11): 1254–63.

Müller, H. Arno J., and Olaf Bossinger. 2003. “Molecular Networks Controlling Epithelial Cell Polarity in Development.” *Mechanisms of Development* 120(11): 1231–56.

Murphy, Michael P. 2009. “How Mitochondria Produce Reactive Oxygen Species.” *The Biochemical journal* 417(1): 1–13.

Muthukkaruppan, V R, L Kubai, and R Auerbach. 1982. “Tumor-Induced Neovascularization in the Mouse Eye.” *Journal of the National Cancer Institute* 69(3): 699–708..

Nakka, Kiran, Claudia Ghigna, Davide Gabellini, and F. Jeffrey Dilworth. 2018. “Diversification of the Muscle Proteome through Alternative Splicing.” *Skeletal Muscle* 8(1).

NikkiЇ, J. et al. 2009. “Familial Breast Cancer Screening Reveals an Alteration in the RAP80 UIM Domain That Impairs DNA Damage Response Function.” *Oncogene* 28(16): 1843–52.

Nilsson, Avlant, and Jens Nielsen. 2016. “Genome Scale Metabolic Modeling of Cancer.” *Metabolic Engineering* 43(part B): 103–12.

Nishida, Naoyo. 2016. “Angiogenesis in Cancer Angiogenesis in Cancer.” *Vascular health and risk management* 2(November): 213–19.

Nogueira-Ferreira, Rita, Rita Ferreira, and Tiago Henriques-Coelho. 2014. “Cellular Interplay in Pulmonary Arterial Hypertension: Implications for New Therapies.” *Biochimica et Biophysica Acta - Molecular Cell Research* 1843(5): 885–93.

Noma, T. et al. 2001. “Structure and Expression of Human Mitochondrial Adenylate Kinase Targeted to the Mitochondrial Matrix.” *Biochemical Journal* 358(1): 225–32.

Orellana-Serradell, Octavio, Daniela Herrera, Enrique Castellon, and Hector Contreras. 2018. “The Transcription Factor ZEB1 Promotes an Aggressive Phenotype in Prostate Cancer Cell Lines.” *Asian Journal of Andrology* 20(3): 294–99.

Ormazabal, Valeska et al. 2018. “Association between Insulin Resistance and the Development of Cardiovascular Disease.” *Cardiovascular Diabetology* 17(1): 1–14.

https://doi.org/10.1186/s12933-018-0762-4.
Osanai-Sasakawa, Aya et al. 2018. “An Anti-ASCT2 Monoclonal Antibody Suppresses Gastric Cancer Growth by Inducing Oxidative Stress and Antibody Dependent Cellular Toxicity in Preclinical Models.” *American journal of cancer research* 8(8): 1499–1513.
Padfield, Gareth J. et al. 2013. “Endothelial Progenitor Cells, Atheroma Burden and Clinical Outcome in Patients with Coronary Artery Disease.” *Heart* 99(11): 791–98.
Pahwa, Rajesh et al. 2019. “Neuromodulation: Technology at the Neural Interface An Acute Randomized Controlled Trial of Noninvasive Peripheral Nerve Stimulation in Essential Tremor.”
Palmieri, Ferdinando. 2004. “The Mitochondrial Transporter Family (SLC25): Physiological and Pathological Implications.” *Pflugers Archiv European Journal of Physiology* 447(5): 689–709.
Palmieri, Ferdinando, and Magnus Monné. 2016. “Discoveries, Metabolic Roles and Diseases of Mitochondrial Carriers: A Review.” *Biochimica et Biophysica Acta - Molecular Cell Research* 1863(10): 2362–78. http://dx.doi.org/10.1016/j.bbamcr.2016.03.007.
Palucka, A. Karolina, and Lisa M. Coussens. 2016. “The Basis of Oncoimmunology.” *Cell* 164(6): 1233–47.
Pan, Qun et al. 2008. “Deep Surveying of Alternative Splicing Complexity in the Human Transcriptome by High-Throughput Sequencing.” *Nature Genetics* 40(12): 1413–15.
Park, Chan Soon et al. 2018. “Association between Adult Height, Myocardial Infarction, Heart Failure, Stroke and Death: A Korean Nationwide Population-Based Study.” *International Journal of Epidemiology* 47(1): 289–98.
Park, Simon J et al. 2018. “An Overview of MCT1 and MCT4 in GBM: Small Molecule Transporters with Large Implications.” *American journal of cancer research* 8(10): 1967–76. http://www.ncbi.nlm.nih.gov/pubmed/30416849.
Parra-Bonilla, Glenda et al. 2010. “Critical Role for Lactate Dehydrogenase A in Aerobic Glycolysis That Sustains Pulmonary Microvascular Endothelial Cell Proliferation.” *American Journal of Physiology - Lung Cellular and Molecular Physiology* 299(4).
Parsa, C.J, M.A. Daneshmand, J.G. Gaca, and J Scott Rankin. 2011a. “Arterial Bypass Grafting of the Coronary Circulation.” *HSR Proceedings in Intensive Care and Cardiovascular Anesthesia* 3(4): 227–34.
Parsa, C J, M A Daneshmand, J G Gaca, and J S Rankin. 2011b. “Arterial Bypass Grafting of the Coronary Circulation.” *HSR proceedings in intensive care & cardiovascular anesthesia* 3(4): 227–34.
Patra, Krushna C., and Nissim Hay. 2014. “The Pentose Phosphate Pathway and Cancer.” *Trends in Biochemical Sciences* 39(8): 347–54.
Pellagatti, Andrea et al. 2018. “Impact of Spliceosome Mutations on RNA Splicing in Myelodysplasia: Dysregulated Genes/Pathways and Clinical Associations.” *Blood* 132(12): 1225–40.
Pober, Jordan S., Wang Min, and John R. Bradley. 2009. “Mechanisms of Endothelial Dysfunction, Injury, and Death.” *Annual Review of Pathology: Mechanisms of Disease* 4(1): 71–95.
Py, Bénédicte F., Mi Sung Kim, Helin Vakifahmetoglu-Norberg, and Junying Yuan. 2013. “Deubiquitination of NLRP3 by BRCC3 Critically Regulates Inflammasome Activity.” *Molecular Cell* 49(2): 331–38.
Rabl, Julius et al. 2019a. “Structural Basis of BRCC36 Function in DNA Repair and Immune Regulation.” *Molecular Cell* 75(3): 483-497.e9.
Radisky, Derek C., and Mark A. LaBarge. 2008. “Epithelial-Mesenchymal Transition and the Stem Cell Phenotype.” *Cell Stem Cell* 2(6): 511–12.
Rajabi, Mehdi, and Shaker A. Mousa. 2017. “The Role of Angiogenesis in Cancer Treatment.” *Biomedicines* 5(2).
Rakic, Marijana et al. 2018. “Possible Role of Circulating Endothelial Cells in Patients after Acute Myocardial Infarction.” *Medical hypotheses* 117: 42–46.

Rathore, Vedika. 2018. “Risk Factors of Acute Myocardial Infarction: A Review.” *Eurasian Journal of Medical Investigation*.

Riganti, Chiara, and Massimo Massaia. 2013. “Inhibition of the Mevalonate Pathway to Override Chemoresistance and Promote the Immunogenic Demise of Cancer Cells: Killing Two Birds with One Stone.” *OncoImmunology* 2(9).

Rizzuto, Rosario, Diego De Stefani, Anna Raffaello, and Cristina Mammucari. 2012. “Mitochondria as Sensors and Regulators of Calcium Signalling.” *Nature Reviews Molecular Cell Biology*.

Rohatgi, Anand et al. 2014. “HDL Cholesterol Efflux Capacity and Incident Cardiovascular Events.” *New England Journal of Medicine* 371(25): 2383–93.

Ros, S et al. 2017. “6-Phosphofructo-2-Kinase/Fructose-2,6-Biphosphatase 4 Is Essential for P53-Null Cancer Cells.” *Oncogene* 36(23): 3287–99.

Ros, Susana, and Almut Schulze. 2013. “Balancing Glycolytic Flux: The Role of 6-Phosphofructo-2-Kinase/Fructose 2,6-Bisphosphatases in Cancer Metabolism.” *Cancer & Metabolism* 1(1).

Rosen, Eliot M. 2013. “BRCA1 in the DNA Damage Response and at Telomeres.” *Frontiers in genetics* 4: 85.

Ryan, John J. et al. 2015. “Right Ventricular Adaptation and Failure in Pulmonary Arterial Hypertension.” *Canadian Journal of Cardiology* 31(4): 391–406.

Ryu, Jae Yong, Hyun Uk Kim, and Sang Yup Lee. 2015. “Reconstruction of Genome-Scale Human Metabolic Models Using Omics Data.” *Integrative Biology* 7(8): 859–68. http://xlink.rsc.org/?DOI=C5IB00002E.

Sammeth, Michael, Sylvain Foissac, and Roderic Guigó. 2008. “A General Definition and Nomenclature for Alternative Splicing Events.” *PLoS Computational Biology* 4(8).

Sánchez-Cabo, Fátima et al. 2011. “Insights into Global Mechanisms and Disease by Gene Expression Profiling.” *Methods in molecular biology (Clifton, N.J.)* 719: 269–98.

Sánchez-Cid, Lourdes et al. 2017. “Oncotarget 83384 Www.Impactjournals.Com/Oncotarget MicroRNA-200, Associated with Metastatic Breast Cancer, Promotes Traits of Mammary Luminal Progenitor Cells.” *Oncotarget* 8(48): 83384–406. www.impactjournals.com/oncotarget/.

Sandoo, Aamer et al. 2015. “The Endothelium and Its Role in Regulating Vascular Tone.” *The Open Cardiovascular Medicine Journal* 4(1): 302–12.

Santos, Maria José et al. 2011. “Hemorheological Parameters Are Related to Subclinical Atherosclerosis in Systemic Lupus Erythematosus and Rheumatoid Arthritis Patients.” *Atherosclerosis*.

Scanlon, C. S., E. A. Van Tubergen, R. C. Inglehart, and N. J. D’Silva. 2013. “Biomarkers of Epithelial-Mesenchymal Transition in Squamous Cell Carcinoma.” *Journal of Dental Research* 92(2): 114–21.

VAN SCHAFTINGEN, Emile, Béatrice LEDERER, Ramon BARTRONS, and Henri-Géry -G HERS. 1982. “A Kinetic Study of Pyrophosphate: Fructose-6-Phosphate Phosphotransferase from Potato Tubers: Application to a Microassay of Fructose 2,6-Bisphosphate.” *European Journal of Biochemistry* 129(1): 191–95.

Schneider, Caroline A., Wayne S. Rasband, and Kevin W. Eliceiri. 2012. “NIH Image to ImageJ: 25 Years of Image Analysis.” *Nature Methods* 9(7): 671–75.

Schoors, Sandra et al. 2014. “Partial and Transient Reduction of Glycolysis by PFKFB3 Blockade Reduces Pathological Angiogenesis.” *Cell metabolism* 19(1): 37–48.

Schrijvers, Dorien M. et al. 2005. “Phagocytosis of Apoptotic Cells by Macrophages Is Impaired in Atherosclerosis.” *Arteriosclerosis, Thrombosis, and Vascular Biology* 25(6): 1256–61.

Schulte, Michael L. et al. 2018. “Pharmacological Blockade of ASCT2-Dependent Glutamine Transport Leads to Antitumor Efficacy in Preclinical Models.” *Nature Medicine* 24(2): 194–202.

Scully, R et al. 1997. “Dynamic Changes of BRCA1 Subnuclear Location and Phosphorylation State Are Initiated by DNA Damage.” *Cell* 90(3): 425–35.

Seib, Todd Michael, Sarjubhai Amratbhai Patel, and Richard James Bridges. 2011. "Regulation of the System x - C Cystine/Glutamate Exchanger by Intracellular Glutathione Levels in Rat Astrocyte Primary Cultures." *GLIA* 59(10): 1387–1401.

Semenza, Gregg L. 2008. "Tumor Metabolism : Cancer Cells Give and Take Lactate." *the Journal of Clinical Investigation* 118(12): 3835–37.

Seo, Minsuh, and Yong-Hwan Lee. 2014. "PFKFB3 Regulates Oxidative Stress Homeostasis via Its S-Glutathionylation in Cancer." *Journal of molecular biology* 426(4): 830–42.

Serrano-Gomez, Silvia Juliana, Mazvita Maziveyi, and Suresh K. Alahari. 2016. "Regulation of Epithelial-Mesenchymal Transition through Epigenetic and Post-Translational Modifications." *Molecular Cancer* 15(1): 1–14. http://dx.doi.org/10.1186/s12943-016-0502-x.

Shah, Nikunj R., and Michael Mahmoudi. 2015. "The Role of DNA Damage and Repair in Atherosclerosis: A Review." *Journal of Molecular and Cellular Cardiology* 86: 147–57.

Shah, Svati H. et al. 2010. "Association of a Peripheral Blood Metabolic Profile with Coronary Artery Disease and Risk of Subsequent Cardiovascular Events." *Circulation: Cardiovascular Genetics* 3(2): 207–14.

Shapiro, H. M., P. J. Natale, and L. A. Kamentsky. 1979. "Estimation of Membrane Potentials of Individual Lymphocytes by Flow Cytometry." *Proceedings of the National Academy of Sciences of the United States of America* 76(11): 5728–30.

Sherwood, Louis M., Edith E. Parris, and Judah Folkman. 1971. "Tumor Angiogenesis: Therapeutic Implications." *New England Journal of Medicine* 285(21): 1182–86.

Shkreta, Lulzim, and Benoit Chabot. 2015. "The RNA Splicing Response to DNA Damage." *Biomolecules* 5(4): 2935–77.

Shu, Yuxin et al. 2016. "Phosphorylation of PPARγ at Ser84 Promotes Glycolysis and Cell Proliferation in Hepatocellular Carcinoma by Targeting PFKFB4." *Oncotarget* 7(47): 76984–94.

De Silva, Sumadee, Kamani Hemamala Tennekoon, and Eric Hamilton Karunanayake. 2019. "Overview of the Genetic Basis toward Early Detection of Breast Cancer." *Breast Cancer: Targets and Therapy* Volume 11: 71–80.

Sinha, Sanjay, Dharini Iyer, and Alessandra Granata. 2014. "Cellular and Molecular Life Sciences Embryonic Origins of Human Vascular Smooth Muscle Cells: Implications for in Vitro Modeling and Clinical Application." *Cell. Mol. Life Sci* 71: 2271–88.

Sitia, S. et al. 2010a. "From Endothelial Dysfunction to Atherosclerosis." *Autoimmunity Reviews* 9(12): 830–34.

Smith, P. K. et al. 1985. "Measurement of Protein Using Bicinchoninic Acid." *Analytical Biochemistry* 150(1): 76–85.

Smolders, Valérie Françoise et al. 2019. "Metabolic Alterations in Cardiopulmonary Vascular Dysfunction." *Frontiers in Molecular Biosciences* 5(JAN): 1–14.

Sobhian, Bijan et al. 2007. "RAP80 Targets BRCA1 to Specific Ubiquitin Structures at DNA Damage Sites." *Science (New York, N.Y.)* 316(5828): 1198–1202.

Solyom, Szilvia et al. 2012. "Breast Cancer-Associated Abraxas Mutation Disrupts Nuclear Localization and DNA Damage Response Functions." *Science Translational Medicine* 4(122).

Son, Jaekyoung et al. 2013. "Glutamine Supports Pancreatic Cancer Growth through a KRAS-Regulated Metabolic Pathway." *Nature* 496(7443): 101–5. http://dx.doi.org/10.1038/nature12040.

Stamm, S. 2006. "ASD: A Bioinformatics Resource on Alternative Splicing." *Nucleic Acids Research* 34(90001): D46–55.

Stapor, Peter C. et al. 2014. "Pericyte Dynamics during Angiogenesis: New Insights from New Identities." *Journal of Vascular Research* 51(3): 163–74.

Stegemann, Christin, Raimund Pechlaner, Peter Willeit, and Sarah R Langley. 2014. "Lipidomics Profiling and Risk of Cardiovascular Disease in the Prospective Population-Based Bruneck Study Christin." *Circulation* 129(18): 1821–31.

Stemmler, Marc P., Rebecca L. Eccles, Simone Brabletz, and Thomas Brabletz. 2019. “Non-Redundant Functions of EMT Transcription Factors.” *Nature Cell Biology* 21(1): 102–12.

Subramanian, Aravind et al. 2005. “Gene Set Enrichment Analysis: A Knowledge-Based Approach for Interpreting Genome-Wide Expression Profiles.” *Proceedings of the National Academy of Sciences of the United States of America* 102(43): 15545–50.

Suganuma, Kazuto et al. 2010. “Energy Metabolism of Leukemia Cells: Glycolysis versus Oxidative Phosphorylation.” *Leukemia and Lymphoma* 51(11): 2112–19.

Sun, Lin et al. 2017. “Decreased Expression of Acetyl-CoA Synthase 2 Promotes Metastasis and Predicts Poor Prognosis in Hepatocellular Carcinoma.” *Cancer Science* 108(7): 1338–46.

Thangavelu, K, Qing Yun Chong, Boon Chuan Low, and J Sivaraman. 2014. “Structural Basis for the Active Site Inhibition Mechanism of Human Kidney-Type Glutaminase (KGA).” *Scientific reports* 4: 3827.

Theodorou, Kosta, and Reinier A. Boon. 2018. “Endothelial Cell Metabolism in Atherosclerosis.” *Frontiers in Cell and Developmental Biology* 6(AUG).

Thiery, Jean Paul. 2003. “Epithelial-Mesenchymal Transitions in Development and Pathologies.” *Current Opinion in Cell Biology* 15(6): 740–46.

Thomson, Timothy M., Cristina Balcells, and Marta Cascante. 2019. “Metabolic Plasticity and Epithelial-Mesenchymal Transition.” *Journal of Clinical Medicine* 8(7): 967.

Tomlinson, Darren C. et al. 2012. “FGFR1-Induced Epithelial to Mesenchymal Transition through MAPK/PLCγ/COX-2-Mediated Mechanisms” ed. Surinder K. Batra. *PLoS ONE* 7(6): e38972.

Townsend, Nick et al. 2016. “Cardiovascular Disease in Europe: Epidemiological Update 2016.” *European Heart Journal*.

Townsend, Nick, Melanie Nichols, Peter Scarborough, and Mike Rayner. 2015. “Cardiovascular Disease in Europe - Epidemiological Update 2015.” *European Heart Journal* 36(40): 2696–2705.

Traore, Mahama A., and Steven C. George. 2017. “Tissue Engineering the Vascular Tree.” *Tissue Engineering - Part B: Reviews* 23(6): 505–14.

Trimboli, Anthony J. et al. 2008. “Direct Evidence for Epithelial-Mesenchymal Transitions in Breast Cancer.” *Cancer Research* 68(3): 937–45.

Trzpis, Monika, Pamela M.J. McLaughlin, Lou M.F.H. De Leij, and Martin C. Harmsen. 2007. “Epithelial Cell Adhesion Molecule: More than a Carcinoma Marker and Adhesion Molecule.” *American Journal of Pathology* 171(2): 386–95.

Tura, Olga et al. 2013. “Late Outgrowth Endothelial Cells Resemble Mature Endothelial Cells and Are Not Derived from Bone Marrow.” *Stem cells (Dayton, Ohio)* 31(2): 338–48..

Typas, Dimitris et al. 2015. “The De-Ubiquitylating Enzymes USP26 and USP37 Regulate Homologous Recombination by Counteracting RAP80.” *Nucleic acids research* 43(14): 6919–33.

Unterluggauer, Hermann et al. 2008. “Premature Senescence of Human Endothelial Cells Induced by Inhibition of Glutaminase.” *Biogerontology* 9(4): 247–59.

Valencia-Nuñez, Diana M et al. 2017. “Endothelial Vascular Markers in Coronary Surgery.” *Heart and vessels* 32(11): 1390–99.

Vega-Naredo, I et al. 2014. “Mitochondrial Metabolism Directs Stemness and Differentiation in P19 Embryonal Carcinoma Stem Cells.” *Cell Death and Differentiation* 21(10): 1560–74.

Verdegem, Dries, Stijn Moens, Peter Stapor, and Peter Carmeliet. 2014. “Endothelial Cell Metabolism: Parallels and Divergences with Cancer Cell Metabolism.” *Cancer and Metabolism* 2(1).

Virmani, Renu et al. 2005. “Atherosclerotic Plaque Progression and Vulnerability to Rupture: Angiogenesis as a Source of Intraplaque Hemorrhage.” *Arteriosclerosis, thrombosis, and vascular biology* 25(10): 2054–61.

Vizán, Pedro et al. 2009. “Characterization of the Metabolic Changes Underlying Growth Factor Angiogenic Activation: Identification of New Potential Therapeutic Targets.” *Carcinogenesis* 30(6): 946–52.

Walden, Miriam et al. 2019. “Metabolic Control of BRISC-SHMT2 Assembly Regulates Immune Signalling.” *Nature* 570(7760): 194–99.

Wang, Bin et al. 2007. “Abraxas and RAP80 Form a BRCA1 Protein Complex Required for the DNA Damage Response.” *Science (New York, N.Y.)* 316(5828): 1194–98.

Wang, Eric T. et al. 2008. “Alternative Isoform Regulation in Human Tissue Transcriptomes.” *Nature* 456(7221): 470–76.

Wang, Yang et al. 2018. “Outcome and Prognostic Value of Treatment for Brain Metastases and the Primary Tumor in Patients with Breast Cancer Brain Metastases.” *Clinical neurology and neurosurgery* 170: 43–46.

Ward-Caviness, Cavin K et al. 2017. “Improvement of Myocardial Infarction Risk Prediction via Inflammation-Associated Metabolite Biomarkers.” *Heart*.

Warzecha, Claude C., Shihao Shen, Y. Xing, and Russ P. Carstens. 2009. “The Epithelial Splicing Factors ESRP1 and ESRP2 Positively and Negatively Regulate Diverse Types of Alternative Splicing Events.” *RNA biology* 6(5): 546–62.

Warzecha, Claude C, Shihao Shen, Yi Xing, and Russ P Carstens. “The Epithelial Splicing Factors ESRP1 and ESRP2 Positively and Negatively Regulate Diverse Types of Alternative Splicing Events.” *RNA biology* 6(5): 546–62.

Weber, Anika Maria, and Anderson Joseph Ryan. 2015. “ATM and ATR as Therapeutic Targets in Cancer.” *Pharmacology and Therapeutics* 149: 124–38.

Willard, Abbott L., and Ira M. Herman. 2012. “Vascular Complications and Diabetes: Current Therapies and Future Challenges.” *Journal of Ophthalmology* 2012.

Wong, Chi Chun et al. 2016. “SLC25A22 Promotes Proliferation and Survival of Colorectal Cancer Cells With KRAS Mutations and Xenograft Tumor Progression in Mice via Intracellular Synthesis of Aspartate.” *Gastroenterology* 151(5): 945-960.e6.

Wong, Justin J-L, Amy Y M Au, William Ritchie, and John E J Rasko. 2016. “Intron Retention in MRNA: No Longer Nonsense: Known and Putative Roles of Intron Retention in Normal and Disease Biology.” *BioEssays : news and reviews in molecular, cellular and developmental biology* 38(1): 41–49.

Wu, Jiaxue et al. 2009. “Histone Ubiquitination Associates with BRCA1-Dependent DNA Damage Response.” *Molecular and cellular biology* 29(3): 849–60.

Wu, Jiaxue, Lin Yu Lu, and Xiaochun Yu. 2010. “The Role of BRCA1 in DNA Damage Response.” *Protein and Cell* 1(2): 117–23.

Wu, Song, Wei Zhu, Patricia Thompson, and Yusuf A. Hannun. 2018. “Evaluating Intrinsic and Non-Intrinsic Cancer Risk Factors.” *Nature Communications* 9(1).

Würtz, Peter et al. 2012. “High-Throughput Quantification of Circulating Metabolites Improves Prediction of Subclinical Atherosclerosis.” *European heart journal* 33(18): 2307–16.

Xia, Ning, Andreas Daiber, Ulrich Förstermann, and Huige Li. 2017. “Antioxidant Effects of Resveratrol in the Cardiovascular System.” *British Journal of Pharmacology*.

Xu, Yilin et al. 2014. “Cell Type-Restricted Activity of HnRNPM Promotes Breast Cancer Metastasis via Regulating Alternative Splicing.” *Genes and Development* 28(11): 1191–1203.

Xu, Yiming et al. 2017. “Regulation of Endothelial Intracellular Adenosine via Adenosine Kinase Epigenetically Modulates Vascular Inflammation.” *Nature Communications* 8(1).

Xu, Zhan et al. 2018. “Rice RAD51 Paralogs Play Essential Roles in Somatic Homologous Recombination for DNA Repair.” *The Plant journal : for cell and molecular biology* 95(2): 282–95.

Yamamoto, Takehiro et al. 2014. “Reduced Methylation of PFKFB3 in Cancer Cells Shunts Glucose towards the Pentose Phosphate Pathway.” *Nature communications* 5: 3480. Yan, Jun et al. 2007. “The Ubiquitin-Interacting Motif-Containing Protein RAP80 Interacts with BRCA1 and Functions in DNA Damage Repair Response.” *Cancer Research* 67(14): 6647–56.

Yang, Lifeng, Sriram Venneti, and Deepak Nagrath. 2017. “Glutaminolysis: A Hallmark of Cancer Metabolism.” *Annual Review of Biomedical Engineering* 19(1): 163–94.

Yang, Yueqin et al. 2016. “Determination of a Comprehensive Alternative Splicing Regulatory Network and Combinatorial Regulation by Key Factors during the Epithelial-to-Mesenchymal Transition.” *Molecular and Cellular Biology* 36(11): 1704–19.

Yersal, Ozlem, and Sabri Barutca. 2014. “Biological Subtypes of Breast Cancer: Prognostic and Therapeutic Implications.” *World journal of clinical oncology* 5(3): 412–24.

Yi, Mei et al. 2019. “6-Phosphofructo-2-Kinase/Fructose-2,6-Biphosphatase 3 and 4: A Pair of Valves for Fine-Tuning of Glucose Metabolism in Human Cancer.” *Molecular Metabolism* 20(December 2018): 1–13. https://doi.org/10.1016/j.molmet.2018.11.013.

Yilmaz, L. Safak, and Albertha JM Walhout. 2017. “Metabolic Network Modeling with Model Organisms.” *Current Opinion in Chemical Biology* 36: 32–39. http://dx.doi.org/10.1016/j.cbpa.2016.12.025.

Yin, Zhengyu et al. 2012. “RAP80 Is Critical in Maintaining Genomic Stability and Suppressing Tumor Development.” *Cancer Research* 72(19): 5080–90.

Zardi, Enrico M., and Antonella Afeltra. 2010. “Endothelial Dysfunction and Vascular Stiffness in Systemic Lupus Erythematosus: Are They Early Markers of Subclinical Atherosclerosis?” *Autoimmunity Reviews* 9(10): 684–86.

Zavadil, Jiri et al. 2008. “Epithelial-Mesenchymal Transition.” *Cancer research* 68(23): 9574–77.

Zhang, Cheng, and Qiang Hua. 2016. “Applications of Genome-Scale Metabolic Models in Biotechnology and Systems Medicine.” *Frontiers in Physiology* 6.

Zhang, Junran, and Simon N. Powell. 2005. “The Role of the BRCA1 Tumor Suppressor in DNA Double-Strand Break Repair.” *Molecular Cancer Research* 3(10): 531–39.

Zhao, Guang Yu et al. 2007. “A Critical Role for the Ubiquitin-Conjugating Enzyme Ubc13 in Initiating Homologous Recombination.” *Molecular cell* 25(5): 663–75.

Zheng, Hui et al. 2013. “A BRISC-SHMT Complex Deubiquitinates IFNAR1 and Regulates Interferon Responses.” *Cell Reports* 5(1): 180–93.

Zorova, Ljubava D et al. 2018. “Mitochondrial Membrane Potential HHS Public Access Author Manuscript.” *Anal Biochem* 552: 50–59. https://www.ncbi.nlm.nih.gov/pmc/articles/PMC5792320/pdf/nihms902260.pdf.

8. APPENDIX 1

APPENDIX 1

A1.1 Production and transduction of lentiviral and retroviral particles (Chapter 4.2)

Full-length human ESRP1, ESRP2, RAP80 cDNAs were obtained from the IMAGE consortium as an insert in pBluescriptR with an ampicillin resistance

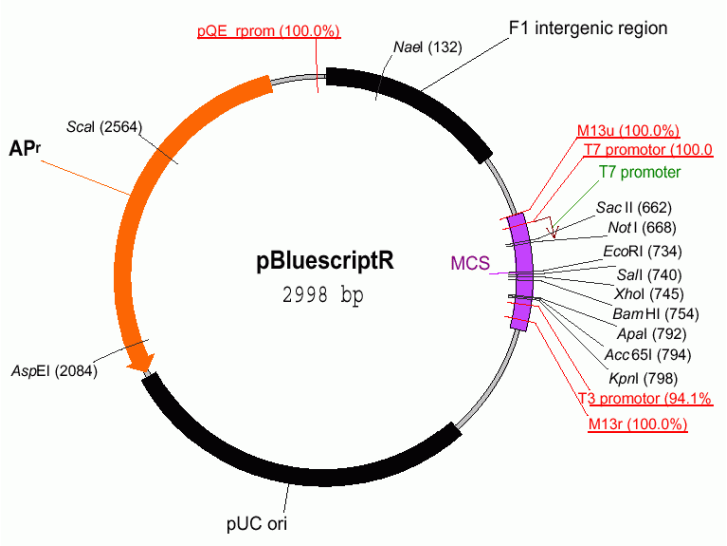

Figure A1: pBluescriptR plasmid map

In order to transfer these cDNAs into mammalian expression vectors, the selected cDNAs were amplified by PCR, adding 2 restriction sites: BamH1, at the 5' end and Sal1 at its 3' end. Sequences coding for the hemaglutinin (HA) tag were also included at the 3' of both cDNAs, in order to promote the detection by Western blotting and immunocytochemistry.

The amplified cDNAs were cloned into the correspondent vector which contains in its multiple cloning sites (MCS/or polylinker) the BamH1 and SalI restriction sites (the same included into the gene construct). The vector plasmid was digested with BamHI and SalI, purified by electrophoresis in agarose gel, and then ligated with the cDNAs. After transformation into competent bacteria, plasmid DNA was purified and sequenced to

confirm the correct insertion. This procedure yielded the retroviral expression constructs pBABE-puro/ESRP1 and pBABE-puro/ESRP2, and the lentiviral expression constructs pLk0.puro/ESRP1, pLk0.puro ESRP2, pLk0.puro/RAP80.

The control plasmid used in this study are pBABE- and pLk0.puro-empty vectors, respectively for over expression and silencing of the selected genes (ESRP1/ESRP2/UIMC-1-RAP80).

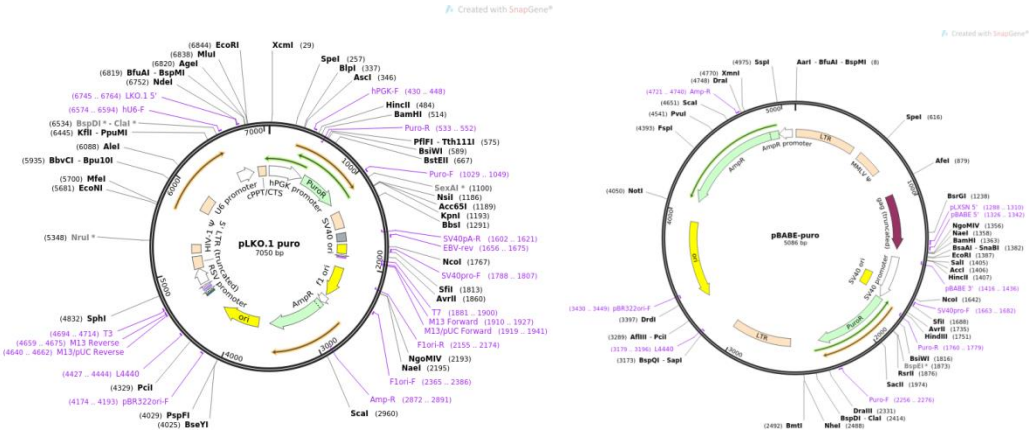

Figure A2: pLk0.puro (#8453) and pBABE (#1764) -empty vectors full sequence maps from AddGene.

The lentivirus packaging cell line HEK293T was co-transfected with these DNAs together with pCMVdeltaR8.91 and pVSV-G (Clontech) and the retrovirus packaging cell line Phoenix was co-transfected with the selected DNAs, for 12 h using Metafectene (BIONTEX) or XtremeGene-9 (Sigma-Aldrich) as vehicles.

Supernatants were collected during the following 48 h and filtered through 0.45 µm methylcellulose filters (Millipore). Target cells were infected using supernatants (or dilutions with fresh medium) supplemented with 8 µg/mL hexadimethrine bromide (polybrene), at 37 ºC for 24 h. Infected cells were allowed to recover in fresh medium for 24-48 h. Cells with integrated viral sequences were selected for 5 days in medium supplemented with 5 µg/mL puromycin (Biomol).

TableA1: Genes target sequences for the generation of the cell variants

Gene	Clone ID	Target Sequence
RAP80 (UIMC1)	TRCN0000060428	CCCACAAAGATTGAACGACATCCGGCCCA CGACATCTCGAGATGTCGTTCAATCTTTGT
ESRP1	TRCN000012678	GCTCAGGGTCGAAGGAAC TTCATGAAGAGCTGAGTG
ESRP2	TRCN0000013004	GCTCAGGGTCGAAGGAAC GCAGTGCTGAAGAGGGG

A.1.2 Sequence of ESRP1

Blue highlighting indicates alternate exons.
Red highlighting indicates amino acids encoded across a splice junction.

Nucleotide Sequence (2046 nt)

ATGACGGCCTCTCCGGATTACTTGGTGGTGCTTTTTGGGATCACTGCTGGGGCCACCGGGGCCAAGCTAG
GCTCGGATGAGAAGGAGTTGATCCTGCTGTTCTGGAAAGTCGTGGATCTGGCCAACAAGAAGGTGGGACA
GTTGCACGAAGTGCTAGTTAGACCGGATCAGTTGGAACTGACGGAGGACTGCAAAGAAGAAACTAAAATA
GACGTCGAAAGCCTGTCCTCGGCGTCGCAGCTGGACCAAGCCCTCCGACAGTTTAACCAGTCAGTGAGCA
ATGAACTGAATATTGGAGTAGGGACTTCCTTCTGTCTCTGTACTGATGGGCAGCTTCATGTCAGGCAAAT
CCTGCATCCTGAGGCTTCCAAGAAGAATGTACTATTACCTGAATGCTTCTATTCCTTTTTTGATCTTCGA
AAAGAATTCAAGAAATGTTGCCCTGGTTCACCTGATATTGACAAACTGGACGTTGCCACAATGACAGAGT
ATTTAAATTTTGAGAAGAGTAGTTCAGTCTCTCGATATGGAGCCTCTCAAGTTGAAGATATGGGGAATAT
AATTTTAGCAATGATTTCAGAGCCTTATAATCACAGGTTTTCAGATCCAGAGAGAGTGAATTACAAGTTT
GAAAGTGGAACTTGCAGCAAGATGGAACTTATTGATGATAACACCGTAGTCAGGGCACGAGGTTTACCAT
GGCAGTCTTCAGATCAAGATATTGCAAGATTCTTCAAAGGACTCAATATTGCCAAGGGAGGTGCAGCACT
TTGTCTGAATGCTCAGGGTCGAAGGAACGGAGAAGCTCTGGTTAGGTTTGTAAGTGAGGAGCACCGAGAC
CTAGCACTACAGAGGCACAAACATCACATGGGGACCCGGTATATTGAGGTTTACAAAGCAACAGGTGAAG
ATTTCCTTAAAATTGCTGGTGGTACTTCCAATGAGGTAGCCCAGTTTCTCTCCAAGGAAAATCAAGTCAT
TGTCCGCATGCGGGGGCTCCCTTTCACGGCCACAGCTGAAGAAGTGGTGGCCTTCTTTGGACAGCATTGC
CCTATTACTGGGGGAAAGGAAGGCATCCTCTTTGTCACCTACCCAGATGGTAGGCCAACAGGGGACGCTT
TTGTCCTCTTTGCCTGTGAGGAATATGCACAGAATGCGTTGAGGAAGCATAAAGACTTGTTGGGTAAAAG
ATACATTGAACTCTTCAGGAGCACAGCAGCTGAAGTTCAGCAGGTGCTGAATCGATTCTCCTCGGCCCCT
CTCATTCCACTTCCAACCCCTCCCATTATTCCAGTACTACCTCAGCAATTTGTGCCCCCTACAAATGTTA
GAGACTGTATACGCCTTCGAGGTCTTCCCTATGCAGCCACAATTGAGGACATCCTGGATTTCCTGGGGGA
GTTCGCCACAGATATTCGTACTCATGGGGTTCACATGGTTTTGAATCACCAGGGCCGCCCATCAGGAGAT
GCCTTTATCCAGATGAAGTCTGCGGACAGAGCATTTATGGCTGCACAGAAGTGTCATAAAAAAAACATGA
AGGACAGATATGTTGAAGTCTTTCAGTGTTCAGCTGAGGAGATGAACTTTGTGTTAATGGGGGGCACTTT
AAATCGAAATGGCTTATCCCCACCGCCATGTAAGTTACCATGCCTGTCTCCTCCCTCCTACACATTTCCA
GCTCCTGCTGCAGTTATTCCTACAGAAGCTGCCATTTACCAGCCCTCTGTGATTTTGAATCCACGAGCAC
TGCAGCCCTCCACAGCGTACTACCCAGCAGGCACTCAGCTCTTCATGAATTACACAGCGTACTATCCCAG
CCCCCCAGGTTCGCCTAATAGTCTTGGCTACTTCCCTACAGCTGCTAATCTTAGCGGTGTCCCTCCACAG
CCTGGCACGGTGGTCAGAATGCAGGGCCTGGCCTACAATACTGGAGTTAAGGAAATTCTTAACTTCTTCC
AAGGTTACCAGTATGCAACCGAGGATGGACTTATACACACAAATGACCAGGCCAGGACTCTACCCAAAGA
ATGGGTTTGTATTTAA

Translation (681 aa):

MTASPDYLVVLFGITAGATGAKLGSDEKELILLFWKVVDLANKKVGQLHEVLVRPDQLELTEDCKEETKI
DVESLSSASQLDQALRQFNQSVSNELNIGVGTSFCLCTDGQLHVRQILHPEASKKNVLLPECFYSFFDLR
KEFKKCCPGSPDIDKLDVATMTEYLNFEKSSSVSRYGASQVEDMGNIILAMISEPYNHRFSDPERVNYKF
ESGTCSKMELIDDNTVVRARGLPWQSSDQDIARFFKGLNIAKGGAALCLNAQGRRNGEALVRFVSEEHRD
LALQRHKHHMGTRYIEVYKATGEDFLKIAGGTSNEVAQFLSKENQVIVRMRGLPFTATAEEVVAFFGQHC
PITGGKEGILFVTYPDGRPTGDAFVLFACEEYAQNALRKHKDLLGKRYIELFRSTAAEVQQVLNRFSSAP
LIPLPTPPIIPVLPQQFVPPTNVRDCIRLRGLPYAATIEDILDFLGEFATDIRTHGVHMVLNHQGRPSGD
AFIQMKSADRAFMAAQKCHKKNMKDRYVEVFQCSAEEMNFVLMGGTLNRNGLSPPPCKLPCLSPPSYTFP
APAAVIPTEAAIYQPSVILNPRALQPSTAYYPAGTQLFMNYTAYYPSPPGSPNSLGYFPTAANLSGVPPQ
PGTVVRMQGLAYNTGVKEILNFFQGYQYATEDGLIHTNDQARTLPKEWVCI

A.1.2.1 Sequence of ESRP2

Nucleotide Sequence (2154nt)

ATGACTCCGCCGCCGCCGCCGCCCCCTCCCCCGGGCCCTGACCCCGCGGCCG
ACCCCGCCGCGGACCCCTGCCCCTGGCCCGGATCACTGGTCGTCCTCTTCGGGGCTACGG
CGGGTGCGCTGGGACGGGACCTGGGCTCGGACGAGACCGACTTAATCCTCCTAGTTTGGC
AAGTGGTTGAGCCGCGGAGCCGCCAGGTGGGGACGCTGCACAAATCGCTGGTTCGTGCCG
AGGCGGCCGCACTGAGTACGCAGTGCCGCGAGGCGAGCGGCCTGAGCGCCGACAGCCTGG
CGCGGGCAGAGCCGCTGGACAAGGTGCTGCAGCAGTTCTCACAGCTGGTGAACGGGGATG
TGGCTTTGCTGGGCGGGGGCCCCTACATGCTCTGCACTGATGGGCAGCAGCTATTGCGAC
AGGTCCTGCACCCCGAGGCCTCCAGGAAGAACCTGGTGCTCCCCGACATGTTCTTCTCCT
TCTATGACCTCCGAAGAGAATTCCATATGCAGCATCCAAGCACCTGCCCTGCCAGGGACC
TCACTGTGGCCACCATGGCACAGGGTTTAGGACTGGAGACAGATGCCACAGAGGATGACT
TTGGGGTCTGGGAAGTCAAGACAATGGTAGCTGTTATCCTCCATCTACTCAAAGAGCCCA
GCAGTCAATTGTTTTCGAAGCCCGAGGTGATAAAGCAGAAATACGAGACGGGGCCTTGCA
GCAAGGCTGATGTGGTGGACAGTGAGACTGTGGTACGGGCTCGTGGGTTGCCGTGGCAGT
CATCAGACCAGGACGTGGCTCGCTTCTTCAAAGGGCTCAACGTGGCCAGGGGTGGTGTAG
CACTCTGCCTCAACGCCCAGGGCCGCAGAAATGGCGAGGCCCTCATCCGCTTTGTGGACA
GCGAGCAGCGGGACCTAGCGCTGCAGAGACACAAGCACCACATGGGCGTCCGCTATATTG
AGGTGTATAAAGCGACAGGGGAGGAGTTTGTAAAGATTGCAGGGGGCACATCACTAGAGG
TGGCTCGTTTCTTGTCACGGGAAGACCAAGTGATCCTGCGGCTGCGGGGACTGCCCTTCT
CGGCTGGGCCAACGGACGTGCTTGGCTTCCTGGGGCCAGAGTGCCCAGTGACTGGGGGTA
CCGAGGGGCTGCTCTTTGTGCGCCATCCTGATGGCCGGCCGACTGGTGATGCCTTCGCCC
TCTTTGCTTGTGAGGAGCTGGCACAGGCTGCACTGCGCAGGCACAAGGGCATGCTGGGTA
AGCGATACATTGAACTCTTCCGGAGCACTGCAGCCGAAGTGCAGCAGGTCTTGAACCGCT
ATGCATCCGGCCCACTCCTTCCTACACTGACTGCCCCACTGCTGCCCATCCCCTTCCCAC
TGGCACCTGGGACTGGGAGGGACTGTGTACGCCTCCGAGGCCTGCCCTACACGGCCACCA
TTGAAGACATCCTGAGCTTTCTGGGGGAGGCAGCAGCTGACATTCGGCCCCACGGTGTAC
ACATGGTGCTCAACCAGCAGGGCCGGCCATCGGGCGATGCCTTCATTCAGATGACATCAG
CAGAGCGAGCCCTAGCTGCTGCTCAGCGTTGCCATAAGAAGGTGATGAAGGAGCGCTACG
TGGAGGTGGTCCCCTGTTCCACAGAGGAGATGAGCCGAGTGCTGATGGGGGGCACCTTGG
GCCGCAGTGGCATGTCCCCTCCACCCTGCAAGCTGCCCTGCCTCTCACCACCTACCTACA
CCACCTTCCAAGCCACCCCAACGCTCATTCCCACGGAGACGGCAGCTCTATACCCCTCTT
CAGCACTGCTCCCAGCTGCCAGGGTGCCTGCTGCCCCCACCCCTGTTGCCTACTATCCAG
GGCCAGCCACTCAACTCTACCTGAACTACACAGCCTACTACCCAAGCCCCCCAGTCTCCC
CCACCACTGTGGGCTACCTCACTACACCCACTGCTGCCCTGGCCTCTGCTCCCACCTCAG
TGTTGTCCCAGTCAGGAGCCTTGGTCCGCATGCAGGGTGTCCCATACACGGCTGGTATGA
AGGATCTGCTCAGCGTCTTCCAGGCCTACCAGCTACCCGCTGATGACTACACCAGTCTGA
TGCCTGTTGGTGACCCACCTCGCACTGTGTTACAAGCCCCCAAGGAATGGGTGTGTTTGT
AG

Translation (660 aa)

MTPPPPPPPPPGPDPAADPAADPCPWPGSLVVLFGATAGALGRDLGSDETDLILLVWQVV
EPRSRQVGTLHKSLVRAEAAALSTQCREASGLSADSLARAEPLDKVLQQFSQLVNGDVAL
LGGGPYMLCTDGQQLLRQVLHPEASRKNLVLPDMFFSFYDLRREFHMQHPSTCPARDLTV
ATMAQGLGLETDATEDDFGVWEVKTMVAVILHLLKEPSSQLFSKPEVIKQKYETGPCSKA
DVVDSETVVRARGLPWQSSDQDVARFFKGLNVARGGVALCLNAQGRRNGEALIRFVDSEQ
RDLALQRHKHHMGVRYIEVYKATGEEFVKIAGGTSLEVARFLSREDQVILRLRGLPFSAG
PTDVLGFLGPECPVTGGTEGLLFVRHPDGRPTGDAFALFACEELAQAALRRHKGMLGKRY
IELFRSTAAEVQQVLNRYASGPLLPTLTAPLLPIPFPLAPGTGRDCVRLRGLPYTATIED
ILSFLGEAAADIRPHGVHMVLNQQGRPSGDAFIQMTSAERALAAAQRCHKKVMKERYVEV
VPCSTEEMSRVLMGGTLGRSGMSPPPCKLPCLSPPTYTTFQATPTLIPTETAALYPSSAL
LPAARVPAAPTPVAYYPGPATQLYLNYTAYYPSPPVSPTTVGYLTTPTAALASAPTSVLS
QSGALVRMQGVPYTAGMKDLLSVFQAYQLPADDYTSLMPVGDPPRTVLQAPKEWVCL

A.1.3 Cell cycle histograms from Endothelial Cells (patients-derived cells and control, Chapter 4.1)

HCAECs

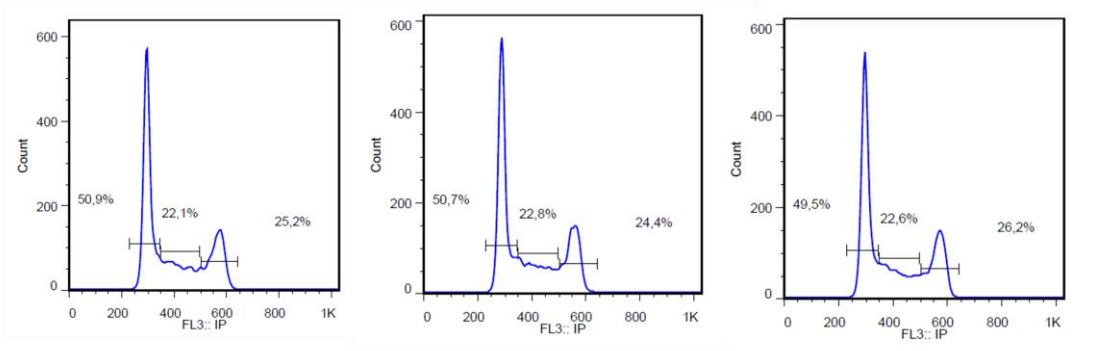

CE-45

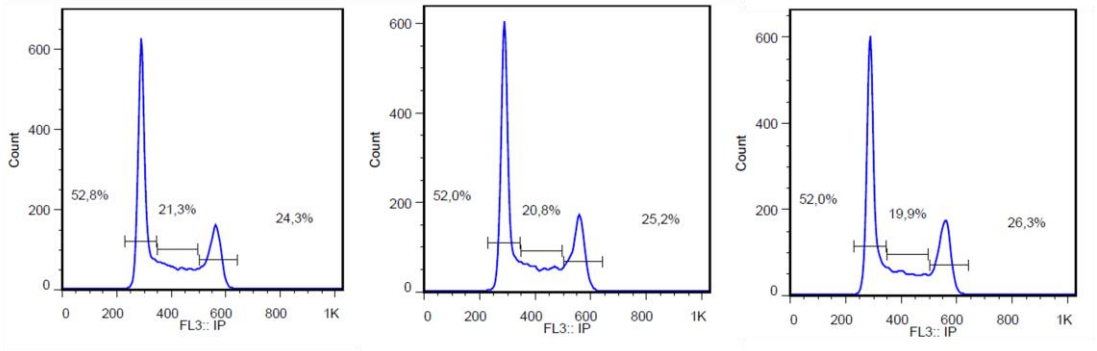

CE-46

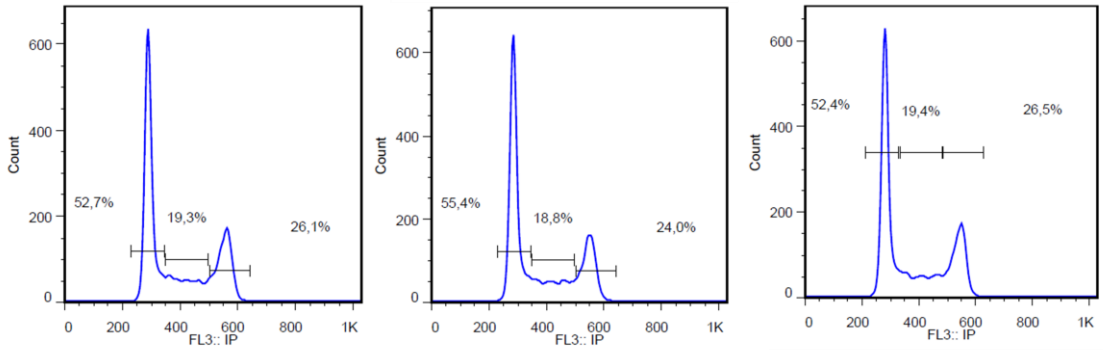

CE-48

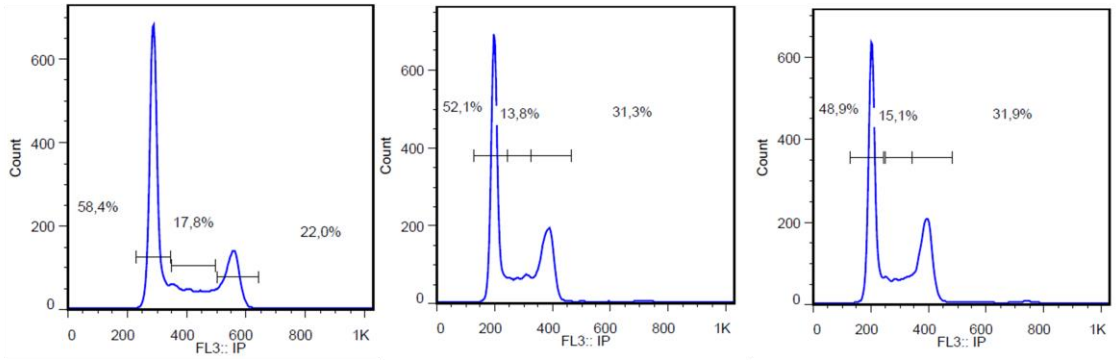

CE-51

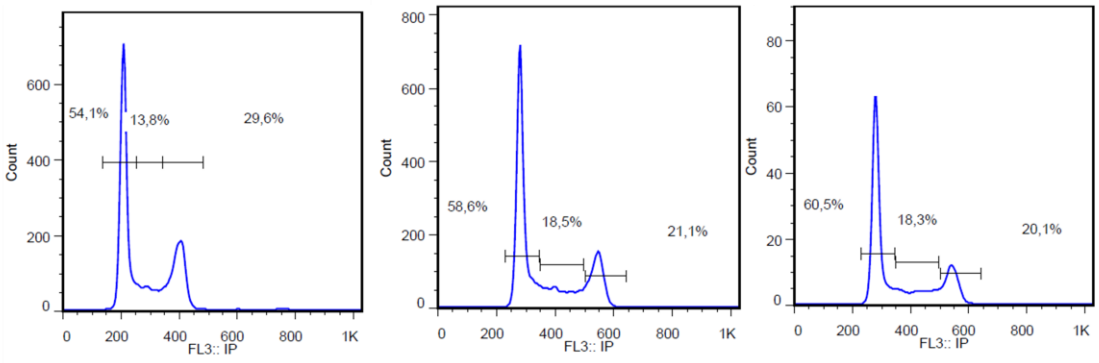

CE-52

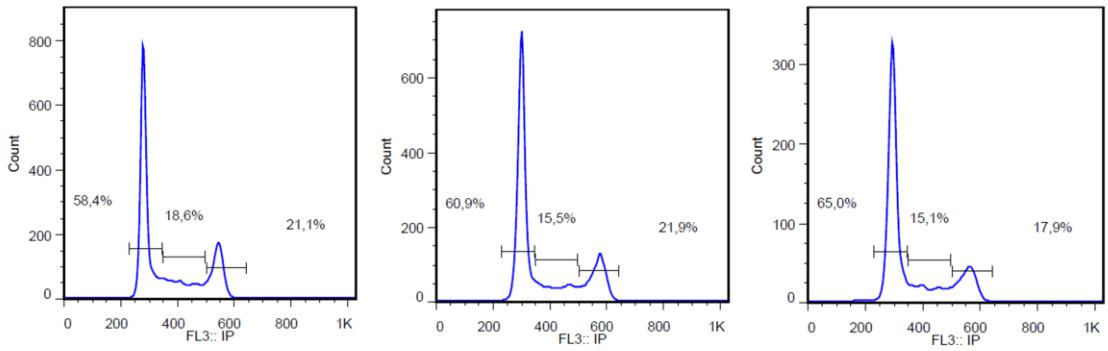

CE-53

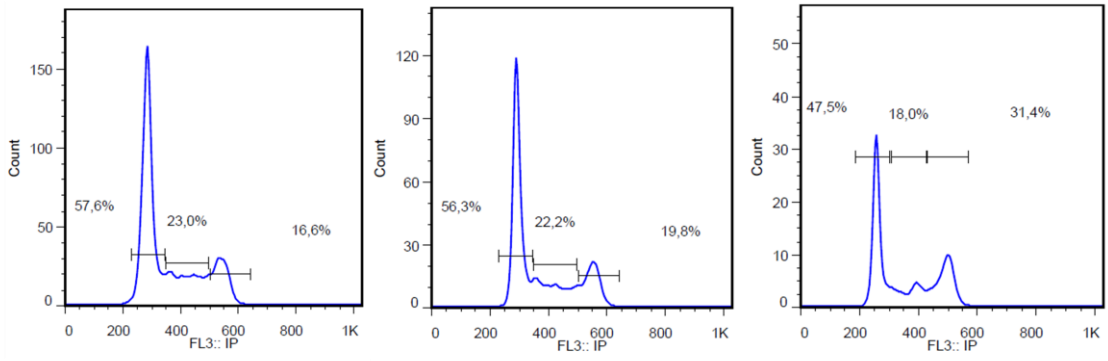

CE-60

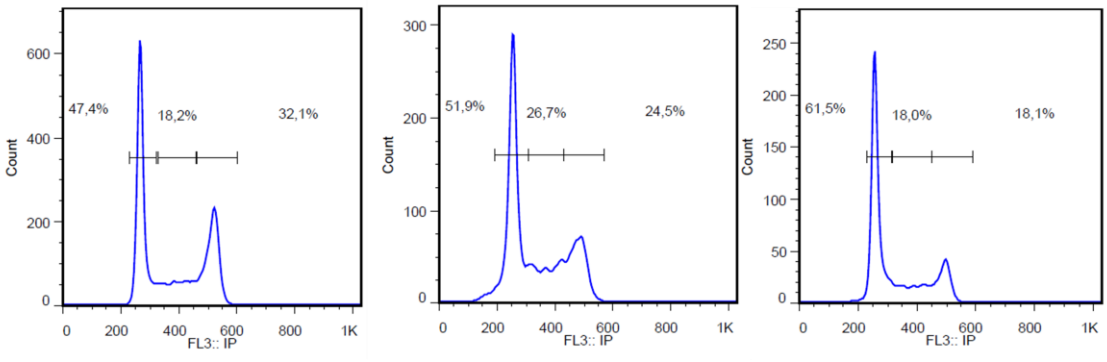
47,4%
18,2%
32,1%
51,9%
26,7%
24,5%
61,5%
18,0%
18,1%
Count
FL3:: IP

CE-61

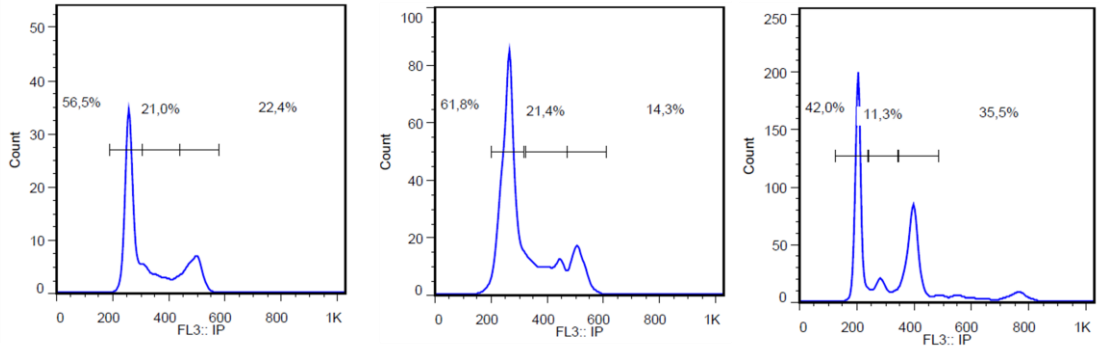
56,5%
21,0%
22,4%
61,8%
21,4%
14,3%
42,0%
11,3%
35,5%
Count
FL3:: IP

APPENDIX 1

Differentially expressed genes (Long list) in AMI patient-derived cells vs. control cell (Chapter 4.1)

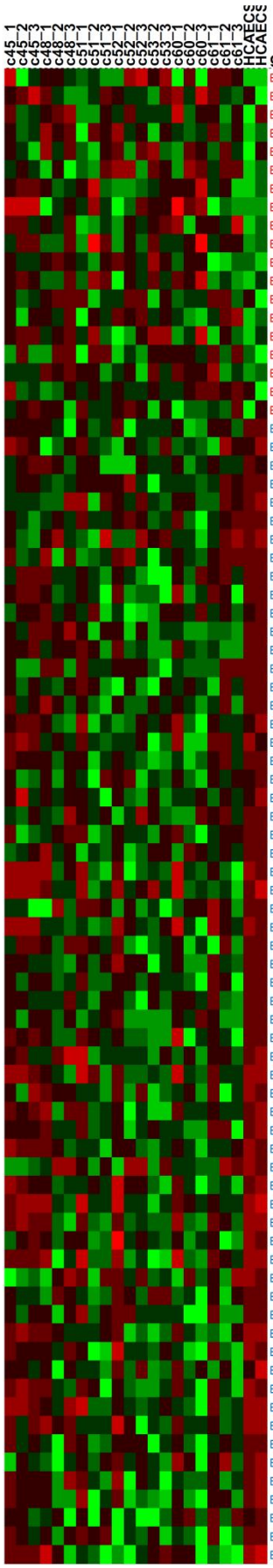

gene	isoform	transcript	_haecs	_haecs				
ENST00000542621.5_ADAMTSL1-008	ADAMTSL1-008	ENST00000542621.5	3,034	0,097	ADAMTSL1-213	ENST00000542621.5	3039	258aa Nonsense mediated decay
ENST00000570001.5_PDXDC1-002	PDXDC1-002	ENST00000570001.5	2,595	0,061	PDXDC1-217	ENST00000570001.5	4828	No protein Retained intron
ENST00000584265.1_MRC2-002	MRC2-002	ENST00000584265.1	2,486	0,084	AC080038.1-202	ENST00000584265.1	2025	No protein Retained intron
ENST00000550957.1_DGKA-035	DGKA-035	ENST00000550957.1	2,450	0,066	DGKA-228	ENST00000550957.1	224	No protein Retained intron
ENST00000580684.5_LINC00667-005	LINC00667-005	ENST00000580684.5	2,384	0,116	LINC00667-203	ENST00000580684.5	1009	No protein lincRNA
ENST00000475656.6_FAM175A-002	FAM175A-002	ENST00000475656.6	2,357	0,088	ABRAXAS1-202	ENST00000475656.6	2718	74aa Nonsense mediated decay
ENST00000534180.1_FTH1-002	FTH1-002	ENST00000534180.1	2,349	0,058	FTH1-210	ENST00000534180.1	983	50aa Nonsense mediated decay
ENST00000412485.1_LINC02154-001	LINC02154-001	ENST00000412485.1	2,348	0,297	LINC02154-201	ENST00000412485.1	1497	No protein lincRNA
ENST00000482847.5_ALAD-002	ALAD-002	ENST00000482847.5	2,309	0,061	ALAD-208	ENST00000482847.5	3247	No protein Retained intron
ENST00000519511.1_STC2-003	STC2-003	ENST00000519511.1	2,273	0,129	STC2-203	ENST00000519511.1	582	No protein Retained intron
ENST00000517910.1_KB-1732A1.1-001	KB-1732A1.1-001	ENST00000517910.1	2,198	0,064	GASAL1-201	ENST00000517910.1	2770	No protein lincRNA
ENST00000549807.1_RP11-818F20.5-0	RP11-818F20.5-001	ENST00000549807.1	2,190	0,112	AC089983.1-201	ENST00000549807.1	701	No protein Antisense
ENST00000469269.1_TGM2-007	TGM2-007	ENST00000469269.1	2,170	0,087	TGM2-205	ENST00000469269.1	3467	No protein Retained intron
ENST00000578586.1_OGFOD3-004	OGFOD3-004	ENST00000578586.1	2,118	0,112	OGFOD3-206	ENST00000578586.1	3796	No protein Retained intron
ENST00000608792.1_LINC00702-003	LINC00702-003	ENST00000608792.1	2,109	0,198	LINC00702-203	ENST00000608792.1	6300	No protein lincRNA
ENST00000464445.1_ARHGAP22-012	ARHGAP22-012	ENST00000464445.1	2,099	0,148	ARHGAP22-208	ENST00000464445.1	520	No protein Retained intron
ENST00000503059.1_NNT-008	NNT-008	ENST00000503059.1	2,086	0,055	NNT-203	ENST00000503059.1	634	11aa Nonsense mediated decay
ENST00000564311.5_RNPS1-024	RNPS1-024	ENST00000564311.5	2,070	0,055	RNPS1-209	ENST00000564311.5	870	156aa Nonsense mediated decay
ENST00000270361.15_CAPN10-008	CAPN10-008	ENST00000270361.15	2,043	0,251	CAPN10-201	ENST00000270361.15	2453	274aa Nonsense mediated decay
ENST00000473757.5_STAG3L5P-005	STAG3L5P-005	ENST00000473757.5	-2,004	0,084	STAG3L5P-205	ENST00000473757.5	1255	Retained intron
ENST00000606008.1_RP11-348P10.2-0	RP11-348P10.2-001	ENST00000606008.1	-2,011	0,120	AC124045.1-201	ENST00000606008.1	1953	No protein lincRNA
ENST00000475770.5_KRIT1-007	KRIT1-007	ENST00000475770.5	-2,017	0,062	KRIT1-221	ENST00000475770.5	2411	No protein Retained intron
ENST00000449005.5_LINC01128-004	LINC01128-004	ENST00000449005.5	-2,020	0,062	LINC01128-207	ENST00000449005.5	874	No protein lincRNA
ENST00000507888.1_NSUN2-008	NSUN2-008	ENST00000507888.1	-2,022	0,081	NSUN2-207	ENST00000507888.1	715	No protein Retained intron
ENST00000554058.1_RP11-488C13.5-0	RP11-488C13.5-002	ENST00000554058.1	-2,024	0,062	VASH1-AS1-201	ENST00000554058.1	871	No protein lincRNA
ENST00000579591.1_CDKN2B-003	CDKN2B-003	ENST00000579591.1	-2,025	0,165	CDKN2B-203	ENST00000579591.1	1069	No protein Retained intron
ENST00000405068.3_EXOC7-005	EXOC7-005	ENST00000405068.3	-2,034	0,109	EXOC7-204	ENST00000405068.3	2958	No protein Retained intron
ENST00000486960.5_SF1-009	SF1-009	ENST00000486960.5	-2,040	0,114	SF1-217	ENST00000486960.5	719	No protein Retained intron
ENST00000547870.1_HNRNPA1-016	HNRNPA1-016	ENST00000547870.1	-2,043	0,216	HNRNPA1-207	ENST00000547870.1	920	No protein Retained intron
ENST00000532075.1_CD151-018	CD151-018	ENST00000532075.1	-2,049	0,115	CD151-221	ENST00000532075.1	786	No protein Retained intron
ENST00000555807.1_ACIN1-016	ACIN1-016	ENST00000555807.1	-2,049	0,089	ACIN1-218	ENST00000555807.1	928	No protein Retained intron
ENST00000530353.1_ZNF251-002	ZNF251-002	ENST00000530353.1	-2,055	0,064	ZNF251-204	ENST00000530353.1	2342	No protein Retained intron
ENST00000476737.1_MYH10-009	MYH10-009	ENST00000476737.1	-2,057	0,101	MYH10-209	ENST00000476737.1	592	No protein Retained intron
ENST00000553251.5_ANKRD13A-007	ANKRD13A-007	ENST00000553251.5	-2,064	0,120	ANKRD13A-210	ENST00000553251.5	3315	No protein Retained intron
ENST00000623550.1_B2M-005	B2M-005	ENST00000623550.1	-2,066	0,059	B2M-213	ENST00000623550.1	2329	No protein Retained intron
ENST00000503339.5_FRYL-008	FRYL-008	ENST00000503339.5	-2,069	0,125	FRYL-206	ENST00000503339.5	3482	No protein Retained intron
ENST00000565793.5_ADAMTS7-004	ADAMTS7-004	ENST00000565793.5	-2,071	0,157	ADAMTS7-202	ENST00000565793.5	4249	No protein Retained intron
ENST00000557041.1_TMEM55B-002	TMEM55B-002	ENST00000557041.1	-2,078	0,071	PIP4P1-207	ENST00000557041.1	3453	No protein Retained intron
ENST00000565978.1_RP11-549B18.1-0	RP11-549B18.1-001	ENST00000565978.1	-2,082	0,083	AC017100.1-201	ENST00000565978.1	1169	No protein Antisense
ENST00000540492.1_REXO2-004	REXO2-004	ENST00000540492.1	-2,092	0,070	REXO2-210	ENST00000540492.1	1088	No protein Retained intron
ENST00000493286.1_PPARA-005	PPARA-005	ENST00000493286.1	-2,093	0,065	PPARA-210	ENST00000493286.1	1564	No protein Retained intron
ENST00000420981.2_SERPINB9P1-002	SERPINB9P1-002	ENST00000420981.2	-2,098	0,107	SERPINB9P1-20	ENST00000420981.2	983	No protein lincRNA
ENST00000601252.1_TIMM50-005	TIMM50-005	ENST00000601252.1	-2,115	0,060	TIMM50-214	ENST00000601252.1	1737	104aa Nonsense mediated decay
ENST00000488288.1_RPL24-004	RPL24-004	ENST00000488288.1	-2,138	0,200	RPL24-205	ENST00000488288.1	1857	No protein Retained intron
ENST00000515394.1_FAM193B-013	FAM193B-013	ENST00000515394.1	-2,145	0,114	FAM193B-218	ENST00000515394.1	589	No protein Retained intron
ENST00000590237.1_KEAP1-009	KEAP1-009	ENST00000590237.1	-2,146	0,216	KEAP1-205	ENST00000590237.1	451	No protein Retained intron
ENST00000467105.1_RPL3-004	RPL3-004	ENST00000467105.1	-2,165	0,118	RPL3-212	ENST00000467105.1	1396	No protein Retained intron
ENST00000478085.5_SGSM3-003	SGSM3-003	ENST00000478085.5	-2,170	0,140	SGSM3-209	ENST00000478085.5	4218	No protein Retained intron
ENST00000550585.5_PCBP2-009	PCBP2-009	ENST00000550585.5	-2,175	0,079	PCBP2-218	ENST00000550585.5	2543	112aa Nonsense mediated decay
ENST00000486652.5_WDR26-002	WDR26-002	ENST00000486652.5	-2,178	0,093	WDR26-208	ENST00000486652.5	2867	208aa Nonsense mediated decay
ENST00000567250.5_SF3B3-008	SF3B3-008	ENST00000567250.5	-2,179	0,137	SF3B3-208	ENST00000567250.5	1084	No protein Retained intron
ENST00000533077.5_GRK2-003	GRK2-003	ENST00000533077.5	-2,182	0,054	GRK2-213	ENST00000533077.5	3453	No protein Retained intron
ENST00000482111.1_EIF1-004	EIF1-004	ENST00000482111.1	-2,183	0,145	EIF1-205	ENST00000482111.1	1428	No protein Retained intron
ENST00000559746.1_THBS1-003	THBS1-003	ENST00000559746.1	-2,188	0,084	THBS1-207	ENST00000559746.1	563	No protein Retained intron
ENST00000490277.1_TPT1-006	TPT1-006	ENST00000490277.1	-2,202	0,083	TPT1-207	ENST00000490277.1	1851	No protein Retained intron
ENST00000601356.1_AP2A1-002	AP2A1-002	ENST00000601356.1	-2,215	0,093	AP2A1-208	ENST00000601356.1	2238	No protein Retained intron
ENST00000338447.10_NAA40-013	NAA40-013	ENST00000338447.10	-2,217	0,096	NAA40-201	ENST00000338447.10	4707	No protein Retained intron
ENST00000575741.1_RP11-235E17.6-0	RP11-235E17.6-001	ENST00000575741.1	-2,229	0,052	AC027796.4-201	ENST00000575741.1	874	No protein Antisense
ENST00000518464.5_DST-019	DST-019	ENST00000518464.5	-2,243	0,050	DST-218	ENST00000518464.5	2967	No protein Retained intron
ENST00000500682.1_RP11-277P12.20-	RP11-277P12.20-00	ENST00000500682.1	-2,247	0,117	AC022075.1-201	ENST00000500682.1	2830	No protein Antisense
ENST00000556436.1_SRSF5-017	SRSF5-017	ENST00000556436.1	-2,272	0,081	SRSF5-214	ENST00000556436.1	611	No protein Retained intron
ENST00000475298.5_CCNL1-003	CCNL1-003	ENST00000475298.5	-2,320	0,059	CCNL1-216	ENST00000475298.5	2362	172aa Nonsense mediated decay
ENST00000591248.5_CDC37-002	CDC37-002	ENST00000591248.5	-2,323	0,068	CDC37-209	ENST00000591248.5	1377	No protein Retained intron
ENST00000431043.1_SNHG5-009	SNHG5-009	ENST00000431043.1	-2,342	0,114	SNHG5-207	ENST00000431043.1	998	No protein Retained intron
ENST00000592700.2_RPS15-003	RPS15-003	ENST00000592700.2	-2,354	0,186	RPS15-211	ENST00000592700.2	1602	No protein Retained intron
ENST00000610230.1_RP11-131L23.2-0	RP11-131L23.2-001	ENST00000610230.1	-2,358	0,094	AL360219.1-201	ENST00000610230.1	366	No protein lincRNA
ENST00000555870.5_MIPOL1-004	MIPOL1-004	ENST00000555870.5	-2,361	0,060	MIPOL1-210	ENST00000555870.5	7434	180aa Nonsense mediated decay
ENST00000588277.1_PPP1R12C-008	PPP1R12C-008	ENST00000588277.1	-2,367	0,088	PPP1R12C-205	ENST00000588277.1	419	No protein Retained intron
ENST00000569997.1_COX4I1-002	COX4I1-002	ENST00000569997.1	-2,376	0,066	COX4I1-217	ENST00000569997.1	3946	No protein Retained intron
ENST00000463727.1_PTPRE-001	PTPRE-001	ENST00000463727.1	-2,403	0,127	PTPRE-205	ENST00000463727.1	3944	No protein Retained intron
ENST00000525522.5_RNH1-008	RNH1-008	ENST00000525522.5	-2,414	0,054	RNH1-209	ENST00000525522.5	3281	No protein Retained intron
ENST00000498238.1_RSRP1-003	RSRP1-003	ENST00000498238.1	-2,417	0,094	RSRP1-207	ENST00000498238.1	2941	No protein Retained intron
ENST00000603767.1_AC108938.5-001	AC108938.5-001	ENST00000603767.1	-2,418	0,086	AC112229.3-201	ENST00000603767.1	3202	248aa Nonsense mediated decay
ENST00000565801.1_MAN2C1-025	MAN2C1-025	ENST00000565801.1	-2,429	0,051	MAN2C1-227	ENST00000565801.1	712	No protein Retained intron
ENST00000523471.5_MTUS1-025	MTUS1-025	ENST00000523471.5	-2,524	0,069	MTUS1-224	ENST00000523471.5	828	No protein Retained intron
ENST00000498309.1_UQCRQ-003	UQCRQ-003	ENST00000498309.1	-2,555	0,060	UQCRQ-206	ENST00000498309.1	874	No protein Retained intron
ENST00000395788.3_C6orf48-009	C6orf48-009	ENST00000395788.3	-2,594	0,061	C6orf48-208	ENST00000395788.3	815	No protein lincRNA
ENST00000561679.5_KIAA0895L-003	KIAA0895L-003	ENST00000561679.5	-2,703	0,076	KIAA0895L-203	ENST00000561679.5	2824	No protein Retained intron
ENST00000509031.5_PPA2-008	PPA2-008	ENST00000509031.5	-2,924	0,247	PPA2-216	ENST00000509031.5	1177	63aa Nonsense mediated decay
ENST00000420627.5_FLNA-021	FLNA-021	ENST00000420627.5	-2,960	0,310	FLNA-205	ENST00000420627.5	8225	604aa Nonsense mediated decay
ENST00000624952.1_PRAL-001	PRAL-001	ENST00000624952.1	-3,516	0,050	PRAL-201	ENST00000624952.1	3286	No protein

9. APPENDIX 2

APPENDIX 1

Table A2: Most significant differential isoforms in prostate cancer subpopulations PC-3/Mc vs. PC-3/S, PC-3Soe.ESRP1 and PC-3/Soe.ESRP2 variants vs. PC-3/S. Red: Protein coding; Blue: Retained Introns or Non-sense mediated decay (Chapter 4.2)

Gene Symbol	Transcript	PC-3M/PC-3S	ESRP1-PC-3S	ESRP2-PC-3S
HSPA8	ENST00000534319.1	13,6303761	2,37905151	2,23771876
	ENST00000526110.1	-2,0144989	-2,2738124	-5,9490549
	ENST00000524590.1	-7,5581277	-5,5276644	-6,2843666
FCHO1	ENST00000600676.1	12,4912978	4,47356407	3,16577159
	ENST00000595594.1	3,55354504	2,65074314	2,72866609
	ENST00000539407.1	-5,978369	-5,9230642	-3,9888841
EIF4G1	ENST00000421110.1	11,9483283	3,24270841	3,01362144
	ENST00000450424.1	-2,6018605	-8,9688519	-5,579366
OVCA2	ENST00000263084.5	11,8972432	7,0064316	2,65033809
	ENST00000572195.1	-12,290879	-8,2844791	-4,8778813
DIDO1	ENST00000266070.4	11,7618894	11,4903716	7,26487443
	ENST00000395343.1	-8,3737894	-3,4062573	-2,8800005
CEP70	ENST00000468900.1	11,7201967	3,87445419	6,6739677
	ENST00000489254.1	-4,5726939	-2,7527048	-2,3691304
FGFR1	ENST00000397091.5	11,5735029	7,0804957	7,89850309
	ENST00000356207.5	6,00281964	5,39807829	6,30992772
	ENST00000526742.1	5,34594168	3,23004997	4,69033629
	ENST00000447712.2	3,0858739	2,82336609	3,50727922
	ENST00000335922.5	2,83201145	2,05781676	2,71954643
	ENST00000466021.1	-3,057476	-2,016156	-1,7716251
	ENST00000326324.6	-3,7092097	-2,4981208	-2,6951858
	ENST00000397103.1	-4,1970604	-2,6418689	-2,8709554
	ENST00000425967.3	-4,528972	-3,1306108	-3,5520013
	ENST00000470826.1	-4,7584794	-7,5279985	-7,2941417
E4F1	ENST00000564139.1	10,1151595	5,80804654	4,87121716
	ENST00000565090.1	11,3408693	9,38172	9,45925731
	ENST00000563643.1	-5,1100152	-4,3591755	-2,4538275
	ENST00000301727.4	-9,9377357	-5,6653353	-7,8806438
CLDND1	ENST00000510545.1	11,3175296	3,66845499	11,3732737
	ENST00000394181.2	3,20883569	2,93856181	4,43550818
	ENST00000508902.1	-2,5857063	-2,7328844	-1,9336033
	ENST00000437922.1	-7,3189608	-3,2081765	-2,0081082
PYROXD1	ENST00000536935.1	11,0793725	3,7838533	5,60555669
	ENST00000375266.4	-6,2952049	-6,2399002	-3,2195687
PLS3	ENST00000537301.1	11,0082325	4,24287705	8,31887235
	ENST00000289290.3	-8,5525609	-4,3298293	-2,7224772
NFYC	ENST00000372651.1	10,941793	7,63235913	6,00714453
	ENST00000447388.3	2,91577166	3,81472513	5,84285802
	ENST00000525290.1	-2,1982766	-2,7052104	-2,3930594
	ENST00000372654.1	-2,9889084	-7,1645578	-2,6965719
PPFIBP1	ENST00000537927.1	10,806002	7,55026939	11,1455967
	ENST00000545381.1	0,52709024	2,39477433	2,36317812
	ENST00000318304.8	-5,5139176	-2,0218541	-4,0588677
TFDP2	ENST00000479040.1	10,7698249	7,06181259	8,35084544
	ENST00000477292.1	8,95710046	3,6010101	2,04916461
	ENST00000488107.2	4,91003672	2,62082365	2,01514876
	ENST00000397991.4	-2,1829491	-3,0679549	-2,6892717
	ENST00000467667.1	-5,5008273	-7,9398581	-5,3149566

RUVBL2	ENST00000221413.6	10,6707647	2,92691867	4,97714695
	ENST00000595002.1	-3,698023	-2,3923737	-6,9667517
STAT6	ENST00000454075.3	10,564201	6,37100805	2,67579511
	ENST00000557563.1	-2,298544	-5,6750288	-4,6210399
PRKAR1B	ENST00000537384.1	10,1319567	5,97536965	3,46897399
	ENST00000488474.1	-6,5534852	-6,2113261	-2,7594517
USP28	ENST00000260188.5	10,0878699	3,47325212	5,1010024
	ENST00000544967.1	-4,2722862	-3,6978088	-2,178386
ZNF707	ENST00000454097.1	9,99199787	7,86489705	4,58316397
	ENST00000531985.1	4,06606925	2,72546492	4,52246247
	ENST00000358656.4	-5,3437039	-2,3149303	-2,7798294
MST1R	ENST00000424150.2	9,95826213	5,86374719	9,33615705
	ENST00000344206.4	3,47589507	3,81892457	3,61971778
	ENST00000411578.2	-8,3425044	-4,4380642	-5,7486626
NARF	ENST00000581743.1	9,79963034	4,23604193	4,56820935
	ENST00000578820.1	5,21320567	2,36067115	4,11331139
	ENST00000584965.1	-3,3898936	-2,6810176	-3,5510396
PLSCR3	ENST00000575543.1	9,54759963	3,24768512	7,50611363
	ENST00000576362.1	4,76606352	2,72758773	3,2444807
	ENST00000574401.1	-7,1426152	-3,5167966	-4,0790121
	ENST00000573070.1	-7,228721	-6,8624142	-6,6084558
NAP1L4	ENST00000469089.1	9,50275753	5,78162996	6,04175803
	ENST00000534372.1	5,07079314	4,96269024	3,11384841
	ENST00000532325.1	3,74506362	3,46910671	2,8540138
	ENST00000448187.1	-4,9546731	-2,9980567	-4,6651116
PLXNB2	ENST00000449103.1	9,48616309	8,53355433	8,94119569
	ENST00000359337.4	-11,746376	-8,561451	-8,1858825
NDRG1	ENST00000517331.1	9,46175551	4,81557541	3,3197689
	ENST00000521544.1	-3,2389849	-2,2216011	-3,3745945
	ENST00000323851.7	-3,5535583	-7,8215877	-4,4850752
CHD4	ENST00000544484.1	9,37384754	4,41605255	7,77436226
	ENST00000309577.6	-8,1577738	-2,0493231	-8,5238596
RDBP	ENST00000444811.2	9,26128117	3,02173992	7,83257156
	ENST00000441998.1	8,69346748	2,9242372	6,50886133
	ENST00000375425.5	7,0691476	2,75918793	3,02109247
	ENST00000436289.2	-3,8152487	-2,179771	-2,1326007
BAG6	ENST00000362049.6	9,21365904	2,4324284	2,82306583
	ENST00000435080.1	-4,2157724	-3,2640466	-4,0265861
CD44	ENST00000360158.4	9,16106102	7,51486976	11,7872432
	ENST00000433354.2	7,74965036	5,50826881	6,85556498
	ENST00000433892.2	5,60078998	5,48443336	5,09757488
	ENST00000533222.1	4,03044109	4,00991019	3,92790917
	ENST00000425428.2	-2,6954355	-3,3972954	-2,9812845
	ENST00000278386.6	-2,7370933	-4,1759019	-3,7447758
	ENST00000352818.4	-7,3149297	-7,259625	-4,1956834
IMPDH1	ENST00000470772.1	9,00469915	8,20063172	9,23727016
	ENST00000480861.1	6,99872873	6,97335674	7,59117762
	ENST00000496200.1	4,21081039	6,74470102	3,54267809
	ENST00000378717.4	3,36072042	6,19847977	3,30566067

	ENST00000338791.6	-10.269339	-10.214(	
IL6ST	ENST00000502326.3	8,98421689	5,25672408	7,52581428
	ENST00000336909.5	-2,1319082	-4,2885187	-2,644454
PAN2	ENST00000547994.1	8,97254135	5,44338579	4,36318497
	ENST00000425394.2	-3,1884147	-7,4644821	-7,8858726
CKAP5	ENST00000312055.5	8,9307444	3,43023954	2,64034644
	ENST00000354558.3	-4,3378798	-4,3785098	-2,5106108
SCRN3	ENST00000437944.1	8,88066941	3,1933755	4,97447875
	ENST00000548868.1	-5,7883825	-4,5693581	-6,0160966
WDR52	ENST00000465636.1	8,84775862	5,55183824	7,16138882
	ENST00000308346.6	3,48558269	2,89330565	4,52939386
	ENST00000488854.2	2,2218036	2,85298667	4,31368975
	ENST00000393845.2	-5,4888041	-4,3246955	-2,9433972
ITGB4	ENST00000584558.1	8,784371	7,53291102	6,39677512
	ENST00000449880.2	8,08430597	2,6180375	3,64961013
	ENST00000339591.3	-4,7823982	-4,0965634	-6,8718451
MAPKAP1	ENST00000373498.1	8,77775142	3,68617548	3,74312395
	ENST00000496658.1	2,8863785	2,69273577	2,74949048
	ENST00000265960.3	-8,8103391	-4,2744286	-7,8525036
APLP2	ENST00000533713.1	8,74464952	4,12232793	4,8828712
	ENST00000527702.1	6,5179246	3,42046378	3,85094068
	ENST00000345598.5	4,36415041	2,18329506	3,12944773
	ENST00000529235.1	-8,2713778	-4,4526698	-4,2941993
FRS2	ENST00000549921.1	8,71705549	9,41781236	6,07204145
	ENST00000299293.2	3,83320747	4,48431891	2,74514303
	ENST00000550389.1	-4,6090963	-5,0530557	-4,4235217
CYB561	ENST00000392975.2	8,69289186	5,35950578	2,62313572
	ENST00000360793.3	-8,4065227	-2,1858184	-2,4937846
USP19	ENST00000417901.1	8,68236272	6,96957923	8,29023283
	ENST00000491859.1	2,85255642	4,41393807	3,5009246
	ENST00000465902.1	2,61049353	3,25408958	2,87757584
	ENST00000306026.5	-4,1420095	-7,3976097	-4,4654566
	ENST00000434032.2	-11,890929	-8,8158585	-6,7806331
PLD3	ENST00000409735.4	8,54117607	3,29061979	3,30579196
	ENST00000409281.1	-11,040491	-3,0964487	-3,8879927
SLC24A6	ENST00000553238.1	8,52184427	4,41636121	6,27425784
	ENST00000548186.1	-6,4065858	-6,3681038	-6,8553835
ACY1	ENST00000464587.1	8,50877633	6,13809477	5,54277961
	ENST00000476351.1	-2,4004939	-2,8157684	-5,2868143
SOGA2	ENST00000359865.3	8,4894446	4,61987673	7,71559245
	ENST00000306285.7	-8,0567572	-3,1762255	-8,4228429
WBP2	ENST00000591399.1	8,47477119	8,63247683	5,39395582
	ENST00000416574.2	-3,0922399	-2,7187706	-3,8153631
	ENST00000591831.1	-3,5473834	-4,0771189	-9,4999021
DEDD	ENST00000464113.1	8,44225712	2,77278648	5,04737262
	ENST00000535389.1	-6,0206308	-2,3328194	-3,7210368
UBXN11	ENST00000494942.1	8,43018228	8,54932043	6,94977129
	ENST00000357089.4	5,70968625	3,86324543	6,41566519
	ENST00000374223.1	2,90855189	2,54013039	3,25707399

	ENST00000436301.2	-2,4603049	-3,4105357	-3,4263746
	ENST00000374217.2	-4,1066868	-4,3042956	-4,0661583
	ENST00000475591.1	-9,5457031	-6,7004975	-9,923491
ARHGEF39	ENST00000343259.3	8,38965202	3,90111381	2,8937657
	ENST00000378387.3	-5,6402194	-2,8472776	-2,7754026
CLK3	ENST00000563842.1	8,37742223	5,95550316	4,27990682
	ENST00000564468.1	3,59988831	3,42044966	2,42621542
	ENST00000483723.1	2,8369935	2,88345169	2,05493304
	ENST00000566126.1	-4,9764651	-2,9330184	-2,1755737
PCYT1A	ENST00000416798.2	8,36968246	7,97423033	7,43225914
	ENST00000460677.1	7,16287114	4,86035171	4,7408583
	ENST00000473978.1	-4,7689902	-4,8986516	-5,0922359
ERBB2	ENST00000406381.2	8,36683785	11,5581465	5,53194724
	ENST00000582788.1	-4,3530384	-7,9946408	-2,9572077
UIMC1	ENST00000377227.4	8,34163824	5,50433072	4,98379918
	ENST00000512031.1	2,11990291	2,52144221	2,27049317
	ENST00000506128.5	-8,7271484	-4,2960383	-2,1273855
DPH1	ENST00000576891.2	8,30755113	6,93648257	2,19549109
	ENST00000263083.6	-6,8090707	-6,9662242	-2,1278483
FLII	ENST00000584444.1	8,30268346	2,75994188	6,45542514
	ENST00000545457.2	5,83573372	2,68864746	2,7457714
	ENST00000578101.1	-2,1732792	-4,4987077	-3,6881973
	ENST00000478416.1	-2,3298214	-4,9904698	-5,3087853
	ENST00000582626.1	-4,3168571	-5,0399453	-7,6097991
FDFT1	ENST00000529464.1	8,28871528	4,57635205	3,81328972
	ENST00000525954.1	7,96677481	3,71514085	2,07268878
	ENST00000538689.1	-5,6107702	-4,0407332	-3,0162237
	ENST00000530337.1	-5,6749731	-4,1424789	-3,3448563
DIXDC1	ENST00000315253.5	8,24086286	3,19096197	4,59980543
	ENST00000440460.2	2,16931768	2,50949046	2,59205322
	ENST00000524385.1	-3,2781155	-3,0057641	-2,7481714
	ENST00000530411.1	-3,8964272	-3,2531574	-4,0864245
MLST8	ENST00000565330.1	8,1977792	3,14764271	4,51046793
	ENST00000301725.7	7,59271065	3,09199101	4,11112936
	ENST00000566653.1	-7,9997014	-7,9443966	-8,3657871
ADAM15	ENST00000271836.6	8,12422416	7,46944128	6,75296785
	ENST00000355956.2	6,76155055	4,9349436	6,33984598
	ENST00000473905.2	3,37436961	4,47236661	4,69312955
	ENST00000356955.2	3,00538618	3,80759064	3,86497154
	ENST00000449910.2	-3,8007835	-3,339807	-3,3461322
	ENST00000359280.4	-5,4399296	-5,5013787	-5,6461505
PTK2	ENST00000521986.1	8,11999424	5,22110868	3,75662064
	ENST00000520045.1	7,43038355	4,40537001	3,47692596
	ENST00000521059.1	4,41014604	4,26557445	3,39019909
	ENST00000523539.1	-6,2081864	-3,4176596	-3,8390501
	ENST00000521907.1	-6,507689	-4,6433721	-4,3984079
	ENST00000538769.1	-8,2146294	-6,3822654	-5,5887443
NUP62	ENST00000352066.3	8,11469256	3,99714237	4,91838618
	ENST00000599186.1	-2,7134239	-3,9300597	-3,5706616

	ENST00000597723.1	-4,2328998	-5,2472035	-5,0456895
NUP62CL	ENST00000484614.1	4,92021539	7,15550051	2,45853471
	ENST00000372461.3	-2,0866526	-4,7647787	-2,3364192
ITPR1	ENST00000493491.1	8,08266992	2,48262419	3,80460143
	ENST00000544951.1	6,56525687	2,04718595	2,44648202
	ENST00000463980.1	-2,863563	-4,9415593	-3,2329736
KIAA1199	ENST00000356249.5	8,04773339	2,98650721	8,40812262
	ENST00000394685.3	-5,702298	-6,1242518	-9,4294807
RAI14	ENST00000507276.1	8,04211902	2,41682138	4,46046322
	ENST00000513974.1	-5,9172938	-3,5948498	-2,6005744
MYO5A	ENST00000356338.6	7,97899111	6,89195998	5,56107521
	ENST00000399231.3	2,34787671	3,62862511	4,72556034
	ENST00000358212.6	-7,0267347	-2,8027356	-4,2620174
SEC23A	ENST00000537403.1	7,97258398	2,03347956	5,01183875
	ENST00000554645.1	-2,5100399	-3,3546036	-4,2287347
USP3	ENST00000538686.2	7,92203476	3,74830222	3,29676092
	ENST00000380324.3	5,09734606	3,24767962	2,74037641
	ENST00000268049.7	4,91190317	2,17507387	2,10160989
	ENST00000559257.1	-3,019533	-2,2270259	-3,2746222
	ENST00000540797.1	-6,4614908	-3,329166	-3,3856188
ACSS2	ENST00000481284.1	7,90988706	4,19809236	2,56842125
	ENST00000484354.1	-7,953448	-2,2155128	-2,9753619
B3GALNT1	ENST00000392780.1	7,90547168	4,86973519	6,97312329
	ENST00000468268.1	3,19959804	3,57629405	3,6255907
	ENST00000320474.4	-6,1634074	-3,8062934	-8,9761272
PRDM10	ENST00000360871.3	7,85700112	7,92702749	3,27578625
	ENST00000358825.5	-11,136587	-11,081282	-7,3090445
KLC1	ENST00000557575.1	7,82066089	4,12744328	4,04038567
	ENST00000445352.4	4,05369013	2,37519239	2,85839772
	ENST00000246489.7	-5,9508631	-3,5904742	-4,7330231
CSNK1G3	ENST00000510842.2	7,80578332	10,9154129	5,57221571
	ENST00000345990.4	5,18207816	4,96156721	3,9528293
	ENST00000360683.2	2,56454081	3,47301188	3,36048352
	ENST00000511130.2	-5,7908534	-5,1243761	-5,0356149
	ENST00000521364.1	-10,745981	-7,9032477	-6,758193
NCOA1	ENST00000406961.1	7,79955689	7,05443772	6,68764645
	ENST00000288599.5	-4,4743785	-4,3344753	-2,2807035
	ENST00000348332.3	-6,755965	-6,7006602	-8,2162633
RAD51AP1	ENST00000536886.1	7,76958437	2,87647713	5,29974559
	ENST00000535558.1	-3,4622535	-5,3267586	-7,5202656
SH3TC1	ENST00000506360.1	7,68570532	5,16401987	4,88128376
	ENST00000245105.3	-4,9517061	-2,2646305	-3,6750726
TET2	ENST00000265149.5	7,67125141	3,56943857	3,61291811
	ENST00000380013.4	2,82542538	3,03456633	2,73661022
	ENST00000545826.1	-9,5411041	-3,865113	-4,1247191
NADK	ENST00000341991.3	7,61145619	8,68094804	5,98240771
	ENST00000497186.1	4,45238849	5,19895049	3,30102957
	ENST00000480499.1	-5,9943936	-4,7874221	-6,3795587
ARHGEF1	ENST00000354532.3	7,59463348	9,70323986	9,14694757

	ENST00000599846.1	-4,9896159	-2,812929	-5,7762076
	ENST00000594044.1	-7,370777	-3,8008598	-5,8761905
MARK2	ENST00000413835.2	7,52403175	3,5987096	6,98150185
	ENST00000513765.2	-8,1559805	-7,9203482	-3,3854392
ASB13	ENST00000357700.6	7,49776586	4,43704555	2,86653996
	ENST00000479033.1	-3,180212	-4,8815283	-2,4113115
NEDD4L	ENST00000400345.3	7,47934366	4,26254759	5,48135227
	ENST00000456173.2	3,87903996	3,43834862	4,35958717
	ENST00000256832.7	3,22354932	2,65766852	4,0100587
	ENST00000585970.1	-3,5541173	-2,3613583	-4,1794172
	ENST00000382850.4	-4,4051891	-2,5869815	-4,7749589
TMBIM6	ENST00000549385.1	7,44523175	2,83612662	5,46578999
	ENST00000550040.1	3,20696799	2,18350559	3,71836347
	ENST00000550445.1	-3,4479295	-3,5964667	-3,2584238
OCIAD1	ENST00000444354.2	7,42290732	5,51122344	3,39033064
	ENST00000264312.7	3,30051056	3,45081455	2,44254587
	ENST00000511102.1	-2,3761447	-2,2794514	-7,4468635
NOL8	ENST00000421075.2	7,3928711	3,99548839	6,00512561
	ENST00000432670.2	5,99420107	3,68698265	4,77891854
	ENST00000442668.2	3,49986197	3,04058258	3,88458961
	ENST00000538215.1	3,22788232	2,95493301	2,17559566
	ENST00000545444.1	-3,2554224	-6,6427161	-7,0641066
TACC1	ENST00000330691.6	7,37106493	7,19988034	9,37489267
	ENST00000443286.2	6,67549073	5,5836656	7,54759075
	ENST00000379931.3	3,35464224	3,88613757	3,50626197
	ENST00000276520.8	-2,5804879	-3,1697291	-2,9949328
	ENST00000522904.1	-7,4961477	-3,4484362	-6,1742365
COMMD4	ENST00000562789.1	7,35145525	6,08824454	6,30643499
	ENST00000562610.1	2,94474767	3,20648425	3,34596165
	ENST00000565517.1	2,18139979	3,08805084	2,6609012
	ENST00000564068.1	2,09498402	2,96316368	2,56085048
	ENST00000567023.1	-2,77058	-2,2361273	-3,7239952
	ENST00000568877.1	-6,0515506	-4,0639163	-3,813663
AP4M1	ENST00000445208.1	7,34466425	4,61645672	4,52074947
	ENST00000446007.1	5,36989012	2,01016452	1,60701258
	ENST00000429084.1	-4,4003815	-2,4630405	-2,5110575
CERS5	ENST00000546406.1	7,34065558	5,52921887	2,56211696
	ENST00000551697.1	-3,0137224	-2,0769455	-3,9631692
	ENST00000550919.1	-3,2729105	-6,7456064	-6,5223896
DYNC1I2	ENST00000410079.3	7,33157455	6,76487406	4,66888171
	ENST00000409317.1	3,36407092	6,00143701	3,91542735
	ENST00000409453.1	-5,5987728	-6,9619717	-5,1844926
NISCH	ENST00000479054.1	7,32394459	7,34079357	7,14541952
	ENST00000345716.4	-4,3874112	-4,4399165	-2,1698574
USP47	ENST00000527733.1	7,31285037	8,39929881	7,25554734
	ENST00000539466.1	-3,5208543	-6,8736967	-4,2464257
WDR90	ENST00000546516.1	7,30676574	3,26111914	6,77089172
	ENST00000552683.1	-4,0382543	-2,2042088	-2,239734
BCLAF1	ENST00000531224.1	7,2670878	3,76392802	3,86068264

	ENST00000353331.4	-4,6566437	-2,7739171	-4,8450338
TOP3A	ENST00000585031.1	7,25939264	10,0125311	9,44462979
	ENST00000321105.5	-2,8238136	-3,1279509	-3,2997786
	ENST00000469739.2	-3,3772565	-3,8950654	-3,8564773
CC2D2A	ENST00000503292.1	7,24986478	5,17199141	3,56180263
	ENST00000512702.1	-7,6145639	-4,2353149	-6,3281025
ATP11C	ENST00000327569.3	7,24735428	3,95680811	4,66180756
	ENST00000433868.1	5,43111713	3,60646344	4,27495068
	ENST00000359686.2	5,04784008	2,6774081	3,41218314
	ENST00000361648.2	-2,912784	-2,962135	-5,4226197
	ENST00000450801.1	-3,880475	-3,6091747	-6,6093861
SEC31B	ENST00000484848.1	7,24604169	4,52555012	4,21707994
	ENST00000479697.1	-4,0219705	-3,0270625	-2,3909492
MEF2A	ENST00000453228.2	7,2323931	3,90261971	5,52457718
	ENST00000557942.1	6,16313698	3,57257634	4,61685492
	ENST00000558983.1	2,17554088	2,77455095	3,68154481
	ENST00000557785.1	-4,5465787	-7,7596148	-5,1898859
TRAPPC9	ENST00000438773.2	7,22519922	9,22098037	9,21700108
	ENST00000389328.4	-4,6835095	-4,1924928	-8,2935438
WARS	ENST00000556579.1	7,21903688	6,2048995	5,74261281
	ENST00000355338.2	4,06146249	3,76744779	4,67150472
	ENST00000344102.5	3,85699418	2,11248774	4,43634012
	ENST00000555031.1	-2,5277489	-3,1967482	-5,926207
	ENST00000557239.1	-5,0157136	-6,0209443	-6,3325715
	ENST00000554820.1	-6,0762491	-12,235629	-6,4423348
CREM	ENST00000490511.1	7,21196847	3,52947226	3,21761092
	ENST00000474931.1	-5,7719279	-2,174573	-1,7788369
	ENST00000472813.1	-5,8765212	-3,441145	-2,8527155
	ENST00000496019.1	-6,5421789	-5,2382816	-3,0662945
	ENST00000374721.2	-8,1128338	-5,5526321	-4,0499864
	ENST00000469517.1	-9,5019912	-5,619046	-5,2100695
SLC12A6	ENST00000397702.2	7,20306459	6,42757375	6,0659275
	ENST00000451844.2	-10,195314	-10,140009	-7,8861643
ZHX3	ENST00000540170.1	7,05434297	4,82279686	2,81484925
	ENST00000560364.1	-6,1740179	-8,3448127	-2,5735936
SUN1	ENST00000457861.1	7,17928126	4,0231748	6,62514062
	ENST00000425407.2	3,32240881	4,01877857	4,17062174
	ENST00000456758.2	-2,9420871	-2,2458349	-2,3301258
	ENST00000401592.1	-3,7339914	-2,9588621	-2,811708
	ENST00000450881.1	-7,2107323	-6,9223568	-3,5816111
HNRNPC	ENST00000554455.1	7,16587955	3,89568716	6,11899844
	ENST00000449098.1	4,80144883	3,10846336	3,80527444
	ENST00000553753.1	4,40951383	2,26039238	3,05319486
	ENST00000554539.1	-3,7463694	-3,3089525	-2,8900961
	ENST00000555137.1	-10,994315	-7,4202595	-6,733195
PSMA6	ENST00000556506.1	7,14200655	11,0911524	10,5963493
	ENST00000553809.1	4,62404694	6,39628489	5,71144846
	ENST00000540871.1	3,54246389	3,7863392	3,71001223
	ENST00000554843.1	-3,8788548	-3,9222466	-3,8134699

	ENST00000556221.1	-4,5485055	-5,286444	-5,2337789
TECR	ENST00000597607.1	7,11105122	3,68591829	4,52534112
	ENST00000598987.1	-5,7772629	-3,1281919	-2,2812417
SLC38A7	ENST00000219320.4	7,11100281	4,26128599	7,46282932
	ENST00000564100.1	-4,4717643	-3,751205	-6,6026861
PCBP2	ENST00000550927.1	7,08882704	6,51804305	2,53722772
	ENST00000359462.5	-3,3388668	-2,17262	-2,2742689
MACF1	ENST00000567887.1	7,04272003	4,98360396	9,42131015
	ENST00000446276.1	4,19206592	2,00111428	8,85416504
	ENST00000422234.2	-7,3400586	-4,7073331	-4,4565864
	ENST00000317713.7	-11,156514	-5,7339081	-11,5226
EHMT2	ENST00000375530.4	7,02183934	9,30175695	11,3584043
	ENST00000375537.4	-8,6028991	-4,9796277	-9,2282147
TXNRD2	ENST00000400521.1	7,00512177	2,45305283	3,44972609
	ENST00000462330.1	-3,785947	-3,1764399	-4,2470364
PCBP4	ENST00000355852.2	7,00286922	3,15995857	4,49933903
	ENST00000490063.1	2,68717	2,6469395	3,28126898
	ENST00000461554.1	-2,4929473	-2,3474455	-2,4943094
POLL	ENST00000370172.1	7,00179807	5,54143204	8,94892438
	ENST00000430045.1	3,62440248	4,95862345	4,91201588
	ENST00000436284.2	-2,3209024	-2,3830452	-4,2310109
	ENST00000456836.2	-2,3783848	-4,0793625	-4,8580311
	ENST00000370169.1	-3,0929636	-6,1423125	-5,8288645
PHF17	ENST00000452328.2	6,99018089	2,40459569	7,29713541
	ENST00000514740.1	-7,3828287	-9,7627726	-11,750389
TMEM161A	ENST00000592369.1	6,96637446	5,76876617	6,52688101
	ENST00000162044.8	5,16337	2,51671482	4,35642101
	ENST00000591031.1	-4,0318496	-3,2460369	-2,0292715
CNOT8	ENST00000523698.1	6,95483919	3,31837916	6,53899766
	ENST00000285896.6	-3,8632796	-2,5565281	-2,2518105
CCDC57	ENST00000389641.4	6,94111555	5,74091388	2,51977958
	ENST00000392347.1	-6,6559292	-5,7049972	-5,0764455
CAST	ENST00000510500.1	6,9394569	6,93551147	8,45257795
	ENST00000508197.1	5,37762474	6,77689933	7,96702814
	ENST00000510756.1	3,02955864	3,66747608	4,73960082
	ENST00000515663.1	2,23445062	2,96559848	3,7275561
	ENST00000505143.1	2,12944864	2,5114645	3,60297257
	ENST00000359176.4	-3,5846802	-2,9815344	-2,8133391
	ENST00000511049.1	-7,2381594	-3,1817834	-3,9507659
C16orf62	ENST00000539322.1	6,92949628	3,90305772	8,4336843
	ENST00000544670.1	-5,554099	-2,9251776	-9,3907003
ELL	ENST00000594635.1	6,89806789	6,54393183	5,19300601
	ENST00000596915.1	-3,8853497	-6,1661071	-4,5664989
ELP3	ENST00000524103.1	6,85411031	3,56296719	6,35589637
	ENST00000542181.1	-4,823542	-5,0917053	-4,6212041
RBM39	ENST00000253363.6	6,84790727	5,8239241	6,75932894
	ENST00000427743.1	5,78210408	3,14282937	5,3313588
	ENST00000475651.1	3,78465542	2,98134575	3,03718466
	ENST00000374038.3	3,57270033	2,94771322	2,95127251

	ENST00000397370.3	2,37454672	2,11465375	2,86806974
	ENST00000412738.1	-3,6485839	-4,2793662	-3,9294831
JMJD8	ENST00000567120.1	6,83791511	5,27224147	5,65599919
	ENST00000563088.1	-3,4754204	-4,3961757	-4,1855544
RPGR	ENST00000318842.6	6,8204121	6,92630234	6,98659542
	ENST00000338898.3	-2,8615146	-2,6029182	-3,8730012
WDR73	ENST00000434634.2	6,81895965	5,79807929	7,68065079
	ENST00000559015.1	2,13622903	4,65948198	5,61461017
	ENST00000398528.3	-2,7225097	-2,7655631	-3,1373173
	ENST00000559994.1	-5,8961061	-3,7203102	-5,6396503
ETV1	ENST00000242066.5	6,81291006	3,32566757	5,40014754
	ENST00000403527.1	6,2165225	3,30008826	3,80442512
	ENST00000405218.2	-6,9764341	-2,9979351	-2,0941963
	ENST00000405192.2	-8,8253835	-3,9839391	-4,2124204
DIS3L2	ENST00000360410.4	6,80171034	9,97493889	5,82701337
	ENST00000390005.5	6,2542703	5,35241618	5,5492942
	ENST00000325385.7	-2,2057498	-3,792208	-2,9629701
DNM1L	ENST00000381000.4	6,76655115	5,5870365	6,97557977
	ENST00000266481.6	6,57861113	2,49136391	6,72982338
	ENST00000548750.1	5,99517752	2,07197891	2,97248656
	ENST00000358214.5	-2,8270784	-2,7410443	-4,6136687
	ENST00000547312.1	-5,0325349	-5,6527566	-6,6991412
CCDC111	ENST00000515774.1	6,76205674	4,53084183	5,80221566
	ENST00000512834.1	3,35390496	3,03725488	2,50485847
	ENST00000314970.6	-7,2073385	-3,4219421	-2,3881138
CASP8	ENST00000323492.7	6,75704248	4,06403308	2,20688457
	ENST00000392263.2	-2,1291655	-3,3172744	-2,1809623
	ENST00000450491.1	-4,8259702	-3,5124241	-4,5628721
	ENST00000432109.2	-4,9989601	-3,725739	-4,7480228
NEK6	ENST00000423785.1	6,75424903	3,90059387	3,49679102
	ENST00000373600.3	-3,643208	-4,0749689	-4,6511765
	ENST00000539416.1	-7,6564096	-4,5513684	-5,8559191
LIMS1	ENST00000449684.2	6,72679215	5,58578001	4,49102704
	ENST00000332345.6	-3,5432582	-6,6017591	-4,4983206
SHMT2	ENST00000553949.1	6,7147899	5,71465015	5,97703196
	ENST00000554975.1	6,52657351	5,44328165	5,15928871
	ENST00000553529.1	6,4861551	2,91737498	4,58863695
	ENST00000553474.1	4,97626604	2,58237072	4,53307726
	ENST00000553324.1	-3,2673414	-2,418664	-2,9828093
	ENST00000557740.1	-4,487581	-3,7179935	-6,0588876
	ENST00000555563.1	-8,6089872	-4,8102897	-6,3803186
NF1	ENST00000456735.2	6,70009667	6,25293563	3,94720442
	ENST00000581113.1	6,11813505	4,48640849	2,67642496
	ENST00000356175.3	3,80884561	4,13490276	2,3933548
	ENST00000579081.1	-7,0838219	-2,3138064	-5,0431583
KLC3	ENST00000470402.1	6,67125139	2,39296059	7,73087028
	ENST00000391946.2	-8,4009	-2,1998303	-8,7669857
FRYL	ENST00000507873.2	6,6462778	3,71339962	3,50426423
	ENST00000537810.1	3,62698808	3,14559877	2,41474057

	ENST00000507711.1	3,57855766	2,5319657	2,37328477
	ENST00000503339.1	3,10040474	2,07837109	2,19127569
	ENST00000503238.1	-8,1278075	-4,3109424	-3,5264916
KIAA1841	ENST00000453873.1	6,63616498	3,32145792	5,6309895
	ENST00000402291.1	-6,0571535	-3,268297	-2,1335763
TRIT1	ENST00000492612.1	6,61006897	5,31817209	5,21237489
	ENST00000469476.1	2,11818871	2,68312162	3,40014563
	ENST00000046894.5	2,08492175	2,09751477	2,93111918
	ENST00000462797.1	-2,1696051	-6,3343871	-4,0392561
CCDC132	ENST00000544910.1	6,60419923	3,37852192	5,2750589
	ENST00000535481.1	5,05515738	2,12412702	3,69153749
	ENST00000305866.5	-12,027657	-3,8707883	-2,3925056
PRMT5	ENST00000553641.1	6,60319761	6,82328591	7,30183528
	ENST00000556616.1	5,85805225	4,24981829	6,15793974
	ENST00000216350.8	5,6448234	4,08314587	5,06436759
	ENST00000554910.1	4,75386046	3,3258126	3,64268954
	ENST00000397441.2	3,34926349	3,00843778	2,47604408
	ENST00000555454.1	-3,2490402	-8,5090883	-7,8321169
ANXA6	ENST00000377751.5	6,59756716	6,56433644	4,79003481
	ENST00000519644.1	-2,9674506	-2,5771866	-2,9985771
OS9	ENST00000413095.2	6,58683877	4,8666732	3,77231337
	ENST00000546916.1	6,01115049	2,79066973	3,25754678
	ENST00000257966.8	4,9005551	2,45731684	2,1123246
	ENST00000389142.5	-2,0084904	-2,8784944	-5,3775486
SF3B2	ENST00000533595.1	6,57869276	4,18340008	2,27608829
	ENST00000530322.1	-5,8859359	-3,2352725	-5,793439
LTBP3	ENST00000530866.1	6,56328231	3,62401857	4,25090139
	ENST00000301873.5	-3,5712297	-2,725321	-3,2301759
	ENST00000322147.4	-6,5030737	-3,7182505	-3,2331027
HDAC6	ENST00000430858.1	6,53705571	2,82984286	5,6089617
	ENST00000481929.1	-5,1154045	-2,7285134	-5,5689926
	ENST00000477528.1	-5,2753659	-3,5101967	-6,7407554
	ENST00000376619.2	-5,4209749	-5,6719855	-10,357091
MTRR	ENST00000264668.2	6,52500757	4,34882993	3,94705951
	ENST00000513439.1	5,33554427	3,7176585	2,50072319
	ENST00000508047.1	-2,8888986	-6,7240768	-2,1602261
COMMD3	ENST00000489125.1	6,5141647	3,2699695	6,36142393
	ENST00000470045.1	-2,9482023	-2,5499303	-4,0303333
MAP3K3	ENST00000584573.1	6,51240489	4,66901249	3,07894118
	ENST00000577395.1	-7,8939163	-2,5607291	-6,0440847
CABIN1	ENST00000454754.1	6,5110725	3,10190165	3,03984703
	ENST00000263119.5	-5,9332	-4,1541952	-3,0345993
ARHGEF28	ENST00000513042.2	6,51081527	3,08472699	6,23083577
	ENST00000296799.4	5,46492792	2,79920363	2,85838617
	ENST00000426542.2	-9,9980302	-3,7676324	-2,354214
NAA60	ENST00000574380.1	6,50670135	7,72627862	7,94986557
	ENST00000414063.2	2,74330991	6,11299375	4,90640792
	ENST00000573580.1	2,7198578	5,65196428	3,11705203
	ENST00000571107.1	-3,1900429	-4,4884909	-2,7427953

	ENST00000575754.1	-3,7273624	-7,554059	-3,0785963
NELF	ENST00000392812.4	6,48906016	3,02790258	4,27066419
	ENST00000541195.1	-2,383392	-2,4517393	-4,2255846
	ENST00000371482.1	-2,5367378	-6,6223134	-4,3093417
IMPA2	ENST00000588927.1	6,48873122	3,80565735	2,47006879
	ENST00000588752.1	-2,7723892	-2,2846933	-2,2386918
SYNE1	ENST00000341594.5	6,48386069	3,62079724	5,42463411
	ENST00000367256.5	2,34677258	3,30240642	3,08935644
	ENST00000265368.4	2,31110789	3,28527286	2,50520152
	ENST00000367255.5	-3,6578877	-2,9451032	-2,7531085
	ENST00000490135.2	-3,8999829	-3,290219	-3,6013879
	ENST00000367251.3	-5,2504119	-5,0180552	-6,4236003
ST6GALNAC6	ENST00000291839.5	6,47343722	7,39988499	6,66406327
	ENST00000373142.1	4,22877716	5,49687703	4,81970457
	ENST00000542456.1	2,29757723	2,96363125	2,15829037
	ENST00000373146.1	-5,4852491	-8,8449513	-8,5540771
MTIF2	ENST00000403721.1	6,4674471	3,47611078	5,91836608
	ENST00000441307.1	2,42710757	2,54410081	5,25690344
	ENST00000417741.1	-5,8782643	-5,7696175	-3,0851366
MCRS1	ENST00000549000.1	6,46662806	3,33284092	7,46448763
	ENST00000552206.1	-4,6660117	-6,0038863	-5,0681393
LTBP4	ENST00000598677.1	6,44977229	8,51641589	8,13501445
	ENST00000600509.1	6,17374399	4,92334576	7,66208296
	ENST00000598717.1	5,72745824	3,2014192	6,97608475
	ENST00000595183.1	4,49694697	2,95460277	5,52157616
	ENST00000601209.1	2,85032813	2,69676776	5,00692674
	ENST00000545697.1	-3,5440458	-2,4032034	-2,2626228
	ENST00000602240.1	-5,0398407	-2,9092277	-2,7435107
	ENST00000308370.7	-6,2041987	-4,3852857	-4,0047816
MOK	ENST00000522867.1	6,42583295	4,93754134	8,21231026
	ENST00000193029.6	4,2405397	4,75586138	5,2581411
	ENST00000361847.2	-5,8970649	-2,7895439	-3,4520464
	ENST00000523169.1	-7,5607559	-3,1869461	-3,5570007
MFF	ENST00000452930.1	6,42405849	4,1369225	6,2666267
	ENST00000392059.1	6,15422167	2,26338937	2,66969704
	ENST00000354503.6	-7,9863493	-3,3098951	-4,7405311
	ENST00000353339.3	-10,464938	-4,1076689	-5,4037365
SEMA4B	ENST00000379122.3	6,41893756	5,97835904	5,24878868
	ENST00000559247.1	5,72660779	4,97118748	5,06980113
	ENST00000558051.1	4,69123715	4,32308845	5,02537284
	ENST00000561085.1	-3,5044502	-4,261865	-5,4053562
SYTL2	ENST00000389960.4	6,41234601	5,08012685	6,5700738
	ENST00000529581.1	-8,5078643	-4,168413	-4,3288723
ZNF714	ENST00000597086.1	6,39558753	2,18235266	2,91826876
	ENST00000601416.1	-6,4695776	-2,4512481	-6,8356633
TMEM39B	ENST00000468135.1	6,38697629	5,03041438	2,76057675
	ENST00000438825.1	-2,8799093	-7,2015415	-4,8775447
FXR1	ENST00000475315.1	6,38395318	6,86795325	2,62013017
	ENST00000445140.2	5,29193057	2,74680632	2,35084174

	ENST00000472339.1	-3,6896193	-8,1683595	-4,5033905
MYO1B	ENST00000451437.1	6,38369758	5,15466192	2,41962468
	ENST00000304164.4	-4,9795504	-3,0781743	-5,9208239
FAM219B	ENST00000565772.1	6,3813582	4,53377418	7,14201792
	ENST00000357635.5	-2,9214832	-2,8033744	-3,9395026
	ENST00000563119.1	-3,427325	-2,9373907	-4,8071971
P4HB	ENST00000537205.1	6,37961161	2,94036321	5,3530916
	ENST00000575069.1	-3,2658284	-7,507725	-5,086242
NAV3	ENST00000228327.6	6,37581771	3,26914637	6,17503493
	ENST00000536525.2	-2,6879872	-2,6557934	-2,7759378
PCCB	ENST00000478469.1	6,34315768	3,5877513	3,48088694
	ENST00000469217.1	5,63517912	3,22680699	3,2215663
	ENST00000462542.1	-2,0195912	-4,1587887	-3,9613575
TTLL3	ENST00000397241.1	6,28861671	4,24173128	4,12796713
	ENST00000383827.1	5,29870408	2,68862649	2,62320506
	ENST00000483051.1	-4,719694	-5,3068818	-3,5416214
CNOT10	ENST00000471003.2	6,28271551	2,51549154	5,71544307
	ENST00000485136.1	3,30216209	2,42117933	2,98006857
	ENST00000455381.1	-2,3637729	-4,557056	-3,2163981
CPEB1	ENST00000563800.1	6,28247388	3,82639781	4,02714494
	ENST00000423133.2	-2,3731728	-2,6712335	-1,2151961
ZC3H7A	ENST00000575170.1	6,26366463	3,33485301	9,09648071
	ENST00000571198.1	-3,3150179	-3,9706668	-6,5998662
TIAM2	ENST00000275246.7	6,25130603	2,95793132	7,15787925
	ENST00000456877.2	-4,7913174	-8,1035525	-6,5473878
PTK7	ENST00000230419.4	6,23477211	4,48178185	8,32779473
	ENST00000470019.1	-4,9615815	-3,1445212	-3,9713357
PRDM15	ENST00000447016.2	6,23225195	3,62002959	2,99010271
	ENST00000441787.1	-7,6701377	-3,6732049	-3,114393
MBP	ENST00000382582.3	6,20844835	2,95537167	8,29980414
	ENST00000354542.4	-2,3907187	-3,6000802	-11,162873
GSN	ENST00000341272.2	6,191149	3,72739297	9,71732535
	ENST00000373823.2	-5,5363781	-4,6858891	-6,1956479
RAP1B	ENST00000425247.2	6,19017995	3,88727811	7,5085679
	ENST00000450214.2	5,6688635	3,33249255	3,22321221
	ENST00000540209.1	5,56997024	2,11011419	2,71218857
	ENST00000540781.1	-3,1691165	-2,2054734	-2,7645876
	ENST00000541386.1	-4,9981531	-3,0578415	-3,1761852
POGZ	ENST00000491586.1	6,16292489	6,21509786	4,79571229
	ENST00000540984.1	6,02903641	4,55290235	2,68894749
	ENST00000531094.1	-3,3734022	-2,5322745	-2,7386282
RABGGTA	ENST00000559974.1	6,16025656	2,76682667	2,89938627
	ENST00000558376.1	5,82843977	2,00912257	2,71757774
	ENST00000216840.6	-3,1528889	-2,7529648	-3,5189747
ACLY	ENST00000590735.1	6,15660799	4,48189956	5,35029902
	ENST00000393896.2	-5,8802687	-3,8724465	-10,022672
STARD3	ENST00000578232.1	6,13668851	6,33919115	6,20323417
	ENST00000443521.1	-3,9346565	-5,3411677	-2,734084
FARP1	ENST00000595437.1	6,12660327	5,85837144	9,70541901

	ENST00000598389.1	-3,5490319	-2,3333112	-4,4896084
	ENST00000596467.1	-4,0554454	-5,1328112	-4,5422467
RAD54L	ENST00000488942.1	6,11654634	9,08599986	2,26537312
	ENST00000463715.1	3,52416078	3,72916823	2,21607313
	ENST00000476687.1	-4,7602441	-4,5884868	-5,7697592
ATP11A	ENST00000487903.1	6,11019256	6,50774819	5,40076368
	ENST00000459908.1	-2,3330994	-5,9193829	-3,7752276
AP3D1	ENST00000345016.5	6,09622646	6,81008216	6,73314549
	ENST00000591650.1	-4,6692167	-2,5942223	-6,2269707
MBNL1	ENST00000477171.1	6,08660922	3,57935238	9,98981646
	ENST00000464596.1	-2,7815633	-2,5684957	-3,6170764
	ENST00000357472.3	-6,9494559	-4,0893723	-9,1231428
ERC1	ENST00000589028.1	6,08289683	2,85637449	5,36927008
	ENST00000545948.1	4,65775374	2,15243758	3,37086737
	ENST00000397203.2	-3,1872563	-3,167498	-3,0131562
	ENST00000543086.2	-7,0931175	-6,3213022	-4,6430635
CCT7	ENST00000537131.1	6,06446268	6,90485884	6,19158157
	ENST00000539919.1	-3,2904423	-2,554083	-2,9754735
RSRC2	ENST00000331738.6	6,06239097	3,7629637	5,33874505
	ENST00000354654.2	-4,5154635	-2,8107771	-2,0201772
	ENST00000433877.2	-5,329881	-5,2745762	-2,2074389
CIRBP	ENST00000588230.1	6,05660998	4,57636886	6,47562498
	ENST00000593048.1	2,70064863	3,19611062	6,05460233
	ENST00000587323.1	-2,801009	-3,2008931	-3,0001934
	ENST00000320936.5	-3,2561978	-3,4101939	-3,9210326
	ENST00000586773.1	-4,0449651	-3,7708755	-5,1552911
ZNF385A	ENST00000394313.2	6,03325757	5,38793918	2,99130976
	ENST00000550779.1	-4,3872712	-3,6264523	-2,2471725
	ENST00000551109.1	-6,7649755	-5,2851696	-4,9423778
KIAA0391	ENST00000556121.1	6,02796024	5,41414073	6,4691298
	ENST00000554896.1	2,35391426	4,69385681	5,07593116
	ENST00000250377.7	-4,5964619	-2,5504918	-2,9315417
DDAH2	ENST00000437288.1	6,01552702	7,40574141	6,75257763
	ENST00000416410.1	-3,6315505	-2,7749021	-2,1203662
	ENST00000375787.2	-6,115073	-2,8956513	-2,3264384
	ENST00000375792.3	-6,8604821	-3,8679432	-2,6612432
SUGP2	ENST00000337018.6	6,01417842	4,08199936	3,6587909
	ENST00000597095.1	-6,6282264	-6,4622432	-5,7840618
VMP1	ENST00000586245.1	6,01169298	8,7660531	6,32069606
	ENST00000537567.1	3,90633102	4,62455256	2,87251509
	ENST00000588617.1	3,15678096	4,1853171	2,59405741
	ENST00000588131.1	-3,1409541	-3,4609012	-2,4332666
	ENST00000587945.1	-6,0807081	-3,6637851	-2,6293665
	ENST00000539763.1	-7,0529037	-7,2820567	-3,8162291

frontiers in Molecular Biosciences

REVIEW
published: 22 January 2019
doi: 10.3389/fmolb.2018.00120

Metabolic Alterations in Cardiopulmonary Vascular Dysfunction

Valérie Françoise Smolders[1,2,3,4†], *Erika Zodda*[1,5†], *Paul H. A. Quax*[3,4], *Marina Carini*[5], *Joan Albert Barberà*[2,6], *Timothy M. Thomson*[7,8], *Olga Tura-Ceide*[2,6‡] *and Marta Cascante*[1,8*‡]

[1] Department of Biochemistry and Molecular Biology and Institute of Biomedicine (IBUB), Faculty of Biology, University of Barcelona, Barcelona, Spain, [2] Department of Pulmonary Medicine, Hospital Clínic-Institut d'Investigacions Biomèdiques August Pi I Sunyer (IDIBAPS), University of Barcelona, Barcelona, Spain, [3] Einthoven Laboratory for Experimental Vascular Medicine, Leiden University Medical Center, Leiden, Netherlands, [4] Department of Vascular Surgery, Leiden University Medical Center, Leiden, Netherlands, [5] Department of Pharmaceutical Sciences, Università degli Studi di Milano, Milan, Italy, [6] Centro de Investigación Biomédica en Red (CIBER) de Enfermedades Respiratorias, Madrid, Spain, [7] Institute for Molecular Biology of Barcelona, National Research Council (IBMB-CSIC), Barcelona, Spain, [8] Centro de Investigación Biomédica en Red (CIBER) de Enfermedades Hepáticas y Digestivas, Madrid, Spain

OPEN ACCESS

Edited by:
Lorraine Brennan,
University College Dublin, Ireland

Reviewed by:
Luciana Hannibal,
University Hospital Freiburg, Germany
Lisardo Bosca,
Instituto de Investigaciones Biomédicas, Mexico

***Correspondence:**
Marta Cascante
martacascante@ub.edu

†*Co-first authors*

‡*These authors have contributed equally to this work*

Specialty section:
This article was submitted to Metabolomics, a section of the journal Frontiers in Molecular Biosciences

Received: *13 October 2017*
Accepted: *31 December 2018*
Published: *22 January 2019*

Citation:
Smolders VF, Zodda E, Quax PHA, Carini M, Barberà JA, Thomson TM, Tura-Ceide O and Cascante M (2019) Metabolic Alterations in Cardiopulmonary Vascular Dysfunction. Front. Mol. Biosci. 5:120. doi: 10.3389/fmolb.2018.00120

Cardiovascular diseases (CVD) are the leading cause of death worldwide. CVD comprise a range of diseases affecting the functionality of the heart and blood vessels, including acute myocardial infarction (AMI) and pulmonary hypertension (PH). Despite their different causative mechanisms, both AMI and PH involve narrowed or blocked blood vessels, hypoxia, and tissue infarction. The endothelium plays a pivotal role in the development of CVD. Disruption of the normal homeostasis of endothelia, alterations in the blood vessel structure, and abnormal functionality are essential factors in the onset and progression of both AMI and PH. An emerging theory proposes that pathological blood vessel responses and endothelial dysfunction develop as a result of an abnormal endothelial metabolism. It has been suggested that, in CVD, endothelial cell metabolism switches to higher glycolysis, rather than oxidative phosphorylation, as the main source of ATP, a process designated as the Warburg effect. The evidence of these alterations suggests that understanding endothelial metabolism and mitochondrial function may be central to unveiling fundamental mechanisms underlying cardiovascular pathogenesis and to identifying novel critical metabolic biomarkers and therapeutic targets. Here, we review the role of the endothelium in the regulation of vascular homeostasis and we detail key aspects of endothelial cell metabolism. We also describe recent findings concerning metabolic endothelial cell alterations in acute myocardial infarction and pulmonary hypertension, their relationship with disease pathogenesis and we discuss the future potential of pharmacological modulation of cellular metabolism in the treatment of cardiopulmonary vascular dysfunction. Although targeting endothelial cell metabolism is still in its infancy, it is a promising strategy to restore normal endothelial functions and thus forestall or revert the development of CVD in personalized multi-hit interventions at the metabolic level.

Keywords: acute myocardial infarction, pulmonary hypertension, endothelial dysfunction, cellular metabolism, glycolysis, metabolic targets, systems biology

IMPORTANCE OF CARDIOPULMONARY DISEASES

Cardiovascular diseases (CVD) are leading cause of death in the world. In 2015, The World Health Organization (WHO) estimated that 17.7 million people died from CVD, representing 31% of all global deaths (Townsend et al., 2015). Death from CVD is associated with increasing age, with 1.4 million deaths in individuals under 75 and 700,000 in individuals under 65 (Townsend et al., 2016).

CVD encompass a range of diseases affecting the functions of the heart and blood vessels, driven by diverse underlying mechanisms. In this review, we will focus on acute myocardial infarction (AMI), a type of coronary artery disease, and pulmonary arterial (PAH), and chronic thromboembolic pulmonary hypertension (CTEPH). Both types of CVD share a diseased endothelium conducive to atherosclerosis and endothelial hyperproliferation, respectively, with consequent narrowing of arteries, compromised blood flow and reduced oxygen and nutrient supply to the vascular cells, eventually leading to cardiac hypertrophy and myocardial infarction.

Atherosclerosis

Atherosclerosis, or the formation of atherosclerotic plaques, underlies one of the major causes of morbidity and mortality in developed and developing nations (Townsend et al., 2015). The World Health Organization attributes an estimated 16.7 million deaths to atherosclerotic cardiovascular disease (Leopold and Loscalzo, 2005; Hyder et al., 2007). Atherosclerotic plaque formation and rupture is one of most common pathogenic mechanisms of coronary artery disease, stroke, and peripheral artery disease (Grootaert et al., 2015). Atherogenesis is the result of complex sequences of events associated with processes such as endothelial dysfunction, neovascularization, vascular proliferation, apoptosis, matrix degradation, inflammation, oxidative stress, and thrombosis (Hansson, 2005). All these processes affect the inner lining of the artery. Eventually, arteries become thicker by virtue of an accumulation of calcium, fat deposits and inflammatory cells, leading to the formation of the atherosclerotic plaque (Liu et al., 2015). Although the pathophysiological mechanisms of atherosclerosis are yet to be fully unveiled, increasing evidences point to a critical role played by endothelial and metabolic dysregulation involving downregulation of oxidative phosphorylation and fatty acid metabolism. A complete understanding of endothelial metabolic reprogramming underlying atherosclerosis requires further investigation and could open new avenues in the prevention and treatment of this disease (Moreno-Viedma et al., 2016).

Current Therapies in Atherosclerosis and AMI

The four major risk factors for developing atherosclerosis are hypercholesterolemia, diabetes, hypertension, and cigarette smoking (Bergheanu et al., 2017). Recent studies have shown that an adequate control of lipoprotein levels reduces the risk of atherosclerosis events. As such, a modification in daily diet, an increase in physical activity and cessation of smoking constitute the cornerstones of any intervention aimed at the prevention and/or treatment of atherosclerosis. While the role of the other parameters is still not clear, TG (triglycerides), LDL-C (low density lipoprotein cholesterol), and HDL-C (high density lipoprotein cholesterol) remain very strong predictors of premature atherosclerosis (Catapano et al., 2016). Hypercholesterolemia alters vascular permeability, allowing the leaking of LDL cholesterol and deposition on the arterial walls. There, LDL is subject to modifications that include oxidation, enzymatic processing, and aggregation, that render the lipoprotein particles proinflammatory and induce an immune response. As part of this response, monocytes are recruited to the sub-endothelial space where they differentiate into macrophages. Macrophages may also derive from pluripotent cells associated with blood vessels. Regardless of their origin, macrophages in atherosclerotic lesions actively participate in lipoprotein ingestion and accumulation giving rise to foam cells filled with cholesterol-rich lipid droplets. These processes lead to vascular modifications visible as fatty streaks, intimal thickening and ruptured plaques, causing acute coronary disease (Bergheanu et al., 2017). Vulnerable plaques contain monocytes, macrophages and T cells, which accounts for their instability.

The critical role played by LDL-C in atherosclerosis has prompted the development of rational strategies to counter the pathogenic effects of hypercholesterolemia. The use of statins (inhibitors of HMG-CoA reductase, the rate-controlling enzyme of the mevalonate, and cholesterol synthesis pathways) as a pharmacological approach to lower cholesterol levels is one of the most widely used therapies in the treatment of atherosclerosis and acute coronary syndromes, as these drugs show consistent clinical event reductions with a very good safety profile (Adams et al., 2014). Other clinical studies reveal that the use of ezetimibe (an inhibitor of intestinal cholesterol absorption) considerably reduces LDL-C blood levels when combined with statins (Catapano et al., 2016). An alternative approach is the administration of fibrates, a particular class of agonists of the peroxisome proliferator-activated receptor α (PPAR-α) a regulator of lipoprotein metabolism, showing a good effect in lowering TG levels as mono-therapy, even though the results are not as promising as for the statins (Adams et al., 2014). Recently, a large multi-scale and multiethnic study was undertaken to better understand the role of genetic and environmental factors in CVD and to identify genetic variants associated to blood lipids levels (Klarin et al., 2018). By using a genome wide association study (GWAS) on Million Veterans Program (MVP), this work depicted some novel lipid associated coding variants with CVD risk or incidence. Individuals with mutations in ANGPTL4 (Angiopoietin-like4) presented a lower risk to develop diabetes mellitus (type2), those with a loss of function in PCSK9 (Proprotein convertase subtilisin/kexin type 9) showed a reduced risk of abdominal aortic aneurysm, and those treated with inhibitors of PDE3B (Phosphodiesterase 3B), presented reduced levels of triglycerides in blood (Cohen et al., 2006; Willer et al., 2013; Ahmad et al., 2016; Dewey et al., 2017; Graham et al., 2017). These data highlight the complexity in humans to control blood lipid composition and the potential of a genetic approach to develop

novel therapeutic agents for the prevention of cardiovascular disease.

When the combination of healthier diet, lifestyle and pharmacological treatments fail to improve the pathological and clinical conditions in atherosclerotic patients with an associated coronary disease, surgical intervention is considered the best option. Coronary artery thrombosis with complete occlusion typically leads to ST-segment elevation myocardial infarction (STEMI). Partial occlusion, or occlusion in the presence of collateral circulation, results in non-STEMI or unstable angina, an acute coronary syndrome without ST-segment elevation. Once a definitive or likely diagnosis of an acute coronary syndrome without ST-segment elevation has been made, the patient is triaged to either an invasive strategy or an ischemia-guided strategy. An invasive strategy leads to improved outcomes and is favored for the majority of patients (Anderson and Morrow, 2017).

In patients presenting with an unstable condition or with STEMI, urgent Percutaneous Coronary Intervention (PCI) is performed. An ischemia-guided strategy is chosen for patients at low risk of recurrent ischemia, especially for women. Although PCI is currently the intervention of choice for most of these patients, individual coronary anatomy and clinical features may dictate the use of a different approach, such as coronary artery bypass grafting (CABG), a surgery that reinstates cardiac blood flow (Parsa et al., 2011). In some cases, current guidelines also recommend an antiplatelet therapy combined with non-vitamin K antagonist oral anticoagulant (NOACs) therapy (Husted et al., 2014; Steffel et al., 2018). Indeed, the rates of major complications of acute myocardial infarction have declined dramatically with early reperfusion (PCI) associated with antiplatelet therapy (French et al., 2010). Nevertheless, complications are still a leading cause of death and deserve careful consideration. Several new therapeutic approaches, such as reducing inflammation, mitigating reperfusion injury or inducing myocardial regeneration, are under active investigation although, except for angiotensin converting enzyme (ACE) inhibition, have so far not proved beneficial in the acute care setting. Acute myocardial infarction continues to have a major impact on global health and its management remains a crucial challenge for scientific advancement in medicine (Bhatt et al., 2013).

Pulmonary Hypertension

Pulmonary hypertension (PH) is a hemodynamic disease state involving multiple clinical conditions including pulmonary arterial hypertension (PAH) and chronic thromboembolic pulmonary hypertension (CTEPH) (Galiè et al., 2016). They are defined by hemodynamic parameters characterized by a mean pulmonary artery pressure $\geq$ 25 mmHg at rest, measured during right heart catheterization (Galiè et al., 2016). The pathophysiological consequence is a gradual obstruction of the arterial lumen leading to the development of increased resistance of the pulmonary vasculature and, ultimately, right ventricular failure (Galiè et al., 2009; Lang, 2015). PAH is characterized by disease-specific lesions mainly involving the smaller pulmonary arteries ($<$500 μm in diameter). These lesions feature thickening of both the external and medial layers and changes in the endothelial monolayer accompanied by an inflammatory infiltration and formation of complex thrombotic lesions (Galiè et al., 2009). Unlike PAH, where obstruction caused by remodeling likely occurs in the more distal pulmonary arteries, CTEPH is largely associated with prominent obstructions in the main pulmonary arteries caused by unresolved thrombi affecting the medial and intimal layers of the arteries (Humbert, 2010; Lang, 2015). Subsequently, distal pulmonary arteriopathy and microvascular disease can be triggered, indistinguishable from classic PAH (Lang and Madani, 2014; Lang, 2015). PAH and CTEPH are both rare and progressive vascular diseases with poor prognosis if early diagnosis is not performed. Diagnosis is complicated by the lack of biomarkers and patient-specific symptoms (Humbert et al., 2014). Whereas, PAH has an estimated prevalence of 15 to 50 per million population (Humbert et al., 2014), the prevalence of CTEPH is not easy to estimate, due to a long asymptomatic period between the initiating event (pulmonary embolism; PE) and the overt symptomatic disease. With this caution, the prevalence of CTEPH is estimated at between 0.1 and 9.1% after diagnosis of PE (Humbert, 2010; Lang and Madani, 2014). Current therapies for PAH mainly focus on targeting endothelial dysfunction, whereas pulmonary endarterectomy (PEA) is the treatment of choice for CTEPH, with a possible curative outcome (Nogueira-Ferreira et al., 2014; Jenkins, 2015). To date, additional research is needed to learn more about the onset and development of PH. This review will touch the recent findings concerning the endothelium dysfunction and metabolic alterations in PAH and CTEPH, its likely relationship with the disease pathogenesis, and whether pharmacological modifications on cellular metabolism might be a potential future treatment for PH.

Current Therapies in PH

PAH is the most studied condition of all PH clinical groups. Three key vasomotor pathways are the targets of the main approved PAH therapies: (1) prostacyclin, (2) endothelin-1, and (3) nitric oxide-cyclic guanosine monophosphate (cGMP). Interventions on all three pathways aim at restoring the imbalance of endothelial vasodilator and vasoconstrictors mediators. However, because they have little impact on vascular remodeling and coagulation homeostasis, they are not curative for PAH (Humbert et al., 2014).

No targeted therapy is currently available for CTEPH patients and, as mentioned above, pulmonary endarterectomy (PEA) is the treatment of choice in operable patients. Features for determining patient operability are the accessibility of the thromboembolic material and patient comorbidities influencing the peri- and post-operative risk. Effective PEA results in improvement of clinical symptoms, normalization of hemodynamics, and increased survival (Jenkins, 2015). For patients who suffer from inoperable CTEPH or persistent/recurrent CTEPH, Riociguat was recently approved as the only pharmaceutical targeted treatment of CTEPH based on the findings from the CHEST study (Hoeper, 2015) and the PATENT-1 study (Galiè and Ghofrani, 2013). Riociguat is a

member of the family of soluble guanylate cyclase stimulators (sGC). It has a two-faceted mode of action, on the one hand by increasing the sensitivity of sGC to endogenous NO, and on the other hand by stimulating sGC activity independently of NO, resulting in restoration of the NO-sGC-cGMP (cyclic guanosine monophosphate) pathway, accompanied with vasodilation and anti-fibrotic, anti-proliferative and anti-inflammatory effects (Hoeper, 2015). The drug significantly improves the patients' exercise capacity and pulmonary vascular resistance and possibly constitutes a first targeted therapy for CTEPH (Ghofrani et al., 2013).

The limited benefits of existing therapies for PAH and the high risk associated with PEA for CTEPH patients have fostered recent studies that explore new therapeutic avenues. An emerging topic suggests the occurrence of potentially actionable metabolic abnormalities in pulmonary hypertension. We will now focus on recent observations on the role of EC dysfunction and metabolism in the pathophysiology of PAH and CTEPH and the therapeutic opportunities they may provide.

ENDOTHELIAL CELLULAR ENERGY METABOLISM

The endothelium is a dynamic organ consisting of a single layer of endothelial cells (ECs) lining the entire vascular system. Independently of their anatomic location (artery, arteriole, capillary, venule, vein) all endothelial share the common function of maintenance of vessel homeostasis (Pober et al., 2009; Sandoo et al., 2010). The control of vessel functions involves regulation of the blood flow, vascular tone, physical barrier, blood coagulation, and the inflammatory response. A balanced production of various hormones, neurotransmitters, and vasoactive factors is crucial for maintaining a homeostatic vessel function (Sandoo et al., 2010). An important vasoactive factor is eNOS-derived nitric oxide (NO), that promotes vasodilatation and inhibits important events that contribute to the development of vascular remodeling diseases, such as platelet aggregation, adhesion of leukocytes, and oxidative stress (Förstermann and Sessa, 2012). NO produced by the endothelium also plays an important role in mitochondrial respiration to maintain the oxygen gradient in oxygen limiting situations (Dromparis and Michelakis, 2013). When the NO precursor arginine and the eNOS cofactor tetrahydrobiopterin (BH_4) are not available, eNOS fails to produce NO and may promote the formation of reactive oxygen species (ROS), causing endothelial dysfunction and leading to atherosclerosis and PH pathogenesis (Förstermann and Sessa, 2012).

The importance of maintaining physiological and homeostatic EC functions is underlined by the development of major diseases like cardiovascular disease, diabetes, and cancer, consequent to endothelial dysfunction (Goveia et al., 2014). The endothelium can be disrupted by EC damage or apoptosis which leads to a re-endothelialization response and in some cases to the selection of ECs with an altered phenotype (Pober et al., 2009; Nogueira-Ferreira et al., 2014). Environmental stresses, such as oxidative stress and metabolic disturbances, are important sources of endothelial dysfunction, injury, and death (Pober et al., 2009).

Glycolysis

When exposed to hypoxic conditions, mitochondrial alterations or growth factors, ECs can rapidly shift from a quiescent cellular mode to an angiogenic state accompanied with changes in their cell metabolism. Under basal conditions, ECs rely mostly (>80%) on glycolysis for generating their cellular energy and thus leaving the circulating oxygen available for underlying oxygen-requiring tissues (De Bock et al., 2013b; Dromparis and Michelakis, 2013; Goveia et al., 2014). In pathological conditions with sustained suppressed oxidative phosphorylation (OXPHOS), glycolytic flux is increased regardless of the oxygen supply as long as glucose is available (Warburg effect) promoting the development of highly proliferative vascular disorders (Parra-bonilla et al., 2010; Dromparis and Michelakis, 2013). This predominantly reliance on glycolysis over the use of more efficient mitochondrial oxidation is supported by the presence of fewer mitochondria when compared to cell types relying on mitochondrial respiration. Regardless the presence of sufficient oxygen to maintain mitochondrial respiration, glycolytic flux quickly converts pyruvate to lactate, followed by an increase in glucose uptake (Parra-bonilla et al., 2010). Sustained upregulation of glycolysis and suppression of OXPHOS is often accompanied with a normoxic activation of HIF1α, leading to activation/upregulation of several glycolytic enzymes and further suppressing mitochondrial respiration (Dromparis and Michelakis, 2013).

The glycolytic enzyme phosphofructokinase-2/fructose-2,6-biphosphatase 3 (PFKFB3) is important for maintaining glycolysis and it has been shown that PFKFB3 inactivation reduces EC proliferation (De Bock et al., 2013b). PFKFB3 catalyzes the synthesis of fructose-2,6-biphosphate (Fru-2,6-P_2), an allosteric activator of phosphofructokinase 1 (PFK-1) and a potent stimulator of glycolysis. Partial reduction of the glycolytic flux by PFKFB3 inhibition was shown to be sufficient to impair EC proliferation without induction of cell death as caused by 2DG (2-deoxy-D-glucose) (Schoors et al., 2014). Another important glycolytic enzyme is the mitochondrial "gate-keeper" enzyme pyruvate dehydrogenase (PDH) that acts as a promoter of the entry of pyruvate in mitochondria (Cottrill and Chan, 2013). PDH can be phosphorylated and inhibited through the activity of pyruvate dehydrogenase kinases (PDKs), resulting in a reduced mitochondrial contribution to energy production and concomitant promotion of aerobic glycolysis (Ryan and Archer, 2015).

PDKs are induced by HIF1α and PDHs are additionally inhibited by altered mitochondrial Ca^{2+} signaling (Dromparis and Michelakis, 2013). Upon PDH inhibition, pyruvate, rather than entering the mitochondrial respiratory chain, is converted to lactate by the enzyme lactate dehydrogenase (LDH) allowing the transformation of NADH to NAD^+, which is crucial for maintaining further glycolysis. Lactate is released to the extracellular microenvironment via monocarboxylate transporter 4 (MCT4). It can also enter the cells through monocarboxylate transporter 1 (MCT1) and used to feed

the TCA cycle under low oxygen conditions, promoting the so-called "reverse Warburg effect," a process that illustrates the symbiotic relationship between lactate-producing and lactate-consuming normal and pathological cells (Semenza, 2008), an important adaptive mechanism to continuously changing micro-environmental conditions (Semenza, 2008; Draoui and Feron, 2011). Moreover, the increase in lactate production generates an extracellular acidification of the microenvironment which promotes the activity of certain metalloproteases that disrupt the extracellular matrix, which also leads to an infiltration of the vascular wall with inflammatory cells and other cell types (Bonuccelli et al., 2010).

Glycolysis is also connected to the pentose phosphate pathway (PPP), a metabolic pathway that generates NADPH and ribose-5-phosphate, essential for the biosynthesis of lipids and nucleotides. PPP plays a pivotal role in the production of NADPH moieties which provide the reducing equivalents necessary for the synthesis of fatty acids and for the scavenging of ROS to promote cell survival (Patra and Hay, 2014). The altered metabolic profile of mitochondrial suppression along with increased glycolytic rates causing a dysfunctional vasculature is similar to that of other rapidly proliferating healthy and malignant cell types, in which a shift occurs from mitochondrial respiration to lactate-producing aerobic glycolysis in order to sustain their rapid growth and to block apoptosis (Vander Heiden et al., 2009; Parra-bonilla et al., 2010; De Bock et al., 2013a).

Mitochondrial Respiration

Mitochondria are considered the quintessential cellular engine since its primary function is energy production in the form of adenosine triphosphate (ATP). ATP is essential to sustain cellular bioenergetic demands, glucose being the principal carbon substrate needed to generate ATP. OXPHOS is the mitochondrial metabolic pathway that enables cells to synthesize ATP from oxidation of nutrients. For each glucose molecule that enters the glycolytic pathway, 2 pyruvate molecules are produced with a net energy of 2 ATP molecules. Subsequent pyruvate uptake into mitochondria results in 36 ATP molecules with minimal production of lactate under physiological conditions (Vander Heiden et al., 2009; Parra-bonilla et al., 2010). This process is oxygen-dependent and, considering its high efficiency, it is the predominant source of energy in mammalian cells(Parra-bonilla et al., 2010). Individual cell growth is controlled by environmental nutrient availability; therefore, cells only take up nutrients for cell division when stimulated by growth factors to avoid abnormal proliferation. In addition to ATP, active cell division requires nucleotides, amino acids, and lipids. To maintain cell growth and concomitant increase in biomass, part of the glucose must be redirected to the generation of critical macromolecular precursors such as acetyl-CoA, glycolytic intermediates, and ribose for the biosynthesis of, respectively, fatty acids, non-essential amino acids, and nucleotides (Vander Heiden et al., 2009). In order to promote this flow of carbon substrates toward biomass accumulation, rapidly growing cells are endowed with mechanisms that favor glycolysis over mitochondrial oxidation.

Although the major function of mitochondria is ATP production, these organelles are also important regulators of cell survival, ion homeostasis (H^+, Ca^{2+}) and cellular redox status (Collins et al., 2012). Tight regulation of the mitochondrial ion status is of great importance in tissues with limited oxygen consumption, like the vasculature and the lung, which facilitate the diffusion of oxygen to more oxygen-requiring tissues. Disturbances in mitochondrial ion status have direct and indirect consequences on cell function, growth, and survival (Dromparis and Michelakis, 2013). Altered mitochondrial morphology and function prompted by factors such as NO status have been associated with vascular endothelial dysfunction and to diverse pathological conditions, including cardiovascular disorders, muscular degeneration, and cancer (Collins et al., 2012; Dromparis and Michelakis, 2013). Mitochondrial metabolism contributes actively to the production of reactive oxygen species (ROS). Mitochondria regulate redox signaling to and from mitochondria and initiate cellular apoptosis (Rizzuto et al., 2012). Oxidative stress is considered a major contributor to the destruction of well-balanced homeostatic mechanisms, causing cell injury either through direct oxidation of cellular proteins, lipids, and DNA or via cell death signaling pathways (Leopold and Loscalzo, 2005; Sinha et al., 2014).

The sensitivity of cells to glycolytic and OXPHOS inhibitors (such as2DG, and Oligomycin, respectively) can be used to help unveil the cell dependency on a specific energy-generating pathway (Suganuma et al., 2010). Such studies have shown that, in spite of the importance of the glycolytic pathway, especially under hypoxic conditions, the majority of cells use a combination of OXPHOS and glycolysis as a strategy for energy production, pointing out the importance of metabolic plasticity for cell survival under shifting environments and the complexity of metabolic adaptations in disease (Moreno-Sánchez et al., 2007).

ROS-Oxidative Stress

During OXPHOS, electrons from NADH and $FADH_2$ molecules (electron donors) are transferred to electron acceptors, such as oxygen. These redox reactions are carried out by protein complexes located in the mitochondrial inner membrane, and release energy which is used to form ATP (Vega-Naredo et al., 2014). Small amounts of these electrons form prematurely mitochondria-derived reactive oxygen species (mROS), such as superoxide (O_2^-). ROS are oxygen-containing chemically reactive species which play important signaling roles to sustain fundamental cellular functions under various physiological conditions (Förstermann, 2008). High levels of oxygen and increased mitochondrial activity leads to excessive ROS production overcoming the buffer capacity of usable antioxidant systems results in oxidative stress causing increased cell death and endothelial dysfunction (Leopold and Loscalzo, 2005; Pangare and Makino, 2012; Dromparis and Michelakis, 2013; Li et al., 2014). Mitochondria-based manganese superoxide dismutase (MnSOD, or SOD2) has an immediately anti-oxidative effect through the conversion of superoxide to the more stable and diffusible H_2O_2. After leaving mitochondria, physiological levels of hydrogen peroxide (H_2O_2) function as an important signaling system, acting on several redox sensitive targets in the

cytoplasm (HIF1α) and the cell membrane (K^+ channels) and also with some proliferation-related enzymes (Fukai and Ushio-Fukai, 2011; Dromparis and Michelakis, 2013). Several other enzyme systems can produce ROS in the vascular wall, notably NADPH oxidase, xanthine oxidase, and eNOS, a dysfunctional endothelial NO synthase in which oxygen reduction is uncoupled from NO synthesis (Brandes and Kreuzer, 2005; Förstermann, 2008; Li et al., 2014; Xia et al., 2017). These oxidases are multisubunit enzyme complexes that produce superoxide from molecular oxygen and NADPH as electron donor (Drummond et al., 2011).

Imbalances in the cellular oxidative status play significant roles in the pathophysiology of vascular diseases (Santos et al., 2011). Some cells might resort to a metabolic switch to glycolysis as a mechanism to reduce production of ROS and thus to protect themselves from mitochondrial-mediated apoptosis (Ryan and Archer, 2015). The crucial role of oxidative stress in CVDs makes it an attractive target for therapy. However, recent studies in patients with cardiovascular symptoms showed that the use of supplementary antioxidants such as vitamins E and C had little therapeutic effect. This was mainly due to the limited specificity for ROS producing factors and to the requirement of high antioxidant doses which could worsen vascular function (Münzel et al., 2010, 2017). Whilst, novel therapeutic strategies propose to target more precise ROS producing sites such as the mitochondria, it is not an easy task as those are important dose-dependent signaling molecules which could have a detrimental effect on key body functions. Therefore, more detailed studies are needed to elucidate the potential therapeutic effects of antioxidant treatments(Münzel et al., 2017).

THE IMPORTANCE OF THE ENDOTHELIUM IN DISEASE

Endothelial Dysfunction in Acute Myocardial Infarction

Acute myocardial infarction (AMI) is the development of myocardial necrosis caused by an unstable ischemic state. The disorder is diagnosed and assessed based on clinical evaluation, electrocardiogram (ECG), biochemical testing, invasive and non-invasive imaging, and pathological evaluation. The usual triggering event of acute myocardial infarction is the rupture or erosion of a vulnerable, lipid-laden, atherosclerotic coronary plaque. This event results in the exposure of circulating blood to highly thrombogenic core and matrix materials in the plaque (Badimon et al., 2012). In response to various stimuli, the normal endothelium endures phenotypic changes and variations, collectively known as endothelial dysfunction, characterized by a loss of the majority of the homeostatic mechanisms present in normal healthy endothelial cells. Usually, this dysfunction is associated with upregulation of adhesion molecules, enhanced production of ROS, synthesis of pro-inflammatory factors and loss of vascular tone (**Figure 1**) (Sitia et al., 2010). Recent studies suggest that this dysfunction contributes to the progression of the atherosclerotic plaque (Zardi and Afeltra, 2010). The pioneer role played by endothelial dysfunction in vascular pathology is supported by observations that individuals without any clinical sign of atherosclerosis but with high cardiovascular risk already present an endothelial dysfunction indicated by a diminished response to some vasodilators, such as acetylcholine (Zardi and Afeltra, 2010). These findings

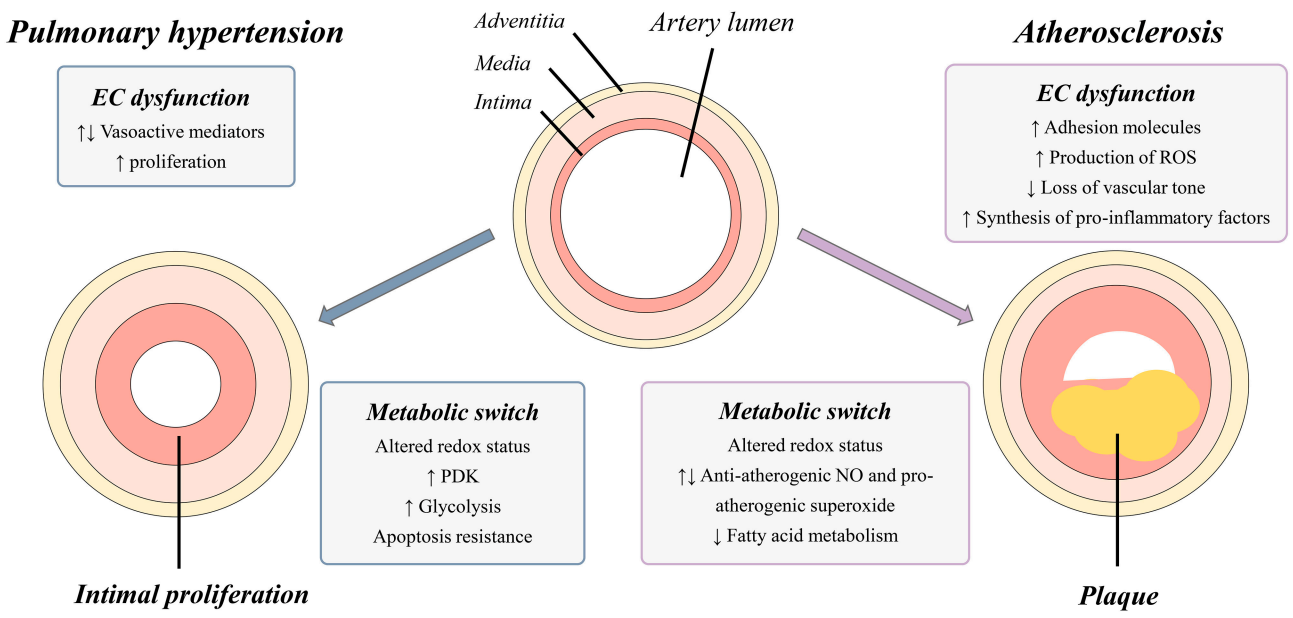

FIGURE 1 | Graphical representation of vascular changes occurring in PH and atherosclerosis. Narrowing of the artery lumen is caused by intimal proliferation (PH) and by plaque formation (atherosclerosis) and is a result of disease specific EC dysfunction and cellular metabolic switches. EC, endothelial cell; PDK, pyruvate dehydrogenase kinases; ROS, reactive oxygen species; NO, nitric oxide; PH, in pulmonary hypertension.

suggest that endothelial dysfunction may precede and constitute a link between different vascular diseases and represents a good predictor of future cardiovascular events, including atherosclerotic diseases and AMI (Sitia et al., 2010). Endothelial dysfunction is considered a systemic vascular process that not only leads to plaque formation, but also determines the clinical course of atherosclerosis progression and associated coronary syndromes. Because several metabolic pathway abnormalities, such as the deregulation of the nitric oxide production and the excessive generation of ROS (**Table 1**), are associated with atherosclerosis, the identification of key metabolic mechanisms underlying such alterations should provide fresh opportunities for the development of new strategies for the treatment of endothelial cell dysfunction in atherosclerosis and related vascular pathologies (Bierhansl et al., 2017).

Metabolic Alterations and Requirements in Acute Myocardial Infarction

Atherosclerosis is characterized by the presence of an uncoupled and reduced eNOS, causing an imbalance between the production of NO, an anti-atherogenic molecule, and superoxide, a pro-atherogenic factor, thereby losing the atheroprotective function of eNOS (Eelen et al., 2015). As such, two general processes are largely responsible for the angiogenic growth observed in early atherogenesis: inflammation and oxidative stress. These metabolic alterations also affect, to a variable degree, vascular remodeling and coagulation homeostasis (Humbert et al., 2014). Beyond eNOS, a critical role in atherogenesis is also played by NADPH oxidase (NOX) enzymes, a large family of enzymes that are pivotal in the generation of ROS in the vasculature. NOX-4 is universally expressed in vascular smooth muscle cells (VSMCs), the primary components of the vascular wall and crucial determinants of vascular homeostasis and disease (Lu et al., 2013). Its expression and activation during the angiogenic process promotes a chain of events leading to vascular inflammation, cellular dysfunction, and atherosclerosis.

Additional metabolic mechanisms may contribute to the generation of a pro-inflammatory environment leading to atherogenesis. For example, the high glycolytic mode encountered in endothelial dysfunction implies a relative reduction in available ATP as compared to cells with OXPHOS-predominant metabolism. This results in diminished intracellular adenosine levels which drives hydrolysis of S-adenosylhomocysteine (SAH) to adenosine and L-homocysteine (Hcy). Reduced SAH levels foster histone H3 lysine 4 hypomethylation and overexpression of a pro-inflammatory gene repertoire (Xu et al., 2017). A recent study (Ward-Caviness et al., 2017) identified three metabolic biomarkers, arginine and two lysophosphatidylcholines (LPC 17:0 and LPC 18:2) associated with incident myocardial infarction (MI). This study also focus on the association between these metabolites and the high-sensitivity C reactive protein (hsCRP), which is a measure for inflammation (Kaptoge et al., 2012). The three biomarkers correlated with each other and with the hsCRP levels, suggesting that inflammation can represent a pathway through which these biomarkers are associated with MI (Cheng et al., 2012). As a consequence of these processes, increased rates of apoptosis are evident in more advanced atherosclerotic plaques. This is a key point in the progression of atherosclerosis and consists of a programmed cell death, morphologically expressed as cellular contraction, condensation of chromatin, and disruption of the cellular membrane. All cells existing in the atherosclerotic plaque, including lymphocytes, endothelial cells, smooth muscle cells, and macrophages, can undergo cellular apoptosis (Schrijvers et al., 2005).

TABLE 1 | Summary main metabolic perturbations in AMI and PH.

	AMI	Pulmonary Hypertension
Nitric Oxide	↓ NO[a,b]	↓ NO[d]
Proliferation	↓ proliferation[c]	↑ proliferation[e]
Metabolism	↓Glycolysis[a]	↓ OXPHOS ↑ Glycolysis[f]
Antioxidants and ROS	↑ mROS[a,b]	↓MnROS (↑O_2^-/↓H_2O_2)[g]

[a]*Eelen et al., 2015;* [b]*Förstermann and Sessa, 2012;* [c]*Lu et al., 2013;* [d]*Budhiraja et al., 2004;* [e]*Humbert et al., 2004; Masri et al., 2007;* [f]*Xu et al., 2007; Xu and Erzurum, 2011; Lewis, 2014; Bujak et al., 2016;* [g]*Archer et al., 2008.*

Future Treatment Options in AMI

Currently, the use of beta blockers and angiotensin-converting enzyme (ACE)-inhibitors are under study for the treatment of AMI, as well as improvements in antithrombotic therapies. Despite the advances of the last decades, a lot is unknown about the biological processes involved in cardiac development and repair for this reason there is a strong need to find new successful therapeutic targets to struggle this disease (Ibanez et al., 2018).

Metabolomic approaches can identify potential biomarkers with predictive value for CVD (Hoefer et al., 2015) and correlate metabolic profiles with risk of death or incident MI (Shah et al., 2010). Several studies focus on the limitations of current vascular biomarkers, like hsCRPs (high sensitive C reactive proteins) and encourage the discovery and validation of novel biomarkers using emerging omics technologies. HDL cholesterol is considered strictly linked to cardiovascular diseases: low HDL cholesterol is associated to a very high cardiovascular risk while high HDL cholesterol seems to be linked to cardiovascular protection (Rohatgi et al., 2014). It has been described, that the key role of HDL is to promote the efflux of the cholesterol and to invert its transport from the periphery to the liver, which seems to be correlated to a low incidence of cardiovascular events, suggesting the potential use of HDL as a new biomarker for coronary heart disease (Hoefer et al., 2015).

The detection of plasma-derived markers which include microparticles (MPs), microvesicles and exosomes in human plasma, has triggered increasing interest for their potential as biomarkers. In particular, levels of MPs expressing CD31 or CD144 seem inversely correlated to the endothelium associated vasodilation highlighting that MPs' levels might be good indicators of vascular lesions and acute endothelial dysfunction (Lacroix et al., 2010). Moreover, the complex composition of these microparticles which comprise proteins, lipids, and nucleic acids represent an interesting onset for omics based analysis (Kanhai et al., 2013). Recent studies have also unveiled that

micro-RNAs (miRNAs) not only present relevant intracellular functions, but also show potential value as cardiovascular disease biomarkers. miRNAs also circulate within microvesiscles and may contribute to forecast heart failure, early atherosclerosis and plaque vulnerability by targeting vascular and cardiac cells (Matsumoto et al., 2013).

Metabolomic studies using general population-based cohorts have recently been performed using LC-MS/MS-based lipidomics and NMR-based approaches to identify species associated with incident CVD with a potential link to systemic inflammation and in particular, pro-inflammatory lipid metabolites have acquired great interest in the cardiovascular disease frame (Hoefer et al., 2015). Molecular lipid profiling by mass spectrometry and nuclear magnetic resonance spectroscopy, as proteomic identification and quantification of small metabolites, can improve the individual cardiovascular risk prediction (Stegemann et al., 2014).

The identification of potential metabolic targets for novel therapeutic approaches for acute myocardial infarction is therefore an interesting approach that should be investigated in earnest in the near future.

Endothelial Dysfunction in Pulmonary Hypertension

The pulmonary vascular barrier consists of three cellular layers: an external layer, the adventitia containing fibroblasts, a medial layer mainly consisting of smooth muscle cells (SMC) lined by an elastic membrane and an internal intima composed of a single layer of endothelial cells in direct contact with the blood circulation (Jeffery and Morrell, 2002). Upon abnormal activation, the normally quiescent endothelium loses its homeostatic function, leading to a disorganization of the three-layer structure of the vascular wall as a key element in the development of pathological lesions (Budhiraja et al., 2004; Xu and Erzurum, 2011). Several endothelium activation stimuli such as ROS, shear stress and inflammation are known to stimulate the endothelium, causing changes in its proliferation status and production of vasoactive mediators and growth factors. In PH, it has been shown that there is an imbalance between vasodilators, such as nitric oxide (NO) and prostacyclin (PG), and vasoconstrictors, such as endothelin-1 (ET-1) and thromboxane, resulting in the disruption of basal pulmonary vascular tone, vascular injury repair and growth (Budhiraja et al., 2004). In addition to changes in vasoactive mediators, it is hypothesized that initial endothelial damage induces a widespread endothelial cell death cascade leading to an apoptosis-resistant population, from which rapidly proliferating cells regenerate the vascular lining (**Figure 1**) (Masri et al., 2007). Additionally, endothelium injury also causes exposure of the medial and adventitial layer to growth factors, inducing the proliferation of fibroblasts and smooth muscle cells (Budhiraja et al., 2004). Furthermore, disease-related alterations in the function and expression of specific ion channels in pulmonary artery smooth muscle cells (PASMC) and endothelial cells contribute to increased vascular tone, proliferation., and decreased apoptosis in PAH. Well-studied as important contributors to continuous vasoconstriction and remodeling of pulmonary arteries are dysfunctional K^+ channels and altered levels of cytosolic Ca^{2+}(Makino et al., 2017). Regulatory dysfunctions in fibroblasts are an additional factor leading to impaired vascular function and remodeling. Studies in PAH have shown a rise in the deposition of extracellular matrix (ECM) proteins in the adventitia facilitating the migration of fibroblasts to the medial and endothelium layers (Stenmark et al., 2006). The overall result is the emergence of an aberrant apoptosis-resistant, highly proliferative pulmonary vascular endothelium together with disruptions in both fibroblasts and PASMC layers.

Previous research has suggested that PAH ECs derived from obstructive plexiform lesions are likely associated with alterations of cellular functions involved in apoptotic and proliferative processes (Humbert et al., 2004). PAH ECs display faster growth rates as compared to non-diseased pulmonary ECs, as shown by enhanced cellular survival signals and increased cell division. This increased ability to maintain cell viability is accompanied with an upregulation of pro-survival factors and continuous activation of signal transducers and activators of transcription (STATs), such as STAT3, with a known involvement in cell growth regulation (Masri et al., 2007).

In CTEPH, several studies have highlighted the existence of an altered cellular phenotype in cells derived from large arteries. Pulmonary arterial ECs (PAECs) derived from CTEPH patients showed enhanced mitogenic activity *in vitro* (Quarck et al., 2012). This was concomitant with the presence of small-vessel abnormalities such as thickening of the medial layer and increased proliferative characteristics of cells lining the internal intimal layer, and formation of obstructive plexiform lesions comparable with features seen in PAH, which suggests the possibility that both diseases might develop from a common endothelial dysfunction that contribute to vascular remodeling (Piazza and Goldhaber, 2011). A deeper understanding of the cellular processes behind these endothelial abnormalities might therefore shed light on the precise mechanisms that underlie the pathological changes occurring in the vascular wall of PAH and CTEPH.

Metabolic Alterations and Requirements in Pulmonary Hypertension

To better understand pulmonary vascular remodeling processes, we will take a closer look at the metabolic alterations and requirements of ECs in PH. As described above, endothelial cells are highly dynamic and rely mostly on glycolysis for their energy production and, when stimulated, they further boost the glycolytic rate to support their higher growth rates.

Both *in vitro* and *in vivo* studies have described an increase in glycolytic rate and lactate release in PAECs derived from PAH patients, as compared to non-diseased PAECs (Xu et al., 2007; Xu and Erzurum, 2011). These findings suggest that glucose metabolism is the primary energy source in PAEC. Additionally, PAH PAEC showed decreased oxygen consumption and maintained similar ATP levels under normoxia and hypoxia, compared to control PAECs (Xu et al., 2007). Despite a

significant scientific effort in the past years, we are still not able to fully understand regulatory mechanisms that promote the switch from oxidative glucose metabolism to glycolysis. A possible explanation is an impaired mitochondrial function, including pathological activation of pyruvate dehydrogenase kinase (PDK) activity and MnSOD deficiency (Archer et al., 2008; Hernandez-saavedra et al., 2017). It has been shown that pyruvate dehydrogenase kinases (PDK) are highly expressed in PAH, which may imply a stronger inhibition of PDH and thus a proneness toward aerobic glycolysis (Cottrill and Chan, 2013; Ryan and Archer, 2015). Reduced levels of MnSOD in PAH disturb the cellular redox status leading to an accumulation of superoxide anion O_2^- and a reduced production of signaling moleculeH_2O_2 followed by normoxic activation of the redox-sensitive HIF1α. This pseudohypoxic state, decreased MnSOD and increased PDK in the presence of normal PO_2, further favors glycolysis and causes a cascade of downstream pathways promoting proliferation and inhibiting apoptosis trough increased cytosolic Ca^{2+} and K^+ concentrations, respectively, both induced by a downregulation of $K_{v1,5}$ channel (Archer et al., 2008).

Recent metabolic studies focus on the less invasive technique, metabolomics of biofluids in PH. Despite contrasting reports using this approach regarding PAH (Zhao et al., 2014; Bujak et al., 2016), it is a promising technique in search of disease specific biomarkers. Metabolic profiling in PH has complement findings from *in vitro* and *in vivo* studies regarding increased glycolysis and has additionally found an increase in PPP, decrease in fatty acid oxidation (FAO) and impaired TCA (Lewis, 2014; Bujak et al., 2016). All these observations point to similarities in metabolic profiles between diseased endothelia in PAH and rapidly growing cells, thus suggesting the existence of a Warburg effect in PAH PAECs together with the presence of mitochondrial abnormalities as summarized in **Table 1**. It will be interesting to determine whether CTEPH ECs also present similar pathophysiological metabolic processes.

Future Treatment Options in PAH and CTEPH

The above described metabolic transformations in PAH ECs (enhanced glycolytic flows and diminished oxidative metabolism) bear similarities to the metabolic profiles of hyperproliferative ECs. On that basis, pharmacological blockade of PFKFB3, which restraints angiogenesis (Schoors et al., 2014), offers a window of opportunity to rein in the hyperproliferative state in PAH ECs by reducing their glycolytic rate (Goveia et al., 2014). *In vitro* studies indicated that a dose-dependent inhibition of PFKFB3 by small compounds such as 3PO (3-(3-pyridinyl)-1-(4-pyridinyl)-2-propen-1-one) successfully reduced glycolysis partially (35–40%) although sufficiently to impair EC proliferation (Schoors et al., 2014). The enhanced expression of the PDK enzymes in PAH and CTEPH ECs offers an additionally opportunity for new targeted therapies. Preclinical intervention models of pulmonary hypertension have been studied to evaluate the efficacy of PDK inhibition in limiting and/or overturning pulmonary vascular changes (Harvey and Chan, 2017). The small molecule dichloroacetate (DCA), a pyruvate analog, has a relatively high specific binding to PDK (McMurtry, 2004). In rat models of monocrotaline-induced PAH (MCT-PAH), DCA was shown to prevent and reverse pulmonary vascular remodeling. Further, DCA induced apoptosis in the MCT-PAH pulmonary arteries (PAs) and suppressed cell growth rates measured by bromodeoxyuridine (BrdU) uptake in the medial layer of remodeled MCT-PAH PAs with little impact on normal pulmonary vascular cells in rats and humans, making it a promising small molecule for targeted restoration of normal metabolic dysfunctions in PAH ECs (Stacpoole et al., 2003; McMurtry, 2004; Ryan and Archer, 2015). A recently published work demonstrated in a first-in-human clinical trial that PDK inhibition has a positive effect on the hemodynamics of PAH patients, further supporting the potential of DCA as a pharmacological agent in this disease (Michelakis et al., 2017). Growing evidence of the existence of metabolic remodeling beyond the glycolytic pathway leads to a growing list of possible metabolic targets. One of these targets is the methylation of SOD2 (MnSOD) which suppresses expression of this redox enzyme. 5-AZA (5-aza-2′-deoxycytidine) inhibits methylation of SOD2 followed by restoration of the mitochondrial respiration (Harvey and Chan, 2017). Nevertheless, future metabolic studies in larger PAH patients groups and CTEPH patients will be as necessary as additional steps in unraveling further pathophysiological mechanisms. However, one needs to bear in mind the challenges of metabolic therapies linked to interpatient variations and target selectivity but also due to the complexity of cell metabolism itself. Together with the search for new pharmacological interventions, a broad metabolomic screening is indispensable in the search for biomarkers in PAH and CTEPH that may help early diagnosis and uncover metabolic-mediated remodeling in PH.

CONCLUSIONS AND PROSPECTS

There is increasing evidence that endothelial dysfunction in cardiopulmonary vascular disorders is associated with disease-specific metabolic alterations in endothelial cells. Such reorganization of metabolic networks is a double-edged sword as, on the one hand, it can function as a defense mechanism against disease-associated external insults, such as changes in glucose or oxygen availability, while, on the other hand, it can contribute to the generation of toxic end-products, anomalous accumulation of metabolic intermediates and alterations in energetic and redox metabolism that compromise physiological endothelial functions. This review points out current metabolic changes that have a great impact on the onset and progression of both atherosclerosis and PH. Endothelial cells' ability to easily switch between glycolysis, OXPHOS, PPP, and FAO makes the cellular metabolic switch a complex and challenging target in the search for future pharmacological interventions.

Targeting endothelial cell metabolism is a promising strategy to restore normal endothelial function and it has been reported that moderate inhibition of PFKFB3 can block pathological angiogenesis and normalize EC dysfunction, whereas strong inhibition can result in vessel disintegration (Conradi et al., 2017). This strategy could be useful to restore endothelial

cell function in pulmonary arterial hypertension (PAH), and possible also in CTEPH, both characterized by abnormal growth and enhanced glycolysis of pulmonary artery endothelial cells (Caruso et al., 2017). The main metabolic perturbations in pathological ECs in atherosclerosis, acute myocardial infarction and PH impact distinct pathways that lead to an imbalance in NO metabolism and ROS production. These diverse metabolic alterations in different EC dysfunctional pathologies highlight the need to apply metabolic network modeling approaches to identify key players that may be specific of endothelial metabolic dysfunctions and to rationally design interventions to target pathological EC metabolism for therapeutic benefit. Although the key players in glycolysis and energetic metabolism as well as in NO and ROS balance have been described, and communalities among different cell types and tissues have been reported, we still have only partial knowledge on the weight of each enzyme on the metabolic network fluxes in different cell types or in pathological vs. healthy states. Techniques and algorithms developed in the past few years permute an accurate modeling of metabolic network fluxes that, in conjunction with "omics" approaches, lay the foundations for unbiased and large-scale identification of targets with the greatest potential for specifically modulating metabolic pathway flux in disease conditions.

For medium-scale metabolic network models, among the main approaches used to model metabolic pathways are those based on the use of stable-isotope tracers (such as ^{13}C labeled metabolites). Computational tools to reconstruct metabolic flux maps from the quantification of the incorporation of ^{13}C-atoms into metabolites have been developed in recent years (e.g., Young, 2014; Antoniewicz, 2015; Foguet et al., 2016).

Models considering the kinetic properties of each enzyme in the metabolic network, in combination with methodologies such as Metabolic Control Analysis (MCA), a methodology to quantitatively evaluate the relative contribution and importance of each metabolic step in controlling overall metabolic flux distribution, have also been successfully used to predict putative drug targets (Hornberg et al., 2007). The control that each individual enzyme has on the flux through a metabolic pathway is quantified using MCA methodology in terms of the so-called "flux control coefficients." MCA can be used also to compare metabolic flux distribution in healthy vs. pathological condition. These comparisons will permit to identify the steps with the greatest potential for target specific metabolic adaptations accompanying pathological states and restore the flux distribution in health condition.

For large-scale models, constraint-based genome-scale metabolic models (GSMMs) have been developed and used in the last years to successfully predict putative therapeutic targets in different types of cancer (Ryu et al., 2015; Nilsson and Nielsen, 2016; Zhang and Hua, 2016; Yilmaz and Walhout, 2017). In brief, GSMMs mainly use transcriptomics and other "omics" data to constraint metabolic flux maps as well as flux balance analysis (FBA) methods to optimize for a cellular objective function. The main challenge in this approach is to appropriately define the objective function. To identify drug targets that impact abnormal endothelial cell growth, the most used objective function has been the maximization of biomass production. Using this approach, putative drug targets have been identified relevant to cancer through a systematic search for essential genes and combinations of target genes interacting in a synthetic lethal fashion able to impair biomass production.

As a word of caution, although topology, stoichiometry and chemical reaction properties are the major constraints on metabolic network flux, the consequences of inhibiting an enzyme activity on the overall network flux redistribution will depend on the relative concentrations of the different enzymes in the network (Cascante et al., 2002; De Atauri et al., 2011; Kell and Goodacre, 2014). Relative levels of enzyme concentrations in human metabolic networks are different not only in different tissues and in health vs. disease conditions but also between individuals which can result in different patient responses to identical metabolic drug interventions. Endothelial cell metabolic alterations associated with cardiopulmonary vascular disorders have been mainly studied using immortalized cell models and there is a shortage of studies characterizing ECs from patient tissues, a necessary next step forward in the field.

The therapeutic possibilities of targeting EC metabolism to improve cardiopulmonary vascular dysfunction are still understudied. However, we predict that deeper characterization of metabolic reprogramming in patient-derived cells and systemic approaches that integrate "omics" data into comprehensive metabolic network flux models will soon permit to identify putative key players in endothelial dysfunction associated with cardiovascular disorders and to design personalized multi-hit interventions at the metabolic level to restore physiological endothelial functions.

Finally, growing interest has focused on the modulation of gut microbiota as a therapeutic strategy in cardiovascular diseases. Microbiota stability is essential in human physiology, as it is involved in the regulation of many host functions such as blood pressure control, glucose tolerance, insulin sensitivity, and body weight control among others. Since hypertension and metabolic disturbances are well-known risk factors of CVD development, it is inevitable to touch in this review the possible role of gut microbiota and its impact on the cardiovascular system (Serino et al., 2014; Tang et al., 2017). In humans, the bacterial proportion of the gut microbiota consists of mainly Firmicutes and Bacteroidetes phyla and its ratio is an important indicator of microbiota stability (Tang et al., 2017). Since gut microbes primarily use ingested nutrients as fuel, it is not surprising that changes in dietary patterns alters the gut composition and its functions (Gentile and Weir, 2018). One way of interaction between the gut microbiota and the host is through production of metabolites that are biologically active or further metabolized by the host (Tang et al., 2017). A meaningful example is trimethylamine (TMA), a metabolite produced by Firmicutes phyla that promotes foam cell formation through its hepatic oxidized form TMA-N-oxide (TMAO) (Serino et al., 2014). Increased levels of this atherogenic microbial metabolite have been associated with increased risks of cardiovascular events (Serino et al., 2014; Tang et al., 2017). Individual differences in the composition of the gut bacteria, combined to the plasticity of the microbiota, indicate that a gut microbiota-targeted strategy could be a promising approach for the prevention and the treatment of

several metabolic diseases. Despite, to date, little evidence have provided direct evidence of mechanistic or causal roles of gut microbiota in human cardiovascular disease suggesting that the relationship between human and gut microbiota must be further investigated (Griffin et al., 2017; Gentile and Weir, 2018).

AUTHOR CONTRIBUTIONS

VS, EZ, OT-C and MCas conceived, designed, and wrote the manuscript. PQ, MCar, JB, and TT contributed to the writing of the manuscript and revised the article critically for significant intellectual content. VS and EZ equally contributed to this work.

FUNDING

The project leading to this work has received funding from the European Commission Horizon 2020 research and innovation program under the MOGLYNET H2020-MSCA-ITN-EJD grant (agreement No 675527). MCas has received support from Generalitat de Catalunya-AGAUR (ICREA Academia Prize 2015 and 2014SGR1017).

REFERENCES

Adams, S. P., Sekhon, S. S., and Wright, J. M. (2014). Rosuvastatin for lowering lipids (review). *Cochrane Database Syst. Rev.* 11, 1–262. doi: 10.1002/14651858.CD010254.pub2

Ahmad, F., Chung, Y. W., Tang, Y., Hockman, S. C., Liu, S., Khan, Y., et al. (2016). Phosphodiesterase 3B (PDE3B) regulates NLRP3 inflammasome in adipose tissue. *Sci. Rep.* 6, 1–13. doi: 10.1038/srep28056

Anderson, J. L., and Morrow, D. A. (2017). Acute myocardial infarction. *N. Engl. J. Med.* 376, 2053–2064. doi: 10.1056/NEJMra1606915

Antoniewicz, M. R. (2015). Methods and advances in metabolic flux analysis: a mini-review. *J. Ind. Microbiol. Biotechnol.* 42, 317–325. doi: 10.1007/s10295-015-1585-x

Archer, S. L., Gomberg-maitland, M., Maitland, M. L., Rich, S., Garcia, J. G., and Weir, E. K. (2008). Mitochondrial metabolism, redox signaling, and fusion : a mitochondria-ROS-HIF-1-Kv1. 5 O2-sensing pathway at the intersection of pulmonary hypertension and cancer. *Am. J. Physiol. Hear. Circ. Physiol.* 294, 570–578. doi: 10.1152/ajpheart.01324.2007

Badimon, L., Padró, T., and Vilahur, G. (2012). Atherosclerosis, platelets and thrombosis in acute ischaemic heart disease. *Eur. Hear. J. Acute Cardiovasc. Care* 1, 60–74. doi: 10.1177/2048872612441582

Bergheanu, S. C., Bodde, M. C., and Jukema, J. W. (2017). Pathophysiology and treatment of atherosclerosis: current view and future perspective on lipoprotein modification treatment. *Netherlands Hear. J.* 25, 231–242. doi: 10.1007/s12471-017-0959-2

Bhatt, D. L., Stone, G. W., Mahaffey, K. W., and Gibson, C. M. (2013). Effect of platelet inhibition with cangrelor during PCI on ischemic events. *N. Engl. J. Med.* 368, 1303–1313. doi: 10.1056/NEJMoa1300815

Bierhansl, L., Conradi, L. C., Treps, L., Dewerchin, M., and Carmeliet, P. (2017). Central role of metabolism in endothelial cell function and vascular disease. *Physiology* 32, 126–140. doi: 10.1152/physiol.00031.2016

Bonuccelli, G., Tsirigos, A., Whitaker-Menezes, D., Pavlides, S., Pestell, R. G., Chiavarina, B., et al. (2010). Ketones and lactate "fuel" tumor growth and metastasis: evidence that epithelial cancer cells use oxidative mitochondrial metabolism. *Cell Cycle* 9, 3506–3514. doi: 10.4161/cc.9.17.12731

Brandes, R. P., and Kreuzer, J. (2005). Vascular NADPH oxidases: molecular mechanisms of activation. *Cardiovasc. Res.* 65, 16–27. doi: 10.1016/j.cardiores.2004.08.007

Budhiraja, R., Tuder, R. M., and Hassoun, P. M. (2004). Endothelial dysfunction in pulmonary hypertension. *Circulation* 109, 159–165. doi: 10.1161/01.CIR.0000102381.57477.50

Bujak, R., Mateo, J., Blanco, I., Izquierdo-García, J. L., Dudzik, D., Markuszewski, M. J., et al. (2016). New biochemical insights into the mechanisms of pulmonary arterial hypertension in humans. *PLoS ONE* 11:e0160505. doi: 10.1371/journal.pone.0160505

Caruso, P., Dunmore, B. J., Schlosser, K., Schoors, S., Dos Santos, C., Perez-Iratxeta, C., et al. (2017). Identification of miR-124 as a major regulator of enhanced endothelial cell glycolysis in pulmonary arterial hypertension via PTBP1 and PKM2. *Circulation* 136, 2451–2467. doi: 10.1161/CIRCULATIONAHA.117.028034

Cascante, M., Boros, L. G., Comin-Anduix, B., de Atauri, P., Centelles, J. J., and Lee, P. W. (2002). Metabolic control analysis in drug discovery and disease. *Nat. Biotechnol.* 20, 243–249. doi: 10.1038/nbt0302-243

Catapano, A. L., Graham, I., De Backer, G., Wiklund, O., Chapman, M. J., Drexel, H., et al. (2016). 2016 ESC/EAS Guidelines for the management of dyslipidaemias. *Eur. Heart J.* 37, 2999–3058l. doi: 10.1093/eurheartj/ehw272

Cheng, S., Rhee, E. P., Larson, M. G., Lewis, G. D., McCabe, E. L., and Shen, D. (2012). Metabolite profiling identifies pathways associated with metabolic risk in humans. *Circulation* 125, 2222–2231. doi: 10.1007/978-1-62703-673-3

Cohen, J. C., Boerwinkle, E., Mosley, T. H., and Hobbs, H. H. (2006). Sequence variations in PCSK9, low LDL, and protection against coronary heart disease. *N. Engl. J. Med.* 354, 1264–1272. doi: 10.1056/NEJMoa054013

Collins, Y., Chouchani, E. T., James, A. M., Menger, K. E., Cochemé, H. M., and Murphy, M. P. (2012). Mitochondrial redox signalling at a glance. *J. Cell Sci.* 125(Pt 4):801–806. doi: 10.1242/jcs.110486

Conradi, L. C., Brajic, A., Cantelmo, A. R., Bouché, A., Kalucka, J., Pircher, A., et al. (2017). Tumor vessel disintegration by maximum tolerable PFKFB3 blockade. *Angiogenesis* 20, 599–613. doi: 10.1007/s10456-017-9573-6

Cottrill, K. A., and Chan, S. Y. (2013). Metabolic dysfunction in pulmonary hypertension: the expanding relevance of the warburg effect. *Eur. J. Clin. Invest.* 43, 855–865. doi: 10.1126/scisignal.2001449

de Atauri, P., Benito, A., Vizán, P., Zanuy, M., Mangues, R., Marín, S., et al. (2011). Carbon metabolism and the sign of control coefficients in metabolic adaptations underlying K-ras transformation. *Biochim. Biophys. Acta Bioenerg.* 1807, 746–754. doi: 10.1016/j.bbabio.2010.11.015

De Bock, K., Georgiadou, M., and Carmeliet, P. (2013a). Role of endothelial cell metabolism in vessel sprouting. *Cell Metab.* 18, 634–647. doi: 10.1016/j.cmet.2013.08.001

De Bock, K., Georgiadou, M., Schoors, S., Kuchnio, A., Wong, B. W., Cantelmo, A. R., et al. (2013b). Role of PFKFB3-driven glycolysis in vessel sprouting. *Cell* 154, 651–663. doi: 10.1016/j.cell.2013.06.037

Dewey, F. E., Gusarova, V., O'Dushlaine, C., and Gottesman, O. (2017). Inactivating variants in ANGPTL4 and risk of coronary artery disease. *N. Engl. J. Med.* 374, 1123–1133. doi: 10.1056/NEJMoa1510926

Draoui, N., and Feron, O. (2011). Lactate shuttles at a glance: from physiological paradigms to anti-cancer treatments. *Dis. Model. Mech.* 4, 727–732. doi: 10.1242/dmm.007724

Dromparis, P., and Michelakis, E. D. (2013). Mitochondria in vascular health and disease. *Annu. Rev. Physiol.* 75, 95–126. doi: 10.1146/annurev-physiol-030212-183804

Drummond, G. R., Selemidis, S., Griendling, K. K., and Sobey, C. G. (2011). Combating oxidative stress in vascular disease: NADPH oxidases as therapeutic targets. *Nat. Rev. Drug Discov.* 10, 453–471. doi: 10.1038/nrd3403

Eelen, G., de Zeeuw, P., Simons, M., and Carmeliet, P. (2015). Endothelial cell metabolism in normal and diseased vasculature. *Circ. Res.* 116, 1231–1244. doi: 10.1161/CIRCRESAHA.116.302855

Foguet, C., Marin, S., Selivanov, V. A., Fanchon, E., Lee, W. N., Guinovart, J. J., et al. (2016). HepatoDyn: a dynamic model of hepatocyte metabolism that integrates 13C isotopomer data. *PLoS Comput. Biol.* 12:e1004899. doi: 10.1371/journal.pcbi.1004899

Hypertension. 2019 Oct; 74(4):947-956. doi: 10.1161/HYPERTENSIONAHA.119.13472. Epub 2019 Aug 26.

Differentially expressed proteins in patient derived primary endothelial cells of acute myocardial infarction

Sarath Babu Nukala[1,2]*, Luca Regazzoni[1], Giancarlo Aldini[1], Erika Zodda[2], Marta Cascante[2], Marina Carini[1], and Alfonsina D'Amato[1]*.

[1]Department of Pharmaceutical Sciences, Università degli Studi di Milano, Milan, 20133, Italy.
*
[2]Department of Biochemistry and Molecular Biology and Institute of Biomedicine (IBUB), Faculty of Biology, University of Barcelona, Barcelona, Spain.

Correspondence: alfonsina.damato@unimi.it; sarath.nukala@unimi.it

Short title: Label free quantitative protein profiling in AMI

1. ABSTRACT:

Endothelial dysfunction is one of the primary factors in the onset and progression of acute myocardial infarction (AMI). However, the comprehensive role of pathological endothelial dysfunctionality in the disease progression mechanism remains unclear. An altered protein expression profiling in combination with protein network analysis was employed by using the mass spectrometry-based label-free quantification approach. 2246 proteins were identified and quantified, of which 335 significantly were differentially regulated in AMI endothelial cells compared to the control group. The differentially regulated protein profiles reveal the alteration of a) metabolism of RNA, b) platelet activation, signaling and aggregation, c) neutrophil degranulation, d) metabolism of amino acids and derivatives, e) cellular responses to stress, and f) response to elevated platelet cytosolic Ca^{2+} pathways. Increased production of oxidants and decreased production of anti-oxidant biomarkers as well as down regulation of protein which had an antioxidant property strongly explained the correlation of the role of oxidative stress in AMI. In conclusion, this is the first ever quantitative proteomics study, analysing patient-derived pathological endothelium dysfunction. These results deliver an exclusive representation of the endothelial proteome in AMI, contributing to the understanding of pathophysiology and building the foundation for the identification of new drug targets.

Key words:

Endothelium dysfunction, AMI patient cells, protein profiling, high-resolution quantitative mass spectrometry, protein networks.

2. Introduction:

Vascular endothelium plays a key role in the maintenance of vascular homeostasis and it also acts as a multifunctional organ for vascular tone regulation. Endothelial dysfunction is more frequently observed in the manifestation of cardiovascular risk factors and significantly contributes to the development of atherogenesis, hypertension, peripheral vascular disease, chronic kidney failure, diabetes, viral infections, coronary artery disease, and myocardial ischemia[1–5]. It is characterized by several features including the association of increased production of reactive oxygen species (ROS), growth factors, adhesive molecules; impaired redox status and fibrinolytic ability; a discrepancy in the functions of endothelium-mediated vasodilation, prothrombic and proinflammatory responses[6–8]. However, the occurrence of alterations in endothelial function causes the morphological changes in the atherosclerotic plaques, lesions and also significantly involves in the development of further clinical complications[9].

Acute myocardial infarction (AMI) is one of the leading causes of morbidity and mortality throughout the world and the appearance of this disease predominantly increasing in most of the developing countries. Approximately 15.9 million cases were reported in 2015[10]. It is a subgroup of an acute coronary syndrome, usually occurs with a reduction in myocardial perfusion that leads to the cell necrosis due to the formation of thrombus in coronary arteries. The rupture of an atherosclerotic plaque and unstable angina exposes the blood to thrombogenic lipids, which leads to the activation of clotting factors and platelets. Thin fibrous cap and lipid-rich core coronary plaques are more prone to rupture. Previous studies have shown that circulating microparticles from patients with AMI causes the endothelial dysfunction and it also occurs severely in young acute ST-elevation myocardial infarction patients correlated with the thrombolysis irrespective of conventional risk factors[11,12].

Emerging data specifies that new pathological blood vessel responses and endothelial dysfunctionality are associated with metabolic alterations in endothelial cells (ECs). Therefore, the affiliation of endothelial dysfunction to the AMI reflects the tendency to develop cardiovascular diseases. However, the underlying mechanisms associated with dysfunctional endothelium may be multidimensional and have not been clarified yet. Therefore, identification of insights and causes resulting in dysfunctional ECs are crucial to the understanding of the disease and to the development of new therapeutic tools. In this study, we aimed to identify the differentially regulated proteins associated with the vascular endothelial dysfunctionality of AMI. For this purpose, we used pathological primary ECs isolated from the thrombus material of patients undergoing treatment for AMI. Patient-derived pathological cells provide an exclusive opportunity to identify the definite molecular proceedings.

Proteomics approach provides ideal evidence of individual protein components and their involvement in numerous signaling pathways, networks and complex protein-protein interactions associated with biochemical functions. Therefore, in this present study, we have successfully applied the mass spectrometry-based label-free quantification approach to understanding the molecular mechanisms, complex network and signaling pathways associated with the endothelial dysfunctionality of AMI. Moreover, we have also observed and validated the expression pattern of a few genes at the transcriptome level by performing the RT-PCR analysis.

3. Materials and methods

3.1 Materials:

Gelatin solution, dithiothreitol (DTT), iodoacetamide (IAA), urea, thiourea, 3-[(3-Cholamidopropyl) dimethyl-ammonio]-1-propane sulfonate (CHAPS), and protease inhibitor cocktail were purchased from Sigma Aldrich (St. Louis, USA). Mini-protein Thx any KD gels, T20 cell counter were purchased from Bio-Rad (USA). EGM™-2 BulletKit™ Medium,

HEPES Buffered Saline Solution, Penicillin- streptomycin, Trypsin-EDTA were purchased from Lonza (USA). Sequence grade modified trypsin was purchased from promega (USA).

3.2 Endothelial cell culture and sample preparation: HCAECs were attained from Lonza Clonetics (Walkersville, USA) and used as controls in the present study. HCAEC-AMI cells were provided by Prof. Marta Cascante, University of Barcelona. Both HCAECs and HCAEC-AMI cells were grown on 0.2% gelatine-coated plates with EGM™-2 bulletkit™ medium which contains the EBM™-2 basal medium along with the EGM™-2 singlequots™ kit components, 10% FBS and 1% penicillin-streptomycin antibiotic. All the cell cultures were maintained in a 37°C humidified incubator at 5% CO_2. Total experiments were performed using the cells in passage number 5-9.

3.3 Protein extraction:

Confluent cells were trypsinized and collected by centrifugation at 1200 rpm for 5 min. Harvested cells were washed two times with cold PBS. The cell pellets were resuspended in the solubilization buffer (8M urea in 50mM Tris-HCl, 30mM NaCl, pH: 8.5 and 1% protease inhibitor) and incubated on ice for 5-10 min. Cell lysates were further homogenized by sonication in an ice bath for three times each for 5sec with 30 sec intervals, using an ultra sonicator. Samples were centrifuged at 14000 rpm for 20 min at 4ºC. The protein supernatant was collected into the new Eppendorf tube and pelleted cell debris was discarded. Samples were stored at -80ºC until we use it for further experiments. The protein estimation was carried out by using the Bradford assay.

3.4 In-solution trypsin digestion:

10µg of total protein was resuspended in 50mM ammonium bicarbonate. Reduction was carried out by incubating 5mM final concentration of DTT for 30 min at 52°C, followed by an alkylation with 15mM final concentration of iodoacetamide for 20min in the dark at room

temperature. Trypsin digestion was allowed at 37°C overnight, with an enzyme: substrate ratio of 1:10. The resulting peptides were used for MS analysis.

3.5 nLC-HRMS analysis:

Tryptic peptides were analyzed using a Dionex Ultimate 3000 nano-LC system (Sunnyvale CA, USA) connected to an Orbitrap Fusion™ Tribrid™ Mass Spectrometer (Thermo Scientific, Bremen, Germany) equipped with a nano-electrospray ion source. Peptide mixtures were pre-concentrated onto an Acclaim PepMap 100 - 100µm x 2cm C18 and separated on EASY-Spray column, 15 cm x 75 µm ID packed with Thermo Scientific Acclaim PepMap RSLC C18, 3 µm, 100 Å. The temperature was setting to 35°C and the flow rate was 300 nL min^{-1}. Mobile phases were the following: 0.1% Formic acid (FA) in water (solvent A); 0.1% FA in water/acetonitrile (solvent B) with 2/8 ratio. Peptides were eluted from the column with the following gradient: 4% to 28% of B for 90 min and then 28% to 40% of B in 10 min, and to 95% within the following 6 min to rinse the column. Column was re-equilibrated for 20 min. Total run time was 130 min. One blank was run between triplicates to prevent sample carryover. MS spectra were collected over an m/z range of 375-1500 Da at 120,000 resolutions, operating in the data dependent mode, cycle time 3 sec between master scans. Higher-energy collisional dissociation (HCD) was performed with collision energy set at 35 eV. Each sample was analyzed in three technical triplicates.

3.6 Protein identification and quantification:

Resulting MS raw files from all the technical and biological replicates were analyzed by using MaxQuant software[13] (version 1.6.2.3). Andromeda search engine was used to identify MS/MS based peptide and proteins in MaxQuant comprises a target-decoy approach with less than 1% of FDR. In the present study we used *Uniport_Homosapiens* database. Trypsin was used for enzyme specificity and maximum five number of modifications per peptide was allowed. Methionine oxidation and acetylation (N terminus) was used as a variable modification.

Carbamidomethylation was used as a fixed modification. For the label-free quantification of proteins, we applied MaxLFQ algorithm. Match between the runs option was enabled and remaining default parameters were permitted. The following criteria were applied: S0 value was set to 2 in both sides, permutation-based FDR value set it as 0.05 and q-value report option, -log10 p-value suffix options were enabled. Proteins with the p-value less than 0.05 were considered as statistically significant.

3.7 Statistical analysis:

An open source Perseus software[14] (version 1.6.1.3; Max Planck Institute of Biochemistry, Germany) was used for the identification of statistically significantly differentially regulated proteins. The resulted data generated from MaxQuant was filtered based on the proteins only identified by site, reverse and potential contaminants. The log 2-fold changes of proteins were estimated by using the comparison of mean LFQ intensities between disease and control groups (HCAEC-AMI vs HCAEC). Variabilities of biological replicates were measured with Pearson correlation coefficient values of the LFQ intensities. The differentially regulated proteins with a minimum of two peptides and FDR adjusted p-value < 0.05 were considered as statistically significant.

3.8 Gene ontology, network and pathway analysis:

We used Cytoscape software (version 3.6.0; http://cytoscape.org/index.php) to understand the possible network pathways connected with differentially regulated proteins. In addition, we also used ClueGo plug-in that generally provides data based on the updated GO terms, BioCarta/Kyoto Encyclopedia of Genes and Genomes (KEGG) pathways[15]. Statistical significance of terms was determined with bid of two-sided enrichment/depletion hypergeometric test and Bonferroni p-value correction. Moreover, we also used the function of GO term fusion for further reduction of redundancy. Remaining default parameters were allowed.

3.9 Real Time PCR:

Total RNA isolation and cDNA synthesis were performed using iScript RT-qPCR sample preparation reagent (BioRad) and Maxima First Strand cDNA Synthesis Kit (Thermo Scientific), respectively following the manufacturer's instructions. cDNA was amplified in triplicate using Maxima SYBR Green/ROX qPCR Master Mix (Thermo Scientific) in an ABI PRISM 7000 Sequence detection system. The thermal cycling conditions included 95°C for 10 minutes, followed by 40 cycles of amplification at 95°C for 15 seconds, followed by 60°C for 1 minute. Gene expression was normalized to the housekeeping gene RPLP0.

3.10 Western blot:

Proteins obtained from control and pathological endothelial cells were used to validate the expression pattern by western blot analysis. 30µg of total proteins were electrophoresed on 8% and 12% SDS-PAGE and transferred by the wet-transfer method. Immunodetection analysis was employed for VWF, IDH1, PARP, NRF2, and FABP4 and ACTB targets using the anti-VWF mouse monoclonal antibody (Santa Cruz), anti-IDH1 rabbit polyclonal antibody (Genetex), anti-PARP purified mouse antibody (BD Bioscience), anti-NRF2 rabbit polyclonal antibody (Abcam), anti- FABP4 polyclonal antibody (Abcam), and anti-beta actin (MP Biomed) as primary antibodies and respective anti-mouse and anti-rabbit HRP conjugated secondary antibodies (Abcam). Results were obtained by ECL detection method and expression of all target proteins was investigated against the actin housekeeping protein.

4. Results:

4.1 Identification and differential proteomic analysis of dysfunctional ECs

The aim of this study was to identify the differentially regulated proteins associated with the vascular endothelial dysfunctionality of AMI. For this purpose, pathological primary ECs, isolated from the thrombus material of AMI patients, were used. Patient-derived pathological cells provide an exclusive opportunity to identify the definite molecular proceedings. The mass

spectrometry-based label-free quantitation approach was able to understand the complex network and signaling pathways associated with the endothelial dysfunctionality of AMI. The confluent pathological ECs (HCAEC-AMI) and normal human coronary artery endothelial cells (HCAECs) were collected to extract the protein content. Altered protein expression profiling in combination with gene ontology, network and pathway analysis was employed by using the mass spectrometry-based label-free quantification approach to explore the molecular proceedings (Fig S1). Multi scatter plot analysis of peptide intensities resulted in Pearson coefficients higher than 0.98, attesting the high grade of reproducibility of technical and biological replicates (Fig.S2). 2246 protein and 17653 unique peptides were quantified, consulting the *Uniprot_Homo sapiens* database; the settings of searches were 10 ppm tolerance on peptides, 0.8Da on fragments and less than 1% false discovery rate. The data analysis was performed as specified in our publication[16]. To discriminate the differentially expressed proteins a two-sided t test was applied to two category groups: HCAEC-AMI (disease) and HCAEC (control). The log2 of ratios of disease versus control (fold change) were plotted against the -log10 of p-value, resulting in the Volcano plot of Figure 1.2. All proteins with a fold change higher than 1.5 and p-value less than 0.05 were considered significant outliers. 335 proteins were differentially regulated, of which 40 up and 123 down-regulated proteins with a fold change higher than 1.5-in the HCAEC-AMI ECs compared to the control group. (Table 1a and 1b).

4.2 Endothelial dysfunction and upregulation:

Majority of upregulated proteins in dysfunctional ECs of AMI are originated from proteasome complex, nucleosome, nuclear nucleosome, large ribosomal subunit and cytosolic ribosome (Supplementary Table 1a). The actin-binding protein TMSB10 is showed to be high upregulated in dysfunctional ECs with log2 fold change of 2.68. This protein is involved in the actin filament organization biological process that plays an important role in the organization

of the cytoskeleton. Similarly, we identified an important adhesion protein VWF as upregulated protein with 2.06 log2 fold change variation. It is a key protein that involves in the hemostasis, blood coagulation, platelet degranulation, and activation and extracellular matrix organization. Studies have shown that VWF promotes the formation of a molecular bridge between platelet-surface receptor complex GPIb-IX-V and sub-endothelial collagen matrix, which further increases the binding of plates to the site of vascular injury. The plasminogen activator (PLAT) protein involved in tissue remodeling and degradation was found to be upregulated in the dysfunctional ECs. Along with these proteins, based on our results, a platelet-expressed protein HSD17B12 might play a primary role in the dysfunction of ECs. It has a 3-ketoacyl-CoA reductase activity, suggesting a role in Lipid metabolism and fatty acid biosynthesis. Moreover, statistically significantly associated biological processes and their corresponding proteins were reported in the figure 2a.

4.3 Endothelial dysfunction and down-regulation:

Cytosolic small and large ribosomal subunits and proteasome complex are the major sources of down-regulated proteins (Supplementary Table 1b). These proteins involved in the ribosome biosynthesis, small and large subunit assembly, regulation of cardiac muscle contraction by regulation of the release of sequestered calcium ion, regulation of oxidative stress-induced cell death, cellular response to reactive oxygen species and cellular aldehyde metabolic processes (Figure 2b). UBE2I, SYNE1, and MGST1 showed an extensive down-regulation among all the identified proteins. The MAPEG family (Membrane-Associated Proteins in Eicosanoid and Glutathione metabolism) protein MGST1, involved in the protection of endoplasmic reticulum and outer mitochondrial membrane from oxidative stress. Therefore, the down-regulation of this protein in dysfunctional ECs might indicate the association of increased oxidative stress in endothelial dysfunction of AMI.

4.4 Network and pathway analysis: To better understand the nature of differentially regulated proteins, they were further classified in terms of Reactome pathways. The retrieved data from this analysis showed the association of metabolism of RNA; platelet activation, signaling and aggregation; neutrophil degranulation; metabolism of amino acids and derivatives; platelet degranulation; cellular responses to stress; and response to elevated platelet cytosolic Ca2+ pathways in endothelial dysfunction of AMI (Figure 3).

4.5 Real time PCR:

A total of 13 genes (Supplementary Table 2) were selected to understand its variation at mRNA level by using quantitative real-time PCR method. The expression of these genes was evaluated using HACEC-AMI cell lines against the HCAECs. The genes such as COL8A1, MMRN1, GGT5, MACROD1, and ME3 were found to be upregulated and genes including DPP7, FABP4, ATP2B4, ITGB3, MYL9, FABP5, FERMT3 and STAT3 were found to be down-regulated during the endothelial dysfunction of AMI (Figure-4).

4.6 Validation of proteins with western blot:

To validate the expression of VWF, we used classical western blot analysis. On the other hand, few proteins such as IDH1, PARP, NRF2, and FABP4, whose profusion changed in the cardiovascular diseases, particularly atherosclerosis, were also selected for western blot analysis to see their expression pattern in the endothelial dysfunction associated with AMI. The peak intensity area of each protein band was calculated using ImageJ software and the data illustrated as histograms after analyzing against the ACT as housekeeping protein. As shown in the figure (Figure 5), the relative abundance of VWF protein was analogous to the results from label-free quantification study. In the dysfunctional ECs, we identified increased expression of IDH1, NRF2 and PARP proteins. While FABP4 protein showed the down-regulation.

5. Discussion:

A deep understanding of molecular mechanisms of disease is crucial in the discovery of novel therapeutic strategies and in the early prediction to improve the prognosis. Mass spectrometry-based proteomics is one of the advanced tools to identify early biomarkers in the various biological samples. In the present study, for the first time, the changing of proteome profile of patient-derived HCAEC-AMI cells was analysed.

The endothelium which exists between the circulatory system and surrounding tissues plays an important role in the vascular injury. Based on the stress and tissue needs, ECs can induce prothrombotic or antithrombotic events. Usually, healthy ECs express anticoagulant and antiplatelet agents that can be involved in the prevention of fibrin formation and platelet aggregation. Whereas dysfunctional ECs generate aggregation, fibrin formation along with the platelet adhesion. During the final stage, ECs produce pro-fibrinolytic events to enhance the fibrinolysis for the degradation of the clot. On the other hand, ECs under physiological conditions prevent thrombosis by activating the cascade of anticoagulant and antiplatelet mechanisms. In this study TMSB10 and VWF proteins were highly upregulated. TMSB10 has a role in the organization of the cytoskeleton, while the increased expression of VWF clearly explains an enhanced occurrence of thrombosis. VWF also binds to collagen during the damage occurring to the blood vessels. Collagen plays a key role in the maintenance of integrity and elasticity of normal vessel walls as well as atherosclerotic vessel walls and it stimulates the thrombosis formation and scar formation processes particularly in acute myocardial infraction[17] VWF and over expressed RAP1A, RAP1B proteins are involved in the platelet aggregation, in integrin alpha IIb beta3 signaling and in MAP2K and MAPK activation pathways.

MAPKs is implicated in multiple important cellular processes such as apoptosis, proliferation, motility, differentiation, stress response, and survival. In this study, MAPK3 protein were down-regulated, that correlates with lower proliferation capability. Recent studies showed that

interferon-induced GTP-binding protein MX1 involved in MI and suggested to play a role in the pathology of the disease[18,19]. In this study, MX1 was upregulated with fold change of 2.4, attesting its role in endothelial dysfunction of AMI. Rap1, which controls the EC function, is one of the critical mediators of FGF-induced ERK activation in human angiogenic process[20]. In this study, upregulation of RAP1a and RAP1b in dysfunctional ECs might explain the strong correlation between endothelial dysfunction, platelet aggregation and angiogenesis in AMI. It might also play a role in the vascular EC protection, based on the results of knockdown studies[21].

The identified differentially regulated proteins in patient cells, such as VWF[22], CRYAB[23], MX1[24], CNN2[25,26], PSME2[27], CIAPIN1[28], TAGLN[29], and EDIL3[30] have been reported to be implicated in AMI, myocardial infarction (MI) vascular injury, morphogenesis, and angiogenesis. Furthermore, previous studies have shown the increased synthesis of type VIII collagen in the vascular injury of the development process of atherosclerosis in humans and animal models[31,32]. The identified over expressed HSD17B12 protein is a reductase involved in collagen binding activity and long fatty acid chain metabolism. However, in the case of dysfunctional ECs of CTEPH disease, HSD17B12 shown the down regulation, suggesting different role in both different diseases. MMRN1, belonging to EMILIN family[33], is usually found in platelets, and has an adhesive ligand property in synergy with VWF in platelet adhesion to collagen at the sites of vascular injury[34,35]. The down regulation of MMRN1 protein, was not confirmed by analysis of its gene expression. This lack of correlation is likely due to the differentially regulation of post translated modified form of the protein.

EC apoptosis has a fundamental role in the angiogenesis process and pathological vascular remodelling and regression[36–38]. In this study proteins related to apoptosis pathway resulted differentially regulated. In particular, CYCS, DNM1L, HMGB1, LMNB1, PSMA4, PSMA7, PSMB5, PSMC5, PSMD13, PSME1, YWHAB, YWHAE showed decreased expression and

PSMA2, PSMB3 (1.08-fold change) and PSME2 showed increased expression, attesting their essential role during endothelial reorganization in AMI.

Metabolic alterations and oxidative stress are important influencing factors in the endothelial dysfunctionality of cardiovascular diseases and diabetes[39–41]. Normal ECs constantly produce endothelial nitric oxide synthase (eNOS). The impairment of eNOS–NO system causes the oxidative stress and endothelial dysfunction that further accelerates the atherogenesis. In this investigation, a reduced expression of eNOS activation pathway, described by the down-regulation of CALM1, CALM2, and CALM3 proteins, and the activation of NF-kappaB in B cells, were found. The down-regulation of PARK7, PAWR, PSAP, TXN and UBQLN1 proteins, involved in the regulation of oxidative stress-induced cell death, and the down-regulation of MGST1 protein, involved in the cell protection against oxidative stress, were found. This confirms the involvement of oxidative stress in endothelial dysfunction. The inhibition of vascular oxidative stress and enhancement of eNO production could be a potential therapeutic strategy along with the treatments of established risk factors.

FABP4 is one of the most abundant proteins in fat cells and lipocytes also known as adipocyte cells and it has a major role in proinflammatory activity in macrophages. Previous studies reported overexpression of endothelial FABP4 in response to angiogenic growth actor VEGFA[42]; while other studies demonstrated the correlation between down-regulation of FABP4 and decrease of endothelial cell proliferation[42,43]. According to the gene expression studies, it encourages P38, endothelial nitric-oxide synthase and stem cell factor (SCF)/c-kit pathways[43]. Furthermore, knockdown studies of FABP4 increased the oxidative stress[44]. In the present study, the down-regulation of FABP4 at transcriptome and protein levels was found, accordingly with less proliferation and migration capacity of AMI cells.

Ribosome (including RNA and proteins) is an essential component in the machinery of protein synthesis and ribosomal proteins (RPs) plays a critical role in the cell proliferation,

differentiation, apoptosis, DNA repair, and other cellular processes[45]. Studies have shown that the dysfunction of ribosomal biosynthesis may result in abnormal cell proliferation in metabolic disorders and cancer[46,47]. Moreover, various RPs have been reported to be associated with the progression of cardiovascular diseases[48,49]. However, we observed the down-regulation of several RPs in dysfunctional ECs which are corresponding to the ribosome biogenesis, small and large subunit assembly processes.

In conclusion, the main involved pathways and related proteins have been extensively described by the quantitative and bioinformatic analyses. This can provide new perspectives in drug discovery to treat cardiovascular diseases.

6. Acknowledgements and source of funding:

This present work was funded by Horizon 2020 program of the European Union - Marie Skłodowska-Curie Actions, Innovative Training Networks (ITN), Call: H2020-MSCA-ITN-2015, Number: 675527-MOGLYNET.

7. Disclosures:

None.

8. References:

1 Celermajer DS. Endothelial Dysfunction: Does It Matter? Is It Reversible? *J Am Coll Cardiol* 1997; 30:325–333.

2 Vilahur G, Padró T, Casaní L, Mendieta G, López JA, Streitenberger S, *et al.* Polyphenol-enriched Diet Prevents Coronary Endothelial Dysfunction by Activating the Akt/eNOS Pathway. *Rev Española Cardiol (English Ed* 2015; 68:216–225.

3 Hasdai D, Gibbons RJ, Holmes DR, Higano ST, Lerman A. Coronary endothelial dysfunction in humans is associated with myocardial perfusion defects. *Circulation* 1997; 96:3390–3395.

4 Zeiher AM, Krause T, Schächinger V, Minners J, Moser E. Impaired endothelium-

9. Novelty and significance of the work:

What is new?

This is the first ever study performed to explore the proteomic signatures with patient-derived pathological ECs to unveil underlying pathophysiological mechanisms in endothelial dysfunction associated with AMI.

What is Relevant?

Quantitative proteomic profiling in endothelial dysfunction reveals the biomarker signature of thrombosis, metabolism and oxidative stress.

The overexpression of VWF strongly associated with thrombus formation, platelet aggregation and angiogenesis that might play a key role endothelial dysfunction of AMI.

Increased production of oxidants and decreased production of anti-oxidant biomarkers as well as down regulation of protein which had an antioxidant property strongly explained the correlation of the role of oxidative stress in endothelial dysfunction of AMI.

Summary:

Our mass spectrometry-based label-free quantitative proteomics approach revealed several cardiovascular related biomarkers with AMI occurrence. Thrombus formation, collagen deposition, vascular remodeling, platelet aggregation, metabolic alterations, oxidative stress related events have a potential unfavorable impact on the endothelial dysfunction.

10. Figure and Table Legends:

Figure 1: Distribution of differentially regulated proteins in HCAEC-AMI cells. Volcano Plot obtained by two-sided t test of the groups: HCAEC-AMI (disease) versus HCAEC (control). Green color indicates the down-regulated proteins, red color represents the upregulated ones.

Figure 2: Biological processes associated with up (a) and down (b) regulated proteins found in dysfunctional HCAEC-AMI cells. The significance of the clustering is shown by colour code and the size of nodes.

Figure 3: Main pathways and involved genes found in dysfunctional HACEC-AMI cells. ClueGo analyses enriched and clustered Reactome pathway terms. The significance of the clustering is shown by color code and the size of nodes.

Figure 4: Transcript expression levels of selected genes. The expression of selected genes was normalized with RPLP0 housekeeping gene. The boxes display the relative expression of genes in HCAEC-AMI against the HCAEC expression. Data were shown in log2 fold changes of mean ± SD. Differences were considered significant when $p < 0.05$ (*), $0.001 < p < 0.01$ (**), $p < 0.001$ (***).

Figure 5: Protein levels of selected proteins. Bar graph was plotted with mean ± SEM, the x-axis represents the HCAEC-AMI and HCAEC groups and the y-axis represents the relative expression of a respective protein to control. Differences were considered significant when $p < 0.05$ (*), $0.001 < p < 0.01$ (**), $p < 0.001$ (***). β-actin was used as a housekeeping protein.

Table 1a: List of upregulated proteins associated with endothelial dysfunction in AMI.

Table 1b: List of down-regulated proteins associated with endothelial dysfunctionality in AMI.

11. Figures:

Figure 1:

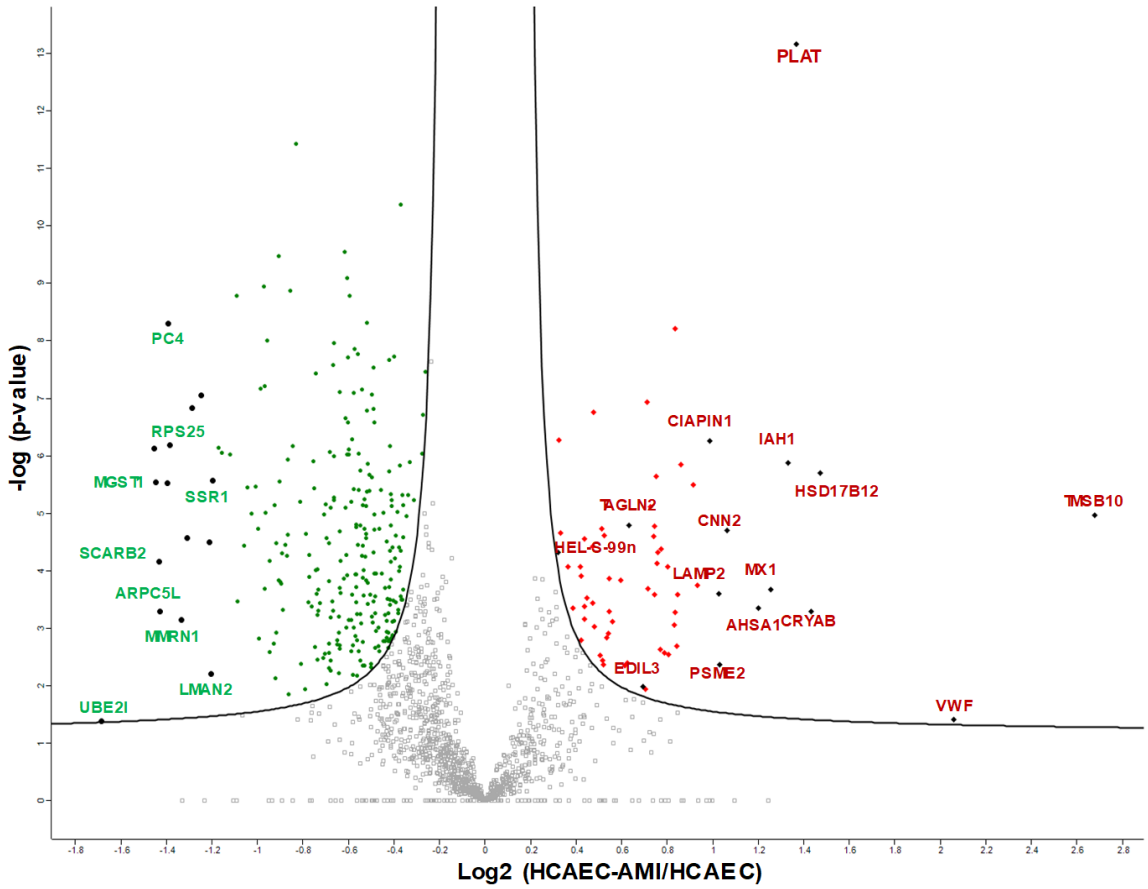
PLAT
PC4
RPS25
MGST1
SSR1
SCARB2
ARPC5L
MMRN1
LMAN2
UBE2I
CIAPIN1
IAH1
HSD17B12
TMSB10
TAGLN2
CNN2
HEL-S-99n
LAMP2
MX1
AHSA1
CRYAB
EDIL3
PSME2
VWF
-log (p-value)
Log2 (HCAEC-AMI/HCAEC)

Figure 2:

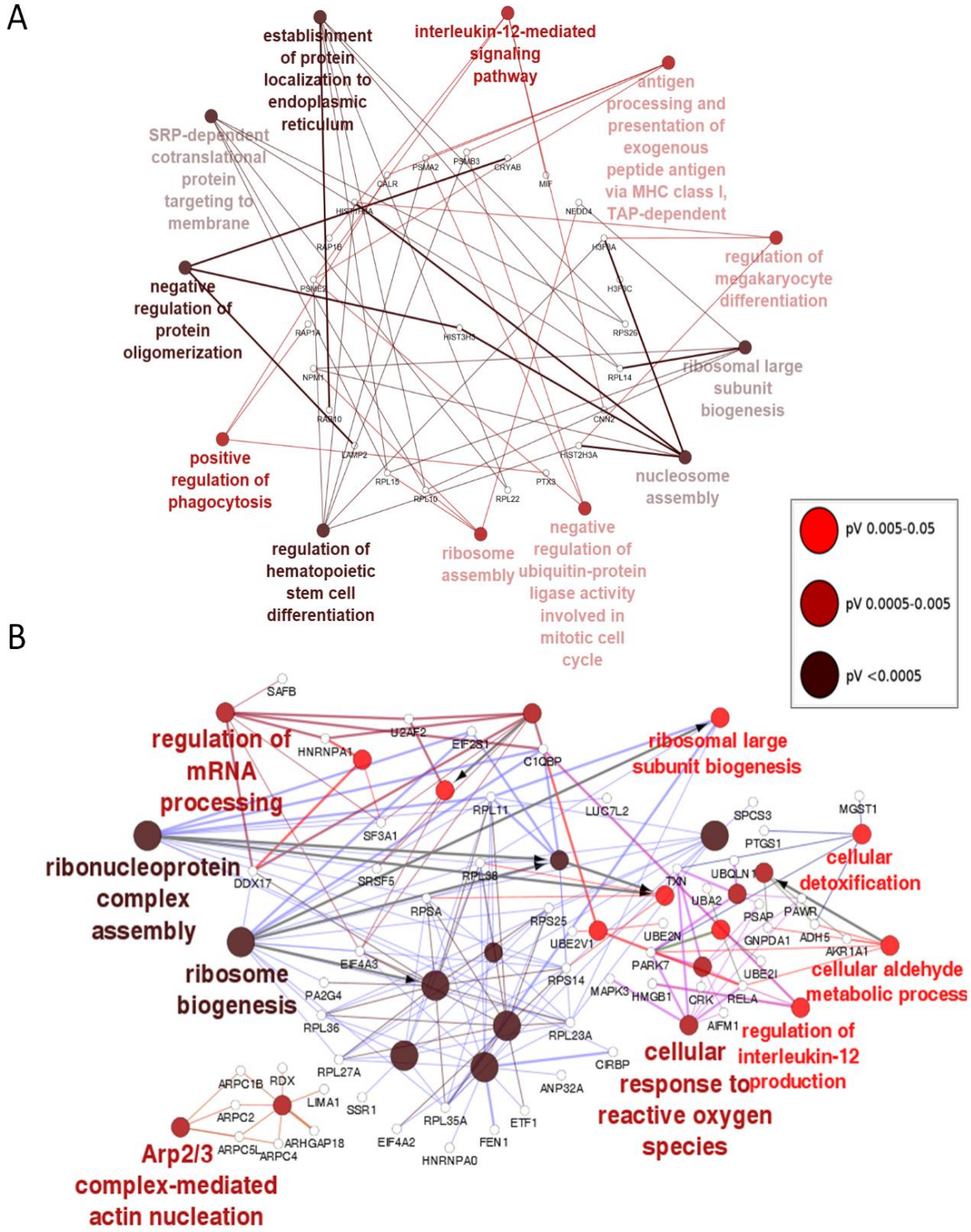
A
establishment of protein localization to endoplasmic reticulum
interleukin-12-mediated signaling pathway
antigen processing and presentation of exogenous peptide antigen via MHC class I, TAP-dependent
SRP-dependent cotranslational protein targeting to membrane
regulation of megakaryocyte differentiation
negative regulation of protein oligomerization
ribosomal large subunit biogenesis
positive regulation of phagocytosis
nucleosome assembly
regulation of hematopoietic stem cell differentiation
ribosome assembly
negative regulation of ubiquitin-protein ligase activity involved in mitotic cell cycle
pV 0.005-0.05
pV 0.0005-0.005
pV <0.0005
B
regulation of mRNA processing
ribosomal large subunit biogenesis
ribonucleoprotein complex assembly
cellular detoxification
ribosome biogenesis
cellular aldehyde metabolic process
regulation of interleukin-12 production
cellular response to reactive oxygen species
Arp2/3 complex-mediated actin nucleation

Figure 3:

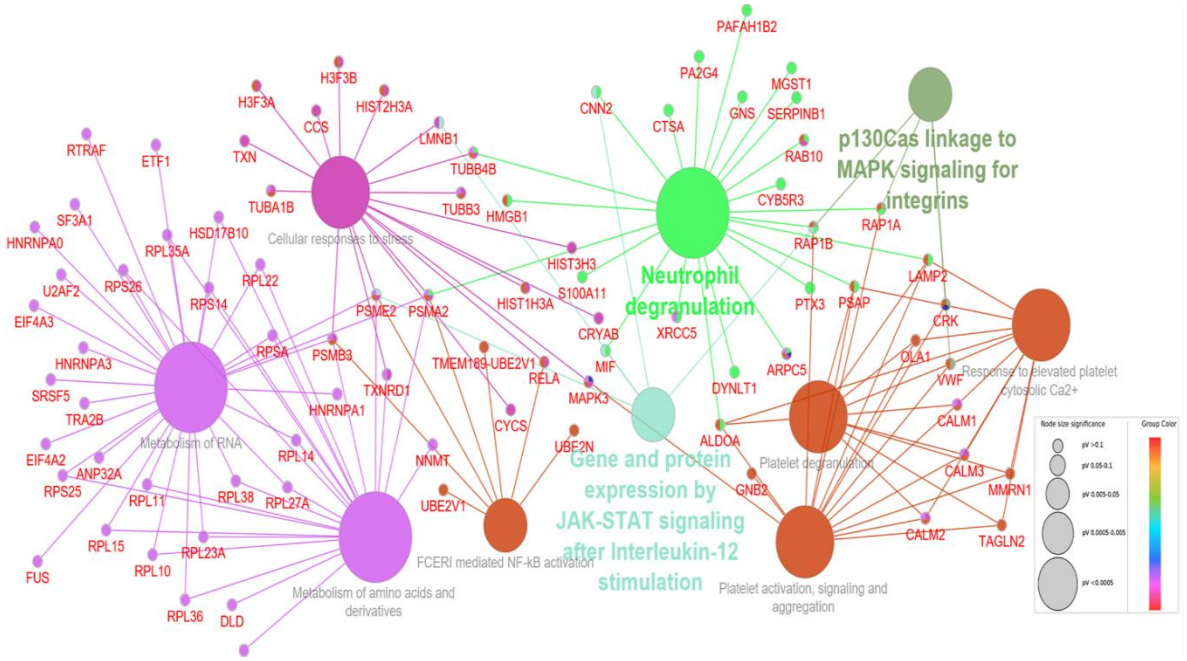

Figure 4:

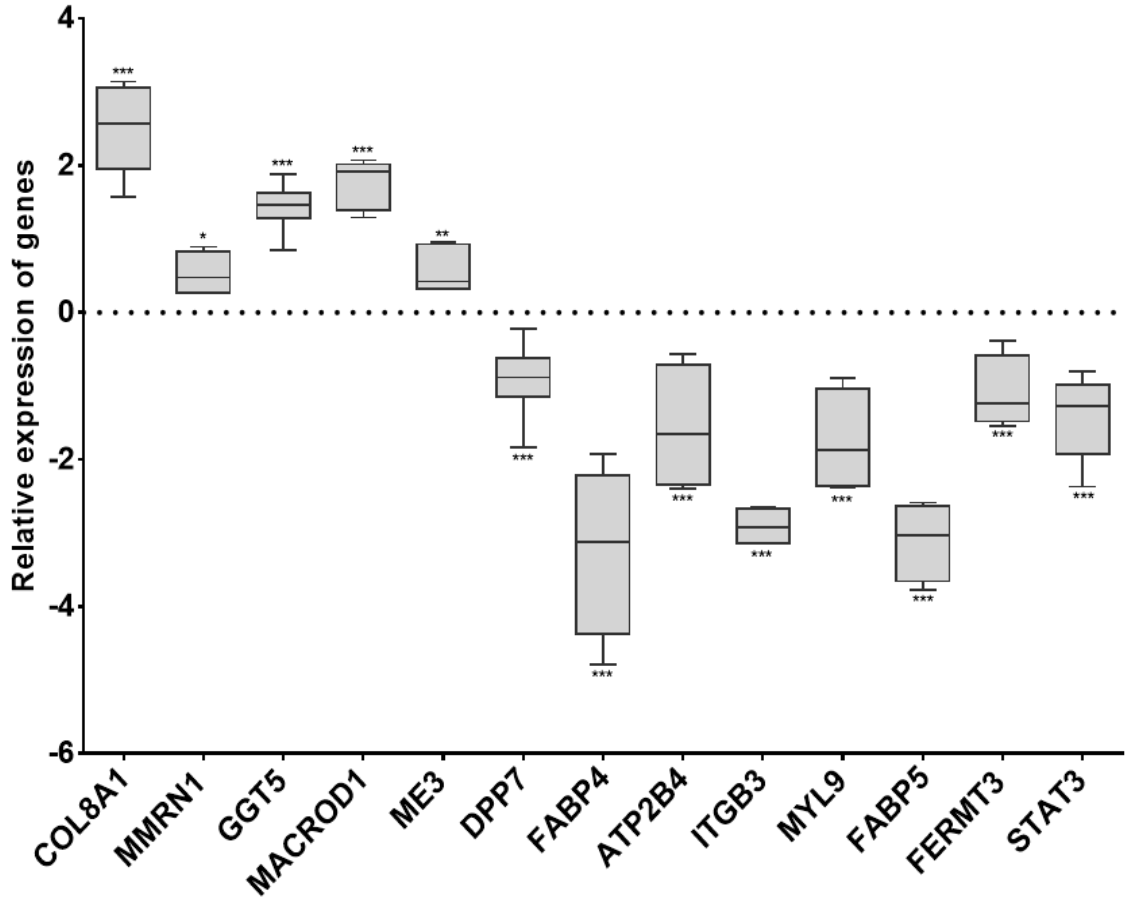

Figure 5:

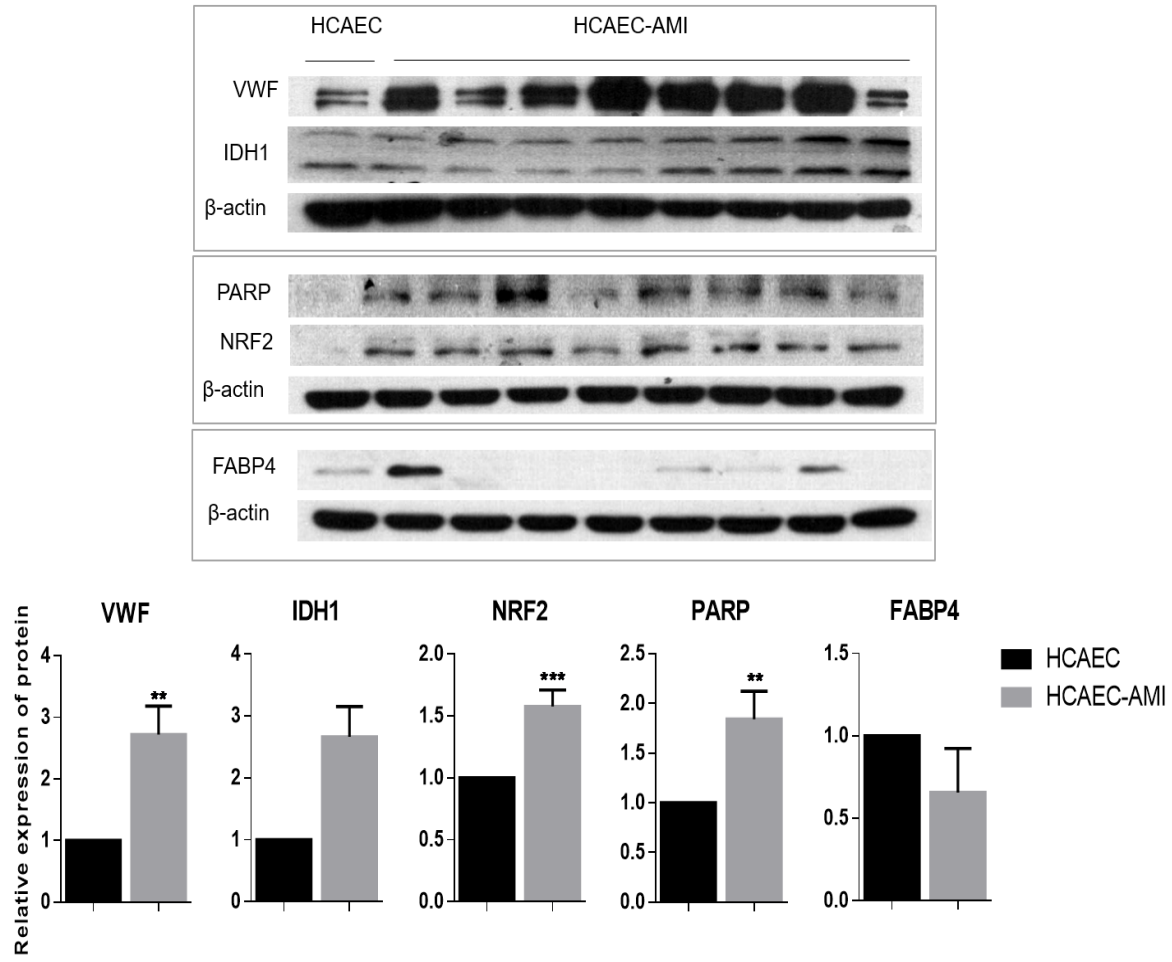

Table 1a:

Protein ID	Protein names	Gene names	Log2 (HCAEC-AMI vs HCAEC)	-LOG(P-value)
P63313	Thymosin beta-10	TMSB10	2.68	4.97
P04275	von Willebrand factor;von Willebrand antigen 2	VWF	2.06	1.41
B4DWS6	Very-long-chain 3-oxoacyl-CoA reductase	HSD17B12	1.47	5.70
E9PR44	Alpha-crystallin B chain	CRYAB	1.43	3.29
B4DRD3	Tissue-type plasminogen activator;Tissue-type plasminogen activator chain A;Tissue-type plasminogen activator chain B	PLAT	1.37	13.16
A0A140VJL6	Isoamyl acetate-hydrolyzing esterase 1 homolog	IAH1	1.33	5.87
P20591	Interferon-induced GTP-binding protein Mx1;Interferon-induced GTP-binding protein Mx1, N-terminally processed	MX1	1.25	3.67
O95433	Activator of 90 kDa heat shock protein ATPase homolog 1	AHSA1	1.20	3.35
B4DDF4	Calponin;Calponin-2	CNN2	1.06	4.70

Q86SZ7	Proteasome activator complex subunit 2	PSME2	1.03	2.36
B4E2S7	Lysosome-associated membrane glycoprotein 2	LAMP2	1.03	3.60
Q6FI81	Anamorsin	CIAPIN1	0.99	6.26
A0A0S2Z4G7	Nucleophosmin	NPM1	0.93	3.75
A0A024R6I3	Transmembrane emp24 domain-containing protein 10	TMED10	0.91	5.50
Q6IBN4	Enoyl-CoA delta isomerase 2, mitochondrial	PECI	0.86	5.85
O94874	E3 UFM1-protein ligase 1	UFL1	0.85	3.59
O15511	Actin-related protein 2/3 complex subunit 5	ARPC5	0.84	2.69
A0A024R3C4	KDEL motif-containing protein 2	KDELC2	0.84	3.28
Q5RLJ0	UPF0568 protein C14orf166	C14orf166	0.83	8.21
Q9UPN1	Serine/threonine-protein phosphatase;Serine/threonine-protein phosphatase PP1-gamma catalytic subunit	PPP1CC	0.83	3.05
A0A024RA52	Proteasome subunit alpha type;Proteasome subunit alpha type-2	PSMA2	0.81	2.55
X5D2T3	60S ribosomal protein L10	RPL10	0.80	4.07
P61026	Ras-related protein Rab-10	RAB10	0.79	2.57
B7ZAY2	Ras-related protein Rap-1b;Ras-related protein Rap-1b-like protein;Ras-related protein Rap-1A	RAP1B	0.77	4.39
Q5U0D2	Transgelin	TAGLN	0.77	2.63
Q6IPH7		RPL14	0.76	4.33
O15231	Zinc finger protein 185	ZNF185	0.76	4.13
P51571	Translocon-associated protein subunit delta	SSR4	0.75	5.64
J3KQ32	Obg-like ATPase 1	OLA1	0.74	4.78
A0A024RB14	40S ribosomal protein S26;Putative 40S ribosomal protein S26-like 1	RPS26	0.74	3.59
Q13509	Tubulin beta-3 chain	TUBB3	0.74	4.60
A0A024R7B7	Hsp90 co-chaperone Cdc37;Hsp90 co-chaperone Cdc37, N-terminally processed	CDC37	0.72	5.11
B7Z3K3	Inositol-3-phosphate synthase 1	ISYNA1	0.71	3.68
B3KT06	Tubulin alpha-1B chain	TUBA1B	0.71	6.93
A0A024R1M8	Apolipoprotein L2	APOL2	0.71	1.95
O43854	EGF-like repeat and discoidin I-like domain-containing protein 3	EDIL3	0.69	1.98
P37802	Transgelin-2	TAGLN2	0.63	4.79
P63172	Dynein light chain Tctex-type 1	DYNLT1	0.63	2.39
B4DFL1	Dihydrolipoyl dehydrogenase;Dihydrolipoyl dehydrogenase, mitochondrial	DLD	0.61	2.36
V9HW44	Platelet-activating factor acetylhydrolase IB subunit beta	HEL-S-303	0.60	3.84

Table 1b:

Protein ID	Protein names	Gene names	Log2 (HCAEC-AMI vs HCAEC)	-LOG(P-value)
H3BPC4	SUMO-conjugating enzyme UBC9	UBE2I	-1.68	1.38
E7ENN3	Nesprin-1	SYNE1	-1.45	6.12
F5H7F6	Microsomal glutathione S-transferase 1	MGST1	-1.45	5.54

A0A1W2PRF6	Lysosome membrane protein 2	SCARB2	-1.43	4.16
B3KPC7	Actin-related protein 2/3 complex subunit 5;Actin-related protein 2/3 complex subunit 5-like protein	ARPC5L	-1.43	3.29
A8K651	Complement component 1 Q subcomponent-binding protein, mitochondrial	C1QBP	-1.39	5.53
Q9BQQ5	60S ribosomal protein L27a	L27a	-1.39	8.30
P62851	40S ribosomal protein S25	RPS25	-1.38	6.19
Q13201	Multimerin-1;Platelet glycoprotein Ia*;155 kDa platelet multimerin	MMRN1	-1.33	3.14
Q9Y5B9	FACT complex subunit SPT16	SUPT16H	-1.31	4.57
Q96FQ6	Protein S100-A16	S100A16	-1.29	6.83
Q6IBA2	Activated RNA polymerase II transcriptional coactivator p15	PC4	-1.25	7.05
Q13151	Heterogeneous nuclear ribonucleoprotein A0	HNRNPA0	-1.21	4.49
B4DWN1	Vesicular integral-membrane protein VIP36	LMAN2	-1.20	2.20
C9J3L8	Translocon-associated protein subunit alpha	SSR1	-1.20	5.57
Q2TAM5	Transcription factor p65	RELA	-1.17	6.14
P29966	Myristoylated alanine-rich C-kinase substrate	MARCKS	-1.15	6.06
H0YN26	Acidic leucine-rich nuclear phosphoprotein 32 family member A	ANP32A	-1.12	6.03
Q53FJ5	Prosaposin;Saposin-A;Saposin-B-Val;Saposin-B;Saposin-C;Saposin-D	PSAP	-1.09	8.79
Q13404	Ubiquitin-conjugating enzyme E2 variant 1	UBE2V1	-1.09	3.47
A0A140VJK1	Glutaredoxin-3	GLRX3	-1.06	4.43
F8W6I7	Heterogeneous nuclear ribonucleoprotein A1;Heterogeneous nuclear ribonucleoprotein A1, N-terminally processed;Heterogeneous nuclear ribonucleoprotein A1-like 2	HNRNPA1	-1.05	5.46
A0A024R3J7	Dolichyl-diphosphooligosaccharide--protein glycosyltransferase subunit STT3A	hCG_2032701	-1.03	5.00
Q9Y3U8	60S ribosomal protein L36	RPL36	-1.01	5.47
P51858	Hepatoma-derived growth factor	HDGF	-1.00	4.74
F5GXX5	Dolichyl-diphosphooligosaccharide--protein glycosyltransferase subunit DAD1	DAD1	-0.99	2.82
Q5T7C4	High mobility group protein B1;Putative high mobility group protein B1-like 1	HMGB1	-0.99	7.17
B4DTT0	N-acetylglucosamine-6-sulfatase	DKFZp686E12166	-0.97	8.94
O14907	Tax1-binding protein 3	TAX1BP3	-0.97	3.69
A0A024R4X0	NADH-cytochrome b5 reductase;NADH-cytochrome b5 reductase 3;NADH-cytochrome b5 reductase 3 membrane-bound form;NADH-cytochrome b5 reductase 3 soluble form	CYB5R3	-0.97	7.22
H9ZYJ2	Thioredoxin	TXN	-0.96	5.01
B5BU25	Splicing factor U2AF 65 kDa subunit	U2AF2	-0.96	8.00
Q86U79	Adenosine kinase	ADK	-0.95	2.58
L7RT18	Adapter molecule crk	CRK	-0.94	4.18
V9HW48	SH3 domain-binding glutamic acid-rich-like protein	HEL-S-115	-0.93	2.73
A0A140VJF4	Biliverdin reductase A	BLVRA	-0.93	5.15
E9PI87	Oxidoreductase HTATIP2	HTATIP2	-0.92	2.13
J3KNF4	Copper chaperone for superoxide dismutase	CCS	-0.92	4.48

Q6FGV9	Phosphomevalonate kinase	PMVK	-0.92	2.92
P20700	Lamin-B1	LMNB1	-0.91	9.48
Q6FGY1	Hippocalcin-like protein 1	HPCAL1	-0.91	3.83
A0A024R258	Ubiquilin-1;Ubiquilin-4	UBQLN1	-0.90	5.55
Q53XX5	Cold-inducible RNA-binding protein	CIRBP	-0.90	3.80
Q59H57	RNA-binding protein FUS	FUS	-0.90	3.77
B4E324	Carboxypeptidase;Lysosomal protective protein;Lysosomal protective protein 32 kDa chain;Lysosomal protective protein 20 kDa chain	CTSA	-0.89	4.30
K7ESE8	Bleomycin hydrolase	BLMH	-0.89	3.32
P46926	Glucosamine-6-phosphate isomerase 1;Glucosamine-6-phosphate isomerase	GNPDA1	-0.88	4.45
B7Z4K8	Basic leucine zipper and W2 domain-containing protein 2	BZW2	-0.87	4.26
B7Z2Z1	Scaffold attachment factor B1	SAFB	-0.87	5.93
Q6IRT1	S-(hydroxymethyl)glutathione dehydrogenase;Alcohol dehydrogenase class-3	ADH5	-0.87	4.62
P15531	Nucleoside diphosphate kinase A	NME1	-0.86	1.85
A2A2D0	Stathmin	STMN1	-0.86	8.87
C9JFR7	Cytochrome c	CYCS	-0.84	6.18
A8K2W3	Serum deprivation-response protein	SDPR	-0.83	11.43
F5GYN4	Ubiquitin thioesterase OTUB1	OTUB1	-0.81	5.20
O75436	Vacuolar protein sorting-associated protein 26A	VPS26A	-0.81	2.38
V9HW74	Ubiquitin carboxyl-terminal hydrolase;Ubiquitin carboxyl-terminal hydrolase isozyme L1	HEL-117	-0.79	1.94
A0A0S2Z410	3-hydroxyacyl-CoA dehydrogenase type-2	HSD17B10	-0.79	4.64
H3BPQ3	Protein NDRG4	NDRG4	-0.78	3.46
Q5T9B9	Endoglin	ENG	-0.77	3.90
A0A087X296	Prostaglandin G/H synthase 1	PTGS1	-0.77	4.28
J3K000	Xaa-Pro dipeptidase	PEPD	-0.76	3.38
A0A024RAV2	ATP-dependent DNA helicase Q1	RECQL	-0.76	5.90
A0A024R3Z6	Basic leucine zipper and W2 domain-containing protein 1	BZW1	-0.75	5.44
P18077	60S ribosomal protein L35a	RPL35A	-0.75	2.68
Q6FH49	Nicotinamide N-methyltransferase	NNMT	-0.74	4.02
V9HWI0	Alcohol dehydrogenase [NADP(+)]	HEL-S-165mP	-0.74	7.43
B3KMZ6	SUMO-activating enzyme subunit 2	UBA2	-0.74	3.60
E9PJ81	UBX domain-containing protein 1	UBXN1	-0.74	2.45
B4DIZ2	Ubiquitin-conjugating enzyme E2 K	UBE2K	-0.74	3.24
A5PLK7	Protein RCC2	RCC2	-0.73	4.02
B0YJ88	Radixin	RDX	-0.73	3.67
A0A024R883	V-type proton ATPase subunit G 1	ATP6V1G1	-0.73	3.30
A0A024R3W7	Elongation factor 1-beta	EEF1B2	-0.73	3.44
Q5IST1	Serine/arginine-rich splicing factor 5	SFRS5	-0.71	2.49
A0A024R8W0	Eukaryotic initiation factor 4A-III;Eukaryotic initiation factor 4A-III, N-terminally processed	DDX48	-0.71	4.98
Q6FHX6	Flap endonuclease 1	FEN1	-0.70	2.56
Q53HS0	Glutamine--tRNA ligase	QARS	-0.70	5.15
O95831	Apoptosis-inducing factor 1, mitochondrial	AIFM1	-0.70	2.02

O15400	Syntaxin-7	STX7	-0.70	4.56
Q5T123	SH3 domain-binding glutamic acid-rich-like protein 3	SH3BGRL3	-0.69	4.48
Q9HDC9	Adipocyte plasma membrane-associated protein	APMAP	-0.69	2.58
Q05BM8	Polypeptide N-acetylgalactosaminyltransferase;Polypeptide N-acetylgalactosaminyltransferase 1;Polypeptide N-acetylgalactosaminyltransferase 1 soluble form	GALNT1	-0.69	3.82
Q9BRL5		CALM3	-0.69	2.73
J3QRT5	Intercellular adhesion molecule 2	ICAM2	-0.69	2.31
F8WCF6	Actin-related protein 2/3 complex subunit 4	ARPC4-TTLL3	-0.68	6.06
I3L2L5	Protein FAM195B	FAM195B	-0.68	3.19
B3KN57	Sorting nexin-2	SNX2	-0.68	5.10
F8VQE1	LIM domain and actin-binding protein 1	LIMA1	-0.68	2.45
D3DP46	Signal peptidase complex subunit 3	SPCS3	-0.68	2.27
A0A024R9D2	Protein LYRIC	MTDH	-0.67	3.46
P35580	Myosin-10	MYH10	-0.67	7.58
K7ES31	Eukaryotic translation initiation factor 3 subunit K	EIF3K	-0.67	3.30
J3KT73	60S ribosomal protein L38	RPL38	-0.66	6.00
P62263	40S ribosomal protein S14	RPS14	-0.66	7.96
P62495	Eukaryotic peptide chain release factor subunit 1	ETF1	-0.66	5.27
Q53XC0	Eukaryotic translation initiation factor 2 subunit 1	EIF2S1	-0.66	5.24
Q96C90	Protein phosphatase 1 regulatory subunit 14B	PPP1R14B	-0.65	2.71
F5H2R5	Rho GDP-dissociation inhibitor 2	ARHGDIB	-0.65	2.80
A4D275	Actin-related protein 2/3 complex subunit 1B	ARPC1B	-0.64	2.92
Q14240	Eukaryotic initiation factor 4A-II;Eukaryotic initiation factor 4A-II, N-terminally processed	EIF4A2	-0.64	3.21
B4E3A8	Leukocyte elastase inhibitor	HEL57	-0.64	2.22
A0A024R1K8	Splicing factor 3A subunit 1	SF3A1	-0.64	*2.65*
H7BY10	60S ribosomal protein L23a	RPL23A	-0.64	3.71
Q96IZ0	PRKC apoptosis WT1 regulator protein	PAWR	-0.64	4.69
A8K719	Core-binding factor subunit beta	CBFB	-0.64	2.71
A0A024RDB0	Ubiquitin-like modifier-activating enzyme 6	UBE1L2	-0.64	7.12
A0A0A6YYJ8	Putative RNA-binding protein Luc7-like 2	LUC7L2	-0.64	3.62
A0A140VJP5	S-adenosylmethionine synthase isoform type-2;S-adenosylmethionine synthase	MAT2A	-0.64	4.18
Q53R19	Actin-related protein 2/3 complex subunit 2	ARPC2	-0.62	3.86
A0A1X7SBZ2	Probable ATP-dependent RNA helicase DDX17	DDX17	-0.62	9.54
A9UK01	Rho GTPase-activating protein 18	ARHGAP18	-0.61	5.11
A0A024RB85	Proliferation-associated protein 2G4	PA2G4	-0.61	6.66
V9HW41	Ubiquitin-conjugating enzyme E2 N	HEL-S-71	-0.61	3.01
Q5VVD0	60S ribosomal protein L11	RPL11	-0.61	4.27
P51991	Heterogeneous nuclear ribonucleoprotein A3	HNRNPA3	-0.61	9.09
A0A024R5Q7	Adenylosuccinate synthetase isozyme 2	ADSS	-0.61	6.02
Q59GU6	Sorting nexin-1	SNX1	-0.61	3.93
P13010	X-ray repair cross-complementing protein 5	XRCC5	-0.60	6.59
C9J9K3	40S ribosomal protein SA	RPSA	-0.60	7.71

Published in final edited form as:
Stem Cells. 2016 May ; 34(5): 1163–1176. doi:10.1002/stem.2286.

Metabolic reprogramming and dependencies associated with epithelial cancer stem cells independent of the epithelial-mesenchymal transition program

Esther Aguilar[1], **Igor Marin de Mas**[1], **Erika Zodda**[1,2], **Silvia Marin**[1], **Fionnuala Morrish**[3], **Vitaly Selivanov**[1], **Óscar Meca-Cortés**[2], **Hossain Delowar**[2], **Mònica Pons**[2], **Inés Izquierdo**[1], **Toni Celià-Terrassa**[2,§], **Pedro de Atauri**[1], **Josep J Centelles**[1], **David Hockenbery**[3], **Timothy M Thomson**[2,*], and **Marta Cascante**[1,*]

[1]Department of Biochemistry and Molecular Biology, Faculty of Biology, University of Barcelona, Diagonal 643, Barcelona 08028, Spain

[2]Department of Cell Biology, Molecular Biology Institute, National Research Council (IBMB-CSIC), Baldiri Reixac 15-21, Barcelona 08028, Spain

[3]Fred Hutchinson Cancer Research Center, 1100 Fairview Avenue N, Seattle, WA 98109, USA

Abstract

In solid tumors, cancer stem cells (CSCs) can arise independently of epithelial-mesenchymal transition (EMT). In spite of recent efforts, the metabolic reprogramming associated with CSC phenotypes uncoupled from EMT is poorly understood. Here, by using metabolomic and fluxomic approaches, we identify major metabolic profiles that differentiate metastatic prostate epithelial CSCs (e-CSCs) from non-CSCs expressing a stable EMT. We have found that the e-CSC program in our cellular model is characterized by a high plasticity in energy substrate metabolism, including an enhanced Warburg effect, a greater carbon and energy source flexibility driven by fatty acids and amino acid metabolism and an essential reliance on the proton buffering capacity conferred by glutamine metabolism. An analysis of transcriptomic data yielded a metabolic gene signature for our e-CSCs consistent with the metabolomics and fluxomics analysis that correlated with tumor progression and metastasis in prostate cancer and in 11 additional cancer types. Interestingly, an integrated metabolomics, fluxomics and transcriptomics analysis allowed us to identify key metabolic players regulated at the post-transcriptional level, suggesting potential biomarkers and therapeutic targets to effectively forestall metastasis.

[*]Corresponding authors: Marta Cascante, Ph.D., University of Barcelona, Diagonal 643, Barcelona 08028, Spain. Telephone: +34-93-402-1593; Fax: +34-93-402-1559; martacascante@ub.edu; and Timothy M Thomson, M.D., Ph.D., IBMB-CSIC, Baldiri Reixac 15-21, Barcelona 08028, Spain. Telephone: +34-93-402-0199; Fax: +34-93-403-4979; titbmc@ibmb.csic.es.
[§]Current address: Department of Molecular Biology, Princeton University, Washington Road, Princeton, NJ 08544, USA

Author Contributions

E.A.: conception and design, collection and assembly of data, data analysis and interpretation and manuscript writing; I.M.M., V.S., P.A. and J.J.C.: data analysis and interpretation; E.Z., H.D., M.P. and I.I.: collection and assembly of data; S.M.: conception and design and manuscript writing; F.M. and D.H.: conception and design, provision of study material and manuscript writing; O.M-C. and A.C-T.: provision of study material; T.M.T and M.C.: conception and design, data analysis and interpretation, manuscript writing and final approval of manuscript.

Keywords

Cancer stem cells; epithelial-mesenchymal transition; metabolic flux analysis; Warburg effect; mitochondrial metabolism; glutaminolysis

Introduction

Tumors represent heterogeneous collections of neoplastic and non-neoplastic cells with divergent phenotypes engaged in complex interactions [1]. Two major operative categories of cancer cells are cancer stem cells (CSCs), endowed with self-renewal and tumor-initiating potentials, and non-CSCs [2]. These two broad functional classes of tumor cells do not necessarily reside in mutually exclusive subpopulations as cell plasticity allows phenotypic switching between CSC and non-CSC states [3].

It has been shown that the epithelial-mesenchymal transition (EMT) can endow cancer cells with stem cell properties, switching from an epithelial program to a motile mesenchymal phenotype [4]. However, increasing evidence suggests that CSC populations in solid tumors may be heterogeneous, including a substantial proportion of epithelial stem cells in which stemness is uncoupled from EMT, suggesting new mechanism driving metastatic colonization [5]. In addition, recent studies have demonstrated cooperative interactions between cell subpopulations displaying epithelial CSCs (e-CSCs) and non-CSCs that potentiate the metastatic behavior of the combined tumor cell populations [6–9]. The existence of intrinsic tumor cell heterogeneity has important implications in cancer drug resistance and therefore the identification of the most salient signaling and biochemical networks that characterize CSC and EMT phenotypes, including their prevalent metabolic states, is essential in order to design tumor subpopulation-specific therapies.

Although several common metabolic features of cancer cells have been extensively described, such as energy production via enhanced glycolysis (Warburg effect) [10, 11], few studies have been reported on metabolic states specific to CSCs and even fewer to metastatic CSCs. For example, CSCs have been reported either to display enhanced aerobic glycolysis with a concomitant reduction in mitochondrial activity [12] or to preferentially maintain oxidative phosphorylation (OXPHOS) and β-oxidation [13]. On the other hand, the induction of an epithelial-mesenchymal transition (EMT), which can lead to the acquisition of CSC properties in cancer cells [4], has been associated with reduced mitochondrial metabolism and enhanced glycolysis through the suppression of fructose-1,6-bisphosphatase [14] or the inhibition of cytochrome C oxidase [15]. Moreover, inhibition of the enzyme citrate synthase [16] or succinate dehydrogenase subunit B [17] results in a bioenergetic disorder that contributes to the acquisition of an EMT phenotype. There are also evidences that EMT-driven CSCs can metabolize alternative high-energy metabolites, displaying the phenomenon known as “reverse Warburg effect” [18]. In contrast, it has also been shown that mitochondrial biogenesis sustains stem-like properties [19] or support propagation and motility of circulating cancer cells expressing EMT traits [20]. All these observations lead to a complex scenario in which it is difficult to clearly associate a specific metabolic reprogramming associated with CSCs independent of EMT that supports the processes of

invasion and metastasis. Hence, a consensus is still lacking on major characteristics that distinguish CSCs from non-CSCs.

To address this deficit, we have performed a comprehensive metabolic characterization of a dual cell model derived from the PC-3 cell line [6] consisting in one highly metastatic subpopulation (PC-3M) enriched in e-CSC features and a second non-metastatic and highly invasive subpopulation (PC-3S) lacking features of CSC (non-CSCs) and displaying a stable EMT. Regardless of tissue of origin of these cells, this model is unique in that CSC and EMT properties are fully uncoupled and displayed by distinct cell subpopulations and thus it offers an ideal cell model to uncover molecular mechanisms and pathways, including metabolic reprogramming, that can be specifically ascribed to either process.

From the integrated analysis of their main bioenergetic pathways and carbon sources, studied by a combination of metabolomics and fluxomics approaches, we have found that our e-CSC subpopulation, in contrast to the mesenchymal-like non-CSC subpopulation, exhibits a strong Warburg effect and a high potential to use alternative mitochondrial substrates, both metabolic features being essential to sustain its stem cell phenotype. Our results also highlight the contribution of amino acids metabolism and specially point out the importance of glutamine to compensate the acidic stress derived from the Warburg effect in the e-CSCs. A computational analysis based on transcriptomic data has identified a metabolic gene signature significantly associated with e-CSC that supports our metabolic analysis and correlates with tumor progression and metastasis in prostate cancer and other 11 tumor types. We thus provide an integrated view and selective metabolic dependencies and vulnerabilities of e-CSCs that may open new avenues to design therapeutic strategies aimed at targeting specific CSC and non-CSC subpopulations.

Materials and Methods

(detailed descriptions of all Materials and Methods are provided as online Supplemental Materials)

Cells and cell culture

PC-3M and PC-3S, clonally derived from the human cell line PC-3, and PC-3M cell variants were obtained as described [6]. Cells were cultured at 37°C in a 5% CO_2 atmosphere in RPMI 1640 media (Sigma-Aldrich or Biowest) supplemented with 10 mM glucose and 2 mM glutamine (unless otherwise indicated), 10% Fetal Bovine Serum (FBS) (PAA Laboratories), 1% pyruvate (1 mM) (Biological Industries), 1% streptomycin (100 μg/mL) / penicillin (100 units/mL) (Gibco) and 1% nonessential amino acids (Biological Industries).

Cell proliferation and viability assay

Proliferation and viability were assessed by Hoechst staining measuring emitted fluorescence.

Spheroid formation assay

Cells (6×10^3/well) were seeded on 24-well Ultra Low Attachement culture plates (Corning) in media containing EGF, BFGF, heparine, B27, insulin and hydrocortisone and allowed to grow for 7 days: At the end of the experiment, spheroids were stained, incubating cells with 0.5 mg/mL MTT (3-[4,5-dimethylthiazol-2-yl]-2,5-diphenyltetrazolium bromide) for 2–4 h and then each well was scanned for posterior spheroid quantification, using ImageJ software (free software that can be downloaded from http://imagej.nih.gov/ij/download.html).

Oxygen consumption rate (OCR) and extracellular acidification rate (ECAR)

These parameters were determined with a XF24 Extracellular Flux Analyzer (Seahorse Bioscience).

Concentration of media metabolites

Glucose, lactate, glutamate and glutamine media concentrations were determined by NADH-coupled reactions. All other amino acids were determined by ion-exchange chromatography.

Intracellular ATP, ROS and glutathione levels

ATP levels were quantified with the CellTiter-Glo Luminescent Cell Viability Assay (Promega, Madison, WI). Total intracellular ROS levels were determined using the cell-permeant probe 2',7'-dichlorodihydrofluorescein diacetate (H_2DCFDA) (Invitrogen) and flow cytometry. Total glutathione content was determined by the glutathione reductase enzymatic method.

Enzyme activities

LDH, TKT, G6PDH and GPT specific activities were determined by using NAD(P)H-coupled reactions.

^{13}C-tracer-based metabolomics: GC/MS analysis

Cells were cultured in media containing either 100% or 50% [1,2-$^{13}C_2$]-glucose, 100% [U-$^{13}C_6$]-glucose or 100% [U-$^{13}C_5$]-glutamine. ^{13}C-isotopologue distributions of metabolites were determined by mass spectrometry-coupled gas chromatography (GC/MS). GC/MS spectral data were corrected by regression analysis to eliminate contribution from natural enriched isotopes in derivatization reagents.

Quantification of metabolic fluxes

Metabolic flux distribution was evaluated through computer simulations of the measured distribution of ^{13}C isotopologues of metabolites implemented in Isodyn [21].

Statistical analysis

Two-tailed Student’s t-test for independent samples was applied where appropriate. In figures, bars represent mean ± standard deviation (SD), * indicates significance at p-value < 0.05, **; $p < 0.01$ and ***; $p < 0.001$; ns, not significant. All experiments shown were performed at least in triplicate

Results

Glycolysis is essential to support cell growth and stemness features of e-CSCs

As a cellular model to help elucidate major bioenergetic pathways of cells that display CSC properties uncoupled from EMT, we resorted to a dual cell model derived from the PC-3 cell line [6] consisting in one highly metastatic subpopulation (PC-3M) enriched in e-CSC features and a second non-metastatic and highly invasive subpopulation (PC-3S) lacking features of CSC (non-CSCs) and displaying a stable EMT. The CSC features of PC-3M cells have been thoroughly characterized by us [6] and supported by their expression of markers characteristic of stem cells such as KLF4, MYC, SOX2 or LIN28, strong enrichment in an embryonic cell (ES)-like gene module [22] and a MYC-centered gene module [23]. Regardless of tissue of origin of these cells, this model is unique in that CSC and EMT properties are fully uncoupled and displayed by distinct cell subpopulations and thus it offers an ideal cell model to uncover molecular mechanisms and pathways, including metabolic reprogramming, that can be specifically ascribed to either process.

We first studied the state of glycolysis in our PC-3M (e-CSCs) and PC-3S (non-CSCs) dual-cell model. The extracellular acidification rate (ECAR), a surrogate for lactic acid derived from glycolysis, was significantly higher in PC-3M cells than in PC-3S cells (Fig. 1A). Consistently, PC-3M cells consumed more glucose and produced more lactate (Fig. 1B) and exhibited a significantly higher lactate dehydrogenase (LDH) activity than PC-3S cells (Fig. 1C). Studies with incorporation of [1,2-$^{13}C_2$]-glucose indicated that both glycolysis and the pentose phosphate pathway (PPP) contribute to the increased lactate production in PC-3M cells (Fig. 1D and Supplemental Table 1). These data suggest a more robust Warburg effect in PC-3M cells as compared to PC-3S cells.

To further analyze the preference of PC-3M cells for glycolysis over oxidative phosphorylation, we evaluated the level of suppression of mitochondrial respiration after treatment with high glucose concentrations, or Crabtree effect [24]. Glucose treatment elicited a significantly greater reduction of mitochondrial respiration in PC-3M cells than PC-3S cells (Fig. 1E), illustrating a preference of the e-CSC subpopulation for metabolizing glucose through glycolysis. Glucose deprivation or treatment with the glycolytic inhibitor 2-deoxyglucose (2-DG) decreased the proliferation of PC-3M cells more than PC-3S cells (Fig. 1F), partly explained by cell death (Supplemental Fig. 1A) and an accumulation in the G1 phase of the cell cycle (Supplemental Fig. 1B).Treatment with 2-DG decreased cellular ATP levels in both cell subpopulations but more so in PC-3M cells (Fig. 1G). Cell growth in anchorage-independent conditions is a functional assay that correlates with stemness. PC-3M cells have a better ability than PC-3S cells to form spheroids under such conditions (Fig. 1H). Furthermore, we found that disruption of glycolysis by 2-DG treatment significantly affected the capacity of PC-3M cells to grow in suspension (Fig. 1I), highlighting the importance of glycolysis for capacity of PC-3M cells to grow in suspension as spheroids.

To determine the involvement of EMT and self-renewal gene networks for the above glycolytic phenotype, PC-3M cells were induced to acquire an EMT through forced overexpression of Snai1 (PC-3M/Snai1), or their self-renewal properties inhibited through

knockdown of the pluripotency factors SOX2, KLF4 and MYC (PC-3M/SKMkd). Both genetic manipulations caused a reduced glycolytic phenotype (Fig. 1J) and diminished the sensitivity of PC-3M cells to 2-DG (Fig. 1K). Therefore, the marked glycolytic phenotype and glucose dependence observed in PC-3M cells requires the maintenance of robust epithelial and self-renewal gene programs.

Mesenchymal-like non-CSCs are more dependent on mitochondrial function than e-CSCs

The above results demonstrate a marked Warburg effect and a higher dependence on glycolysis in PC-3M cells than PC-3S cells. We further investigated the reliance of these cells on mitochondrial respiration using four mitochondrial drugs (Fig. 2A). Oligomycin, an ATP synthase inhibitor, reduced more oxygen consumption rate (OCR) (Fig. 2B) and had a more significant dose-dependent proliferation inhibitory effect (Supplemental Fig. 2) in PC-3S cells than PC-3M cells, suggesting a greater dependence on mitochondrial metabolism for cell growth of the non-CSC subpopulation. However, this drug did not significantly affect ATP levels in either subpopulation (Fig. 2C). Exposure of cells to trifluorocarbonylcyanide phenylhydrazone (FCCP), a mitochondrial uncoupling agent, boosted OCR more in PC-3S cells than PC-3M cells (Fig. 2B), indicative of a significantly higher mitochondrial respiratory capacity of the non-CSC subpopulation. Moreover, exposure to the mitochondrial complex I and III inhibitors rotenone and antimycin reduced OCR in both cell subpopulations, although significantly more in PC-3S cells (Fig. 2B). Consistent with mitochondrial metabolic activity being the main source of reactive oxygen species (ROS) [25], PC-3S cells exhibited higher basal levels of ROS than PC-3M cells (Fig. 2D). In support of the importance of the epithelial and pluripotency gene programs for these metabolic readouts, PC-3M/Snai1 and PC-3M/SKMkd variants were more sensitive than parental PC-3M cells to all mitochondrial drugs (Fig. 2E).

We next stained cells with MitoTracker to investigate the possible association of mitochondrial morphology with the above bioenergetics phenotypes (Supplemental Figure 2). PC-3M cells exhibited fragmented mitochondrial networks consistent with extensive mitochondrial fission, which has been associated with less efficient OXPHOS and a higher reliance on anaerobic glycolysis for bioenergetics [26]. In contrast, the mitochondrial morphologies in PC-3S cells were more compact, consistent with active fusion events [27], a process coupled to a robust mitochondrial function and bioenergetics [28]. Thus, the non-CSC subpopulation displays a mitochondrial organization predicted to support a better coupled mitochondrial respiratory chain for the generation of ATP.

A higher flexibility of mitochondrial metabolism is required for spheroid growth of e-CSCs

To investigate the degree of metabolic flexibility of these cells in the use of alternative carbon substrates, we evaluated the consumption of glutamine under glucose deprivation and with 2-DG treatment. These conditions caused enhanced glutamine consumption in PC-3M cells but not PC-3S cells (Fig. 2F), suggesting that PC-3M cells are more adept at using alternative carbon substrates. This was further explored by evaluating baseline OCR in full media (with glucose and glutamine), in restricted media (lacking glucose or glutamine) or minimal media (lacking glucose and glutamine). PC-3M cells showed higher baseline OCR values than PC-3S cells in all restricted media conditions, while no differences were

detected in full media (Fig. 2G). This illustrates a robust switching to alternative carbon sources in PC-3M cells and also indicates that, although PC-3M cells preferentially metabolize glucose through glycolysis rather than oxidative metabolism, their mitochondrial respiration is functional and can be boosted when prompted. Interestingly, baseline OCR values for PC-3S cells in the absence of glutamine were lower than those in full media conditions ($p = 0.004$) (Fig. 2G), suggesting that glutamine is essential for the mitochondrial respiration of PC-3S cells but not PC-3M cells.

To test the ability of PC-3M cells to use alternative mitochondrial substrates, we analyzed the consumption of ketogenic amino acids, which can be degraded into acetyl-CoA. PC-3M cells consumed more glutamine (Fig. 2F) and the ketogenic amino acids leucine, isoleucine, lysine, threonine, tyrosine, tryptophan and phenylalanine than PC-3S cells (Fig. 2H). We examined the contribution of fatty acid β-oxidation by exposing cells to the carnitine palmitoyltransferase 1 (CPT1) inhibitor etomoxir, which impairs fatty acid β-oxidation, thus reducing OCR [29]. Etomoxir treatment decreased OCR in PC-3M cells more than in PC-3S cells (Supplemental Fig. 2). Consistently, PC-3M cells expressed higher CPT1 protein levels than PC-3S cells (Supplemental Fig. 2). To test if oxidation of fatty acids and glutamine as well as global synthesis of mitochondrial ATP are essential for the ability of PC-3M cells to grow in suspension, we treated these cells with the drugs bis-2-(5-phenylacetamido-1,3,4-thiadiazol-2-yl)ethyl sulfide (BPTES) (glutaminase inhibitor), etomoxir and oligomycin (Fig. 2I). Spheroid growth was significantly inhibited after these treatments, demonstrating that the alternative metabolic activities regarding mitochondrial metabolism are essential to sustain the stemness state of e-CSCs in our cell model.

The tricarboxylic acid (TCA) cycle in e-CSCs is mainly fueled by glutamine due to post-transcriptional inactivation of pyruvate dehydrogenase (PDH)

To investigate the contribution of glucose to TCA cycle intermediates, cells were cultured with [1,2-$^{13}C_2$]-glucose and the isotopologue distribution for citrate, glutamate, fumarate, malate and aspartate determined by GC/MS (Supplemental Table 2). We observed that PC-3S cells incorporated label into TCA cycle intermediates more efficiently than PC-3M cells (Supplemental Table 2, 24 h). The labeling of pyruvate was similar in both cell types, suggesting that the e-CSC subpopulation diverts more pyruvate derived from glycolysis away from mitochondria than the non-CSC subpopulation, consistent with a marked Warburg effect. The relative rates of pyruvate oxidation in the TCA cycle were investigated by calculating the ratio of the m2 isotopologues of the above mentioned metabolites (m2TCA) to the m2 pyruvate isotopologue (m2Pyr) (Fig. 3A). We found lower ratios of m2TCA to m2Pyr in PC-3M cells than in PC-3S cells (Fig. 3B), indicative of decreased incorporation of labeled pyruvate into the TCA cycle.

Next, to investigate the contribution of glutamine to the TCA cycle in our cell model, we analyzed the incorporation of ^{13}C in the TCA cycle intermediates after incubation with [U-$^{13}C_5$]-glutamine (Supplemental Table 3). We compared m4 isotopologues (fumarate, malate, citrate, aspartate) and m5 isotopologues (glutamate) to evaluate the glutamine oxidative pathway (Fig. 3C). We observed that the contribution of glutamine to these labeling patterns was more pronounced in PC-3M cells than in PC-3S cells (Fig. 3D, left).

Analysis of m5 citrate and m3 aspartate, malate and fumarate indicated that the metabolism of glutamine through reductive carboxylation (Fig. 3C) is more active in PC-3M cells than in PC-3S cells (Fig. 3D, right). These results are consistent with a higher ability of PC-3M cells for using alternative metabolic pathways to sustain energy production and to rapidly adapt to changes in nutrient availability.

PDH is a key enzyme that mediates the entry of pyruvate to mitochondria whose activity is regulated by its phosphorylation status through the activity of pyruvate dehydrogenase kinase (PDHK) [30]. Treatment of cells with the PDHK inhibitor dichloroacetic acid (DCA) or the LDH inhibitor oxamate resulted in a more pronounced increase in mitochondrial respiration in PC-3M cells than in PC-3S cells, particularly in response to DCA (Fig. 3E–F). This suggests that PDH has a lower baseline activity in PC-3M cells than in PC-3S cells. Indeed, PDH was markedly more phosphorylated (i.e. less active) in PC-3M cells than in PC-3S cells (Fig. 3G, inset) and transcript levels for PDHK1 were higher and the PDH phosphatase PDP2 lower in PC-3M cells than in PC-3S cells (Fig. 3G).

We next used Isodyn [21] to integrate ^{13}C-based isotopologue distributions (Supplemental Tables 2 and 3) and biochemical data (Supplemental Table 4) to estimate comparative metabolic flux distributions relative to glucose uptake in central carbon metabolic networks in both cell types (Supplemental Fig. 3). The resulting metabolic flux simulations involving TCA cycle-related reactions lend further support to the occurrence of an enhanced entry of pyruvate *via* PDH into the TCA cycle, increased TCA cycle fluxes (CS, citakg and akgfum) and a higher flux associated with mitochondrial respiration (resp) in PC-3S cells than in PC-3M cells, consistent with a higher diversion of glucose into mitochondrial metabolism (Fig. 3H).

Glutaminolysis protects cells from acidity generated from a marked Warburg effect: an Achilles heel of e-CSCs

To explore the role of an enhanced glutamine metabolism in PC-3M cells, we first determined the expression levels of glutaminase (GLS1), a direct MYC target frequently expressed at high levels in rapidly proliferating cells and CSCs [31, 32]. GLS1 was expressed at significantly higher levels in PC-3M cells than PC-3S cells, in particular the glutaminase C (GAC) isoform (Fig. 4A–B). The higher expression levels of GAC *vs.* the kidney-type glutaminase (KGA) in PC-3M cells were partly dependent on the maintenance of an epithelial gene program, as shown by a diminished GAC/KGA ratio in PC-3M/Snai1 cells as compared to control PC-3M cells (Fig. 4B). Exposure to the glutaminase inhibitor BPTES inhibited the proliferation of PC-3M cells more significantly than that of PC-3S cells (Fig. 4C), associated with a decreased proportion of cells in the S phase of the cell cycle (Supplemental Fig. 4). The sensitivity of PC-3M cells to growth inhibition by BPTES was attenuated by overexpression of Snai1 (Fig. 4C), illustrating that the strong dependence on glutaminolysis of PC-3M cells relies on the maintenance of an epithelial gene program.

Both PC-3M and PC-3S cells increased lactate production upon treatment with BPTES (Fig. 4D), suggesting the participation of metabolic compensatory mechanisms, and thus we tested the effects on viability of a combined inhibition of glutaminolysis and glycolysis. We observed a marked additive effect on cell death by combining BPTES and 2-DG treatments

in PC-3M cells but not in PC-3S cells (Fig. 4E), indicating that glycolysis and glutaminolysis are essential for the optimal growth and survival of PC-3M cells.

Glutamine metabolism has been described to be important for several cancer cell types, but its differential essentiality for heterogeneous tumor cell subpopulations has not been addressed thus far [33, 34]. Because glutamine is an anaplerotic TCA cycle substrate [35], growth inhibition by BPTES is expected to be rescued by the cell-permeable α-ketoglutarate (α-KG) analog dimethyl α-ketoglutarate (DMK). Remarkably, cell growth was not rescued by DMK in BPTES-treated PC-3M or PC-3S cells (Fig. 4F), suggesting that glutamine exerts a survival function independent of its anaplerotic function. Glutamine contributes to other metabolic pathways, including synthesis of glutathione, NADPH production and pH homeostasis [36, 37]. In their basal state, PC-3S cells contained higher levels of ROS (Fig. 2D) and total intracellular glutathione (Fig. 4G) than PC-3M cells. Thus, the non-CSC subpopulation potentially counteracts higher levels of ROS with an accumulation of glutathione. Although ROS levels did not increase significantly in either cell subpopulation after BPTES treatment (Fig. 4H), glutathione content was significantly reduced in PC-3S cells (Fig. 4I), demonstrating the importance of glutamine metabolism for glutathione synthesis in these cells.

We next investigated the existence of an alternative mechanism underlying the differential sensitivity of PC-3M cells to glutaminase inhibition. An additional function of glutamine is to provide resistance to acidic conditions through the release of ammonia [36]. Compared to cells grown in standard pH 7.9 media, incubation in more acidic media (pH 7.1) had a more significant impact on the proliferation of PC-3M cells than PC-3S cells (Fig. 4J). Addition of BPTES elicited an additive growth inhibitory effect that was more pronounced for PC-3M cells (Fig. 4J), as did depletion of sodium bicarbonate ($NaHCO_3$) (Fig. 4J). PC-3M/Snai1 and PC-3M/SKMkd cells showed enhanced resistance to BPTES treatment at low pH compared to control PC-3M cells (Fig. 4K), confirming the importance of the epithelial and pluripotency gene programs in conferring sensitivity to glutaminase inhibition. These observations suggest that the glutaminase reaction contributes to the buffering of surplus protons produced by PC-3M cells through their marked Warburg effect and consequent lactate production.

e-CSCs are characterized by an enhanced serine, glycine and one-carbon (SGOC) metabolism

Metabolic reprogramming during tumor progression induces alterations in biochemical states and preferences for amino acids that are closely linked to the Warburg effect [38, 39]. Glucose metabolism can be diverted from the glycolytic intermediate 3-phosphoglycerate towards the synthesis of serine, which in turn may be converted to glycine and participate in one-carbon metabolism [40]. Both amino acids provide essential precursors for the synthesis of proteins, nucleic acids and lipids [41] and the importance of the SGOC network in cancer has been analyzed in depth [42]. We analyzed the consumption and production profiles of serine and glycine and their isotopologue distributions after incubating cells with a ^{13}C-enriched glucose tracer (Supplemental Table 5). PC-3M cells consumed more extracellular serine than PC-3S cells, while extracellular glycine was consumed by PC-3M cells and

produced by PC-3S cells (Fig. 5A). After incubation of cells with [U-$^{13}C_6$]-glucose, m3 serine was predominant in PC-3M cells, whereas more evenly distributed representations of m1, m2 and m3 serine isotopologues were found in PC-3S cells (Fig. 5B). The largely homogeneous m3 labeling of serine in PC-3M cells suggests that serine does not accumulate in these cells and is efficiently used as a building block for protein synthesis and/or funneled to catabolic reactions that rapidly transform serine to glycine (Supplemental Fig. 5). In line with this, failure to secrete glycine and relatively low levels of m2 glycine in PC-3M cells (Fig. 5C) suggest that glycine derived from serine is also rapidly used in these cells for biosynthetic purposes or cleaved to further contribute to one-carbon metabolic reactions. In support of this proposal, PC-3M cells expressed 5-fold higher levels than PC-3S cells of glycine decarboxylase (GLDC), the key enzyme catalyzing glycine cleavage (Fig. 5D). Moreover, PC-3M cells also expressed higher levels of many other enzymes involved in serine and one-carbon metabolism (Fig.5D) [40, 43, 44]. Thus, these results suggest that PC-3M cells have a more active SGOC metabolism than PC-3S cells.

Higher NADPH-generating reactions fuel an enhanced fatty acid synthesis and face oxidative stress in non-CSCs

The oxidative branch of the PPP uses glucose-6-phosphate as a substrate to generate NADPH, providing reducing power for other biosynthetic pathways (e.g. fatty acid synthesis) and to counter free radicals and oxidative stress. The non-oxidative branch of the PPP recycles pentose phosphates to glycolytic intermediates. Importantly, the PPP generates ribose-5-phosphate for nucleotide synthesis. Two key PPP enzymes are glucose-6-phosphate dehydrogenase (G6PDH) in the oxidative branch and transketolase (TKT) in the non-oxidative branch. Label incorporation to ribose from [1,2-$^{13}C_2$]-glucose was significantly greater in PC-3M cells than in PC-3S cells (Fig. 6A and Supplemental Table 2B), suggestive of a larger demand for nucleotide biosynthesis to sustain their higher proliferation rate. Analysis of ribose isotopologue distribution revealed an increase in m1 (oxidative PPP) and m2 (non-oxidative PPP) isotopologues in PC-3M cells (Fig. 6B). However, the analysis of the m1/m2 ribose ratio also indicated a differential contribution of the oxidative and non-oxidative branches of the PPP in these cells (Fig. 6C), suggesting that the highly glycolytic PC-3M cells redirect back part of the glucose-based PPP intermediates to glycolysis through the non-oxidative branch, thus resulting in a higher production of lactate through this pathway (Fig. 1D). The differential use of the PPP branches was further supported by the observation of significantly higher enzymatic activity and expression levels of G6PDH in PC-3S cells and TKT in PC-3M cells (Fig. 6D–F).

The above results suggest a higher demand of NADPH in PC-3S cells, likely in order to face higher levels of oxidative stress resulting from accumulation of ROS. Isodyn analysis indicated that the fluxes for NADPH-producing reactions, such as cytosolic malic enzyme (ME) and isocitrate dehydrogenase (participating in the citakg flux), are higher in PC-3S cells than in PC-3M cells (Fig. 3I). Isodyn also predicted an enhanced efflux of citrate from the mitochondrial to the cytosol compartment (citdmc flux) in these cells (Fig. 3I). NADPH reducing equivalents actively participate in many biosynthetic reactions, such as fatty acid synthesis. After incubation of cells with [1,2-$^{13}C_2$]-glucose, greater yields of m2 and m4 labeled palmitate (Fig. 6G) and stearate (Fig. 6H) were detected in PC-3S cells than in

PC-3M cells, suggesting that glucose-derived carbons are more efficiently routed towards fatty acid synthesis in PC-3S cells. Protein expression levels of ATP citrate lyase (ACLY), the primary enzyme responsible for cytosolic fatty acid biosynthesis, were also higher in PC-3S cells than PC-3M cells (Fig. 6I), confirming a greater coupling between glycolysis and fatty acid synthesis.

Trancriptome analysis reveals significant associations between the metabolic fingerprint of e-CSCs and malignant progression of several cancers

To determine the potential significance to tumor progression of those metabolic pathways differentially expressed in the e-CSC *vs.* non-CSC prostate model, we performed a Rank Product analysis [45] of transcriptomic data generated for the PC-3M and PC-3S subpopulations [6]. The resulting PC-3M-overexpresed metabolic gene signature included enzymes involved in the metabolism of serine and glycine (GLDC, CBS), branched-chain amino acids (BCAT1), and glutamate and proline (ASS1, AGMAT), which support the metabolic flexibility accompanying the CSC phenotype. It also included genes that participate in the synthesis of purine nucleotides (GUCY1A3 and PDE3B) as part of reactions that converge on substrates that are actively metabolized in PC-3M cells, such as glycine and one-carbon units from tetrahydrofolate. This analysis allows to examine the metabolic underpinnings of the cellular programs that increase cancer cell aggressiveness and to understand how cellular metabolism contributes to these and other proliferation-independent features of cancer.

Next, by applying Gene Set Enrichment Analysis (GSEA) (Subramanian et al 2005), we found that the PC-3M-overexpressed metabolic gene set was significantly enriched concomitant with malignant progression in prostate cancer (Fig. 7) and in 11 other types of human tumors, including ovarian, bladder, adrenocortical, head and neck, stomach or rectal carcinoma, or melanoma (Supplemental Table 7). These observations link the metabolic pathways and reactions differentially expressed in our CSC vs. non-CSC cell model to human tumor progression.

Discussion

The cancer stem cell hypothesis implies intratumoral phenotypic heterogeneity. Neoplastic cells can reversibly switch between CSC and non-CSC states [3], presenting a hurdle to efforts at targeting specific tumor subpopulations that may escape from therapeutic pressure [46]. A successful strategy to forestall these resistance mechanisms should incorporate the characterization of biochemical and gene networks, including those related with cell metabolism, to uncover endogenous vulnerabilities pertaining to both CSCs and non-CSCs.

Previous studies have failed to discriminate whether the metabolic reprogramming observed in tumor cells with CSC features were explained by EMT [14, 16, 20, 47] or CSC states, which recent studies have found that may occur in cancer cells unlinked to EMT [6, 48]. In order to address this issue, we have undertaken a systematic comparative metabolic characterization of a dual-cell tumor cell model in which CSC and EMT programs are clearly uncoupled. Our comparative analysis sheds light on major metabolic pathways and vulnerabilities accompanying self-renewal and stemness states uncoupled from EMT as

Published evidences suggest a predominance of glycolysis and a Warburg effect in association with breast and lung cancers and glioblastoma CSCs [12, 50–52], which may also display an EMT. Together with such data, our observations lead us to conclude that CSCs engage a Warburg effect, independently of whether their phenotype is associated with an epithelial (our model) or a mesenchymal (other models) gene program. In seeming contradiction, other authors have found that pancreatic CSCs and/or drug-resistant tumor populations preferentially use mitochondrial metabolism over glycolysis for cellular energetics [13, 53]. However, in at least one of these studies it was found that the emergence of CSCs resistant to a specific drug treatment (metformin) was associated with a significantly enhanced glycolytic capacity and lactate production [53], an observation that suggests that enhanced glycolysis may be a feature of the more aggressive CSC subpopulations. In this regard, we note that the PC-3M cells used in our study as our model CSCs are a highly metastatic subpopulation isolated through positive selection *in vivo*. Importantly, our data demonstrate that the expression of EMT features does not necessary correlate with a higher glycolytic phenotype. High glycolytic fluxes likely benefit cells with elevated proliferation rates through the production of glycolytic intermediates for *de novo* biosynthesis of nucleotides, lipids and proteins [54] and previous studies have suggested that the glycolytic metabolism may be a broadly conserved stem cell property [55] and associated with undifferentiated states [56, 57]. The situation described here, in which one tumor cell subpopulation displays high glycolytic activity and marked Warburg effect, while a second subpopulation relies more strongly on mitochondrial metabolism for energy supply, is akin to the so-called “metabolic asymmetry” of tumors [58], in which different cell populations within a tumor, including neoplastic *vs*. non-neoplastic cells, express very different metabolic profiles [59] that contribute to potential co-operation between such subpopulations to foster more aggressive overall phenotypes [60, 61]. Our observations suggest that neoplastic cell subpopulations expressing uncoupled CSC or EMT features may cooperate not only through cell-cell contacts or diffusible protein factors [60], but also through metabolic co-operation.

Amino acid metabolism has been far less explored than glucose metabolism but its biological relevance for the study of tumor progression is gaining ground. Our stable isotope labeling studies also revealed that PC-3M cells actively metabolized the amino acids serine and glycine, while PC-3S cells presented a more limited use of these amino acids as shown by an accumulation of m1, m2 and m3 serine isotopologues and excretion of surplus

glycine. Therefore, differences in the expression levels of genes involved in the SGOC metabolism could be good biomarkers of tumor progression to metastatic disease [42].

Glutaminolysis normally serves to anaplerotically fill the TCA cycle, in particular in cells that shut down the entry of pyruvate into mitochondria as a consequence of PDH inhibition [35]. Interestingly, our analysis showed that, of the different functions of glutamine investigated, its protective role against acidic conditions better explained the growth and survival properties of PC-3M cells. Moreover, several metabolic pathways use glutamate-derived glutamine, including reactions involved in serine metabolism (Supplemental Fig. 5b). Targeting these metabolic pathways could additionally compromise the proliferation and viability of PC-3M cells and, by extension, CSCs, not only because of their specific role in amino acid metabolic networks but also as a consequence of compromised cell pH buffering capacity. In contrast, glutamine metabolism in PC-3S cells contributed substantially to their mitochondrial respiration and was more closely linked to glutathione synthesis which confers protection from oxidative stress. Thus, reasonable strategies to target non-CSCs that constitute part of the tumor bulk and with similar metabolic phenotypes might include interventions to limit antioxidant adaptive responses.

Finally, PC-3M cells displayed a more active non-oxidative branch of the PPP, which may be advantageous for their high glycolytic phenotype, allowing a reversible and dynamic connection between glycolysis and the PPP. In contrast, PC-3S cells showed a preference for the oxidative branch of the PPP, a key source of NADPH to support fatty acid synthesis and redox homeostasis maintenance. PC-3S cells also had a more pronounced fatty acid synthetic activity than PC-3M cells, in which fatty acid oxidation was more prevalent. From these observations, we predict a higher sensitivity of the non-CSC PC-3S cell subpopulation to perturbations in lipogenesis than the e-CSC PC-3M subpopulation, which in turn should be more susceptible to inhibitors of fatty acid β-oxidation.

Additionally, our computational analysis has permitted to further analyze the correlation between the metabolic adaptations and tumor malignancy in prostate cancer as well as in other tumor types. The metabolic pathways associated with the metabolic gene signature characteristic of PC-3M cells are consistent with our metabolomics and fluxomics analysis, which indicates the reliability of the metabolic gene signature inferred from our transcriptomic analysis. Nevertheless, this analysis failed to predict specific reactions that we have found, through our experimental approaches, to be relevant in the metabolic reprogramming of CSCs in our cell model. Thus, unlike the transcriptomic-based computational analysis, metabolomics and fluxomics approaches revealed that PDH is more active in PC-3S than in PC-3M cells, whereas the activities of GLS and CPT1, representatives of glutamine and fatty acid metabolism respectively, were increased in PC-3M cells. This is likely due to the fact that transcriptomic analyses do not consider the functional consequences of post-transcriptional modifications, such as the regulation of PDH activity by phosphorylation, the effects of substrate availability or the need for buffering capacity due to excess of protons derived from a marked Warburg effect.

Conclusion

In summary, we conclude that metabolic programs underlying CSC and EMT phenotypes can be mutually uncoupled and that each can be associated with preferred metabolic dependencies required for optimal cell proliferation and sustaining specific cell phenotypes. In this work, we have tackled the study of complex cellular phenomena associated with tumor progression and malignancy from a novel perspective that combines metabolomic, fluxomic and transcriptomic approaches. These complementary studies have widened the scope of our results, establishing new grounds for targeting tumor cell metabolism with a subpopulation-specific approach, providing insights into mechanisms supporting tumor progression and with potential impacts on the management of metastatic disease.

Supplementary Material

Refer to Web version on PubMed Central for supplementary material.

Acknowledgments

This work was supported by funds to M.C. from MICINN (SAF2011–25726 and SAF2014-56059-R, European Comission FEDER - Una manera de hacer Europa); Agència Catalana d'Ajuts Universitaris i de Recerca (AGAUR) (2014SGR-1017), ICREA Foundation (Generalitat de Catalunya) and European Commission (Metaflux, PITN-GA-2010-264780); to T.M.T. from MICINN (SAF2011-24686), MINECO (SAF2012-40017-C02-01, European Comission FEDER - Una manera de hacer Europa), AGAUR (2009SGR1482), and Xarxa de Referència en Biotecnologia; and to D.H. and F.M. from NIH (5R01CA158921-02). E.A. was supported by a fellowship from the MECD and a travel grant from RTICC; I.M.M. by a EC Marie Curie grant (Metaflux, PITN-GA-2010-264780).

References

1. Merlo LM, Pepper JW, Reid BJ, et al. Cancer as an evolutionary and ecological process. Nat Rev Cancer. 2006; 6:924–935. [PubMed: 17109012]
2. Hanahan D, Weinberg RA. Hallmarks of cancer: the next generation. Cell. 2011; 144:646–674. [PubMed: 21376230]
3. Chaffer CL, Brueckmann I, Scheel C, et al. Normal and neoplastic nonstem cells can spontaneously convert to a stem-like state. Proc Natl Acad Sci U S A. 2011; 108:7950–7955. [PubMed: 21498687]
4. Mani SA, Guo W, Liao MJ, et al. The epithelial-mesenchymal transition generates cells with properties of stem cells. Cell. 2008; 133:704–715. [PubMed: 18485877]
5. Papagerakis S, Pannone G, Zheng L, et al. Oral epithelial stem cells - implications in normal development and cancer metastasis. Exp Cell Res. 2014; 325:111–129. [PubMed: 24803391]
6. Celia-Terrassa T, Meca-Cortes O, Mateo F, et al. Epithelial-mesenchymal transition can suppress major attributes of human epithelial tumor-initiating cells. J Clin Invest. 2012; 122:1849–1868. [PubMed: 22505459]
7. Cleary AS, Leonard TL, Gestl SA, et al. Tumour cell heterogeneity maintained by cooperating subclones in Wnt-driven mammary cancers. Nature. 2014; 508:113–117. [PubMed: 24695311]
8. Tsuji T, Ibaragi S, Shima K, et al. Epithelial-mesenchymal transition induced by growth suppressor p12CDK2-AP1 promotes tumor cell local invasion but suppresses distant colony growth. Cancer Res. 2008; 68:10377–10386. [PubMed: 19074907]
9. Chapman A, Fernandez del Ama L, Ferguson J, et al. Heterogeneous tumor subpopulations cooperate to drive invasion. Cell Rep. 2014; 8:688–695. [PubMed: 25066122]
10. Koppenol WH, Bounds PL, Dang CV. Otto Warburg's contributions to current concepts of cancer metabolism. Nat Rev Cancer. 2011; 11:325–337. [PubMed: 21508971]
11. Warburg O. On respiratory impairment in cancer cells. Science. 1956; 124:269–270. [PubMed: 13351639]

PLOS COMPUTATIONAL BIOLOGY

RESEARCH ARTICLE

Model-driven discovery of long-chain fatty acid metabolic reprogramming in heterogeneous prostate cancer cells

Igor Marín de Mas[1,2,3], Esther Aguilar[1,2], Erika Zodda[1,2,4], Cristina Balcells[1,2], Silvia Marin[1,2], Guido Dallmann[5], Timothy M. Thomson[4], Balázs Papp[3]*, Marta Cascante[1,2]*

1 Department of Biochemistry and Molecular Biomedicine, Faculty of Biology, Universitat de Barcelona, Barcelona, Spain, **2** Institute of Biomedicine of University of Barcelona (IBUB) and Associated Unit with CSIC, Barcelona, Spain, **3** Synthetic and Systems Biology Unit, Institute of Biochemistry, Biological Research Center of the Hungarian Academy of Sciences, Szeged, Hungary, **4** Department of Cell Biology, Barcelona Institute for Molecular Biology (IBMB), National Research Council (CSIC), Barcelona, Spain, **5** Biocrates Life Sciences AG, Innsbruck, Austria

* pappb@brc.hu (BP); martacascante@ub.edu (MC)

Citation: Marín de Mas I, Aguilar E, Zodda E, Balcells C, Marin S, Dallmann G, et al. (2018) Model-driven discovery of long-chain fatty acid metabolic reprogramming in heterogeneous prostate cancer cells. PLoS Comput Biol 14(1): e1005914. https://doi.org/10.1371/journal.pcbi.1005914

Editor: Nathan E Lewis, University of California San Diego, UNITED STATES

Received: July 7, 2017

Accepted: December 1, 2017

Published: January 2, 2018

Data Availability Statement: All relevant data are within the paper and its Supporting Information files.

Funding: This work was supported by the European Commission Seventh Framework Programme FP7 (METAFLUX-Marie Curie FP7-PEOPLE-2010 ITN-264780); the Spanish Government and the European Union FEDER funds (SAF2014-56059-R, SAF2015-70270-REDT and SAF2015-66984-C2-1-R); Generalitat de Catalunya-

Abstract

Epithelial-mesenchymal-transition promotes intra-tumoral heterogeneity, by enhancing tumor cell invasiveness and promoting drug resistance. We integrated transcriptomic data for two clonal subpopulations from a prostate cancer cell line (PC-3) into a genome-scale metabolic network model to explore their metabolic differences and potential vulnerabilities. In this dual cell model, PC-3/S cells express Epithelial-mesenchymal-transition markers and display high invasiveness and low metastatic potential, while PC-3/M cells present the opposite phenotype and higher proliferative rate. Model-driven analysis and experimental validations unveiled a marked metabolic reprogramming in long-chain fatty acids metabolism. While PC-3/M cells showed an enhanced entry of long-chain fatty acids into the mitochondria, PC-3/S cells used long-chain fatty acids as precursors of eicosanoid metabolism. We suggest that this metabolic reprogramming endows PC-3/M cells with augmented energy metabolism for fast proliferation and PC-3/S cells with increased eicosanoid production impacting angiogenesis, cell adhesion and invasion. PC-3/S metabolism also promotes the accumulation of docosahexaenoic acid, a long-chain fatty acid with antiproliferative effects. The potential therapeutic significance of our model was supported by a differential sensitivity of PC-3/M cells to etomoxir, an inhibitor of long-chain fatty acid transport to the mitochondria.

Author summary

The coexistence within the same tumor of a variety of subpopulations, featuring different phenotypes (intra-tumoral heterogeneity) represents a challenge for diagnosis, prognosis and targeted therapies. In this work, we have explored the metabolic differences underlying tumor heterogeneity by building cell-type-specific genome-scale metabolic models

www.impactjournals.com/oncotarget/ Oncotarget, 2017, Vol. 8, (No. 48), pp: 83384-83406

Priority Research Paper

MicroRNA-200, associated with metastatic breast cancer, promotes traits of mammary luminal progenitor cells

Lourdes Sánchez-Cid[1,2,15], Mònica Pons[1], Juan José Lozano[3], Nuria Rubio[4,5], Marta Guerra-Rebollo[4,5], Aroa Soriano[6], Laia Paris-Coderch[6], Miquel F. Segura[6], Raquel Fueyo[1], Judit Arguimbau[1], Erika Zodda[7], Raquel Bermudo[2], Immaculada Alonso[8], Xavier Caparrós[8], Marta Cascante[7], Arash Rafii[9], Yibin Kang[10], Marian Martínez-Balbás[1], Stephen J. Weiss[11], Jerónimo Blanco[4,5], Montserrat Muñoz[12], Pedro L. Fernández[2,13,14] and Timothy M. Thomson[1]

[1] Institute of Molecular Biology, Spanish National Research Council (IBMB-CSIC), Barcelona, Spain

[2] Institut d'Investigacions Biomèdiques August Pi i Sunyer (IDIBAPS), Barcelona, Spain

[3] Networked Biomedical Research Center for Hepatic and Digestive Diseases (CIBER-EHD), Instituto de Salud Carlos III, Madrid, Spain

[4] Networked Biomedical Research Center for Bioengineering, Biomaterials and Nanomedicine (CIBER-BBN), Instituto de Salud Carlos III, Madrid, Spain

[5] Institute of Advanced Chemistry of Catalonia (IQAC-CSIC), Barcelona, Spain

[6] Vall d'Hebron Institut de Recerca (VHIR), Universitat Autònoma de Barcelona, Barcelona, Spain

[7] Department of Biochemistry and Molecular Biology, Faculty of Biology, Universitat de Barcelona, Barcelona, Spain

[8] Department of Obstetrics and Gynecology, Hospital Clinic, Barcelona, Spain

[9] Weill Cornell Medical College, Education City, Ar-Rayyan, Qatar

[10] Department of Molecular Biology, Princeton University, Princeton, NJ, USA

[11] Life Sciences Institute, University of Michigan, Ann Arbor, MI, USA

[12] Department of Oncology, Hospital Clínic, Barcelona, Spain

[13] Department of Pathology, Hospital Clínic, Barcelona, Spain

[14] School of Medicine, University of Barcelona, Barcelona, Spain

[15] Current address: Networked Biomedical Research Center for Bioengineering, Biomaterials and Nanomedicine (CIBER-BBN), Instituto de Salud Carlos III, Madrid, Spain

***Correspondence to**: Timothy M. Thomson, **email**: titbmc@ibmb.csic.es*

*Correspondence to: Pedro L. Fernández, **email**: plfernan@clinic.ub.es*

Keywords: microRNAs, miR-200, epithelial reprogramming, progenitor luminal cells, invasive ductal breast cancer

***Received**: March 06, 2017* ***Accepted**: July 25, 2017* ***Published**: September 07, 2017*

ABSTRACT

MicroRNAs are critical regulators of gene networks in normal and abnormal biological processes. Focusing on invasive ductal breast cancer (IDC), we have found dysregulated expression in tumor samples of several microRNAs, including the miR-200 family, along progression from primary tumors to distant metastases, further reflected in higher blood levels of miR-200b and miR-7 in IDC patients with regional or distant metastases relative to patients with primary node-negative tumors. Forced expression of miR-200s in MCF10CA1h mammary cells induced an enhanced epithelial program, aldehyde dehydrogenase (ALDH) activity, mammosphere growth and ability to form branched tubuloalveolar structures while promoting orthotopic tumor growth and lung colonization *in vivo*. MiR-200s also induced the constitutive activation of the PI3K-Akt signaling through downregulation of PTEN, and the enhanced mammosphere growth and ALDH activity induced in MCF10CA1h cells by miR-200s required the